

UNIVERSITI MALAYA

ORIGINAL LITERARY WORK DECLARATION

Name of Candidate: Khairul Bahiyah binti Md Isa (**I.C/Passport No**): 830518-07-5756

Registration/Matric No: SGR 070061

Name of Degree: Master of Science

Title of Project Paper/Research Report/Dissertation/Thesis (“this Work”):

Electrical and Structural Studies of Polyacrylonitrile (PAN) Complexed with Inorganic Salts.

Field of Study: Polymer Physic and Advanced Materials

I do solemnly and sincerely declare that:

- (1) I am the sole author/writer of this Work;
- (2) This Work is original;
- (3) Any use of any work in which copyright exists was done by way of fair dealing and for permitted purposes and any excerpt or extract from, or reference to or reproduction of any copyright work has been disclosed expressly and sufficiently and the title of the Work and its authorship have been acknowledged in this Work;
- (4) I do not have any actual knowledge nor do I ought reasonably to know that the making of this work constitutes an infringement of any copyright work;
- (5) I hereby assign all and every rights in the copyright to this Work to the University of Malaya (“UM”), who henceforth shall be owner of the copyright in this Work and that and reproduction or use in any form or by any means whatsoever is prohibited without the written consent of UM having been first had and obtained;
- (6) I am fully aware that if in the course of making this Work I have infringed any copyright whether intentionally or otherwise, I may be subject to legal action or any other action as may be determined by UM.

Candidate’s Signature

Date

Subscribed and solemnly declared before,

Witness’s Signature

Date

Name:

Designation:

ABSTRACT

In the present study, polymer electrolyte films composed of polyacrylonitrile (PAN) as a host polymer, ethylene carbonate (EC) as the plasticizer and lithium triflate (LiCF_3SO_3) and sodium triflate (NaCF_3SO_3) as dopant salts were prepared by the solution cast technique. Five systems of polymer electrolytes films have been prepared; these systems are the plasticized-PAN system i.e. PAN-EC system, two salted-PAN systems i.e. PAN- LiCF_3SO_3 and PAN- NaCF_3SO_3 , and two plasticized-salted PAN systems i.e. PAN-EC- LiCF_3SO_3 and PAN-EC- NaCF_3SO_3 . The pure PAN film was prepared as a reference. The ionic conductivity for each system is characterized using impedance spectroscopy. The room temperature conductivity of the pure PAN film and the film containing 24 wt.% EC is $1.51 \times 10^{-11} \text{ Scm}^{-1}$ and $3.43 \times 10^{-11} \text{ Scm}^{-1}$ respectively. The room temperature-conductivity for the highest conducting film in the PAN- LiCF_3SO_3 system and PAN- NaCF_3SO_3 system is $3.04 \times 10^{-4} \text{ S cm}^{-1}$ and $7.13 \times 10^{-4} \text{ S cm}^{-1}$ respectively. On addition of plasticizers, the ionic conductivity of these films is further increases to one order of magnitude, i.e. $1.32 \times 10^{-3} \text{ S cm}^{-1}$ and $5.49 \times 10^{-3} \text{ S cm}^{-1}$ for PAN-EC- LiCF_3SO_3 film and PAN-EC- NaCF_3SO_3 film, respectively. The increase in conductivity is due to the increase in number of mobile ions and this can be implied from the dielectric constant, ϵ_r - frequency plots. The conductivity-temperature and pressure-dependence studies are then performed on the highest conducting film from the PAN- LiCF_3SO_3 system, the PAN- NaCF_3SO_3 system, the PAN-EC- LiCF_3SO_3 system and the PAN-EC- NaCF_3SO_3 system. The plots of conductivity versus inverse temperature for all systems followed the Arrhenius rule. The activation energy, E_a values for the PAN+26wt% LiCF_3SO_3 film, the PAN+24wt% NaCF_3SO_3 film, the PAN+EC+22wt% LiCF_3SO_3 film and the PAN+EC+34wt% NaCF_3SO_3 film have been calculated to be 0.28 eV, 0.23 eV, 0.22 eV and 0.19 eV respectively. It can be observed

that the film containing NaCF_3SO_3 salt has higher ionic conductivity and lower activation energy compared to the film containing LiCF_3SO_3 salt. This result can be explained based on the Lewis acidity of the alkali ions, i.e., the strength of the interaction of cations with the nitrogen atoms from the polymer, PAN. The variations in ionic conductivity in the polymer electrolyte systems with pressure have been carried out at the pressure range between 0.1 atm to 1.0 atm. The conductivity is observed to decrease with increasing pressure for all systems. The activation volume, V^* values for the PAN-26wt% LiCF_3SO_3 film, the PAN-24wt% NaCF_3SO_3 film, the PAN-EC-22wt% LiCF_3SO_3 film and the PAN EC-34wt% NaCF_3SO_3 film have been calculated to be $3.04 \times 10^{-2} \text{ cm}^3 \text{ mol}^{-1}$, $2.86 \times 10^{-2} \text{ cm}^3 \text{ mol}^{-1}$, $1.37 \times 10^{-2} \text{ cm}^3 \text{ mol}^{-1}$ and $1.11 \times 10^{-2} \text{ cm}^3 \text{ mol}^{-1}$, respectively. FTIR spectrum for pure PAN film exhibits the nitrile band, $\text{C}\equiv\text{N}$ at 2247 cm^{-1} and this band shifted to 2244 cm^{-1} in this complex films. This is due to inductive effect created by the interaction between the nitrogen atom in $\text{C}\equiv\text{N}$ with Li^+ and Na^+ ions from the salts. The XRD studies show the occurrence of complexation between the polymer, the plasticizer and the salts. The SEM micrographs show that the presence of the plasticizer in PAN-salt system helped to obtain regular pore structure, which can increase ion mobility and conductivity. DSC studies show that the pure PAN film has glass transition temperature, T_g at $85.4 \text{ }^\circ\text{C}$. The T_g of the film decreases upon addition of the plasticizer and the salts. This result is in good agreement with the conductivity behavior.

ABSTRAK

Dalam kajian ini, filem elektrolit polimer yang mengandungi polimer asas PAN, agen pemplastik, EC dan garam pendopan iaitu litium triflate (LiCF_3SO_3) dan sodium triflate (NaCF_3SO_3) telah disediakan dengan menggunakan teknik tuangan larutan. Terdapat lima sistem elektrolit polimer yang iaitu sistem PAN-EC, sistem PAN- LiCF_3SO_3 , sistem PAN- NaCF_3SO_3 , sistem PAN-EC- LiCF_3SO_3 dan sistem PAN-EC- NaCF_3SO_3 . Filem PAN tulen digunakan sebagai rujukan. Kekonduksian bagi setiap filem dalam semua sistem diukur dengan menggunakan spektroskopi impedan. Kekonduksian pada suhu bilik bagi filem PAN tulen dan PAN-EC adalah masing-masing bernilai $1.51 \times 10^{-11} \text{ S cm}^{-1}$ dan $3.43 \times 10^{-11} \text{ S cm}^{-1}$. Kekonduksian tertinggi bagi filem di dalam sistem PAN- LiCF_3SO_3 dan sistem PAN- NaCF_3SO_3 adalah masing-masing bernilai $3.04 \times 10^{-4} \text{ Scm}^{-1}$ dan $7.13 \times 10^{-4} \text{ S cm}^{-1}$. Kekonduksian terus meningkat apabila agen pemplastik ditambah iaitu kekonduksian tertinggi yang diperolehi bagi sistem PAN-EC- LiCF_3SO_3 dan sistem PAN-EC- NaCF_3SO_3 adalah bernilai $1.32 \times 10^{-3} \text{ S cm}^{-1}$ dan $5.49 \times 10^{-3} \text{ S cm}^{-1}$. Peningkatan nilai-nilai kekonduksian ini adalah disebabkan oleh peningkatan jumlah ion-ion yang bergerak dan ini dapat dibuktikan daripada plot-plot pemalar dielektrik, ϵ_r -frekuensi. Seterusnya, filem-filem yang mempunyai kekonduksian tertinggi daripada setiap sistem digunakan untuk mengkaji kesan suhu dan tekanan kepada filem-filem tersebut. Berdasarkan plot konduktiviti melawan suhu songsangan untuk semua filem, hasil yang diperolehi menunjukkan bahawa kekonduksian dalam julat suhu ini mematuhi hukum Arrhenius. Tenaga pengaktifan, E_a bagi filem PAN+26wt% LiCF_3SO_3 , filem PAN+24wt% NaCF_3SO_3 , filem PAN+EC+22wt% LiCF_3SO_3 dan filem PAN+EC+34wt% NaCF_3SO_3 adalah 0.28 eV, 0.23 eV, 0.22 eV and 0.19 eV. Filem yang mengandungi garam NaCF_3SO_3 mempunyai kekonduksian yang lebih tinggi dan tenaga pengaktifan yang lebih rendah

dibandingkan dengan filem yang mengandungi garam LiCF_3SO_3 . Keputusan ini boleh diterangkan melalui teori keasidan Lewis bagi ion-ion alkali iaitu kekuatan interaksi di antara kation garam dengan atom-atom nitrogen daripada polimer PAN. Kekonduksian didapati berkurangan dengan peningkatan tekanan dari 0.01 MPa hingga 0.09 MPa. Nilai-nilai isipadu pengaktifan, ΔV^* bagi filem PAN+26wt% LiCF_3SO_3 , filem PAN+24wt% NaCF_3SO_3 , filem PAN+EC+22wt% LiCF_3SO_3 dan filem PAN+EC+34wt% NaCF_3SO_3 adalah $3.04 \times 10^{-2} \text{ cm}^3 \text{ mol}^{-1}$, $2.86 \times 10^{-2} \text{ cm}^3 \text{ mol}^{-1}$, $1.37 \times 10^{-2} \text{ cm}^3 \text{ mol}^{-1}$ and $1.11 \times 10^{-2} \text{ cm}^3 \text{ mol}^{-1}$. Spektra FTIR bagi filem PAN tulen menunjukkan frekuensi untuk kumpulan $\text{C}\equiv\text{N}$ (nitril) wujud pada 2247 cm^{-1} dan frekuensinya beranjak kepada 2244 cm^{-1} dalam filem-filem kompleks. Ini adalah disebabkan berlakunya interaksi antara kumpulan $\text{C}\equiv\text{N}$ dalam PAN dengan garam-garam pendopan. Keputusan XRD menunjukkan pengkompleksan berlaku di antara polimer, garam-garam dan agen pemplastik. Imej-imej SEM menunjukkan bahawa kehadiran agen pemplastik dalam sistem-sistem PAN-garam telah menyebabkan wujud struktur berliang yang seragam di mana ianya memudahkan pergerakan ion-ion seterusnya meningkatkan kekonduksian. Kajian DSC menunjukkan PAN tulen mempunyai suhu peralihan ke kaca, T_g pada $85.4 \text{ }^\circ\text{C}$. Nilai T_g ini berkurangan apabila garam dan agen pemplastik ditambah. Keputusan ini adalah selari dengan nilai-nilai kekonduksian.

Acknowledgments

In the name of Allah, the Almighty Lord, the most Gracious and the most Merciful. Alhamdulillah, I thank to God for His Help and Bless, finally, I was able to finish my dissertation successfully. Peace be upon His messenger Muhammad and his honourable family.

I would like to express my deepest gratitude to my supervisor, Assoc. Prof. Dr. Zurina Osman, for her encouragement, excellent guidance, caring, patience and support from the initial to the final level enabled me to develop an understanding of this project.

Special thank to Lisani Othman, who as a good friend, was always willing to help and give her best suggestions. I am also grateful to my lab mates, Azhar Ahmad , Noranis Mohd Ali and Chua Ngeah Boon for their help and long term friendship. Thanks also due to the late Haji Salleh Zakaria, the Materials Science Laboratory assistant at Physics Department for the technical support rendered.

I would also like to convey thanks to the University of Malaya for providing the financial support and laboratory facilities.

I also wishes to express my love and gratitude to my beloved families and my special friend Mohd Amran Ahmad for their understanding and endless love, through the duration of my studies. They were always supporting and encouraging me with their best wishes.

Last but certainly not least, appreciation is expressed to all the individuals who have directly or indirectly assisted me during the preparation of this dissertation.

CONTENTS

<u>CONTENTS</u>	<u>PAGE</u>
Declaration	ii
Abstract	iii
Abstrak	v
Acknowledgements	vii
Contents	viii
List of Figures	xii
List of Tables	xix
List of Published and Presented Papers	xx
CHAPTER 1 : Introduction	
1.1 Background of the Present Work	1
1.2 Objectives of the Present Work	3
1.3 Organization of the Dissertation	4
CHAPTER 2 : Literature Review	
2.1 Polymer	5
2.1.1 Polymerization	6
2.1.2 Polymer properties	7
2.1.2.1 <i>Relationship between chain length and polymer properties</i>	7
2.1.2.2 <i>Crystallinity</i>	7
2.1.2.3 <i>Tensile strength</i>	8
2.1.2.4 <i>Transport Properties</i>	8
2.2 Lewis Theory	8
2.2.1 <i>Lewis's Theory of Chemical Bonding</i>	9

2.2.2	<i>Salts</i>	11
2.3	Ionic Conduction	14
2.4	Polymer electrolytes	17
2.5	Polyacrylonitrile (PAN)	20
2.5.1	<i>PAN-based electrolytes</i>	21
2.6	Plasticization	24
2.7	Solvent	25
2.8	Applications of Polymer Electrolytes	26
2.8.1	<i>Batteries</i>	27
2.8.2	<i>Electrochromic Devices</i>	29
2.8.3	<i>Fuel cells</i>	32
2.8.4	<i>Sensors</i>	34

CHAPTER 3 : Experimental Techniques

3.1	Sample preparation	37
3.1.1	<i>Preparation of PAN-EC, PAN-LiCF₃SO₃ and PAN-NaCF₃SO₃ systems</i>	38
3.1.2	<i>Preparation of PAN-EC-LiCF₃SO₃ system and PAN-EC-NaCF₃SO₃ system</i>	40
3.2	Impedance Spectroscopy	41
3.3	Fourier Transform Infrared Spectroscopy (FTIR)	47
3.4	X-Ray Diffraction (XRD)	49
3.5	Scanning Electron Microscopy (SEM)	52
3.6	Differential Scanning Calorimetry (DSC)	54

RESULTS AND DISCUSSION:

CHAPTER 4 : Electrical Studies

4.1	Impedance Spectroscopy Analysis	57
-----	---------------------------------	----

4.2	Room temperature electrical conductivity studies	57
4.2.1	<i>Pure PAN film</i>	57
4.2.2	<i>PAN - EC system</i>	58
4.2.3	<i>PAN - LiCF₃SO₃ system</i>	60
4.2.4	<i>PAN - NaCF₃SO₃ system</i>	66
4.2.5	<i>PAN - EC - LiCF₃SO₃ system</i>	71
4.2.6	<i>PAN - EC - NaCF₃SO₃ system</i>	76
4.3	Conductivity-temperature dependence studies	81
4.3.1	<i>PAN - LiCF₃SO₃ system</i>	81
4.3.2	<i>PAN - NaCF₃SO₃ system</i>	84
4.3.3	<i>PAN - EC - LiCF₃SO₃ system</i>	87
4.3.4	<i>PAN - EC - NaCF₃SO₃ system</i>	90
4.4	Conductivity-pressure dependence studies	92

CHAPTER 5 : Fourier Transform Infrared (FTIR) Studies

5.1	FTIR Analysis	96
5.2	Pure PAN film	96
5.3	PAN - EC system	98
5.4	PAN - LiCF ₃ SO ₃ system	105
5.5	PAN - NaCF ₃ SO ₃ system	111
5.6	PAN - EC - LiCF ₃ SO ₃ system	117
5.7	PAN - EC - NaCF ₃ SO ₃ system	123

CHAPTER 6 : X-Ray Diffraction (XRD) Studies

6.1	XRD Analysis	128
6.2	Pure PAN film	128
6.3	Pure EC	129

6.4	LiCF ₃ SO ₃ and NaCF ₃ SO ₃ salts	129
6.5	PAN - EC system	131
6.6	PAN - LiCF ₃ SO ₃ system	132
6.7	PAN - NaCF ₃ SO ₃ system	133
6.8	PAN - EC - LiCF ₃ SO ₃ system	134
6.9	PAN - EC - NaCF ₃ SO ₃ system	135
CHAPTER 7 : Scanning Electron Microscopy (SEM) Studies		
7.1	SEM Analysis	136
7.2	Pure PAN film	136
7.3	PAN - EC system	137
7.4	PAN - LiCF ₃ SO ₃ system and PAN - NaCF ₃ SO ₃ system	138
7.5	PAN - EC - LiCF ₃ SO ₃ system and PAN - EC - NaCF ₃ SO ₃ system	139
CHAPTER 8 : Differential Scanning Calorimetry (DSC) Studies		
8.1	DSC analysis	141
8.2	Pure PAN film	141
8.3	PAN - EC system	142
8.4	PAN - LiCF ₃ SO ₃ system and PAN - NaCF ₃ SO ₃ system	143
8.5	PAN - EC - LiCF ₃ SO ₃ system and PAN - EC - NaCF ₃ SO ₃ system	145
CHAPTER 9 : DISCUSSION, CONCLUSION AND SUGGESTIONS FOR FURTHER WORK		148
REFERENCES		153

LIST OF FIGURES	PAGE	
Figure 1.1	Molecular structure of PAN	1
Figure 1.2	The chemical structure of (a) lithium triflate and (b) sodium triflate	2
Figure 2.1	A simple diagram of a chain of monomers	5
Figure 2.2	Macromolecule structure of polypropylene	5
Figure 2.3	Simple chemical structure of polypropylene	6
Figure 2.4	The chemical structure of (a) lithium triflate and (b) sodium triflate	12
Figure 2.5	Ions move in polymer chain	18
Figure 2.6	Molecular structure of polyacrylonitrile (PAN)	21
Figure 2.7	Simple molecular structure of polyacrylonitrile	21
Figure 2.8	The chemical structure of ethylene carbonates (EC)	24
Figure 2.9	The molecular structure of DMF	26
Figure 2.10	Schematic of charge and discharge process for secondary battery	27
Figure 2.11	Conceptual structure of lithium polymer battery	29
Figure 2.12	Internal construction of lithium-polymer battery	29
Figure 2.13	Electrochromic window	31
Figure 2.14	Schematic of a polymer electrolyte membrane fuel cell	33
Figure 2.15	Setup for basic sensor and typical electrochemical sensor	35
Figure 3.1	Sinusoidal Current Response in a Linear System	42
Figure 3.2	Cole-Cole plot	44
Figure 3.3	Experimental Setup for conductivity measurement	46
Figure 3.4	A Schematic of a generic Michelson interferometer	47
Figure 3.5	The sample analysis process (FTIR)	48
Figure 3.6	A schematic of an x-ray diffractometer	50

Figure 3.7	Constructive and destructive interference	50
Figure 3.8	A simple schematic of the Young's double split experiment	51
Figure 3.9	The schematic diagram of SEM experiment	53
Figure 3.10	Experimental setup for DSC	55
Figure 4.1	Cole-Cole plot of pure PAN film	58
Figure 4.2	Conductivity versus amount of EC in the PAN-EC system	60
Figure 4.3	Cole-Cole plots for the PAN films containing (a) 2 wt.% (b) 10 wt.% (c) 26wt.% and (d) 30wt.% and of LiCF_3SO_3 films	62
Figure 4.4	Conductivity versus amount of LiCF_3SO_3 in the PAN- LiCF_3SO_3 system	64
Figure 4.5	Dielectric constant versus frequency for films in the PAN- LiCF_3SO_3 system	65
Figure 4.6	Dielectric loss versus frequency for films in the PAN- LiCF_3SO_3 system	65
Figure 4.7	Cole – Cole plot for the PAN films containing and (a) 2 wt.% (b) 10wt.% (c) 24wt.%, and (d) 30wt% of NaCF_3SO_3	67
Figure 4.8	Conductivity versus amount of NaCF_3SO_3 in the PAN- NaCF_3SO_3 system	69
Figure 4.9	Dielectric constant versus frequency for films in the PAN- NaCF_3SO_3 system	70
Figure 4.10	Dielectric constant versus frequency for films in the PAN- NaCF_3SO_3 system	70
Figure 4.11	Cole – Cole plot for the PAN-EC- LiCF_3SO_3 films containing (a) 2 wt.% (b) 10 wt.% (c) 22 wt.% and (d) 30wt.% LiCF_3SO_3	72
Figure 4.12	Conductivity versus amount of LiCF_3SO_3 in the PAN-EC- LiCF_3SO_3 system	74
Figure 4.13	Dielectric constant versus frequency for films in the PAN-EC- LiCF_3SO_3 system	75
Figure 4.14	Dielectric loss versus frequency for films in the PAN-EC- LiCF_3SO_3 system	75

Figure 4.15	Cole-Cole plot for the PAN-EC-NaCF ₃ SO ₃ films containing (a) 2 wt % (b) 10 wt.% (c) 34 wt.% and (d) 40 wt.% NaCF ₃ SO ₃	77
Figure 4.16	Conductivity versus amount of NaCF ₃ SO ₃ in the PAN-EC-NaCF ₃ SO ₃ system	79
Figure 4.17	Dielectric constant versus frequency for films in the PAN-EC-NaCF ₃ SO ₃ system	80
Figure 4.18	Dielectric loss versus frequency for films in the PAN-EC-NaCF ₃ SO ₃ system	80
Figure 4.19	Arrhenius plot for the highest conducting film in the PAN-LiCF ₃ SO ₃ system	82
Figure 4.20	Dielectric constant versus frequency for the highest conducting film in the PAN-LiCF ₃ SO ₃ system	83
Figure 4.21	Dielectric loss versus frequency for the highest conducting film in the PAN-LiCF ₃ SO ₃ system	84
Figure 4.22	Arrhenius plot for the highest conducting film in the PAN-NaCF ₃ SO ₃ system	85
Figure 4.23	Dielectric constant versus frequency for the highest conducting film in the PAN-NaCF ₃ SO ₃ system	86
Figure 4.24	Dielectric loss versus frequency for the highest conducting film in the PAN-NaCF ₃ SO ₃ system	87
Figure 4.25	Arrhenius plot for the highest conducting film in the PAN-EC-LiCF ₃ SO ₃ system	88
Figure 4.26	Dielectric constant versus frequency for the highest conducting film in the PAN-EC-LiCF ₃ SO ₃ system	89
Figure 4.27	Dielectric loss versus frequency for the highest conducting film in the PAN-EC-LiCF ₃ SO ₃ system	89
Figure 4.28	Arrhenius plot for the highest conducting film in the PAN-EC-NaCF ₃ SO ₃ system.	90
Figure 4.29	Dielectric constant versus frequency for the highest conducting film in the PAN-EC-NaCF ₃ SO ₃ system	91
Figure 4.30	Dielectric loss versus frequency for the highest conducting film in the PAN-EC-NaCF ₃ SO ₃ system	91
Figure 4.31 (a)	The conductivity versus pressure for the highest conducting film in the PAN-LiCF ₃ SO ₃ system	93

Figure 4.31 (b)	The conductivity versus pressure for the highest conducting film in the PAN-NaCF ₃ SO ₃ system	94
Figure 4.31 (c)	The conductivity versus pressure for the highest conducting film in the PAN-EC-LiCF ₃ SO ₃ system	95
Figure 4.31 (d)	The conductivity versus pressure for the highest conducting film in the PAN-EC-NaCF ₃ SO ₃ system	95
Figure 5.1	FTIR spectrum for pure PAN film in the region 400 cm ⁻¹ and 4000 cm ⁻¹	96
Figure 5.2	FTIR spectrum for pure EC in the region 600 cm ⁻¹ and 3000 cm ⁻¹	98
Figure 5.3	FTIR spectra of (a) pure PAN (b) EC (c) PAN + 8 wt.% EC (d) PAN + 16 wt.% EC (e) PAN + 24 wt.% EC (f) PAN + 26 wt.% EC and (g) PAN + 30 wt.% EC	101
Figure 5.4	FTIR spectra of (a) pure PAN film (b) EC (c) PAN + 8 wt.% EC film (d) PAN + 16 wt.% EC film, (e) PAN + 24 wt.% EC film (f) PAN + 26 wt.% EC film and (g) PAN + 30 wt.% EC film	102
Figure 5.5	FTIR spectra of (a) pure PAN film (b) EC (c) PAN + 8 wt.% EC film (d) PAN + 16 wt.% EC film, (e) PAN + 24 wt.% EC film (f) PAN + 26 wt.% EC film and (g) PAN + 30 wt.% EC film	103
Figure 5.6	FTIR spectra of (a) pure PAN film (b) EC (c) PAN + 8 wt.% EC film (d) PAN + 16 wt.% EC film, (e) PAN + 24 wt.% EC film (f) PAN + 26 wt.% EC film and (g) PAN + 30 wt.% EC film	104
Figure 5.7	FTIR spectrum of LiCF ₃ SO ₃ salt	105
Figure 5.8	FTIR spectra of (a) pure PAN film (b) LiCF ₃ SO ₃ (c) PAN + 8 wt.% LiCF ₃ SO ₃ film (d) PAN + 18 wt.% LiCF ₃ SO ₃ film (e) PAN + 22 wt.% LiCF ₃ SO ₃ film (f) PAN + 26 wt.% LiCF ₃ SO ₃ film and (g) PAN + 30 wt.% LiCF ₃ SO ₃ film.	108
Figure 5.9	FTIR spectra of (a) pure PAN film (b) LiCF ₃ SO ₃ (c) PAN + 8 wt.% LiCF ₃ SO ₃ film (d) PAN + 18 wt.% LiCF ₃ SO ₃ film (e) PAN + 22 wt.% LiCF ₃ SO ₃ film (f) PAN + 26 wt.% LiCF ₃ SO ₃ film and (g) PAN + 30 wt.% LiCF ₃ SO ₃ film.	109
Figure 5.10	FTIR spectra of (a) pure PAN film (b) LiCF ₃ SO ₃ (c) PAN + 8 wt.% LiCF ₃ SO ₃ film (d) PAN + 18 wt.% LiCF ₃ SO ₃ film (e) PAN + 22 wt.% LiCF ₃ SO ₃ film (f) PAN + 26 wt.% LiCF ₃ SO ₃ film and (g) PAN + 30 wt.% LiCF ₃ SO ₃ film	110

Figure 5.11	FTIR spectrum of NaCF ₃ SO ₃ salt	111
Figure 5.12	FTIR spectra of (a) pure PAN film (b) NaCF ₃ SO ₃ (c) PAN + 8 wt.% NaCF ₃ SO ₃ film (d) PAN + 18 wt.% NaCF ₃ SO ₃ film (e) PAN + 24 wt.% NaCF ₃ SO ₃ film (f) PAN + 26 wt.% NaCF ₃ SO ₃ film and (g) PAN + 30 wt.% NaCF ₃ SO ₃ film	114
Figure 5.13	FTIR spectra of (a) pure PAN film (b) NaCF ₃ SO ₃ (c) PAN + 8 wt.% NaCF ₃ SO ₃ film (d) PAN + 18 wt.% NaCF ₃ SO ₃ film (e) PAN + 24 wt.% NaCF ₃ SO ₃ film (f) PAN + 26 wt.% NaCF ₃ SO ₃ film and (g) PAN + 30 wt.% NaCF ₃ SO ₃ film	115
Figure 5.14	FTIR spectra of (a) pure PAN film (b) NaCF ₃ SO ₃ (c) PAN + 8 wt.% NaCF ₃ SO ₃ film (d) PAN + 18 wt.% NaCF ₃ SO ₃ film (e) PAN + 24 wt.% NaCF ₃ SO ₃ film (f) PAN + 26 wt.% NaCF ₃ SO ₃ film and (g) PAN + 30 wt.% NaCF ₃ SO ₃ film	116
Figure 5.15	FTIR spectra of (a) pure PAN film (b) EC (c) LiCF ₃ SO ₃ (d) PAN + EC + 8 wt.% LiCF ₃ SO ₃ film (e) PAN + EC + 16 wt.% LiCF ₃ SO ₃ film (f) PAN + EC + 22 wt.% LiCF ₃ SO ₃ film (g) PAN + EC + 28 wt.% LiCF ₃ SO ₃ film and (h) PAN + EC + 36 wt.% LiCF ₃ SO ₃ film.	119
Figure 5.16	FTIR spectra of (a) pure PAN film (b) EC (c) LiCF ₃ SO ₃ (d) PAN + EC + 8 wt.% LiCF ₃ SO ₃ film (e) PAN + EC + 16 wt.% LiCF ₃ SO ₃ film (f) PAN + EC + 22 wt.% LiCF ₃ SO ₃ film (g) PAN + EC + 28 wt.% LiCF ₃ SO ₃ film and (h) PAN + EC + 36 wt.% LiCF ₃ SO ₃ film.	120
Figure 5.17	FTIR spectra of (a) pure PAN film (b) EC (c) LiCF ₃ SO ₃ (d) PAN + EC + 8 wt.% LiCF ₃ SO ₃ film (e) PAN + EC + 16 wt.% LiCF ₃ SO ₃ film (f) PAN + EC + 22 wt.% LiCF ₃ SO ₃ film (g) PAN + EC + 28 wt.% LiCF ₃ SO ₃ film and (h) PAN + EC + 36 wt.% LiCF ₃ SO ₃ film.	121
Figure 5.18	FTIR spectra of (a) pure PAN film (b) EC (c) LiCF ₃ SO ₃ (d) PAN + EC + 8 wt.% LiCF ₃ SO ₃ film (e) PAN + EC + 16 wt.% LiCF ₃ SO ₃ film (f) PAN + EC + 22 wt.% LiCF ₃ SO ₃ film (g) PAN + EC + 28 wt.% LiCF ₃ SO ₃ film and (h) PAN + EC + 36 wt.% LiCF ₃ SO ₃ film	122
Figure 5.19	FTIR spectra of (a) pure PAN film (b) EC (c) NaCF ₃ SO ₃ (d) PAN + EC + 8 wt.% NaCF ₃ SO ₃ film (e) PAN + EC + 16 wt.% NaCF ₃ SO ₃ film (f) PAN + EC + 22 wt.% NaCF ₃ SO ₃ film (g) PAN + EC + 34 wt.% NaCF ₃ SO ₃ film and (h) PAN + EC + 38 wt.% NaCF ₃ SO ₃ film	124

Figure 5.20	FTIR spectra of (a) pure PAN film (b) EC (c) NaCF ₃ SO ₃ (d) PAN + EC + 8 wt.% NaCF ₃ SO ₃ film (e) PAN + EC + 16 wt.% NaCF ₃ SO ₃ film (f) PAN + EC + 22 wt.% NaCF ₃ SO ₃ film (g) PAN + EC + 34 wt.% NaCF ₃ SO ₃ film and (h) PAN + EC + 38 wt.% NaCF ₃ SO ₃ film	125
Figure 5.21	FTIR spectra of (a) pure PAN film (b) EC (c) NaCF ₃ SO ₃ (d) PAN + EC + 8 wt.% NaCF ₃ SO ₃ film (e) PAN + EC + 16 wt.% NaCF ₃ SO ₃ film (f) PAN + EC + 22 wt.% NaCF ₃ SO ₃ film (g) PAN + EC + 34 wt.% NaCF ₃ SO ₃ film and (h) PAN + EC + 38 wt.% NaCF ₃ SO ₃ film	126
Figure 5.22	FTIR spectra of (a) pure PAN film (b) EC (c) NaCF ₃ SO ₃ (d) PAN + EC + 8 wt.% NaCF ₃ SO ₃ film (e) PAN + EC + 16 wt.% NaCF ₃ SO ₃ film (f) PAN + EC + 22 wt.% NaCF ₃ SO ₃ film (g) PAN + EC + 34 wt.% NaCF ₃ SO ₃ film and (h) PAN + EC + 38 wt.% NaCF ₃ SO ₃ film	127
Figure 6.1	X-ray diffractogram of pure PAN film	128
Figure 6.2	X-ray diffractogram of pure EC	129
Figure 6.3	X-ray diffractogram of LiCF ₃ SO ₃ salt	130
Figure 6.4	X-ray diffractogram of NaCF ₃ SO ₃ salt	130
Figure 6.5	X-ray diffractogram of the films in the PAN-EC system	131
Figure 6.6	X-ray diffractogram of the films in the PAN-LiCF ₃ SO ₃ system	132
Figure 6.7	X-ray diffractogram of films in the PAN-NaCF ₃ SO ₃ system	133
Figure 6.8	X-ray diffractogram of the films in the PAN-EC-LiCF ₃ SO ₃ system	134
Figure 6.9	X-ray diffractogram of the films in the PAN-EC-NaCF ₃ SO ₃ system.	135
Figure 7.1	SEM micrograph for pure PAN film	136
Figure 7.2	SEM micrograph for the highest conducting film in the PAN-EC system	137
Figure 7.3 (a)	SEM micrograph for the highest conducting film in the PAN-LiCF ₃ SO ₃ system	138
Figure 7.3 (b)	SEM micrograph for the highest conducting film in the PAN-NaCF ₃ SO ₃ system	139

Figure 7.4 (a)	SEM micrograph for the highest conducting film in PAN-EC-LiCF ₃ SO ₃ system	140
Figure 7.4 (b)	SEM micrograph for the highest conducting film in PAN-EC-NaCF ₃ SO ₃ system	140
Figure 8.1	DSC thermogram of pure PAN	142
Figure 8.2	DSC thermogram of highest conducting film in the PAN-EC system	143
Figure 8.3	DSC thermogram of the highest conducting film in the PAN-LiCF ₃ SO ₃ system	144
Figure 8.4	DSC thermogram of the highest conducting film in the PAN-NaCF ₃ SO ₃ system	145
Figure 8.5	DSC thermogram of the highest conducting film in the PAN-EC-LiCF ₃ SO ₃ system	146
Figure 8.6	DSC thermogram of the highest conducting film in the PAN-EC-NaCF ₃ SO ₃ system	146

LIST OF TABLES		PAGE
Table 2.1	Conductivity values for several polymer electrolytes	20
Table 3.1	Amounts of PAN, EC and salts in each group of polymer electrolytes system	37
Table 3.2	Compositions of EC, LiCF ₃ SO ₃ and NaCF ₃ SO ₃ in PAN-EC system, PAN-LiCF ₃ SO ₃ system, and PAN-NaCF ₃ SO ₃ system	39
Table 3.3	Compositions of EC, LiCF ₃ SO ₃ and NaCF ₃ SO ₃ in PAN-EC-LiCF ₃ SO ₃ system, and PAN-EC-NaCF ₃ SO ₃ system	40
Table 4.1	The compositions, the values of bulk resistance, R_b and the conductivity of films in the PAN-EC system	60
Table 4.2	The compositions, the bulk resistance, R_b and the conductivity, σ of films in the PAN - LiCF ₃ SO ₃ system	64
Table 4.3	The compositions, the values of bulk resistance, R_b and the conductivity of films in the PAN-NaCF ₃ SO ₃ system	69
Table 4.4	The compositions, the values of bulk resistance, R_b and the conductivity of films in the PAN-EC-LiCF ₃ SO ₃ system	74
Table 4.5	The compositions, the values of bulk resistance, R_b and the conductivity of films in the PAN-EC-NaCF ₃ SO ₃ system	79
Table 4.6	The conductivity, σ and activation volume, ΔV^* for PAN-LiCF ₃ SO ₃ , PAN-NaCF ₃ SO ₃ , PAN-EC-LiCF ₃ SO ₃ and PAN-EC-NaCF ₃ SO ₃ systems.	94
Table 5.1	The vibrational mode and wavenumbers of pure PAN film	98
Table 5.2	The vibrational modes and wavenumbers of pure EC	100
Table 5.3	The vibrational modes and wavenumbers of LiCF ₃ SO ₃ salt	107
Table 5.4	The vibrational modes and wavenumbers of NaCF ₃ SO salt	113
Table 8.1	T_g values from the highest conducting film of PAN-EC, PAN-LiCF ₃ SO ₃ , PAN-NaCF ₃ SO ₃ , PAN-EC-LiCF ₃ SO ₃ and PAN-EC-NaCF ₃ SO ₃ systems	147
Table 9.1	The highest conductivity at room temperature for each system	150

LIST OF PUBLISHED AND PRESENTED PAPERS

1. Z. Osman, **K. B. Md. Isa**, A. Ahmad and L. Othman, “A Comparative Study of Lithium and Sodium Salts in PAN-based Ion Conducting Polymer Electrolytes” – accepted for publication in IONICS (2009) DOI: 10.1007/s11581-009-0410-9
2. **K. B. Md. Isa**, N. M. Ali, L. Othman, A. Ahmad K.W. Chew and Z. Osman “Temperature and Pressure Variations of the Ionic Conductivity of PAN-LiCF₃SO₃ Polymer Electrolyte Systems” Presented at International Conference on Functional Materials and Devices 2008 (ICFMD 2008), 16-19 JUNE 2008, KUALA LUMPUR.
3. A.Ahmad , **K.B. Md Isa**, L. Othman and Z. Osman, “ Effects of Adding the Plasticizers on Morphology and Thermal Properties of the PAN ion conducting Polymer Films” Presented at International Conference on Functional Materials And Devices 2008 (ICFMD 2008), 16-19 JUNE 2008, KUALA LUMPUR
4. Z. Osman, **K. B. Md. Isa**, A. Ahmad and L. Othman, “Characterization of Polyacrylonitrile Based Conducting Polymer Electrolytes Films” Presented at 24th Regional Conference on Solid State Science and Technology 2008 (RCSST 2008), 30 Nov-2 Dec 2008, Port Dickson, Negeri Sembilan.
5. **K. B. Md. Isa**, N. M. Ali, L. Othman, A. Ahmad and Z. Osman, “Ionic Conductivity and Dielectric Properties of the PAN-Ion Conducting Polymers” Current issues of Physics in Malaysia, (ed) H. B. Senin, G. Carini, J. Abdullah and D.A. Bradley, American Institute of Physics Conference Proceeding, Vol. 1017 (2008), 264-269
6. Z. Osman, **K. B. Md. Isa** and A. Ahmad, “Preparation and Studies of Polyacrylonitrile Ion Conducting Polymer Electrolytes”, Presented at National Workshop on Functional Materials, 20 June 2009, University of Malaya
7. **K. B. Md. Isa**, A. Ahmad and Z. Osman “Comparative Studies on Polyacrylonitrile (PAN) Polymer Electrolytes Containing Lithium and Sodium Salts”, Presented at Malaysia Polymer International Conference (MPIC), 21-22 Oct 2009, Palm Garden Hotel IOI Resort, Putrajaya
8. A.Ahmad, **K.B. Md Isa** and Z. Osman, “Conductivity and Structural Studies of Plasticized Polyacrylonitrile (PAN) – Lithium Triflate Polymer Electrolytes Films”, Presented at Malaysia Polymer International Conference (MPIC), 21-22 Oct 2009, Palm Garden Hotel IOI Resort, Putrajaya
9. A.Ahmad, **K.B. Md Isa** and Z. Osman, “Effect of Temperature and Pressure on Ionic Conductivity of PAN-based Polymer Electrolytes Containing Inorganic Salts”, Presented at National Physics Conference, 7-9 December 2009, Avillion Legacy Hotel, Malacca, Malaysia

CHAPTER 1:

Introduction

1.1 Background of the Present Work

In this study, polyacrylonitrile (PAN) based polymer electrolyte films are prepared and studied. On the bases of the studies of the pure PAN film, lithium triflate (LiCF_3SO_3) and sodium triflate (NaCF_3SO_3) salts are added as the dopants in order to improve conductivity and to achieve the Li^+ ion conductor and Na^+ ion conductor, respectively. Ethylene carbonate (EC) has been used as a plasticizer.

PAN was used as a host polymer and will provide a medium for the transport of ions. The monomer for PAN is called acrylonitrile. Acrylonitrile has the chemical compound with the formula CH_2CHCN ($\text{C}\equiv\text{N}$). In term of its molecular structure, it consists of a vinyl group linked to a nitrile group. Figure 1 shows molecular structure of PAN. The functional group in this polymer is nitrile group. The nitrogen atoms from nitrile groups are expected to form a coordinate bond with the lithium and sodium ions from the doping salts.

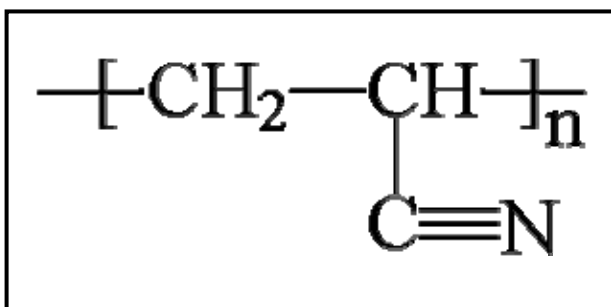


Figure 1.1: Molecular structure of PAN [1]

This study will investigate the effect of adding two triflate based salts with different cation i.e lithium and sodium on the properties of PAN polymer electrolytes. Although most of the interest in polymer electrolytes studies is focused on lithium ion-conducting systems, the sodium ion-conducting systems have also been the subject of much attention for many researchers. One of the earliest studies of polymer electrolytes containing sodium triflate was reported by Schantz et al. [2], where sodium triflate salt has been dissolved in polyether.

The chemical structures of the lithium triflate and sodium triflate are shown in Figure 2(a) and 2(b). Lithium and sodium have similar chemical properties because they are in the same group in the periodic table. However, the sodium is more reactive than lithium. This is because the outermost shell electron in sodium is much further than the one in lithium, the attraction between the electron and the sodium nucleus would be weaker and sodium readily and easily loses its electron to the surrounding and becomes a positive ion. This is one of the most important criteria of inorganic salts in the polymer electrolytes being studied. The same properties are expected in the triflate salt and sodium is expected to dissociate easily from the triflate anion. Triflate anion is larger than other anions such as tetrafluoroborate (BF_4^-) and perchlorate (ClO_4^-). The lattice energy of the salt with larger anion is lower and it is expected to promote greater dissociation of the salt, thereby providing higher conductivity of ions. In the present study, the anion of both salts is the same i.e. triflate. Therefore, the effects of different cations on the conductivity, morphological, structural and thermal properties of PAN-based polymer electrolytes system can be investigated.

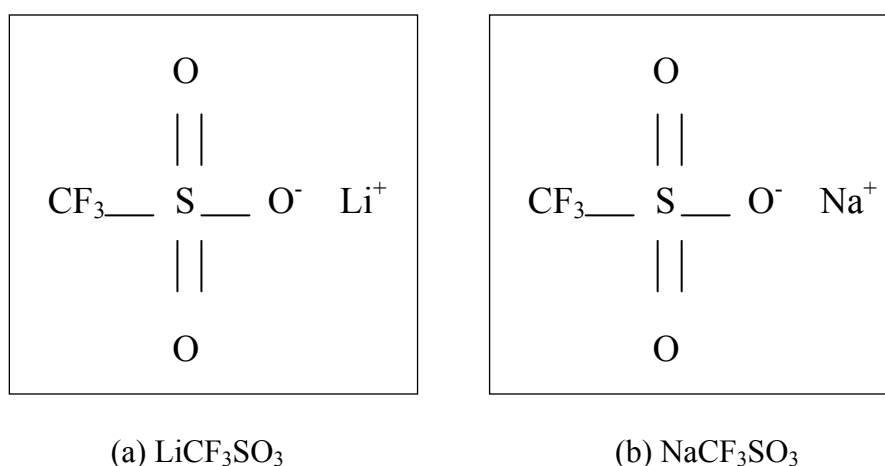


Figure 1.2: The chemical structure of (a) lithium triflate and (b) sodium triflate.

1.2 Objectives of the Present Work

The objectives of this work are to study the electrical and structural properties of PAN-based polymer electrolyte films. More specifically, the aims of this study are:

- 1) To improve the conductivity by doping with LiCF_3SO_3 and NaCF_3SO_3 salts. Conductivity measurements will be carried out by AC impedance spectroscopy. The influence of doping with inorganic salts and plasticizer on the ionic conductivity will be investigated.
- 2) To investigate the conduction mechanism, where conductivity-temperature and conductivity-pressure studies will be carried out. Other immittance responses such as dielectric constant, ϵ_r and dielectric loss, ϵ_i will be calculated in order to understand why conductivity varies with salt concentrations and varies with temperature as well as pressure.
- 3) To study the structural, morphological and thermal properties. The various techniques i.e. Fourier Transform Infrared (FTIR), X-Ray Diffraction (XRD), Scanning Electron Microscopy (SEM) and Differential Scanning Calorimetry (DSC) will be used.

1.3 Organization of the Dissertation

This dissertation is organized into nine chapters. The first chapter provides the background and objectives of the study.

Chapter two of this dissertation presents overview of polymer electrolytes including the basic information of polymer, salts and plasticizer. This chapter also covers ion conduction mechanism and the application of the polymer electrolytes.

Chapter three outlines the experiments carried out to prepare the samples and the techniques used to characterize the samples. The characterization are done by using various techniques include impedance spectroscopy, Fourier Transform Infrared (FTIR), X-Ray Diffraction (XRD), Scanning Electron Microscopy (SEM) and Differential Scanning Calorimetry (DSC). The theoretical background of the experimental techniques will be provided.

Chapter four to chapter eight present the analysis and discussion of the results from all experiments. The results of electrical conductivity studies of the PAN-based polymer electrolytes films at various temperature and pressure using impedance spectroscopy and the effect of different sizes of cations (Li^+ and Na^+) in enhancing the electrical conductivity of PAN film will be presented in chapter four. The structural and morphological studies of the samples are done using FTIR, XRD and SEM. The results will be presented in chapter five, six and seven, respectively. The results of thermal studies using DSC will be discussed in chapter eight. Finally, chapter nine concludes the dissertation with some suggestions for further work.

CHAPTER 2:

Literature Review

2.1 Polymer

The simplest definition of a polymer is something made of many units. The units or “monomers” are small molecules that usually contain ten or less atoms in a row. Carbon and hydrogen are the most common atoms in monomers, but oxygen, nitrogen, chlorine, fluorine, silicon and sulfur may also be present. Think of a polymer as a chain in which the monomers are linked (polymerized) together to make a chain with at least 1000 atoms in a row. This feature gives polymers their special properties.

Macromolecules or polymers are found in the human body, animals, plants, minerals and manufactured products. The macromolecule can have different end units, branches in the chain, variations in the sequence of the monomers, and different monomers repeated in the same chain which leads to the large number of manufactured polymers as well as all of the natural polymers. Today, polymers are studied in the fields of polymer chemistry, polymer physics, and polymer science. Figure 2.1 and 2.2 show the diagram of a chain of monomers and the macromolecule structure of polypropylene, respectively.

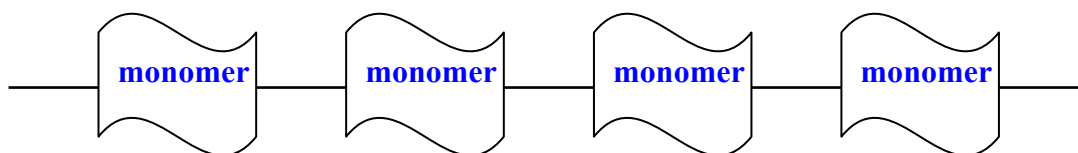


Figure 2.1: A simple diagram of a chain of monomers

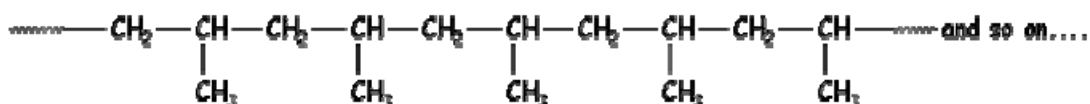


Figure 2.2: Macromolecule structure of polypropylene [3]

To make things simple, we usually only draw one unit of the repeat structure as shown in Figure 2.3.

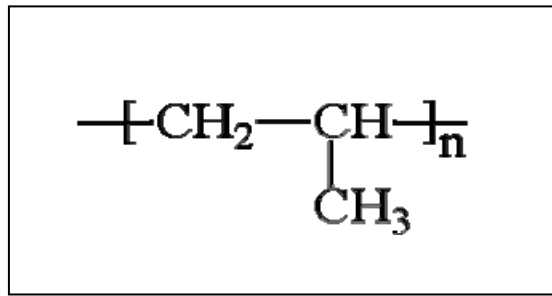


Figure 2.3: Simple chemical structure of polypropylene [3]

2.1.1 Polymerization

Polymerization is the process where small molecules or repeating units are joined together to create large synthetic polymers. The processes of polymerization were divided by Flory (1953) and Carothers (1940) into two groups known as condensation and addition polymerization or in more precise terminology, step-reaction and chain-reaction polymerization. Some common synthetic polymers are Bakelite, neoprene, nylon, PVC (polyvinyl chloride), polystyrene, **polyacrylonitrile** and PVB (polyvinyl butyral).

Today, the applications of synthetic polymers can be found in nearly every industry and area of life. These polymers are widely used as adhesives and lubricants, as well as structural components for products ranging from children's toys to aircraft. They have been employed in a variety of biomedical applications ranging from implantable devices to controlled drug delivery. Polymers such as poly (methylmethacrylate) (PMMA) can be used as photoresist materials in semiconductor manufacturing and low-k dielectrics for use in high-performance microprocessors. Recently polymers have also been employed in the development of flexible polymer-based substrates for electronic displays.

2.1.2 Polymer Properties

2.1.2.1 *Relationship between chain length and polymer properties*

Polymer bulk properties are strongly dependent upon their structure and mesoscopic behavior. A number of qualitative relationships between structure and properties are known. Increasing chain length tends to decrease chain mobility, increase strength and toughness, and increase the glass transition temperature (T_g). The glass transition temperature is a temperature at which the polymer experiences the transition from rubbery to rigid state. The glass transition temperature occurs in amorphous (or glassy and semicrystalline polymers, and is due to a reduction in motion of large segments of molecular chains with decreasing temperature. Upon cooling, glass transition corresponds to the gradual transformation from a liquid to a rubbery material and finally to a rigid solid. Upon heating through glass transition temperature, the amorphous solid polymer transforms from a rigid to a rubbery state.

2.1.2.2 *Crystallinity*

The crystallinity of polymers is characterized by their degree of crystallinity, ranging from zero for a completely noncrystalline polymer to one for a theoretical completely crystalline polymer. Increasing degree of crystallinity tends to make a polymer more rigid. It can also lead to greater brittleness. Polymers with a degree of crystallinity approaching zero or one will tend to be transparent, while polymers with intermediate degrees of crystallinity will tend to be opaque due to light scattering by crystalline or glassy region.

2.1.2.3 *Tensile strength*

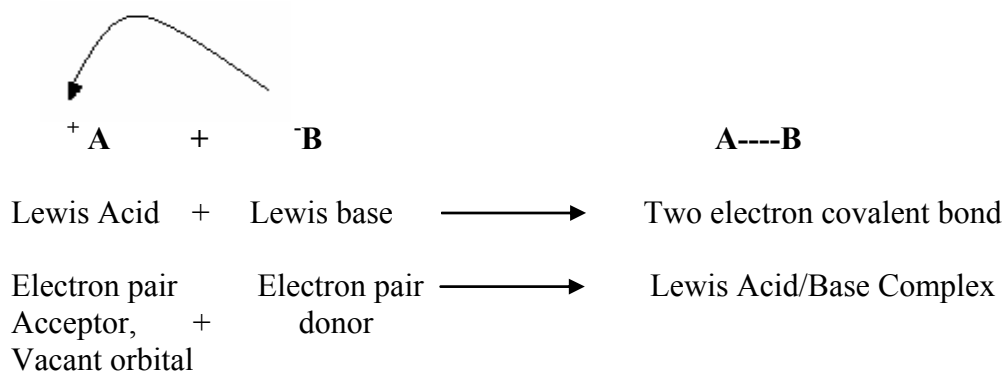
Tensile strength is important for a material that is going to be stretched or under tension. The tensile strength of a material quantifies how much stress the material will endure before failing. This is very important in applications that rely upon a polymer's physical strength or durability. For example, a rubber band with a higher tensile strength will hold a greater weight before snapping. In general tensile strength increases with polymer chain length.

2.1.2.4 *Transport Properties*

Polymers are very poor in electrical conductivity. By doping with an electron donor such as an alkali-metal ion, conductivity of polymers could be increased. Transport properties such as diffusivity relate to how rapidly molecules/ions move through the polymer matrix. These are very important in many applications of polymers for conducting polymer films and membranes. An ion conducting polymer is defined as a polymer that shows conductivity due to transport of ionic species. The ion conducting polymers that can be used as electrolytes are becoming increasingly important because of their potential applications in solid state polymer batteries and fuel cells.

2.2 Lewis Theory

In 1923, Gilbert Newton Lewis proposed this theory, which is based on chemical bond theory [4]. According to the Lewis theory, a base is defined as an electron pair donor and acid is an electron pair acceptor. The positive charge of the acid serves to attract a lone electron pair of the base into the vicinity of the acid so that orbital overlap and bonding may take place.



Several categories of substances can be considered Lewis acids:

- 1) positive ions
- 2) having less than a full octet in the valence shell
- 3) polar double bonds (one end)
- 4) expandable valence shells

Several categories of substances can be considered Lewis bases:

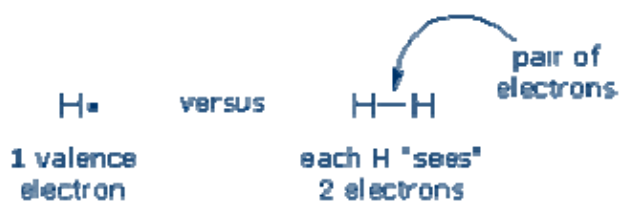
- 1) negative ion
- 2) one or more unshared pairs in the valence shell
- 3) polar double bonds (the other end)
- 4) the presence of a double bond

2.2.1 Lewis' Theory of Chemical Bonding

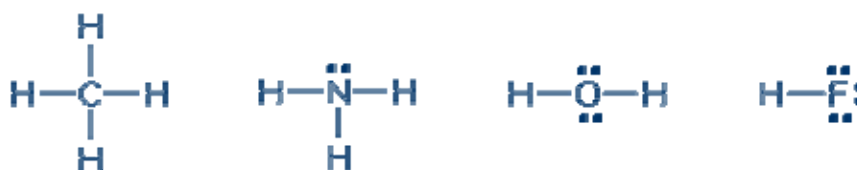
Covalent Bonds

Lewis' second great idea was this: two atoms attract each other (create a covalent bond) by sharing a *pair* of electrons. Lewis claimed that the shared electrons became part of each atom's electron configuration, so sharing effectively boosts each atom's electron count.

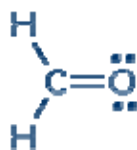
For example, an isolated hydrogen atom possesses only one electron, but *two* hydrogen atoms can share their electrons so that the resulting covalent bond gives each atom an inert gas electron configuration:



Similarly, covalent bonding in the following compounds boosts each atom's electron count and gives the atom a Lewis octet. Each H in ammonia, NH₃, "sees" the 2 electrons it shares with N. At the same time, the N "sees" 8 electrons; the 6 bonding electrons and the 2 nonbonding electrons it "keeps" for itself.



Two atoms can share more than one pair of electrons. The C and O in formaldehyde, CH₂O, share 4 electrons. By forming a double bond, each atom achieves a Lewis octet.



Lewis' theory is numerically strict. A covalent bond involves two electrons, and it occurs between two atoms, and each atom "sees" both electrons to the same degree (the electrons are shared equally). These rules are powerful predictors of bonding behavior (especially the "bond = 2 electrons" rule), but we will eventually encounter molecules that disobey them.

Ions and Ionic Bonds

Charged particles (or ions) exert electrostatic (or Coulomb) forces on each other. Oppositely charged ions create attractive forces and these create ionic bonds. Ionic bonds are electrostatic whether the ions are atomic, like sodium Na^+ and fluoride F^- , or polyatomic, like ammonium NH_4^+ and sulfate SO_4^{2-} . Ionic bonds lead to the formation of neutral compounds called **salts**. Ionic bonds do not change the interacting ions in any major way, so ions maintain their separate charges inside the salt, and are usually discharged as ions when the salt breaks down. For example, sodium sulfate, Na_2SO_4 , dissolves in water by releasing Na^+ and SO_4^{2-} ions.

Lewis' theory helps us identify atoms that can easily form ions. Ions that carry small charges and maintain inert gas electron configurations should form most easily. These requirements are met by the alkali cations (Li^+ , Na^+ , K^+), alkaline earth cations (Mg^{+2} , Ca^{+2}), and halide anions (F^- , Cl^- , Br^- , I^-).

Metals and non-metals nearly always form ionic compounds when they combine. The metals lose electrons and the non-metals gain electrons. Whenever we encounter a formula that combines metals with non-metals, such as Na_2O , we should assume that the compound is ionic and we should assign appropriate charges to each component (Na^+ and O^{2-}).

2.2.2 Salts

A salt is an ionic compound consisting of a cation (Group 1 and 2 cations) combined with an anion. Because they are ionic, salts are strong electrolytes. Most salts have either acidic or base properties, usually due to the anion. Anions exhibit a range of base strength. Whether a salt has base properties or not depend on how strongly the anion functions as a base.

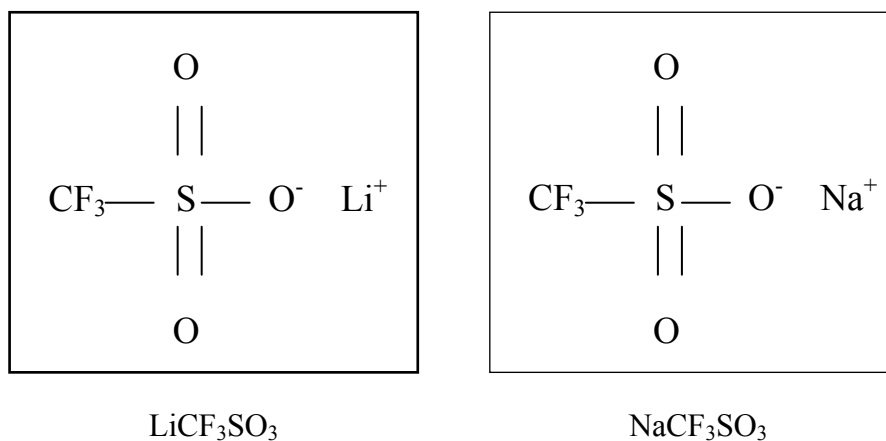
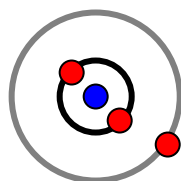


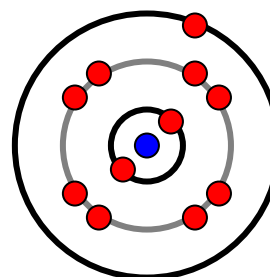
Figure 2.4: The chemical structure of (a) lithium triflate and (b) sodium triflate.

Cations:

Lithium: $1s^2 2s^1$



Sodium: $1s^2 2s^2 2p^6 3s^1$



● Electron

● Nucleus

Figure 2.4 shows the chemical structure of lithium and sodium triflate. Lithium is an alkali metal element that has an atomic number of 3. Lithium has a single valence electron which it will readily lose to form a cation, indicated by the element's low electronegativity. As a result, lithium is easily deformed, highly reactive, and has lower melting and boiling points than most metals. These and many other properties attributable to alkali metals' weakly held valence electron are most distinguished in lithium, as it possesses the smallest atomic radius and thus the highest electronegativity of the alkali group. The atomic number of the element sodium is 11. This means that

there are 11 protons and neutrons in its nucleus, and 11 electrons distributed specially on the energy levels. There are two electrons on the first level, eight on the second, and one on the third. Having only one electron on outermost shell makes it very reactive. The atomic radius of sodium atom is larger than lithium atom which is meant that the Lewis acidity of Na^+ is weaker than Li^+ . The size of radius will play the important role in the interaction between both cations with anion in salts and between cation and the negative charge on the bipolar groups of polymer in polymer electrolytes.

The small ionic radius of lithium ion can provide high volumetric capacity. Thus, lithium ion conducting polymer electrolytes have been more widely studied due to their potential use in rechargeable batteries. The energy of the salts should be lower for which salt with larger anions are most suitable [5]. The lithium salts used for Li^+ conductive polymer electrolytes, such as lithium perchlorate (LiClO_4), lithium tetrafluoroborate (LiBF_4) and lithium triflate (LiCF_3SO_3) have large anions and low lattice energies to promote high conductivity, compared with halides such as lithium chloride (LiCl), lithium iodide (LiI) and lithium bromide (LiBr). Although most of the interest in polymer electrolytes focused on lithium ion-conducting polymer, the sodium ion conducting analogs have also been the subject of much attention. One of the earliest studies polymer electrolytes containing dissolved sodium triflate was reported by Schantz et al [2]. The comparison study of lithium triflate and sodium triflate dissolved in poly(ethylenimine) and poly(ethylene oxide) was reported by many researchers i.e Rhodes et. al, Sanders et. al and York et. al [6-8].

To achieve a better understanding of mechanism of ionic transport, research efforts have been focused on cation-anion interactions [9] and cation-polymer interaction [10], both of which play critical roles in ion transport. Both cation-anion and cation-polymer interactions presumably affect the ionic mobilities and also play a major role in determining the number of charge carriers.

2.3 Ionic conduction

Ionic conductivity of electrolytes depends on the charge carrier concentration, n and carrier mobility, μ , as described by the relation

$$\sigma = \sum \mu_i n_i q_i \quad (2.1)$$

Where n , q and μ representing the charge carrier concentration, charge of mobile carrier and the mobility, respectively. Increases of conductivity value can be related to the increases of mobile charge which is contributed by salt concentration.

Generally, ionic conductivity of solid electrolytes increases with temperature due to the higher segmental motion of polymer chain in the amorphous phase. At higher temperatures, thermal movement of polymer chain segments and dissociation of salts would be improved, which increases ionic conductivity. Experimentally, in homogeneous ion conducting polymers, one observes fairly straightforward behavior of the temperature dependence of the conductivity. The straight or curved lines observed when the conductivity is plotted in Arrhenius coordinates can be fit to the Arrhenius and Vogel-Tamman-Fulcher (VTF) forms. The linear variation of $\ln \sigma$ versus $1000/T$ suggests an Arrhenius type thermally activated process which the conductivity can be expressed as:

$$\sigma = \sigma_0 \exp\left(\frac{-E_a}{kT}\right) \quad (2.2)$$

Where σ_0 is a pre-exponential factor, E_a is activation energy, k is Boltzmann constant and T is the absolute temperature in K. The E_a value can be evaluated from slope of the Arrhenius plot. The steady increase in conductivity with temperature is interpreted as a hopping mechanism between coordinating sites, local structural relaxation and

segmental motion of polymer. Another interesting feature of the conductivity plots is that they are gentle curves and not perfectly straight lines. So, the temperature dependence on the ionic conductivity was not linear and it shows that ion transport in polymer electrolytes was correlated with polymer segmental motion. The conductivity can be expressed as VTF equation:

$$\sigma T = \sigma_0 \exp\{-B/T - T_0\} \quad (2.3)$$

Where B is constant and T_0 normally called the equilibrium (ideal) glass-transition temperature, is related to the (kinetic) measured glass-transition temperature roughly by

$$T_0 \cong T_g - 50K \quad (2.4)$$

The kinetic glass-transition temperature, T_g can be observed as an endotherm in a thermal-analysis measurement. The simplest understanding of bent VTF conductivity behavior is that diffusion can occur only when the diffusing particle moves from one free volume space to another. The availability of free volume is indexed by the quantity $T-T_0$ and one can trivially derive the VTF form of equation (2.3) based on an expansion of the free volume around the equilibrium glass-transition temperature, T_0 .

The free volume model is the simplest way to understand the polymer segment mobility. It states that as temperature increases, the expansivity of the material produces local empty space, free volume, into which ionic carriers, solvated molecules or polymer segments themselves can move. The overall mobility of the material then is determined by the amount of volume present in the material. The free volume is calculated according to the simplest model, by the usual statistical argument of maximizing the number of ways in which the volume can be distributed [11]. One then obtains for the diffusivity D, the form

$$D = BRT \exp(-V^*/V_f) \quad (2.5)$$

which B and V^* are constant, R is the gas constant and V_f is the free volume. When the volume is expanded in terms of the volume at the glass transition temperature plus a linear term, the free volume theory yields the form [12-14]

$$D = D_0 T \exp\left(\frac{-a}{T - (T_g - C_2')}\right) \quad (2.6)$$

where the constants a and C_2' are both inversely proportional to the free volume thermal expansion factor. Cheradame and co-workers [15,16], shows that indeed there is a very close relationship between conductivity and polymer relaxation behavior.

The important concept for understanding of ionic motion in polymer is the issue of coupling between transport and relaxation: when the host polymer relaxes more rapidly, ionic conductivity increases. Angell [17, 18] has generalized these concepts to differentiate two types of amorphous solid ion conducting polymers. He defines a decoupling ratio R as

$$R = \tau_s / \tau_\sigma \quad (2.7)$$

The dimensionless decoupling ratio R is the quotient of two different relaxation times: the structural relaxation time τ_s refers to viscosity or segmental relaxation, while the conductivity relaxation time τ_σ is inversely proportional to the conductivity. If R were close to unity, it would indicate that the ionic motion and the structural relaxation occur on the same time scale, thus suggesting that their rate determining steps are the

same. Angell [19] has noted that for polymeric solid electrolytes $R \sim 10^{-3}$, which implies (since it is substantially less than unity) strong residual ion-ion coupling, resulting in reduced conduction.

The free volume type concepts also can be applied to understand the pressure dependence of ionic conductivity. Ion conducting polymers are soft materials and one might therefore suspect that they would be easily compressible. Accordingly, several investigations [20-22] have been reported in which the ionic conductivity was measured as a function of pressure. The conductivity indeed is observed to decrease with increasing pressure, due to the decreases of free volume in solid electrolytes. Since the free volume, V_f of equation (2.5) will decrease with applied pressure, one expects diffusivity D to fall off exponentially as pressure is increased and free volume decreased. General equation for the pressure dependence of ionic conductivity:

$$\left(\frac{\partial \ln \sigma}{\partial P} \right)_T = -\frac{\Delta V^*}{RT} \quad (2.8)$$

The activation volume, ΔV^* can be determined from a slope of the above relationship.

2.4 Polymer electrolytes

Polymer electrolytes are an interesting new area of polymer physics involving a range of polymer materials which are able to conduct ions and therefore potentially find application in batteries, capacitors and similar electrochemical devices. Polymers are usually good insulators but can be made into ion conducting polymers by doping it with inorganic salts. It is called ion conducting polymer because the electrical conductivity is due to transport of ionic species. In polymer electrolytes, ions can move with the segmental motion of the polymer chain. The term electrolyte means that this ion is

electrically-charged and moves to either a negative (cathode) or positive (anode) electrode. Ions that move to the cathode (cations) are positively charged and those moves to the anode (anions) are negatively charged.

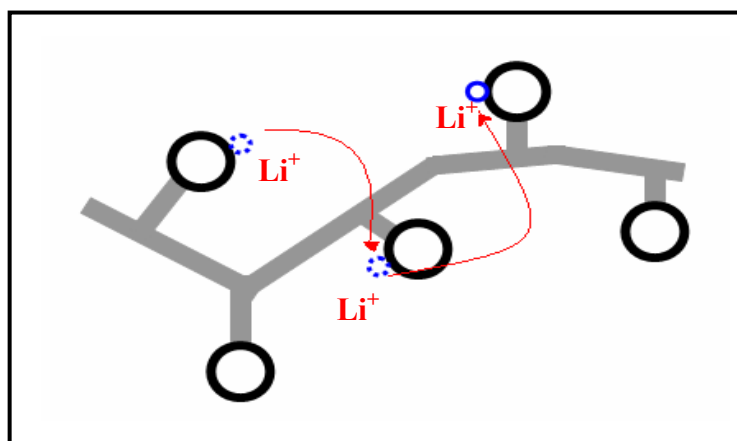


Figure 2.5: Ions move in polymer chain

A polymer must be able to solvate salt; through interaction between the cations of the salt and the lone pair electrons provided by N, O, S or Cl in the polymer. The conductivity mechanism requires the polymer to rearrange its conformation in order for the cations to hop to a new position with little or no energy barrier. There are many principal properties for polymer to act as successful polymer host such as high relative dielectric constant (>10) to dissociate the salts, facile polymer segmental motion and easy processibility into thin film. Generally, ion conducting polymers consist of an inorganic salts dissolved in a polymer host such as polyacrylonitrile (PAN), poly(methyl methacrylate) (PMMA), poly(vinyl chloride) (PVC), poly(propylene oxide) (PPO) and poly(ethylene oxide) (PEO). The polymers will provide a medium for ion to move in polymer electrolytes. The inorganic salt that is usually used in polymer electrolyte research such as lithium perchlorate (LiClO_4), lithium triflate (LiCF_3SO_3), lithium tetrafluoroborate (LiBF_4), lithium hexafluorophosphate (LiPF_6), sodium triflate

(NaCF_3SO_3), copper (I) thiocyanate (CuCNS), and copper triflate (CuCF_3SO_3). The first polymer observed to have the ability to solvate inorganic salt was poly (ethylene oxide) (PEO). The electrical conductivity of this salt-solvating polymer has been reported [23].

There are many types of polymer electrolytes such as (a) solid polymer electrolytes (SPEs) (b) liquid polymer electrolytes and (c) gel polymer electrolytes. SPEs consisting of an ionic conductive polymer matrix and a supporting electrolyte salt were firstly introduced by Fenton et. al [24]. By using a SPEs, a separator is unnecessary and the electrolyte can be prepared as a thin film. Some of the benefits that a solid polymer electrolyte offers are:

- ease of manufacturing
- immunity from leakage
- suppression of lithium dendrite formation
- elimination of volatile organic liquids
- mechanical flexibility.

The first polymer studied as a matrix for SPE was poly (ethylene oxide) (PEO). However, these PEO-based electrolytes showed relatively lower ionic conductivity ($\sim 0.1 \mu\text{S cm}^{-1}$) than liquid electrolytes ($\sim 10 \text{ mS cm}^{-1}$). So, many attempts have been made to modify the structure of solid polymer electrolytes in order to improve their electrical, electrochemical and mechanical properties. These approaches include (a) synthesizing polymer (b) blending two polymer (c) adding plasticizers to polymer electrolytes and (d) adding inert fillers to make composite polymer electrolytes [25].

The ionic conductivity of SPE can be enhanced by the use of plasticizers which are low molecular weight organic compounds such as propylene carbonate (PC) and ethylene carbonate (EC). A plasticizer can be defined as a chemical which reduces the

stiffness of an amorphous polymer. A plasticizer interacts with the polymer chain on the molecular level so as to speed up the viscoelastic response of the polymer and increase the ionic mobilities in the electrolytes significantly.

The range of conductivity of SPE is very large. Table 2.1 shows the conductivity of some polymer electrolytes.

Table 2.1: Conductivity values for several polymer electrolytes.

Polymer electrolytes	Conductivity (S cm ⁻¹) at room temperature	Reference
PEO- LiClO ₄	1.00 x 10 ⁻⁵	[27]
PEO- LiCF ₃ SO ₃	6.00 x 10 ⁻³	[27]
PAN-LiCF ₃ SO ₃	1.32 x 10 ⁻³	[28]
PAN/PEO- LiClO ₄	6.79 x 10 ⁻⁴	[26]
PVC/PAN- LiClO ₄ -EC	7.57 x 10 ⁻⁵	[25]
PVC/PAN- LiClO ₄ -EC-TiO ₂	4.46 x 10 ⁻³	[25]

2.5. Polyacrylonitrile (PAN)

PAN is one of the versatile polymers that are widely used for making membranes due to its good solvent resistance property. Almost all PAN resins are copolymers made from mixtures of monomer with acrylonitrile as the main component. The general chemical structure of PAN is shown in Figure 2.6. Figure 2.7 represents the simplest molecular structure for PAN.

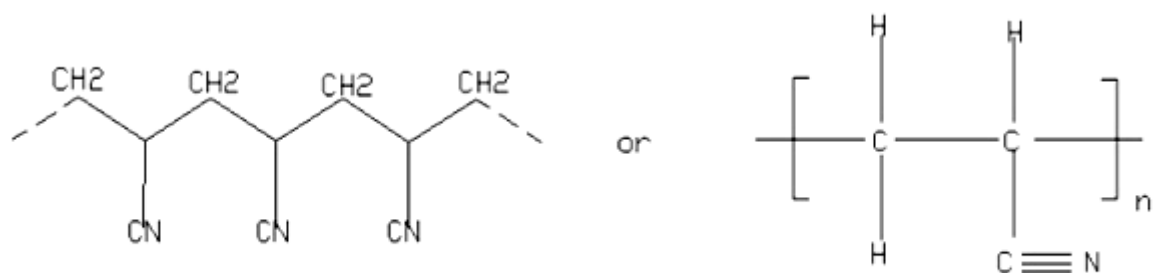


Figure 2.6: Molecular structure of polyacrylonitrile (PAN) [29]

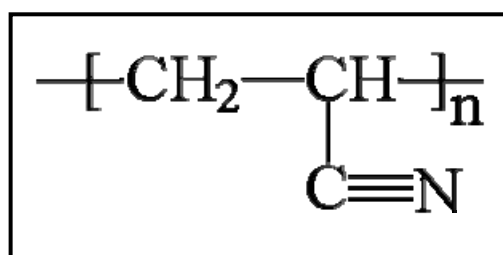


Figure 2.7: Simple molecular structure of polyacrylonitrile [1]

PAN is most commonly used in fiber form. PAN fibers are the chemical precursor of high quality carbon fiber. There are numerous PAN fibers advantages including a high degree of molecular orientation, higher melting point (317 °C) and low density at 25 °C (1.184 g/cm³). The molecular weight of repeat unit is 53.06 g/mol. Its glass transition temperature, T_g is 85.0 °C and it has a functional group in its polymer chain called a nitrile group. In the nitrile group, the carbon atom and the nitrogen atom are triple bonded ($-C\equiv N$) together. The nitrogen atoms from this nitrile group are expected to form a coordinate bond with the cations from the doping salts.

2.5.1 PAN-based Electrolytes

(SPEs)-based on polyacrylonitrile (PAN) with good mechanical properties has had many advantages in the application of secondary rechargeable battery i.e. the ionic conductivity of polymer electrolyte based on PAN depends on ionic mobility. That is,

these systems show decoupled ion transport behavior in wide range temperature [30]. PAN based polymer electrolytes also has very unique mechanism in polymer-in-salt system with much higher salt content than it traditional salt-in-polymer electrolytes [31].

Reich and Michaeli [32] first investigated polyacrylonitrile by examining the conductivity of PAN complexes with hydrated perchlorate salts. The ionic conductivities obtained are in the range 10^{-7} - 10^{-2} S cm⁻¹ but it is unsuitable for use with lithium electrodes because the systems contained water that acts as a plasticizer. Watanabe and his co-workers [33], then prepared hybrid films by dissolving PAN and LiClO₄ in a plasticizer such as propylene carbonate (PC) or ethylene carbonate (EC) and casting the solution on teflon. Watanabe has concluded that the role of polyacrylonitrile is two-fold [33]:

1. It acts as a support forming a mechanically stable film, and
2. It helps to dissolve the LiClO₄ to a level which exceeds the solubility of LiClO₄ in EC alone.

In 1990, Abraham et al. [34] synthesized PAN-based lithium salt electrolytes with ionic conductivity higher than 10^{-3} S cm⁻¹ at room temperature, breaking through the prediction of 10^{-4} S cm⁻¹. These electrolytes are ionically, plasticized-dissolved salt in a polymer matrix. The polymer contributes to the mechanical strength and the plasticizer-dissolved salt allows the relatively high conductivity at ambient temperature.

The use of polyacrylonitrile as a polymer host was also reported by many other researchers. PAN-based ion conducting polymers has many advantages such as:

1. high ionic conductivity of the order of 10^{-3} S cm⁻¹ and good mechanical properties at room temperature [35-36].

-
2. offer a homogeneous, hybrid electrolyte films in which the salt and the plasticizer were molecularly dispersed [37].
 3. it is commercially available
 4. it brings polar groups
 5. it provides physical gels with the usual electrolyte solvents [38]
 6. it has a fire-retardant property when PAN complexes with ethylene carbonate (EC), propylene carbonate (PC) and LiPF_6 [39].

Since the early work of Watanabe et. al [34,40] to later improvements by Abraham et. al [41] research has mostly focused on the temperature dependent conductivity, cycle efficiency and energy density. Factors governing these properties include relative concentrations PAN, EC and the type of salts and the passivation build up between the electrode and the electrolyte [42]. Rajendran et.al [43] have been studied the temperature dependence of the ionic conducting for SPEs containing PAN, LiClO_4 and various compositions of PC and EC in the temperature range 301 to 373 K. The results shown that the highest conductivities is estimated as $4.5 \times 10^{-3} \text{ S cm}^{-1}$ at 301 K for the composition of PAN(21) – LiClO_4 (8) – EC(38) – PC(8). From the measurement of conductivity dependence with temperature, it also indicated that as the temperature increases, the conductivity values also increase and this behaviour is obeys VTF relation [44]. The study of conductivity dependence with pressure has been explored by Larsson et. al [45]. The measurements have been carried out on poly (propyleneglycol) (PPG) complexed with LiCF_3SO_3 for pressures up to 1GPa. The results have indicated that the conductivity decrease with increasing pressure which is due to the strong decrease of the ion mobility.

2.6 Plasticization

In order to enhance the conductivity without affecting the morphological properties at or near ambient temperature, the low molecular weight organic nonaqueous solvent (plasticizer) such as ethylene carbonate is added to the electrolyte.

Figure 2.8 shows the chemical structure of the plasticizer, EC

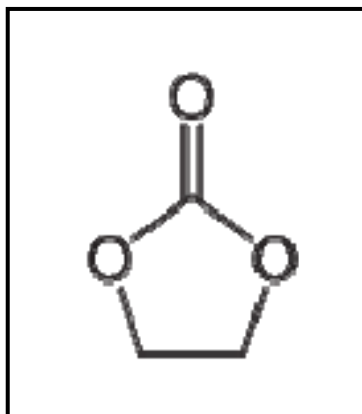


Figure 2.8: The chemical structure of ethylene carbonates (EC) [46].

The functions of the plasticizer in the polymer electrolyte may be summarized as the following [47];

- a) Decreasing the glass transition temperature, T_g of the polymer and dissolving the crystallites of the polymer. This will lead to the increase of the mobility of the segmental chain of the polymer and help the transport of the charge carriers depending on the movement of the segmental chain
- b) Dissolving the salts so as to provide charge carriers for the polymer electrolytes
- c) Interacting with the polymer molecules by way of dipolar interactions and therefore, increasing the polarities of the polymer and the plasticizer itself, which in turn, will help the dissociation of the salts in polymer electrolytes
- d) Destructing the coordination bond of Li^+ and Na^+ ions with PAN and making more ions move into polymer electrolytes

Based on the above functions of the plasticizer in a polymer electrolyte, the requirement of plasticizer for polymer electrolytes:

- a) Compatible with the polymer and the electrodes
- b) Thermodynamically stable
- c) Low viscosity
- d) High dielectric constant
- e) Low melting point and high boiling point
- f) Inexotic and easily obtainable

Ethylene carbonate (EC) has high dielectric constant compared to the others plasticizer such as propylene carbonate (PC) which give it the ability to assist the dissolution and dissociation of salts [33,39]. Therefore, this plasticizer helps to prevent ion aggregation and increase the number of charge carriers thereby enhancing the electrical conductivity.

2.7 Solvent

Solvent is a substance, usually a liquid, that acts as a dissolving agent or that is capable of dissolving another substance. In solutions of solids or gases in a liquid, the liquid is the solvent. In all other homogeneous mixtures (i.e., liquids, solids, or gases dissolved in liquids; solids in solids; and gases in gases), solvent is the component of the greatest amount. The appropriate solvent should be selected based on the inactivity in the reaction conditions, dissolving the reagents as well as reactants, appropriate boiling point and easy removal at the end of the reaction [48- 49].

N, N-Dimethylformamide

N, N-Dimethylformamide (DMF) is a clear liquid with the formula $(\text{CH}_3)_2 \text{NC}(\text{O})\text{H}$. DMF is prepared by the reaction of dimethyl amine and formic acid. The molecular structure for DMF is shown in Figure 2.9. DMF is a stable compound with a relatively low vapour pressure and high boiling point $\sim 153^\circ\text{C}$. The good water solubility, high dielectric constant, high boiling point, and organic properties make DMF suitable to be used as a solvent in industry particularly for acrylic fibres and polyurethanes. In this research work, DMF is used as a solvent to dissolve the PAN, plasticizer and salts. The mixture was continuously stirred at 60°C for 6 hours. Finally, the solution of PAN electrolytes was dried at 52°C in a vacuum oven under 10^{-2} Torr pressure for 3 days to remove DMF residue in the samples.

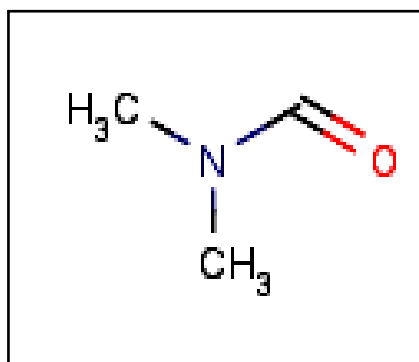


Figure 2.9: The molecular structure of DMF [50]

2.8 Applications of Polymer Electrolytes

Polymer electrolytes have a number of significant advantages over conventional electrolytes in the area of polymer science, chemistry and inorganic chemistry. Development of polymer electrolytes has focused largely on rechargeable batteries for the past a few decades. However, a good potential of polymer electrolytes not only in

all solid state rechargeable batteries but also in other electrochemical devices such as fuel cells, sensors and electrochromic devices.

2.8.1 Batteries

A battery as we know it is a device that stores chemical energy and through an electrochemical/electromotive force converts the stored chemical energy into electric energy via a direct current voltage. A battery cell is the most basic electrochemical unit. A battery cell has three basic parts: the anode, the cathode, and an electrolyte solution. The electrolyte solution is a chemical compound (salt, acid, or base) that when dissolved in a solvent forms a solution that becomes an ionic conductor of electricity. In the battery cell the electrolyte solution is the conducting medium in which the flow of electric current between the electrodes takes place by the migrating electrons.

There are two types of batteries i.e. primary (disposable) and secondary (rechargeable), both of which convert chemical energy to electrical energy. Primary batteries can only be used once because they use up their chemicals in an irreversible reaction. Secondary batteries can be recharged because the chemical reactions they use are reversible; they are recharged by running a charging current through the battery, but in the opposite direction of the discharge current.

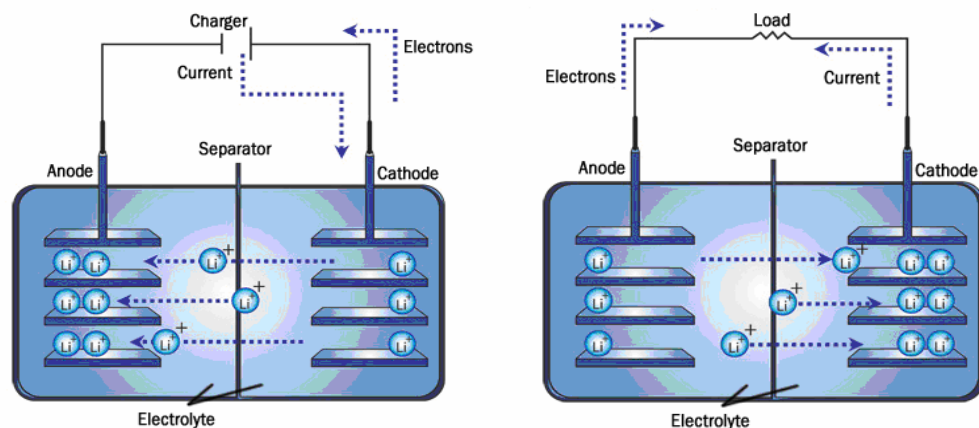


Figure 2.10: Schematic of charge and discharge process for secondary battery [51]

Figure 2.10 shows the schematic of charge and discharge process for rechargeable battery. During the charge reaction, lithium ions in the positive electrode are ionized and moves to the negative electrode through the electrolyte. During the discharge reaction, the lithium ions return to the positive electrode, reverting to its original phase. This simple migration of lithium ions gives the battery a long shelf life and a long cycle life.

Lithium-polymer battery:

Lithium-polymer battery is a battery technology that similar to lithium-ion. It performs the same task with lithium-ion battery, but can be shaped much thinner. The li-polymer differentiates itself from other battery systems in the type of electrolyte used.

The original design, dating back to the 1970s, uses a dry solid polymer electrolyte only. This electrolyte resembles a plastic-like film that does not conduct electricity but allows an exchange of ions (electrically charged atoms or groups of atoms). The polymer electrolyte replaces the traditional porous separator, which is soaked with electrolyte. The dry polymer design offers simplifications with respect to fabrication, ruggedness, safety and thin-profile geometry. There is no danger of flammability because no liquid or gel electrolyte is used. To date, most lithium-polymer applications are widely used for consumer items like cell phones, MP3 players and many Bluetooth enabled devices where low weight and small size are essential.

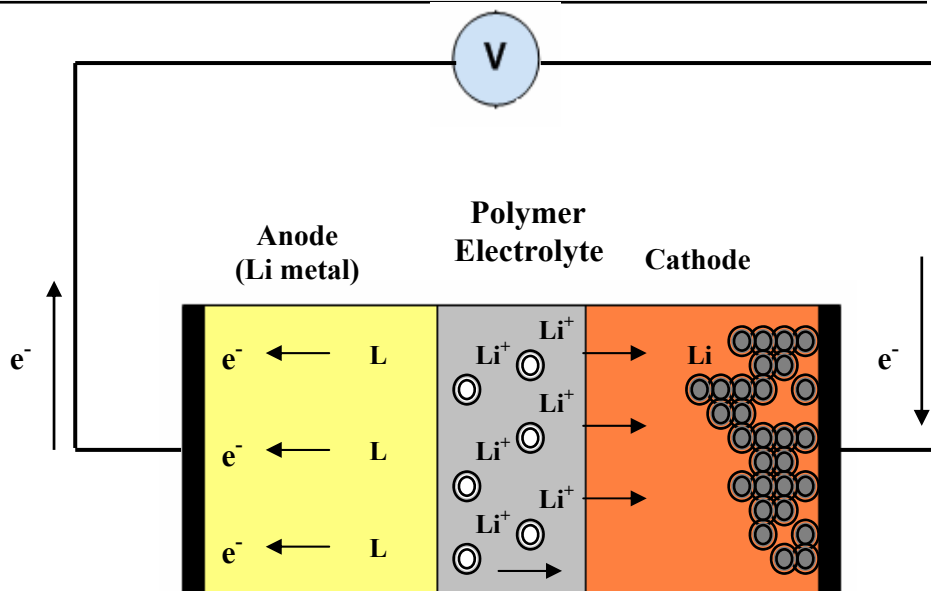


Figure 2.11: Conceptual structure of lithium polymer battery.

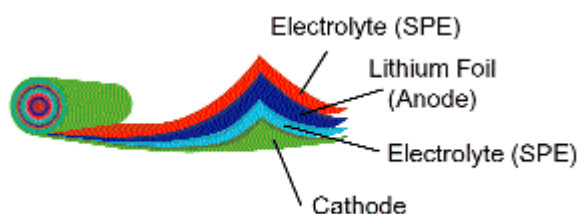


Figure 2.12: Internal construction of lithium-polymer battery [52].

2.8.2 Electrochromic Devices

An electrochromic device (ECD) is able to modify its optical absorption in a reversible and persistent way via the application of potential. The color changes either from transparent to color or from one color to another depending on the electrochromic material and construction of the device. This phenomenon, which can be produced by the application of an electric field, is called electrochromism [53]. ECDs have many potential applications in technology. Thus, the possibility to modulate the diffuse reflectance lends itself to non-emissive display devices of different sizes. Modulation of the specular reflectance opens up possibilities for anti-dazzling rear view mirrors for automobiles and innovative architecture. Passenger cars with EC-based compartment

rear-view mirrors have been available on the market for a few years. Modulation of the luminous transmittance can be used in future buildings for superior day lighting and hence good working conditions, with a minimum electric of lighting. Other application may be for sun-glasses and also for windows in cars, trains, ships, etc. Many EC devices can be viewed as basic design of five layers backed by a glass substrate according to the following:

- i. A transparent electrically conducting film on the glass substrate;
- ii. A thin film of electrochromic material;
- iii. An electrolyte in liquid or solid form;
- vi. A counter electrode operating in conjunction with the electrochromic material; and
- v. An electrically conducting, transparent electrode

The electrochromic material and the counter electrode are mixed conductors for electrons and ions. The materials electrochromic properties include organic compounds (for example polyaniline) or inorganic materials such as prussian blue and oxides such as WO_3 , TiO_2 , and NiO_x . By the application of an electric field between the external conducting electrodes, ions can be inserted into or extracted from the electrochromic film, whose optical properties thereby are altered. Depending on the electrolyte the ions can be H^+ , Li^+ , Na^+ , K^+ , H_3O^+ , OH^- or their complexes[54,55]

The solid electrolyte can be either inorganic, such as hydrated oxide film, or organic (polymer). The requirements of the electrolyte are as follows:

- a) An ionic conductivity greater than $10^{-5} \text{ S cm}^{-1}$, electronic conductivity less than $10^{-12} \text{ S cm}^{-1}$;
- b) Electrochemical stability for extended cycling at operating temperature and during UV irradiation; and
- c) Good adherence to the adjoining materials.

Several proton and ion conducting (such as Na^+ , K^+) polymers for application in these devices have been published [56, 57].

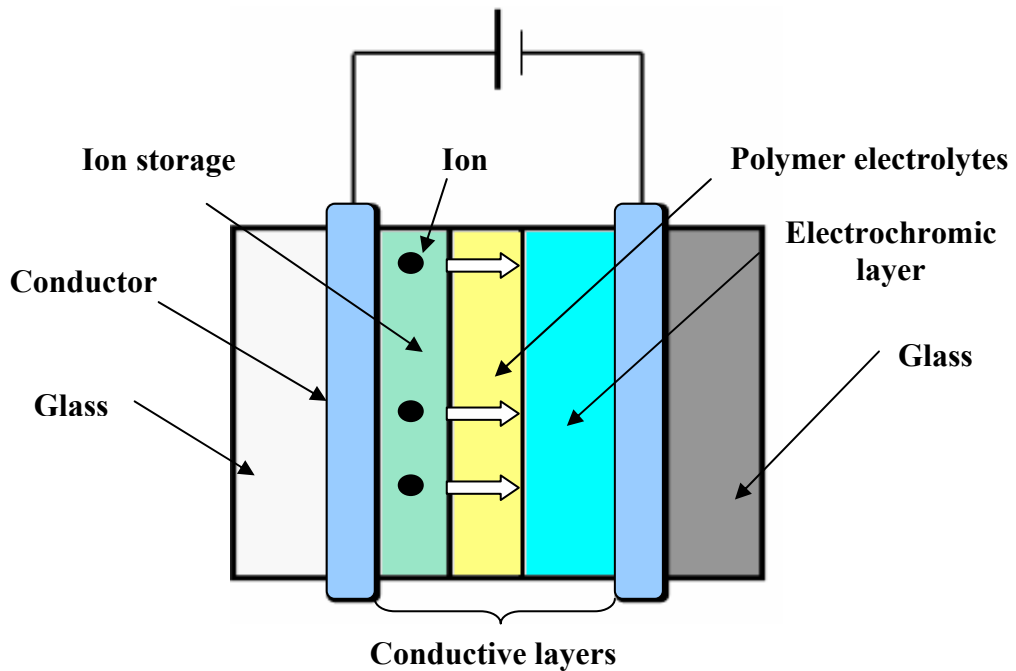


Figure 2.13: Electrochromic window

Figure 2.13 shows the basic design of electrochromic window. Electrochromic windows are windows that can be darkened or lightened electronically. The electrochromic windows consist of up to seven layers of materials. The essential function of the device results from the transport of hydrogen or lithium ions from an ion storage layer and through an ion conducting layer, injecting them into an electrochromic layer. To darken (or "color") the windows, a voltage is applied across the two transparent conducting oxide layers. This voltage drives the ions from the ion storage layer, through the ion conducting layer and into the electrochromic layer. To reverse the process, the voltage is reversed, driving the ions in the opposite direction, out of the electrochromic layer, through the ion conducting layer, and into the ion storage layer. As the ions migrate out of the electrochromic layer, it lightens, and the window becomes transparent again.

2.8.3 Fuel Cells

Functioning similar to a battery, which uses electrochemical conversion, fuel cells take in hydrogen-rich fuel and oxygen and turn them into electricity and heat. The waste product is water. The hydrogen can be derived from gasoline, natural gas, propane or methanol. There are several types of fuel cells currently under development, each with its own advantages, limitations, and potential applications. A few of the most promising types include [58];

- Polymer Electrolyte Membrane (PEM)
- Phosphoric Acid
- Direct Methanol
- Alkaline
- Molten Carbonate
- Solid Oxide
- Regenerative (Reversible)
- Fuel Cell Comparisons

Polymer Electrolyte Membrane Fuel Cells

Polymer electrolyte membrane (PEM) fuel cells also called proton exchange membrane fuel cells deliver high power density and offer the advantages of low weight and volume, compared to other fuel cells. PEM fuel cells use a solid polymer as an electrolyte and porous carbon electrodes containing a platinum catalyst. They need only hydrogen, oxygen from the air, and water to operate and do not require corrosive fluids like some fuel cells. They are typically fuelled with pure hydrogen supplied from storage tanks or onboard reformers. A schematic of a polymer electrolyte membrane hydrogen-oxygen fuel cell is shown in Figure 2.14.

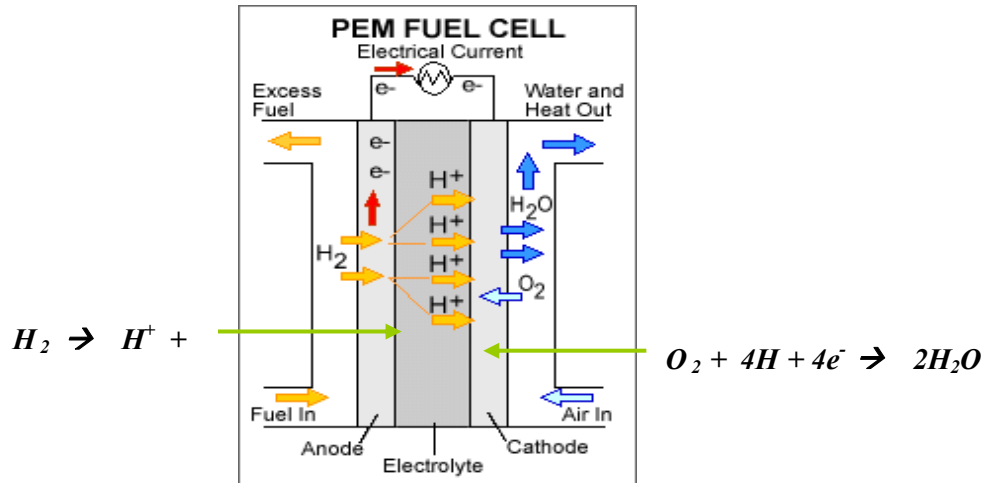


Figure 2.14: Schematic of a polymer electrolyte membrane fuel cell [58]

The hydrogen, which comes into the anode side of the fuel cell, is converted into electrons and hydrogen ions. The electrons are repelled by the anode and flow to the cathode. The cathode accepts the electrons as well as oxygen, which combine with the hydrogen ions from the anode, and converts them into water.

The polymer electrolyte membrane fuel cells operate at relatively low temperatures, around 80°C (176°F). Low temperature operation allows them to start quickly (less warm-up time) and results in less wear on system components, resulting in better durability. However, it requires that a noble-metal catalyst (typically platinum) be used to separate the hydrogen's electrons and protons, adding to system cost. The platinum catalyst is also extremely sensitive to carbon monoxide (CO) poisoning; making it necessary to employ an additional reactor to reduce CO in the fuel gas if the hydrogen is derived from an alcohol or hydrocarbon fuel. This also adds cost. Developers are currently exploring platinum/ruthenium catalysts that are more resistant to CO.

PEM fuel cells are used primarily for transportation applications and some stationary applications. Due to their fast startup time, low sensitivity to orientation, and favorable power-to-weight ratio, PEM fuel cells are particularly suitable for use in passenger vehicles, such as cars and buses.

2.8.4 Sensors

A sensor is a device that takes a physical quantity, measures it, and converts it into information that can be read and understood by an observer. There are a wide variety of means by which a sensor collects and converts data, many of them not involving any electronics at all.

All sensors share one general characteristic: they are transducers. A transducer is a device for transforming one type of energy into another. For example, even a simple mercury thermometer works by taking heat energy and changing it to the expansion or contraction of liquid for the purposes of measurement. Therefore, all sensors can be categorized according to the kind of energy they detect and convert. These categories are: acoustic, chemical, electromagnetic, ionizing radiation, mechanical, optical, and thermal. In particular, biosensors and electrochemical sensors have become increasingly important as biological and biochemical applications continue to emerge. These applications include

- medical diagnostic
- automotive
- food monitoring
- home/environmental monitoring
- biological/chemical warfare (Homeland Security)
- industrial high throughput screening (HTS)

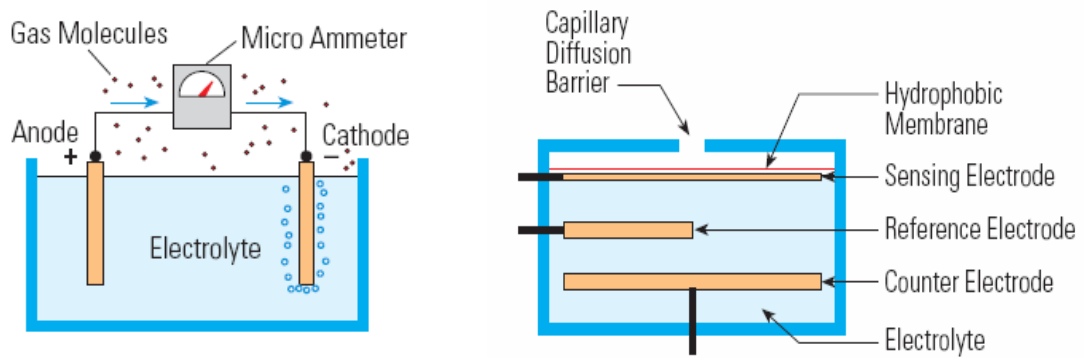


Figure 2.15: Setup for basic sensor and typical electrochemical sensor [59]

Today, solid electrolytes widely used in electrochemical sensor for monitoring hydrogen in industrial processes. Electrochemical sensors are fuel cell-like device consisting of anode, cathode and solid proton conducting electron. Since a few years ago, electrochemical sensors were used for oxygen monitoring. Figure 2.14 shows a setup for basic sensor and typical electrochemical sensor.

Electrochemical sensors operate by reacting with the gas of interest and producing an electrical signal proportional to the gas concentration. A typical electrochemical sensor consists of a sensing electrode (or working electrode), and a counter electrode separated by a thin layer of electrolyte. Gas that comes in contact with the sensor first passes through a small capillary-type opening and then diffuses through a hydrophobic barrier, and eventually reaches the electrode surface. This approach is adopted to allow the proper amount of gas to react at the sensing electrode to produce a sufficient electrical signal while preventing the electrolyte from leaking out of the sensor. The gas that diffuses through the barrier reacts at the surface of the sensing electrode involving either an oxidation or reduction mechanism. These reactions are catalyzed by the electrode materials specifically developed for the gas of interest. With a resistor connected across the electrodes, a current proportional to the gas

concentration flows between the anode and the cathode. The current can be measured to determine the gas concentration. Because a current is generated in the process, the electrochemical sensor is often described as an amperometric gas sensor or a micro fuel cell

Electrochemical sensors can detect various gases but the functions of each markedly different. Similarly, the electrolyte composition and the sensing electrode material are selected based on the chemical reactivity of the target gas. By careful selection of the electrolyte and/or the sensing electrode, one can achieve the selectivity towards the target gas, but the sensitivity may be reduced.

In solid electrolytes, the conductivity depends on ionic mobility rather than electron mobility, where the conductivity is dominated by one type of ion only. Therefore, solid electrolytes play an important role in commercial gas and ion sensor. Solid electrolytes were used in these commercial sensors for determination of oxygen in exhaust gases of automobiles. Solid polymer electrolytes (SPEs) are other membranes of interest for detection of ions in solution as the electrolyte in electrochemical gasses sensors.

CHAPTER 3:

Experimental Techniques

3.1 Sample Preparation

Table 3.1: Amounts of PAN, EC and salts in each group of polymer electrolytes system

Materials Systems	PAN	EC	LiCF ₃ SO ₃	NaCF ₃ SO ₃
Pure PAN	2g	-	-	-
PAN – EC	2g	Varied (2wt.%-30wt.%)	-	-
PAN – LiCF ₃ SO ₃	2 g	-	Varied (2wt.%-30wt.%)	-
PAN – NaCF ₃ SO ₃	2g	-	-	Varied (2wt.%-30wt.%)
PAN - EC - LiCF ₃ SO ₃	2g	Fixed at 24wt.%	Varied (2wt.%-40wt.%)	-
PAN - EC - NaCF ₃ SO ₃	2g	Fixed at 24wt.%	-	Varied (2wt.%-40wt.%)

Table 3.1 shows the amounts of PAN, EC and salts in each group of polymer electrolyte systems that have been prepared in this study. The pure PAN film will be served as a reference. The pure PAN films is prepared by using 2 gram of polyacrylonitrile with 150,000 g/mol from Aldrich and dissolved in dimethylformamide (DMF). The mixtures will continuously stir at 60 °C with a magnetic stirrer for several hours. When complete dissolution is achieved, the solution is then cast into petri dishes and dry in vacuum oven ($<10^{-2}$ Torr) for 3 days at 52°C until the films have formed. Further drying was achieved for 24 hours at 80 °C to remove the residual solvent. The

DMF residue in the films estimated from thermogravimetric analysis (TGA) was less than 5wt%. Then the films were put into desiccator for further drying until characterizations are to be carried out.

3.1.1 Preparation of PAN-EC, PAN-LiCF₃SO₃ and PAN-NaCF₃SO₃ Systems

In these systems, the polymer host polyacrylonitrile (PAN) with the fixed amount of 2 gram was dissolved in dimethylformamide (DMF) solvent. The mixtures were stirred at 60°C until the polymer solutions is homogeneous. EC and salts with varied compositions ranging from 2 wt% to 30 wt% were added to the polymer solution to form a complexation of PAN-EC, PAN-LiCF₃SO₃ and PAN-NaCF₃SO₃. Table 3.2 shows the compositions of EC, LiCF₃SO₃ and NaCF₃SO₃ in PAN-EC system, PAN-LiCF₃SO₃ system, and PAN-NaCF₃SO₃ system.

The mixtures were stirred for 6 hours at 60°C. The solutions is then were cast into glass petri dishes and left to dry under vacuum ($<10^{-2}$ Torr) for 3 days at 40°C until the films have formed. This was followed by further drying in a desiccator until conductivity measurements to be carried out. These films were prepared to investigate the effect of plasticizer and doping salt on electrical conductivity of the PAN film.

Table 3.2: Compositions of EC, LiCF_3SO_3 and NaCF_3SO_3 in PAN-EC system, PAN- LiCF_3SO_3 system, and PAN- NaCF_3SO_3 system

PAN (g)	EC or LiCF_3SO_3 or NaCF_3SO_3 (wt. %)	EC or LiCF_3SO_3 or NaCF_3SO_3 (g)
2	2	0.041
2	4	0.083
2	6	0.128
2	8	0.174
2	10	0.222
2	12	0.273
2	14	0.326
2	16	0.381
2	18	0.439
2	20	0.500
2	22	0.564
2	24	0.632
2	26	0.703
2	28	0.778
2	30	0.857

3.1.2 Preparation of PAN-EC-LiCF₃SO₃ System and PAN-EC-NaCF₃SO₃ System

Table 3.3: Compositions of EC, LiCF₃SO₃ and NaCF₃SO₃ in PAN-EC-LiCF₃SO₃ system, and PAN-EC-NaCF₃SO₃ system.

PAN (g)	EC (g)	LiCF ₃ SO ₃ or NaCF ₃ SO ₃ (wt.%)	LiCF ₃ SO ₃ or NaCF ₃ SO ₃ (g)
2	0.632	2	0.054
2	0.632	4	0.011
2	0.632	6	0.168
2	0.632	8	0.229
2	0.632	10	0.292
2	0.632	12	0.359
2	0.632	14	0.428
2	0.632	16	0.501
2	0.632	18	0.577
2	0.632	20	0.658
2	0.632	22	0.742
2	0.632	24	0.831
2	0.632	26	0.924
2	0.632	28	1.023
2	0.632	30	1.127

The same process as mentioned in Section 3.1.1 is repeated to prepare a film in these systems. In these systems, solutions containing fixed amount of PAN and EC with different amounts of LiCF₃SO₃ and NaCF₃SO₃ varying from 2wt% to 40 wt% were

prepared to form the PAN-EC-LiCF₃SO₃ and PAN-EC-NaCF₃SO₃ system respectively. The amount of EC is fixed at 24 wt% was determined from section 3.1.1. Table 3.3 shows the amounts of LiCF₃SO₃ and NaCF₃SO₃ in PAN-EC-LiCF₃SO₃ and PAN-EC-NaCF₃SO₃ systems. These films were prepared in order to investigate the effect of salt concentration on electrical conductivity of the plasticized PAN system.

The conductivity-temperature dependence and conductivity-pressure dependence studies were performed on the films with the highest room temperature conductivity for the PAN-LiCF₃SO₃ system, the PAN-NaCF₃SO₃ system, the PAN-EC-LiCF₃SO₃ system and the PAN-EC-NaCF₃SO₃ system. The studied temperature and pressure is in the range of 303 K to 373 K and 0.1 atm to 1.0 atm, respectively.

3.2 Impedance Spectroscopy

Impedance Spectroscopy is a non-destructive analytical technique that allows for the characterization of many complex non-linear electrochemical processes under a variety of conditions (e.g., temperature, pressure, etc) using relatively simple equivalent electrical circuits (e.g., resistors, capacitors, inductors). The analysis involves the linear excitation of the electrochemical process by application of small sinusoidal stimulus voltage or current.

Impedance is normally measured using a small excitation signal and the cell's response is pseudo-linear. In a linear (or pseudo-linear) system, the current response to a sinusoidal potential will be a sinusoid at the same frequency but shifted in phase. Figure 3.1 shows the graph of sinusoidal current response in a linear system [60].

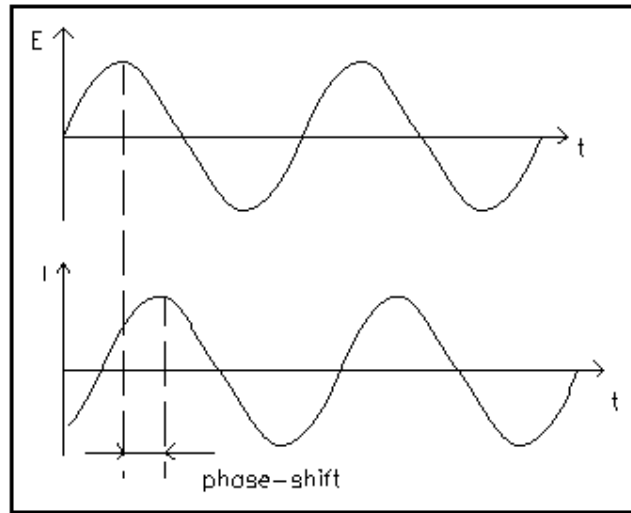


Figure 3.1: Sinusoidal current response in a linear system [60]

The excitation signal, expressed as a function of time, has the form

$$E_t = E_o \sin(\omega t) \quad (3.1)$$

E_t is the potential at time t , E_o is the amplitude of the signal, and ω is the radial frequency. The relationship between radial frequency ω (expressed in radians/second) and frequency f (expressed in Hertz) is:

$$\omega = 2\pi f \quad (3.2)$$

In a linear system, the response signal, I_t , is shifted in phase (ϕ) and has a different amplitude, I_o .

$$I_t = I_o \sin(\omega t + \phi) \quad (3.3)$$

An expression analogous to Ohm's Law allows us to calculate the impedance of the system as:

$$Z = \frac{E_t}{I_t} = \frac{E_o \sin(\omega t)}{I_o \sin(\omega t + \phi)} = Z_o \frac{\sin(\omega t)}{\sin(\omega t + \phi)} \quad (3.4)$$

The impedance is therefore expressed in terms of magnitude, Z_o and phase shift, ϕ with Eulers relationship,

$$\exp(j\phi) = \cos \phi + j \sin \phi \quad (3.5)$$

It is possible to express the impedance as a complex function. The potential is described as;

$$E_t = E_o \exp(j\omega t) \quad (3.6)$$

And the current response as:

$$I_t = I_o \exp(j\omega t - \phi) \quad (3.7)$$

The impedance is then represented as a complex number,

$$Z(\omega) = \frac{E}{I} = Z_o \exp(j\phi) = Z_o (\cos \phi + j \sin \phi) = Z' + jZ'' \quad (3.8)$$

And the phase angle given by:

$$\phi(\omega) = \tan^{-1} \left(\frac{Z''(\omega)}{Z'(\omega)} \right) \quad (3.9)$$

The expression for $Z(\omega)$ is composed of a real and an imaginary part. If the real part is plotted on the X axis and the imaginary part on the Y axis, we get a "Cole-Cole plot" as shown in Figure 3.2.

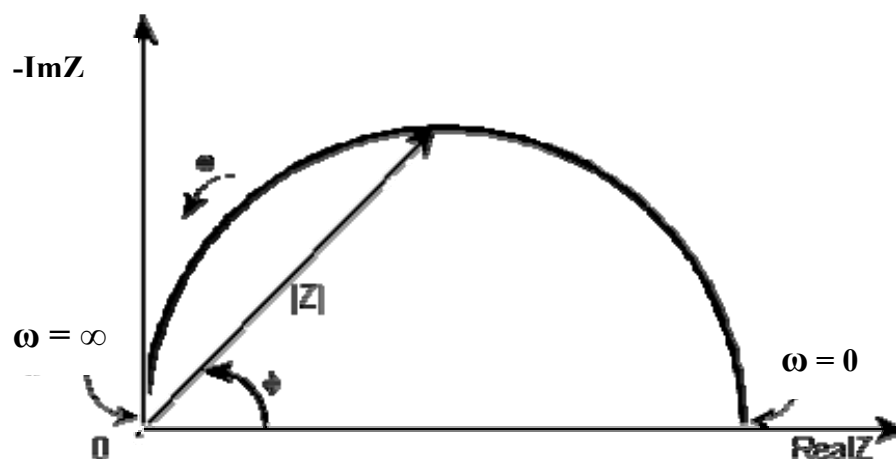


Figure 3.2: Cole-Cole plot [60]

From the Cole-Cole plot with the horizontal and vertical axes having the same scale, the bulk resistance, R_b can be obtained. Whenever R_b was difficult to obtain from the complex impedance data, the impedance data was converted into admittance data and plotted according to the admittance formalism from which $1/R_b$ maybe easier to obtain. The room temperature electrical conductivity of the sample (σ) can then be calculated using the equation:

$$\sigma = \frac{t}{R_b A} \quad (3.10)$$

where t is thickness of the film and A is the cross-sectional area. The conductivity-temperature dependence and conductivity-pressure dependence measurements are carried out to analyze the mechanism of ionic conduction in ion conducting polymers. The linear variation of $\log \sigma$ versus $1000/T$ plot suggests an Arrhenius type thermally activated process [61-62]. The conductivity can be expressed by:

$$\sigma = \sigma_0 \exp\left(\frac{-E_a}{kT}\right) \quad (3.11)$$

where σ_o = a pre-exponential factor
 E_a = the activation energy
 k = Boltzmann constant
 T = the absolute temperature in K

The activation energy, E_a value can be calculated from the slope of the Arrhenius plot [63-64]. Since the ionic conductivity follows an Arrhenius type, we can obtain the activation volume ΔV^* from the plot of conductivities values on logarithmic scale as a function of pressure. The slopes of straight lines plot allow a volume ΔV^* to be determined by the relationship [65]:

$$\left(\frac{\partial \ln \sigma}{\partial P} \right)_T = -\frac{\Delta V^*}{RT} \quad (3.12)$$

The relationship between complex impedance, admittance, permittivity and electrical modulus can be obtained from MacDonald, 1987 [66]. From these relationships and writing $Z = Z_r + jZ_i$ where Z_r and Z_i are the magnitudes of real and imaginary impedance, the equations for the dielectric constant, ϵ_r and the dielectric loss, ϵ_i can be shown as:

$$\epsilon_r = \frac{Z_i}{\omega C_c (Z_r^2 + Z_i^2)} \quad (3.13)$$

$$\epsilon_i = \frac{Z_r}{\omega C_c (Z_r^2 + Z_i^2)} \quad (3.14)$$

Z_r and Z_i are related to the magnitude of the complex impedance via equation, $Z_r(\omega) = Z(\omega) \cos \theta(\omega)$, $Z_i(\omega) = Z(\omega) \sin \theta(\omega)$ and $C_c = \epsilon_o A/t$. ϵ_o is permittivity of

free space, A is the electrolyte-electrode contact area, t is thickness of the sample and $\omega = 2\pi f$ where f is frequency in Hertz.

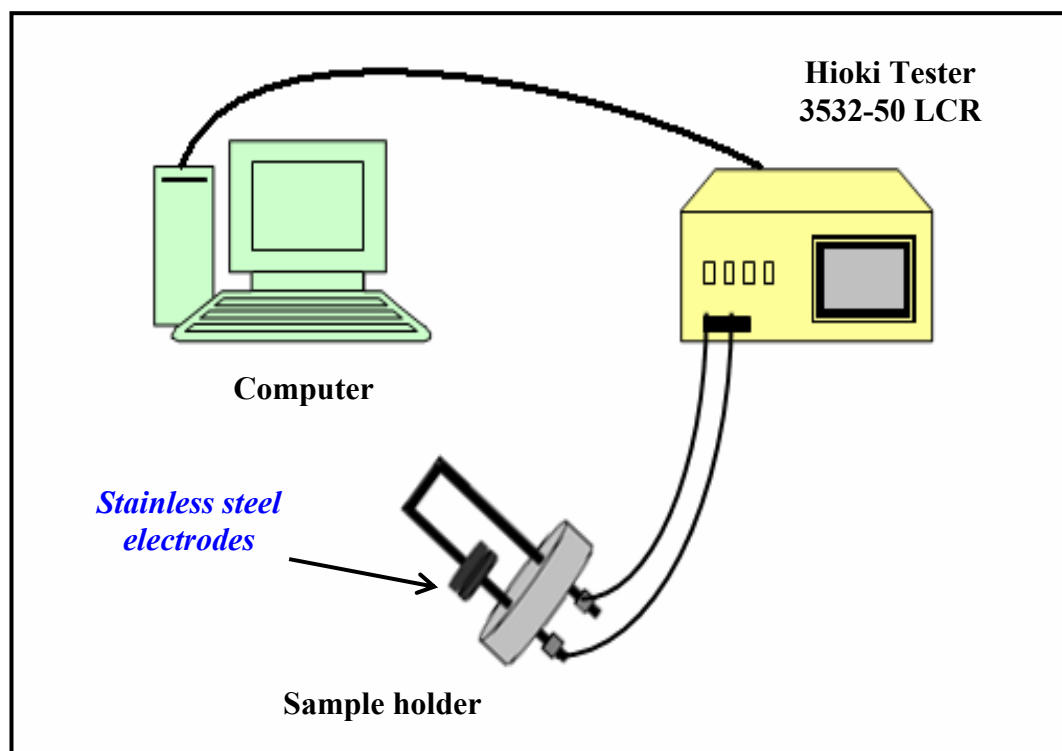


Figure 3.3: Experimental setup for conductivity measurement

In this study, the electrical conductivity of polymer electrolytes was measured using a HIOKI 3532-50 LCR Hi Tester which is interfaced to a computer for data acquisition over the frequency range between 50 Hz and 1 MHz. Figure 3.3 shows the experimental setup for conductivity measurement. The film was placed between two stainless steel electrodes which acted as a blocking electrode for ions. The electrical conductivity is measured six times with different portions of the samples. The conductivity - temperature studies are conducted in the temperature range between 303 K and 373 K while the conductivity-pressure studies with pressure range between 0.01 MPa and 0.09 MPa.

3.3 Fourier Transform Infrared (FTIR)

FTIR is a method of obtaining infrared spectra by first collecting an interferogram of a sample signal using an interferometer, and then performing a Fourier Transform (FT) on the interferogram to obtain the spectrum. FT-IR Spectrometer collects and digitizes the interferogram, performs the FT function, and displays the spectrum. This instrument is the most useful method for identifying chemicals that are either organic or inorganic. It can also be applied to the analysis of solids, liquids and gasses.

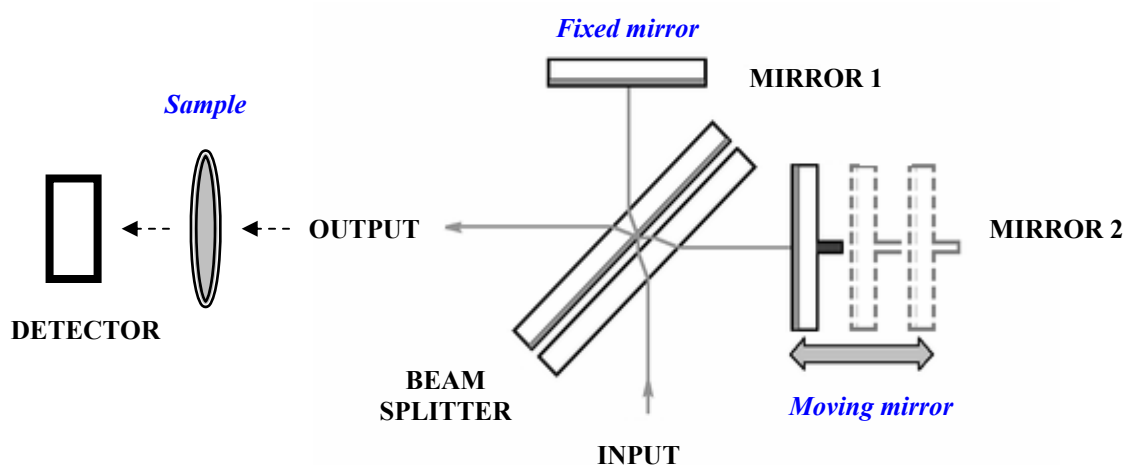


Figure 3.4: A Schematic of a generic Michelson interferometer

FTIR is typically based on a Michelson Interferometer an example is shown in Figure 3.4. The interferometer employs a beam splitter which takes the incoming infrared beam and divides it into two optical beams. The beam splitter is made of a special material that transmits half of the radiation striking it and reflects the other half. Radiation from the source strikes the beam splitter and split into two beams. One beam is transmitted through the beam splitter to the fixed mirror and the second is reflected off the beam splitter to the moving mirror. The fixed and the moving mirrors reflect the radiation back to the beam splitter. Again, half of this reflected radiation is transmitted

and half is reflected at the beam splitter, resulting in one beam passing to the detector and the second back to the source. Because the path that one beam travels is a fixed length and the other is constantly changing as its mirror moves, the signal which exits the interferometer is the result of these two beams “interfering” with each other. The resulting signal is called an interferogram which has the unique property that every data point (a function of the moving mirror position) which makes up the signal has information about every infrared frequency which comes from the source.

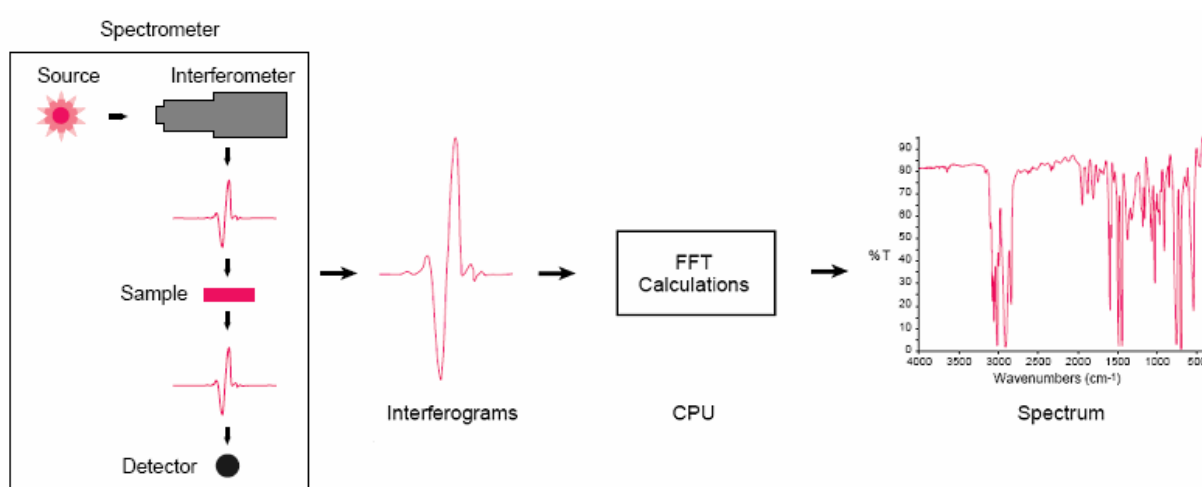


Figure 3.5: The sample analysis process [67]

This means that as the interferogram is measured; all frequencies are being measured simultaneously. Thus, the use of the interferometer results in extremely fast measurements. Because the analyst requires a frequency spectrum (a plot of the intensity at each individual frequency) in order to make an identification, the measured interferogram signal can not be interpreted directly. A means of “decoding” the individual frequencies is required. This can be accomplished via a well-known mathematical technique called the Fourier transformation. This transformation is

performed by the computer which then presents the user with the desired spectral information for analysis.

In this present work, the infrared spectra of all samples were taken with a MAGNA-IR550 Spectrophotometer-Series II in the number region between 4000 cm^{-1} and 400 cm^{-1} . The resolution of this spectrometer was 1 cm^{-1} .

3.4 X-ray diffraction (XRD)

X-ray diffraction is an analytical technique used to determine the structures of materials. A beam of x-rays is diffracted off of the repeating planes of atoms in crystalline samples to produce a diffraction pattern. The orientation of the x-ray and the crystal is the most importance. As the angle between the x-ray beam and the crystal face is varied, the diffraction pattern will change as well. Through analysis of the diffraction pattern, atomic structures can be determined.

A schematic of the x-ray diffractometer is shown in Figure 3.6. The main components are the x-ray source, a goniometer (or crystal orienter), a detection system, and a computer control system. The x-ray source is a high-vacuum tube, and the x-ray beam passes out of the tube through a thin window. A single crystal is generally mounted on the end of a glass fiber. This fiber is then attached to a metal pin which is secured to the goniometer head. The goniometer precisely orients the sample in the x-ray beam. As the x-rays pass through the crystal, the detector collects information to generate a diffraction pattern. Finally, the computer control system processes the information from the detector, and the structure of the crystal is solved.

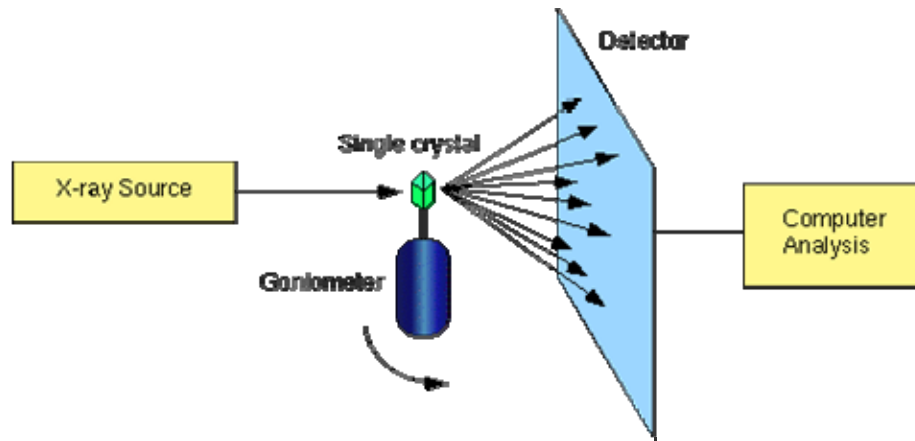


Figure 3.6: A schematic of an x-ray diffractometer [68]

To understand how a diffraction pattern occurs, consider the diffraction patterns of two waves. Two waves of the same wavelength can come together either in phase or out of phase. If the two waves come together in phase, this means that the maxima and minima of both waves are at the same points. In other words, the hills and the valleys from both waves are lined up together. The waves reinforce or cause constructive interference, and the intensity of the resultant wave is increased. Conversely, two waves coming together out of phase have each minimum from one wave combining with a maximum of the other wave. The hills from the first wave line up with the valleys from the second wave while the valleys from the first wave line up with the hills from the second wave. This is called destructive interference and destroys the wave. Figure 3.7 shows constructive and destructive interference.

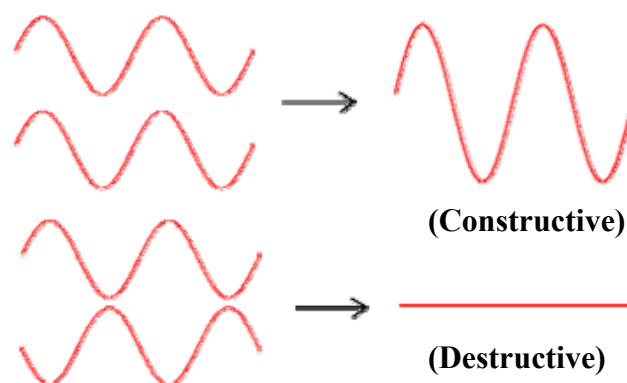


Figure 3.7: Constructive and destructive interference

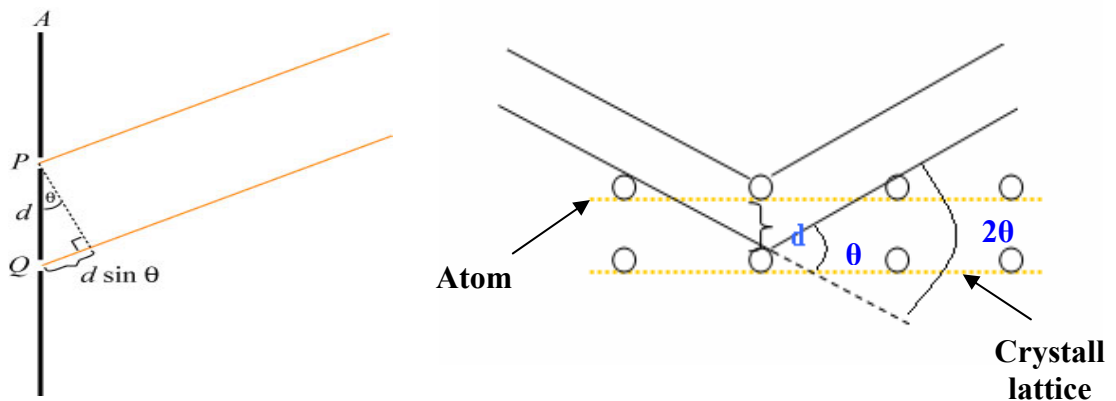
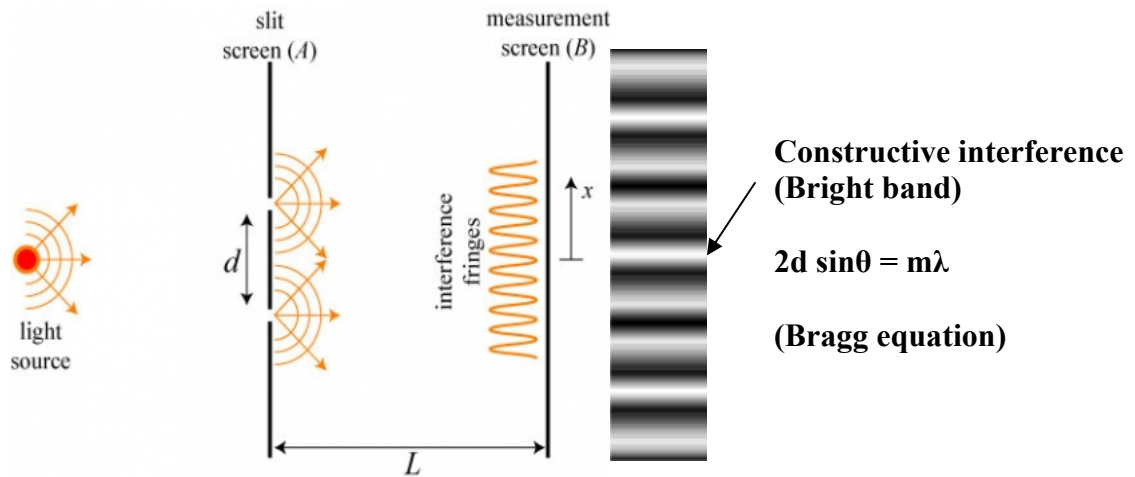


Figure 3.8: A simple schematic of the Young's double slit experiment [69]

In a crystal, x-rays are reflected from the different planes of atoms that are present. If two x-rays travel to two different planes, then one x-ray must travel further than the other. The x-rays may end up out of phase after they are reflected. Only at certain angles of reflection do the two rays remain in phase. In the diffraction pattern, dark areas are caused by destructive interference while brighter areas are caused by constructive interference. Thus, the diffraction pattern can be related to the structure of the crystal, and the position of each atom in a molecule as well as the type and size of a unit cell can be determined by using x-ray diffraction.

Nowadays, the XRD become a very powerful determinative method in the mineral and materials science. There are some limitations, but x-ray diffraction can also be a very straightforward and easy to use in order to determine the identity of the minerals. In this work, x-ray diffractograms are obtained using the XRD PANAnalytical X'Pert Pro machine at the Institute of Science, Universiti Teknologi MARA (UiTM) Shah Alam.

3.5 Scanning Electron Microscopy (SEM)

The Scanning Electron Microscope is a microscope that uses electrons rather than light to form an image. There are many advantages to using the SEM instead of a light microscope. The SEM has a large depth of field, which allows a large amount of the sample to be in focus at one time. The SEM also produces images of high resolution, which means that closely spaced features can be examined at a high magnification. Preparation of the samples is relatively easy since most SEMs only require the sample to be conductive. The combination of higher magnification, larger depth of focus, greater resolution, and ease of sample observation makes the SEM one of the most heavily used instruments in research areas today.

Figure 3.9 shows the schematic diagram of SEM experimental set-up. A beam of electrons is produced at the top of the microscope by an electron gun. The electron beam follows a vertical path through the microscope, which is held within a vacuum. The beam travels through electromagnetic fields and lenses, which focus the beam down toward the sample. Once the beam hits the sample, electrons and x-rays are ejected from the sample. Detectors collect these x-rays, backscattered electrons, and secondary electrons and convert them into a signal that is sent to a screen similar to a television screen. This produces the final image. Because the SEM utilizes vacuum

conditions and uses electrons to form an image, special preparations must be done to the sample. All water must be removed from the samples because the water would vaporize in the vacuum. All metals are conductive and require no preparation before being used. All non-metals need to be made conductive by covering the sample with a thin layer of conductive material. This is done by using a device called a "spin coater." The spin coater uses an electric field and argon gas. The sample is placed in a small chamber that is at a vacuum. Argon gas and an electric field cause an electron to be removed from the argon, making the atoms positively charged. The argon ions then become attracted to a negatively charged gold foil. The argon ions knock gold atoms from the surface of the gold foil. These gold atoms fall and settle onto the surface of the sample producing a thin gold coating.

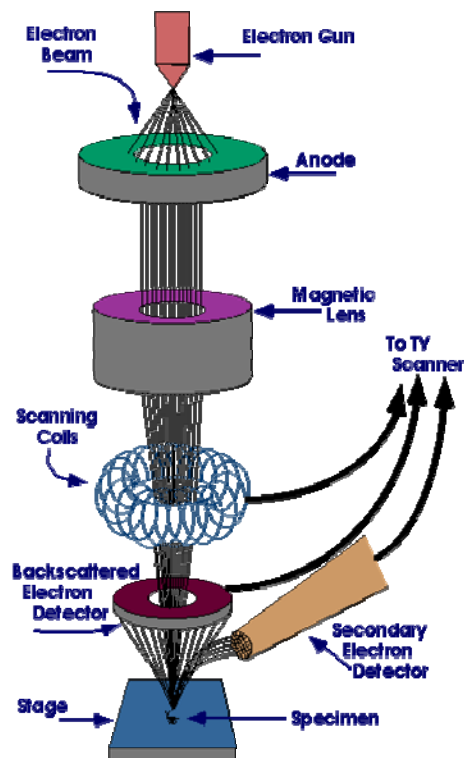


Figure 3.9: The schematic diagram of SEM experiment [70]

The micrographs obtained from SEM provide important information on the surface structure and morphology of almost of any samples. The nature and morphology of a polymer electrolyte film surface is an important property for the polymer electrolytes. In this work, SEM micrographs of the samples are obtained using SEC Mini Digital Scanning Electron Microscope machine.

3.6 Differential Scanning Calorimetry (DSC)

Differential Scanning Calorimetry is a thermo analytical technique in which the difference in the amount of heat required to increase the temperature of a sample and reference are measured as a function of temperature. Both the sample and reference are maintained at nearly the same temperature throughout the experiment. Generally, the temperature program for the DSC analysis is designed such that the sample holder temperature increases linearly as a function of time. Only a few milligrams of material are required to run the analysis.

DSC is commonly used to measure a variety of properties in both organic and inorganic materials, from metals and simple compounds to polymers and pharmaceuticals. The properties measured include:

- Glass transitions temperature, T_g
- Phase changes
- Melting temperature, T_m
- Crystallization temperature, T_c
- Product stability
- Cure / cure kinetics
- Oxidative stability
- Heat capacity and heat of fusion measurements

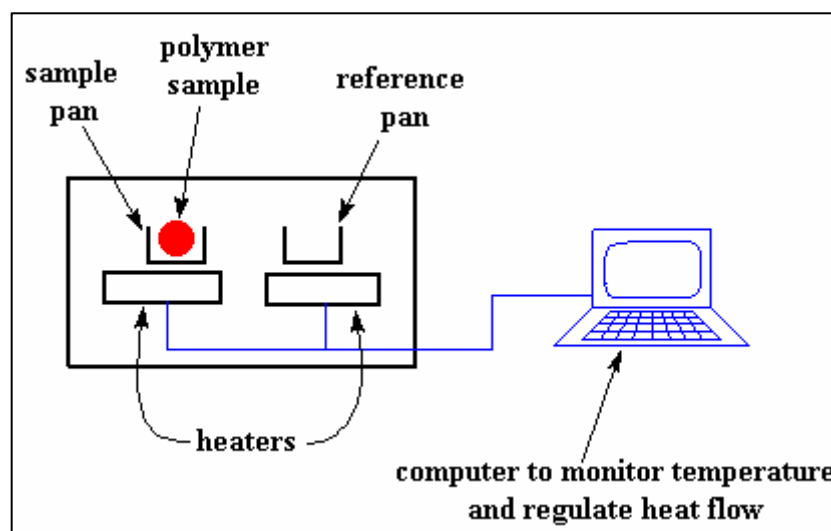


Figure 3.10: Experimental setup for DSC [71]

Figure 3.10 shows the experimental setup for T_g measurement. Glass transitions, T_g may occur as the temperature of an amorphous solid is increased. These transitions appear as a step in the baseline of the recorded DSC signal. This is due to the sample undergoing a change in heat capacity; no formal phase change occurs. When a sample undergoes a physical transformation such as a phase transition, more or less heat will need to flow to it than to the reference (typically an empty sample pan) to maintain both at the same temperature. Whether more or less heat must flow to the sample depends on whether the process is exothermic or endothermic. For example, as a solid sample melts to a liquid it will require more heat flowing to the sample to increase its temperature at the same rate as the reference. This is due to the absorption of heat by the sample as it undergoes the endothermic phase transition from solid to liquid. Likewise, as the sample undergoes exothermic processes (such as crystallization) less heat is required to raise the sample temperature. By observing the difference in heat flow between the sample and reference, differential scanning calorimeters are able to measure the amount of heat absorbed or released during such transitions. DSC may also be used to observe more subtle phase changes, such as glass transitions [71].

In this work, DSC results of the samples are obtained using Perkin Elmer Instrument DSC6 calorimeter at the Chemistry Department, University of Malaya. The temperature range studied was -50 °C to 350 °C. The heating/cooling rate was 10 °C/min. The calibration of temperature and enthalpy was performed with Pyris 6 series thermal software.

CHAPTER 4:

Results and Discussion

-Electrical Studies-

4.1 Impedance Spectroscopy Analysis

The study of electrical conductivity on polymer electrolytes films is very important to investigate the ionic behavior and transport mechanisms of these films. Therefore, impedance spectroscopy analysis was performed on PAN based electrolytes system to obtain the conductivity at room temperature. The impedance was measured from 50 Hz to 1 MHz. The films from the PAN-LiCF₃SO₃ system, the PAN-NaCF₃SO₃ system, the PAN-EC-LiCF₃SO₃ system and the PAN-EC-NaCF₃SO₃ system with the highest room temperature conductivity were used to study the conductivity-temperature and conductivity-pressure dependence. The conductivity-temperature studies were carried out in the temperature range between 303 K and 373 K while the conductivity-pressure studies were carried out in the pressure range between 0.01 MPa and 0.09 MPa.

4.2 Room Temperature Impedance Spectroscopy Studies

4.2.1 Pure PAN Film

Figure 4.1 depicts the Cole-Cole plot of pure PAN film. From the figure, the value of bulk resistance, R_b and conductivity, σ at room temperature is $2.33 \times 10^8 \Omega$ and $1.51 \times 10^{-11} \text{ S cm}^{-1}$, respectively.

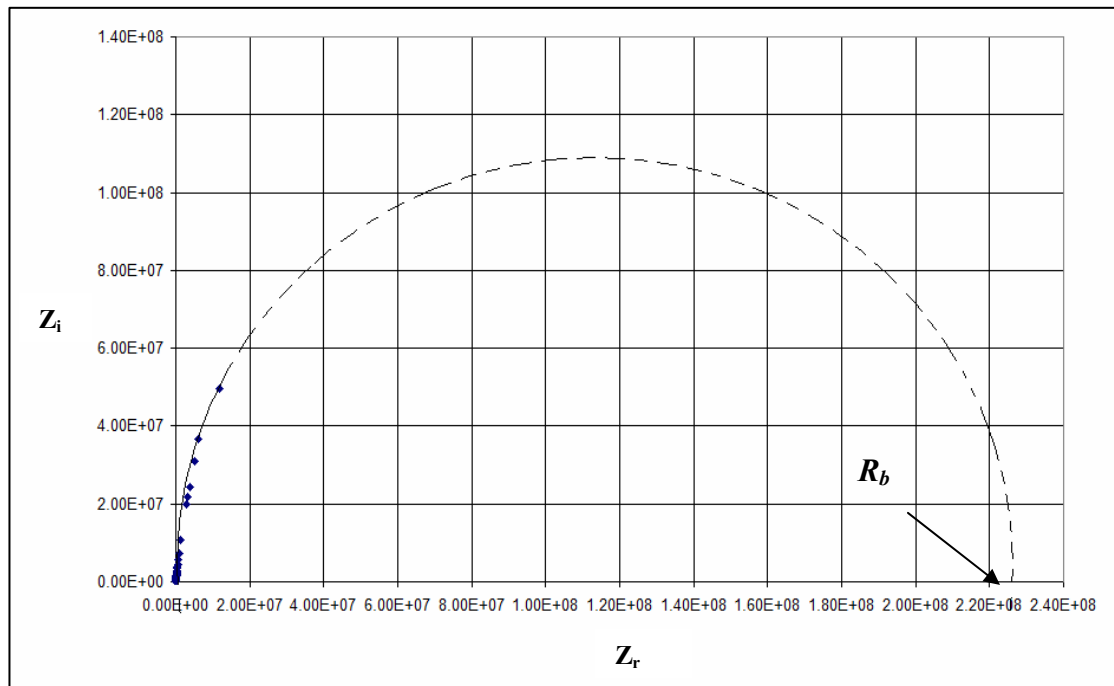


Figure 4.1: Cole-Cole plot of pure PAN film

4.2.2 PAN-EC system

Table 4.1 lists the compositions, the values of bulk resistance, R_b and the conductivities films in the PAN-EC system. The highest conductivity achieved is $3.43 \times 10^{-11} \text{ S cm}^{-1}$ from the film containing 24 wt% of EC. The variation of conductivity of PAN-EC films containing different amounts of EC in weight percentage is presented in Figure 4.2. It can be observed from the figure that the conductivity value of PAN increases when the plasticizer, EC was added. The increase in conductivity value in this system implies that the plasticizer has dissolved the polymer and reduced the rigidity of polymer backbone. This will lead to the increase of the mobility of the segmental chain of the polymer. Since no ions have been introduced into this system, the conductivity is expected not to be high.

Table 4.1: The compositions, the values of bulk resistance, R_b and the conductivity, σ of films in the PAN-EC system.

EC content in PAN-EC system (wt.%)	Average Bulk Resistance, R_b (Ω)	Average Conductivity, $(\sigma \pm \Delta \sigma)$ ($S\ cm^{-1}$)
2	3.51×10^8	$(1.63 \pm 0.12) \times 10^{-11}$
4	3.20×10^8	$(1.92 \pm 0.21) \times 10^{-11}$
6	2.29×10^8	$(2.24 \pm 0.15) \times 10^{-11}$
8	2.24×10^8	$(2.31 \pm 0.30) \times 10^{-11}$
10	2.21×10^8	$(2.96 \pm 0.34) \times 10^{-11}$
12	2.14×10^8	$(3.03 \pm 0.20) \times 10^{-11}$
14	1.56×10^8	$(3.07 \pm 0.32) \times 10^{-11}$
16	1.89×10^8	$(2.74 \pm 0.22) \times 10^{-11}$
18	2.04×10^8	$(2.86 \pm 0.43) \times 10^{-11}$
20	2.02×10^8	$(2.91 \pm 0.44) \times 10^{-11}$
22	2.00×10^8	$(3.17 \pm 0.43) \times 10^{-11}$
24	1.71×10^8	$(3.43 \pm 0.21) \times 10^{-11}$
26	2.68×10^8	$(2.19 \pm 0.14) \times 10^{-11}$
28	3.03×10^8	$(1.89 \pm 0.18) \times 10^{-11}$
30	3.16×10^8	$(1.87 \pm 0.23) \times 10^{-11}$

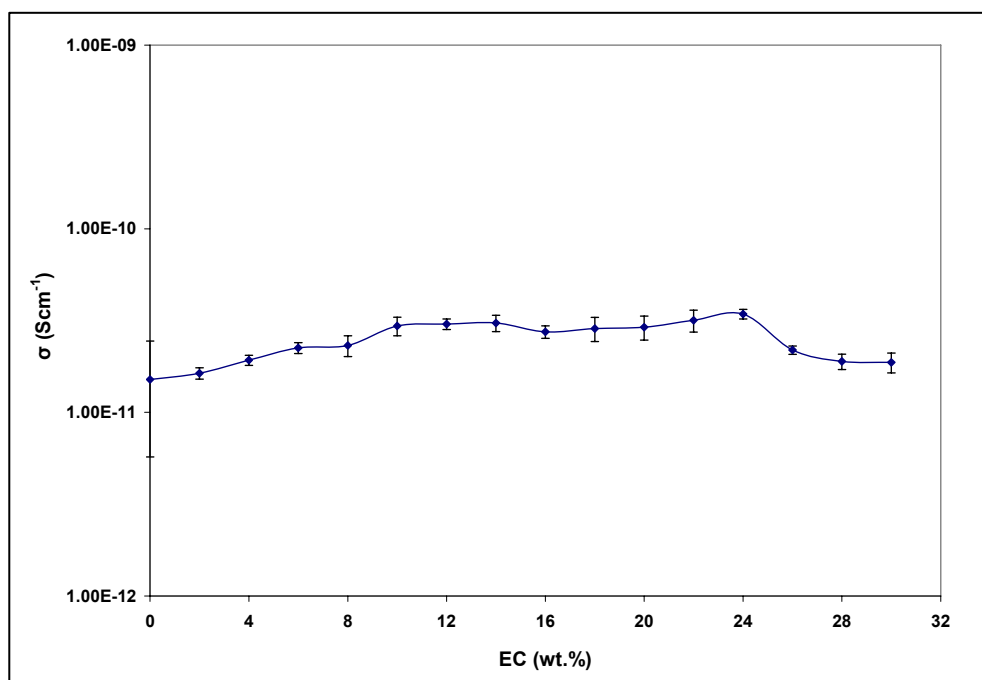


Figure 4.2: Conductivity versus amount of EC in the PAN-EC system.

4.2.3 PAN - LiCF₃SO₃ System

Figure 4.3 depicts the Cole-Cole plots of PAN-LiCF₃SO₃ film containing 2 wt.%, 10 wt.%, 26 wt.% and 30 wt.% of LiCF₃SO₃. It can be observed that from the plot of PAN containing 26 wt% and 30wt% the semicircle at high frequency is completely disappeared. The compositions, the values of bulk resistance, R_b and the conductivities of the films in the PAN-LiCF₃SO₃ system are summarized in Table 4.2. The highest conductivity achieved is 3.04×10^{-4} S cm⁻¹ from the film containing 26 wt% of LiCF₃SO₃. Figure 4.4 shows the variation of conductivity of the system containing different amounts of LiCF₃SO₃ in weight percentage. It can be observed that the conductivity of pure PAN increases when LiCF₃SO₃ was added. The increase in conductivity has been assumed that the lithium ion from LiCF₃SO₃ has interacted with a nitrogen atom from functional group of polymer, PAN structure. Generally, ionic conductivity of electrolytes is depend on the charge carrier concentration, n and charge carrier mobility, μ as described by relation $\sigma = nq\mu$, where n , q and μ representing the

charge carrier concentration, charge of mobile carrier and the mobility, respectively. In the low salt concentrations range, the LiCF_3SO_3 is totally dissociated. The number of mobile ions increases with the increase of LiCF_3SO_3 concentration thus increases the conductivity value. At higher salt concentrations, the decrease in conductivity value can be explained by aggregation of the ions, leading to the formation of ion cluster, thus decreasing the number of mobile charge carriers and hence the mobility [72].

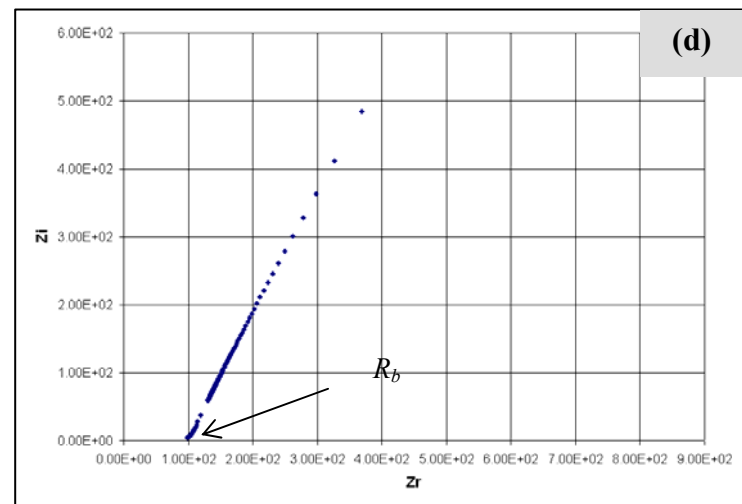
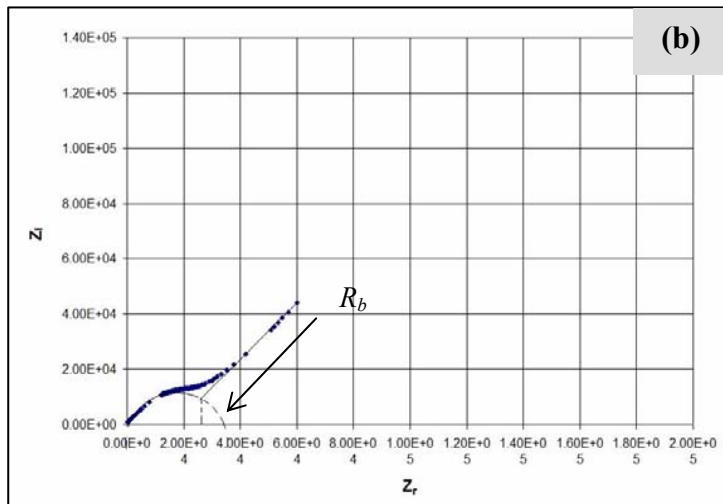
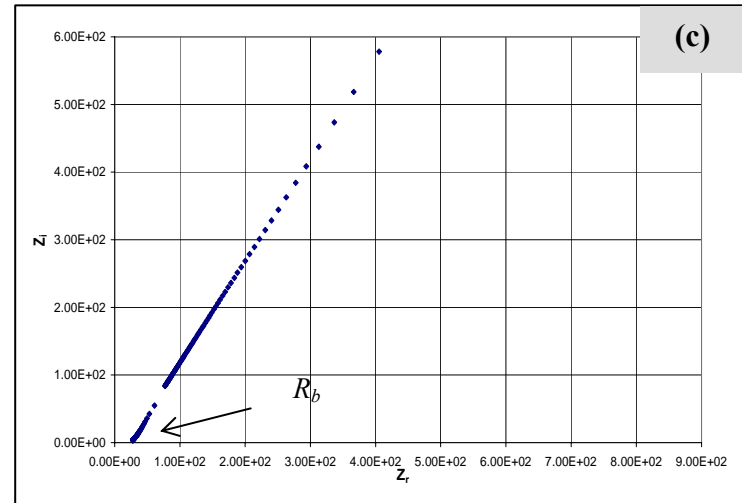
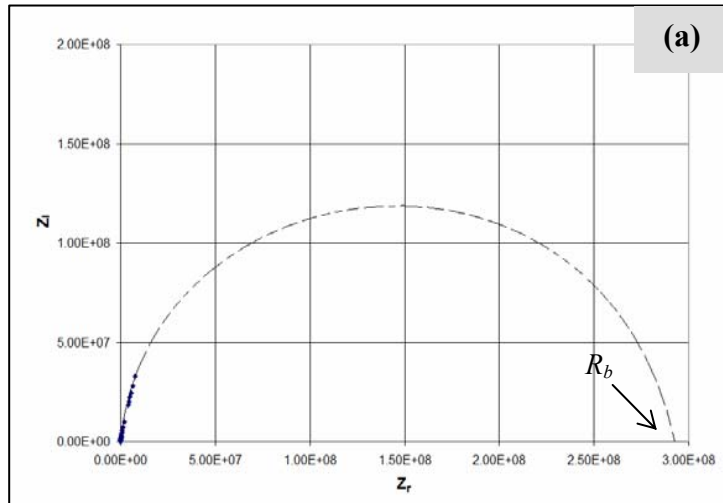


Figure 4.3: Cole-Cole plots for the PAN films containing (a) 2 wt.% (b) 10 wt.% (c) 26wt.% and (d) 30wt.% and of LiCF_3SO_3 films.

Table 4.2: The compositions, the bulk resistance, R_b and the conductivity, σ of films in the PAN - LiCF_3SO_3 system.

LiCF₃SO₃ content in PAN – LiCF₃SO₃ system (wt.%)	Average Bulk Resistance, R_b (Ω)	Average Conductivity, ($\sigma \pm \Delta \sigma$) (S cm⁻¹)
2	2.92×10^8	$(1.72 \pm 0.60) \times 10^{-11}$
4	6.51×10^7	$(1.52 \pm 0.73) \times 10^{-10}$
6	9.63×10^5	$(6.15 \pm 3.50) \times 10^{-9}$
8	5.80×10^4	$(9.11 \pm 3.38) \times 10^{-8}$
10	2.40×10^4	$(2.66 \pm 1.35) \times 10^{-7}$
12	2.50×10^4	$(5.48 \pm 3.89) \times 10^{-7}$
14	5.70×10^3	$(1.42 \pm 0.94) \times 10^{-6}$
16	4.00×10^3	$(2.60 \pm 1.79) \times 10^{-6}$
18	2.07×10^3	$(5.50 \pm 0.42) \times 10^{-6}$
20	5.68×10^2	$(1.40 \pm 0.34) \times 10^{-5}$
22	2.93×10^3	$(2.30 \pm 0.22) \times 10^{-5}$
24	1.53×10^2	$(7.30 \pm 2.02) \times 10^{-5}$
26	3.43×10^1	$(3.04 \pm 0.34) \times 10^{-4}$
28	8.83×10^1	$(1.55 \pm 0.57) \times 10^{-4}$
30	9.93×10^1	$(1.22 \pm 0.32) \times 10^{-4}$

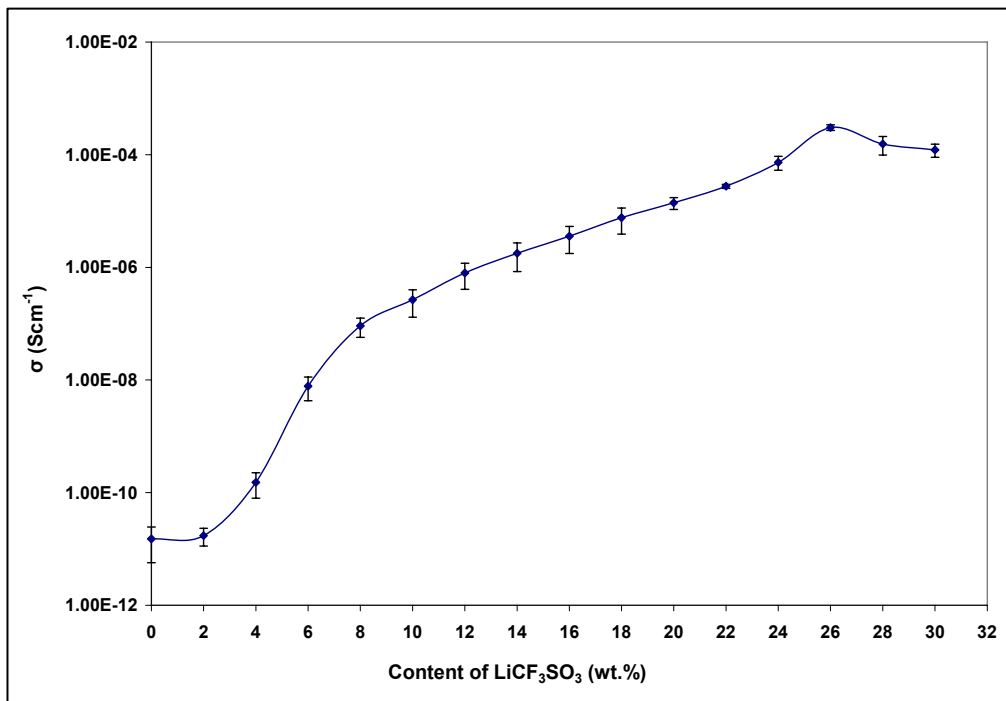


Figure 4.4: Conductivity versus amount of LiCF₃SO₃ in the PAN-LiCF₃SO₃ system

Figure 4.5 and 4.6 show the dielectric constant and dielectric loss versus log frequency for films in the PAN-LiCF₃SO₃ system. The film that has the highest conductivity with 26 wt% of LiCF₃SO₃ in this system has the highest value of dielectric constant, ϵ_r and dielectric loss, ϵ_i . It can be observed that the increase in dielectric constant with salt content is in accordance to the conductivity and vice versa. Dielectric constant is directly related to capacitance. The increase of capacitance implies the increase in the number of ions. Both the real (ϵ_r) and imaginary (ϵ_i) parts of dielectric complex rise sharply towards low frequencies due to the electrode polarization effects [73].

At low frequencies, the periodic reversal of the field direction occurs very slowly so that the ions are able to accumulate in the direction of the field leading to a nett polarization and hence contribute to the high value of ϵ_r and ϵ_i . At high frequencies, the periodic reversal of the electric field occurs very fast. Therefore the polarization due

to the decrease charge accumulation, leads to the observed decrease in the value of ϵ_r and ϵ_i .

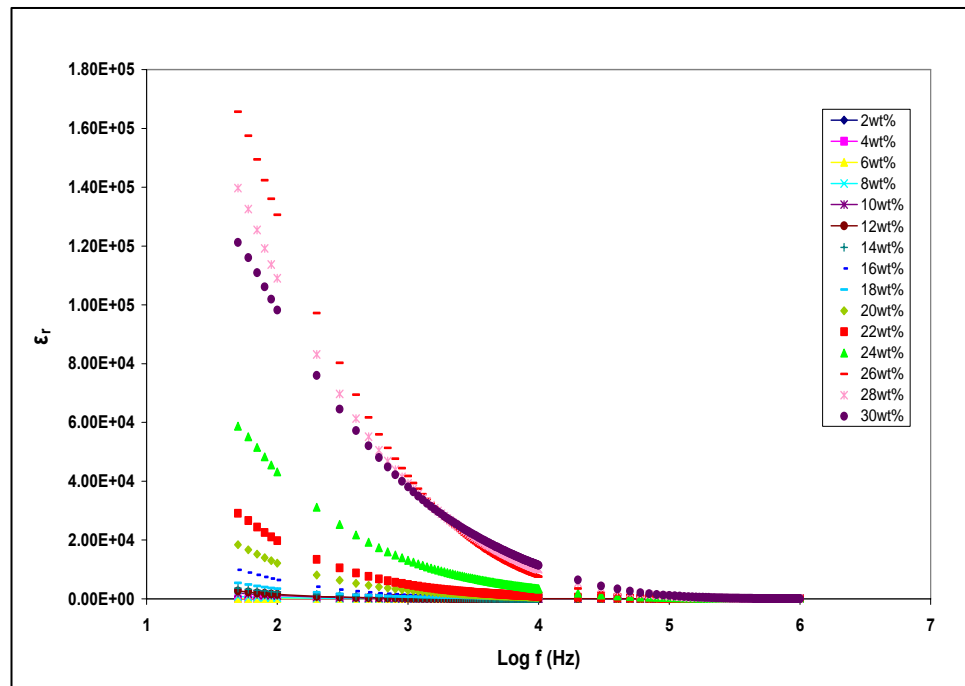


Figure 4.5: Dielectric constant versus frequency for films in the PAN-LiCF₃SO₃ system

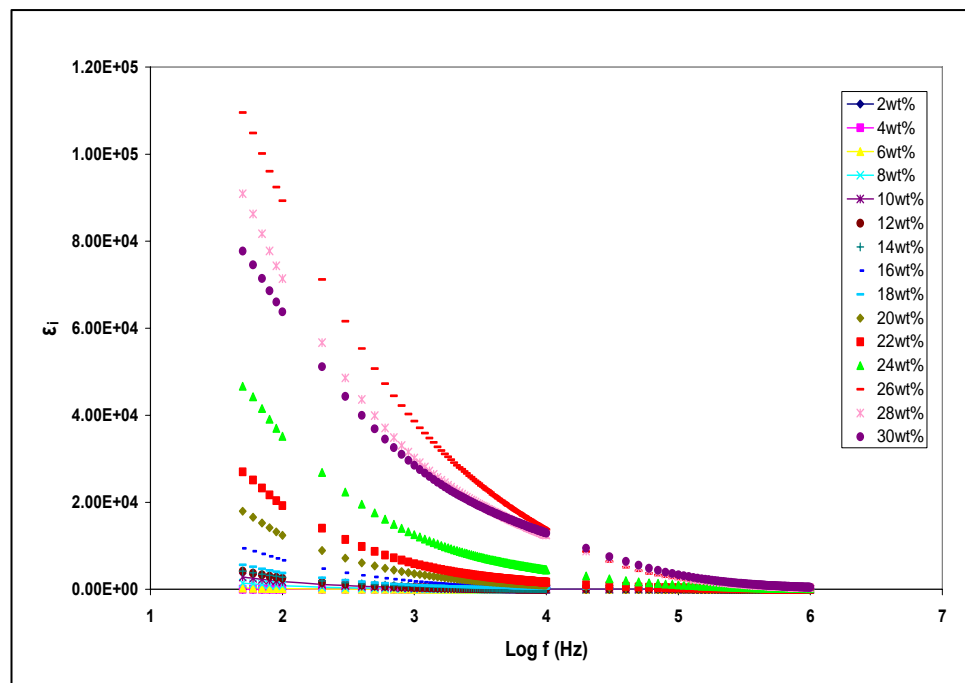


Figure 4.6: Dielectric loss versus frequency for films in the PAN-LiCF₃SO₃ system

4.2.4 PAN - NaCF₃SO₃ System

The Cole-Cole plots for the films containing 2 wt.%, 10 wt.%, 24 wt.% and 30 wt.% of NaCF₃SO₃ in the PAN-NaCF₃SO₃ system have been shown in Figure 4.7. For higher salt concentrations, the semicircle has been found to be absent. This result suggests that, only the resistive component of ion conducting polymer prevails when the ability of PAN to dissolve NaCF₃SO₃ is maximum at 24 wt.%. It can be observed from the Table 4.3, the conductivity values continuously increase when more salt (up to 24 wt.%) has been added. The ionic conductivity as a function of salt concentration is shown in Figure 4.8. The sharp increase in the conductivity value from 6 wt.% to 12 wt.% is due to the increasing of charge carriers concentration and ionic mobility in this system. It can be observed from the figure that the conductivity increases with the increase of the amount of NaCF₃SO₃ up to 24 wt% and decrease with further addition. This is because when the salt content is increased, the number of free ions also increases, thus increases the diffusion of ions through their free volumes. Therefore, the conductivity increased. When more salt was added, the number of free ions also increases until it was saturated. These ions become closer to one another, decreasing the free volumes thus decreasing the conductivity.

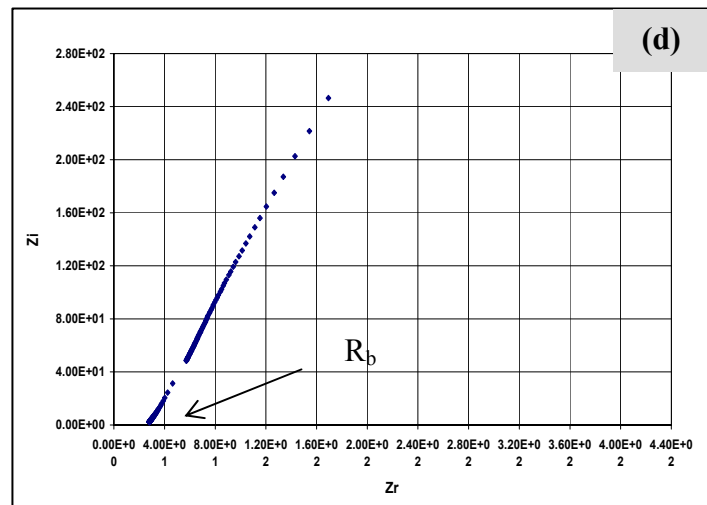
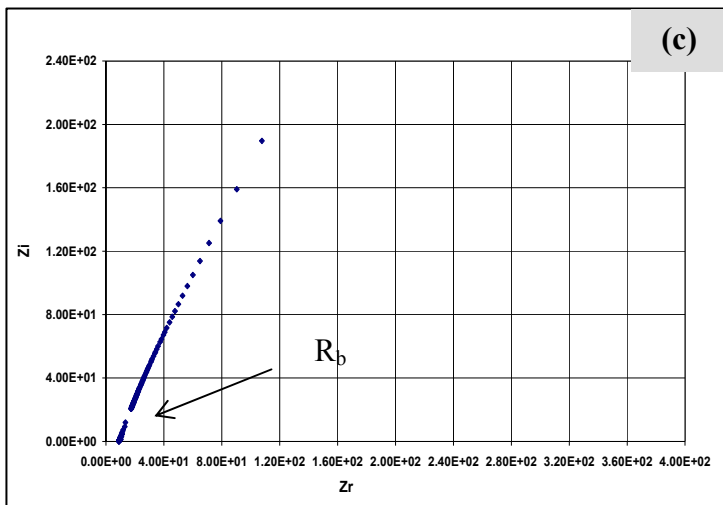
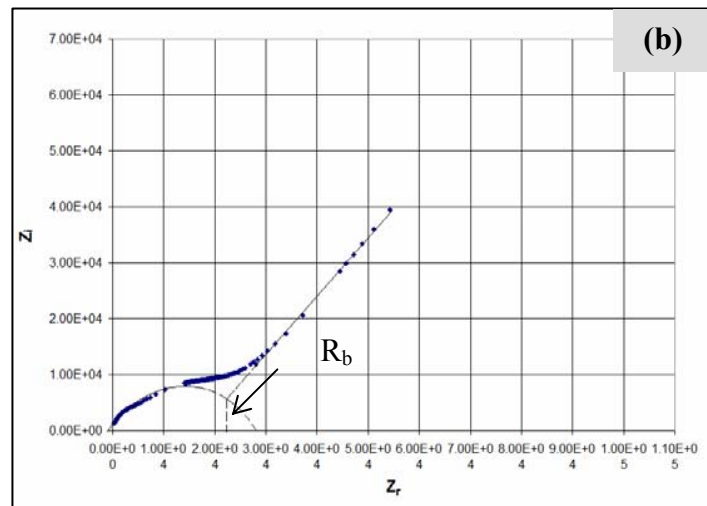
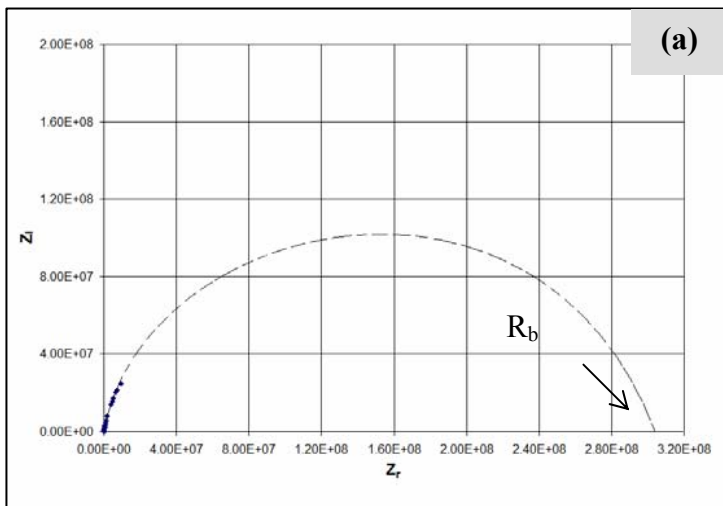


Figure 4.7: Cole – Cole plots for the PAN films containing and (a) 2 wt.% (b) 10wt.% (c) 24wt.%, and (d) 30wt% of NaCF_3SO_3 .

Table 4.3: The compositions, the values of bulk resistance, R_b and the conductivity, σ of films in the PAN - NaCF₃SO₃ system.

NaCF₃SO₃ content in PAN–NaCF₃SO₃ system (wt.%)	Average Bulk Resistance, R_b (Ω)	Average Conductivity ($\sigma \pm \Delta \sigma$) (S cm⁻¹)
2	3.06×10^8	$(2.68 \pm 1.34) \times 10^{-11}$
4	9.93×10^7	$(5.46 \pm 1.96) \times 10^{-11}$
6	2.26×10^7	$(1.90 \pm 0.84) \times 10^{-10}$
8	3.87×10^6	$(1.39 \pm .69) \times 10^{-9}$
10	2.76×10^4	$(1.73 \pm 0.73) \times 10^{-7}$
12	5.90×10^3	$(3.71 \pm 2.32) \times 10^{-6}$
14	7.50×10^2	$(1.10 \pm 0.48) \times 10^{-5}$
16	3.18×10^2	$(2.43 \pm 0.10) \times 10^{-5}$
18	1.02×10^2	$(9.35 \pm 3.82) \times 10^{-5}$
20	1.17×10^2	$(1.75 \pm 0.30) \times 10^{-4}$
22	40.0×10^1	$(2.58 \pm 0.87) \times 10^{-4}$
24	1.33×10^1	$(7.13 \pm 2.55) \times 10^{-4}$
26	3.05×10^1	$(3.99 \pm 0.50) \times 10^{-4}$
28	3.13×10^1	$(3.92 \pm 0.61) \times 10^{-4}$
30	3.17×10^1	$(3.90 \pm 0.97) \times 10^{-4}$

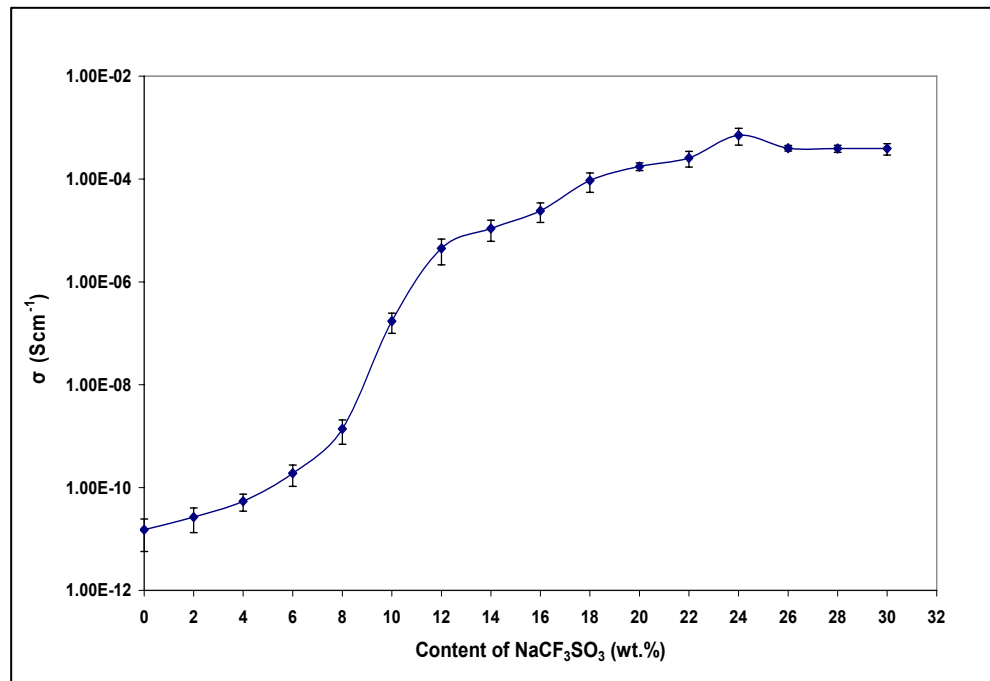


Figure 4.8: Conductivity versus amount of NaCF₃SO₃ in the PAN-NaCF₃SO₃ system

Figure 4.9 and 4.10 show the variation of dielectric constant, ϵ_r and dielectric loss, ϵ_i with frequency for different amounts of NaCF₃SO₃ for films in the PAN-NaCF₃SO₃ system. The trends of the plots are similar to the plot of dielectric constant, ϵ_r and dielectric loss, ϵ_i with frequency for the PAN-LiCF₃SO₃ system indicating that the same phenomenon applies. It can be observed that the dielectric constant, ϵ_r and dielectric loss, ϵ_i increase as frequency decreases. The film that has the highest conductivity with 24 wt% of NaCF₃SO₃ in the PAN-NaCF₃SO₃ system has the highest value of dielectric constant, ϵ_r and dielectric loss, ϵ_i . This infers that the increase in conductivity is due to an increasing the diffusion of ions through their free volume.

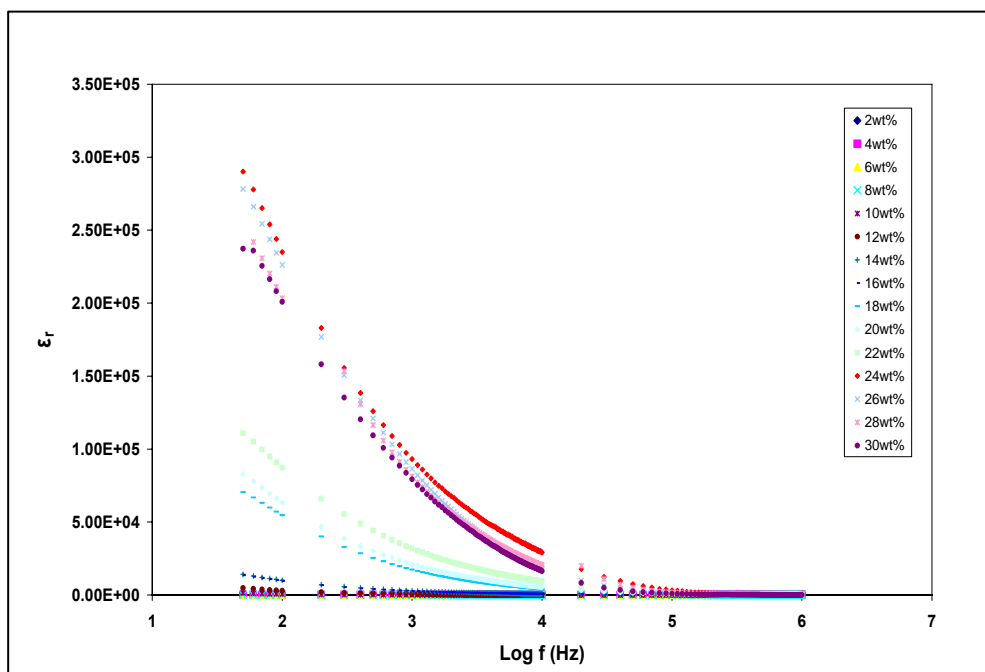


Figure 4.9: Dielectric constant versus frequency for films in the PAN-NaCF₃SO₃ system

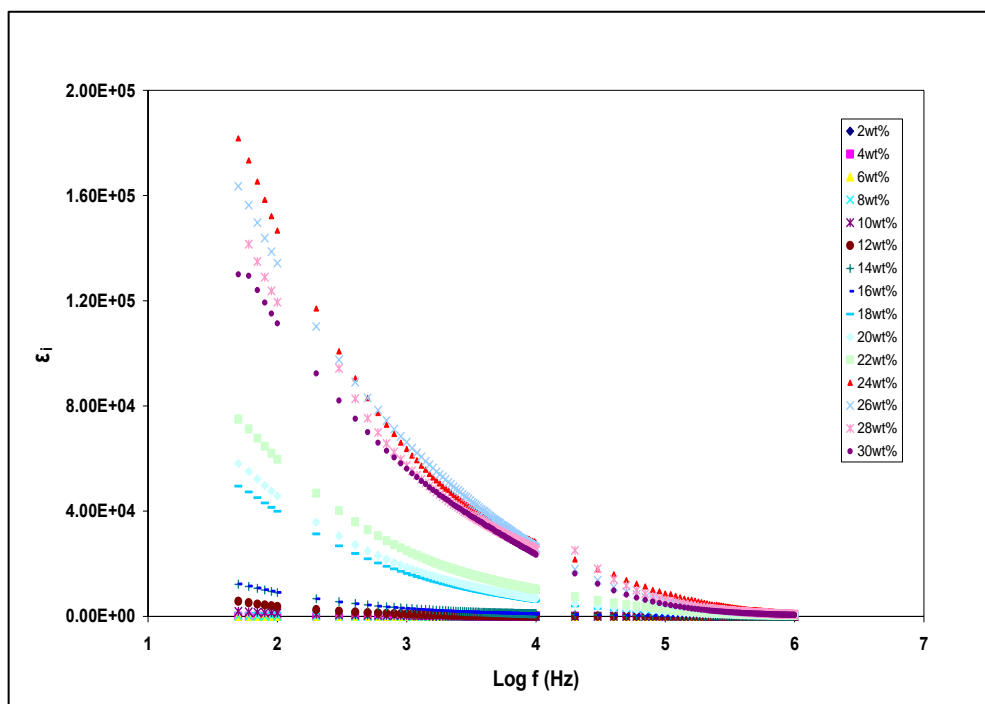


Figure 4.10: Dielectric constant versus frequency for films in the PAN-NaCF₃SO₃ system

4.2.5 PAN - EC - LiCF₃SO₃ System

Figure 4.11 shows the Cole-Cole plots of plasticized PAN films containing 2 wt.%, 10 wt.%, 22 wt.% and 30 wt.% of LiCF₃SO₃. As listed in Table 4.4, the PAN-EC-LiCF₃SO₃ system exhibits the same conductivity trend with the PAN-LiCF₃SO₃ system and the PAN-NaCF₃SO₃ systems which the conductivity is increased as the amount of salt is increased up to 22 wt.% after which the conductivity is decreased. The highest conductivity value for this system is $1.32 \times 10^{-3} \text{ S cm}^{-1}$. It can be observed that the plasticizer, EC has ability to increase the conductivity value of PAN containing LiCF₃SO₃. Hence the plasticizer plays role as the polar medium providing a pathway for conducting by ion transport which decreasing the viscosity of electrolytes directed the movement of the ionic charge carriers along the polymer backbone. Figure 4.12 shows the variation of conductivity of the system containing different amounts of LiCF₃SO₃ in weight percentage.

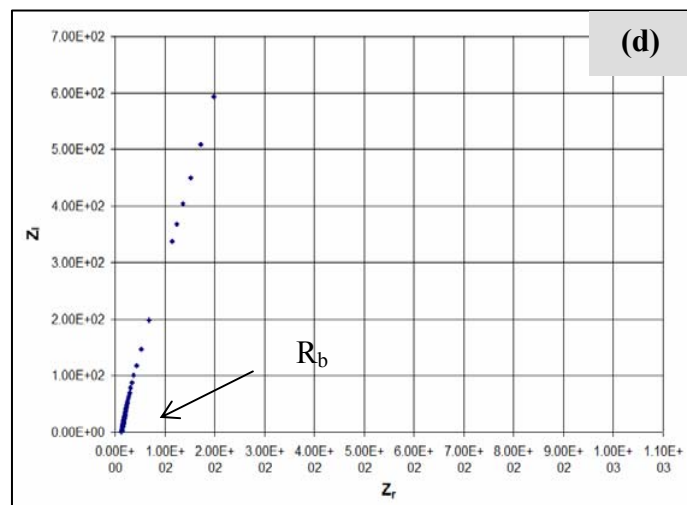
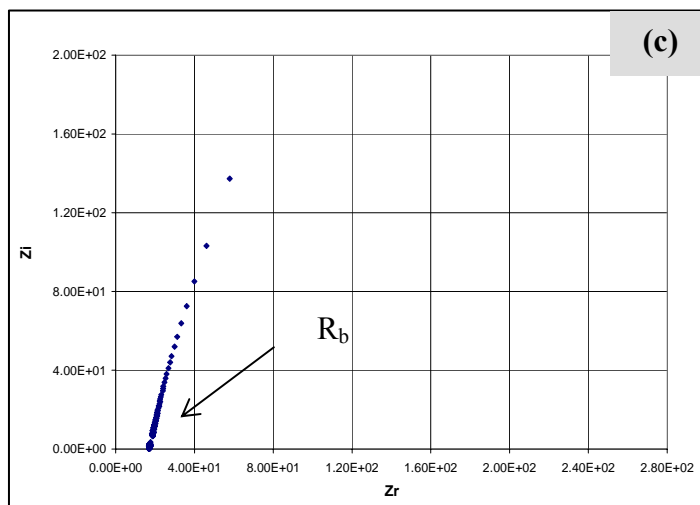
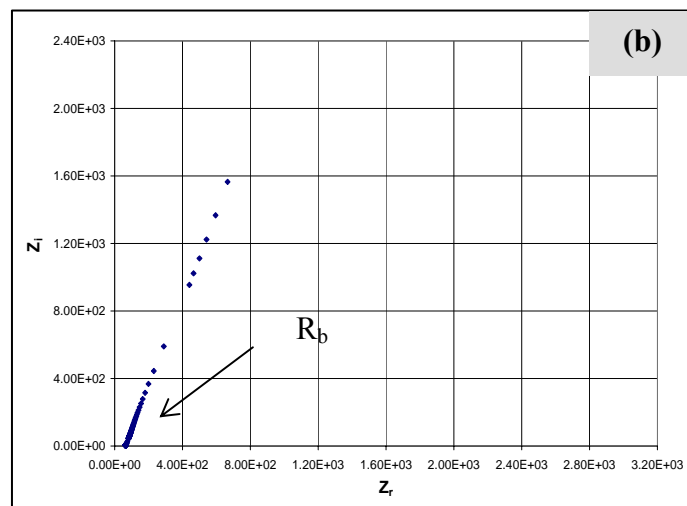
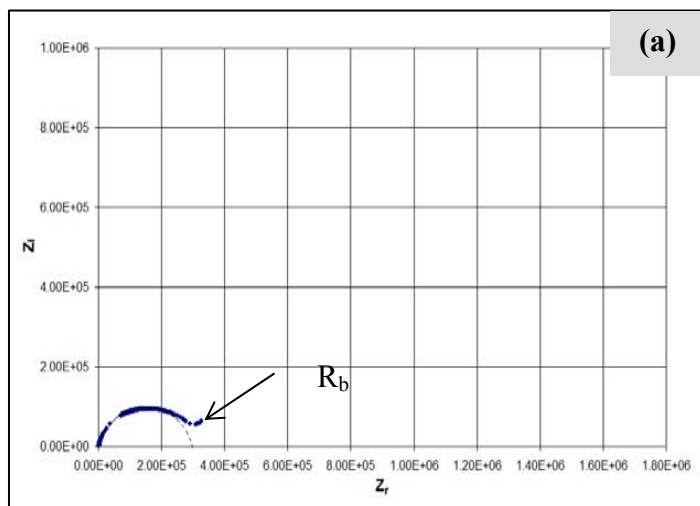


Figure 4.11: Cole – Cole plots for the PAN-EC-LiCF₃SO₃ films containing (a) 2 wt.% (b) 10 wt.% (c) 22 wt.% and (d) 30wt.% LiCF₃SO₃

Table 4.4: The compositions, the values of bulk resistance, R_b and the conductivity, σ of films in the PAN-EC-LiCF₃SO₃ system.

LiCF ₃ SO ₃ content in PAN – EC – LiCF ₃ SO ₃ system (wt.%)	Average Bulk Resistance, R_b (Ω)	Average Conductivity, ($\sigma \pm \Delta \sigma$) (S cm ⁻¹)
2	2.90×10^5	$(1.36 \pm 0.33) \times 10^{-8}$
4	6.14×10^4	$(8.98 \pm 1.29) \times 10^{-8}$
6	3.97×10^4	$(1.46 \pm 0.26) \times 10^{-7}$
8	3.98×10^3	$(2.58 \pm 0.78) \times 10^{-6}$
10	1.57×10^2	$(4.57 \pm 2.22) \times 10^{-5}$
12	1.20×10^2	$(5.73 \pm 1.59) \times 10^{-5}$
14	3.42×10^1	$(1.36 \pm 0.34) \times 10^{-4}$
16	2.85×10^1	$(2.86 \pm 0.60) \times 10^{-4}$
18	2.65×10^1	$(3.27 \pm 1.09) \times 10^{-4}$
20	1.61×10^1	$(6.60 \pm 2.82) \times 10^{-4}$
22	1.29×10^1	$(1.32 \pm 0.39) \times 10^{-3}$
24	1.70×10^1	$(6.73 \pm 0.66) \times 10^{-4}$
26	2.35×10^1	$(4.26 \pm 0.64) \times 10^{-4}$
28	2.17×10^1	$(4.67 \pm 0.67) \times 10^{-4}$
30	16.7×10^1	$(5.17 \pm 1.23) \times 10^{-4}$
32	20.0×10^1	$(4.77 \pm 0.67) \times 10^{-4}$
34	20.0×10^1	$(4.52 \pm 0.71) \times 10^{-4}$
36	2.11×10^1	$(3.75 \pm 0.80) \times 10^{-4}$
38	1.80×10^1	$(4.44 \pm 0.60) \times 10^{-4}$
40	1.75×10^1	$(4.55 \pm 0.56) \times 10^{-4}$

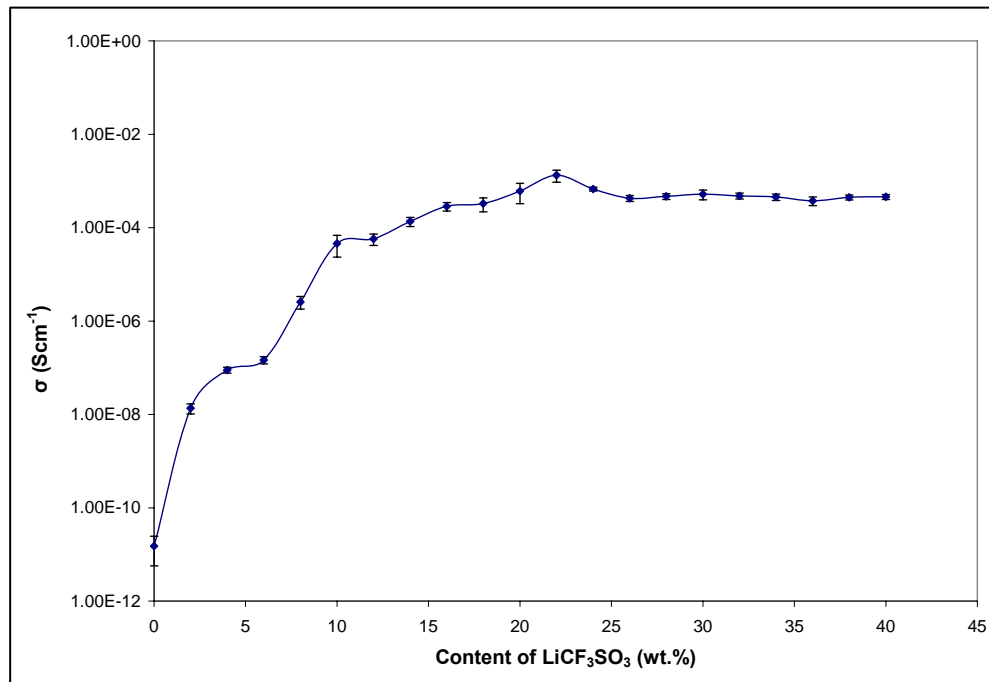


Figure 4.12: Conductivity versus amount of LiCF₃SO₃ in the PAN-EC-LiCF₃SO₃ system

Figure 4.13 and 4.14 show the variations of the dielectric constant, ϵ_r and dielectric loss, ϵ_i with frequency for different amounts of LiCF₃SO₃ in wt% for films in the PAN-EC-LiCF₃SO₃ system. The same behaviour as discussed in PAN-LiCF₃SO₃ system can be observed in these figures. The dielectric constant, ϵ_r and dielectric loss, ϵ_i increase as frequency decreases. The film containing 22 wt% of LiCF₃SO₃ has the highest conductivity value in the PAN-EC-LiCF₃SO₃ system. This film also has the highest dielectric constant, ϵ_r and dielectric loss, ϵ_i values. This infers that the increase in conductivity is due to an increase in the number of free ions. Both dielectric constant, ϵ_r and dielectric loss, ϵ_i approach a constant value at high frequencies.

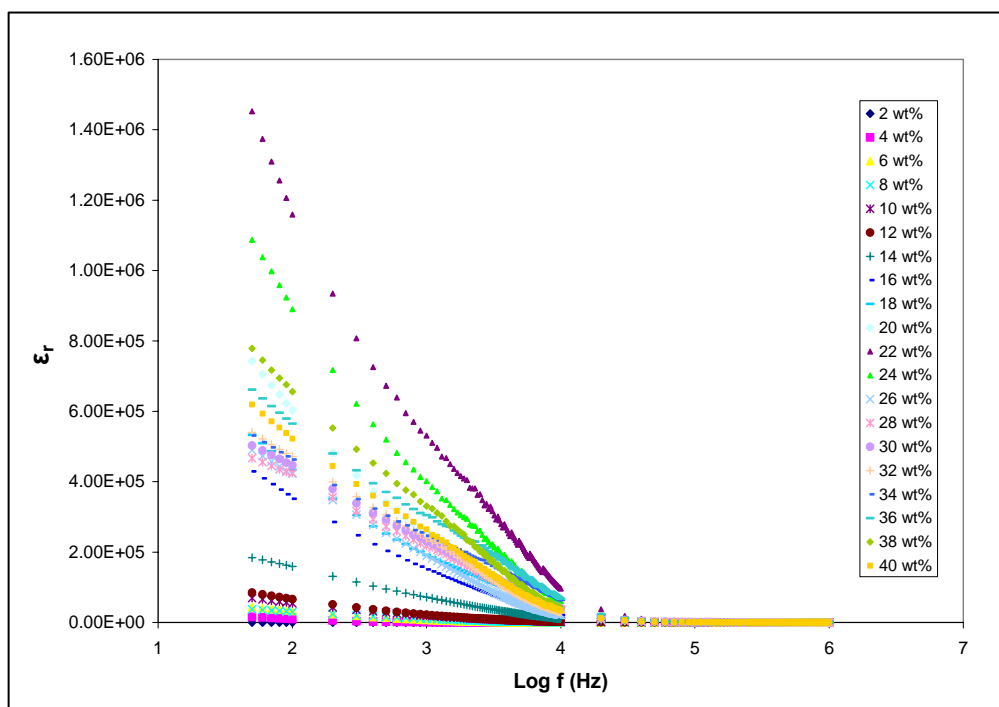


Figure 4.13: Dielectric constant versus frequency for films in the PAN-EC-LiCF₃SO₃ system.

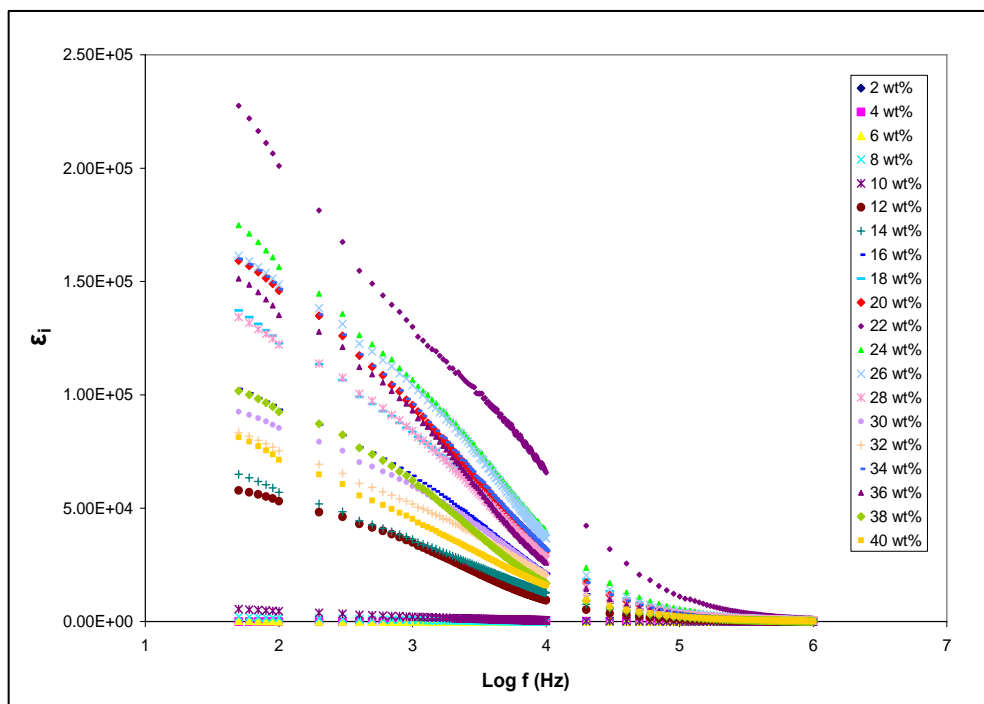


Figure 4.14: Dielectric loss versus frequency for films in the PAN-EC-LiCF₃SO₃ system.

4.2.6 PAN - EC - NaCF₃SO₃ System

Figure 4.15 shows the Cole-Cole plots of plasticized PAN film containing 2 wt.%, 10 wt.%, 34 wt.% and 40 wt.% of NaCF₃SO₃ from the PAN-EC-NaCF₃SO₃ system. From Table 4.5, it can be noted that the conductivity of this system continuously increases until 34 wt% of NaCF₃SO₃ is added and the conductivity decreases with further addition of salt. The maximum conductivity achieved is $5.49 \times 10^{-3} \text{ S cm}^{-1}$. This implies that the plasticizer, EC has dissociated more NaCF₃SO₃ salt than LiCF₃SO₃ salt into ions. The sharp increase in the conductivity value from 2 wt.% to 6 wt.% is due to the increasing of mobility of the charge carriers in this system. At lower concentrations, the ions can move easily in the electrolytes because the plasticizer will help to destruct the coordination bond of Na⁺ with PAN and making more ions move in polymer electrolytes, hence increase the conductivity. When more salt is added, the ion clusters are formed in the salted PAN based polymer electrolyte system. There is ion association in the PAN system containing NaCF₃SO₃. The association among the free ion i.e. Na⁺ will reduce the mobility of the charge carrier. In this case, EC will play a vital role in dissociate the saturated amounts of salt in this system to become free ion.

At higher salt concentrations, the number of free Na⁺ ions also increases and makes these ions become closer to one another. Since the ions become so close to one another, thus the conductivity decreased. Figure 4.16 shows the variation of conductivity of the system containing different amounts of NaCF₃SO₃ in weight percentage.

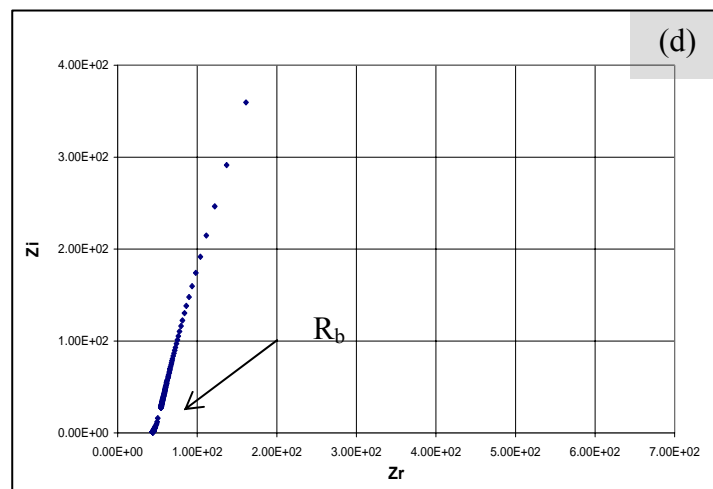
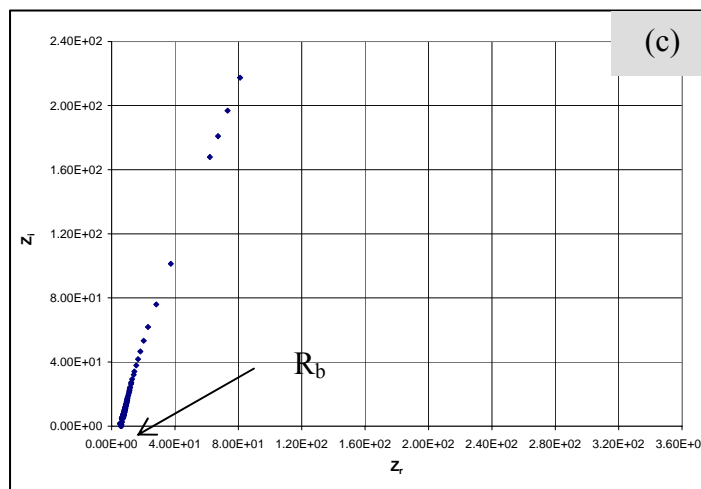
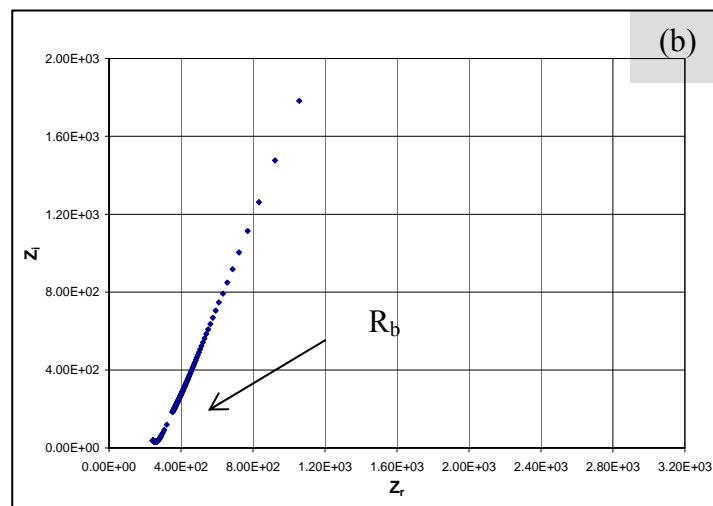
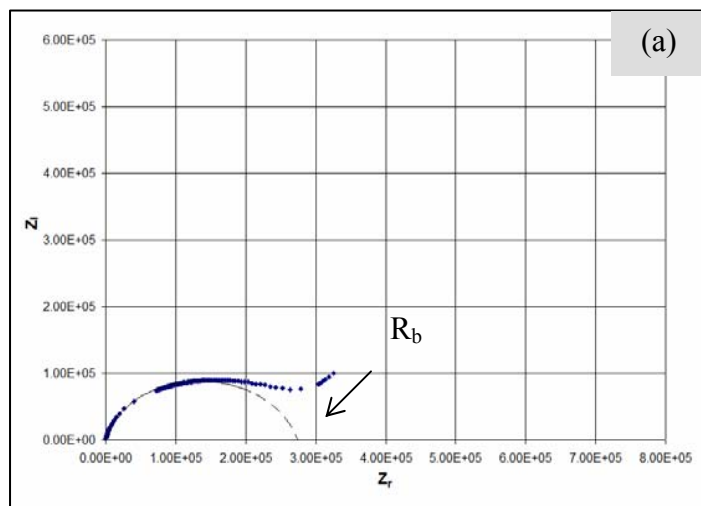


Figure 4.15: Cole-Cole plots for the PAN-EC- NaCF_3SO_3 films containing (a) 2 wt % (b) 10 wt.% (c) 34 wt.% and (d) 40 wt.% NaCF_3SO_3

Table 4.5: The compositions, the values of bulk resistance, R_b and the conductivity, σ of films in the PAN-EC-NaCF₃SO₃ system

NaCF ₃ SO ₃ content in PAN – EC – NaCF ₃ SO ₃ system (wt.%)	Average Bulk Resistance, R_b (Ω)	Average Conductivity, ($\sigma \pm \Delta \sigma$) (S cm ⁻¹)
2	2.74×10^5	$(1..52 \pm 0.42) \times 10^{-8}$
4	6.47×10^3	$(7.61 \pm 1.07) \times 10^{-7}$
6	5.66×10^2	$(1.13 \pm 0.01) \times 10^{-5}$
8	4.67×10^2	$(1.51 \pm 0.52) \times 10^{-5}$
10	2.62×10^2	$(2.68 \pm 0.59) \times 10^{-5}$
12	1.49×10^2	$(7.36 \pm 1.83) \times 10^{-5}$
14	1.26×10^2	$(1.29 \pm 0.21) \times 10^{-4}$
16	5.20×10^1	$(2.04 \pm 0.65) \times 10^{-4}$
18	4.01×10^1	$(2.34 \pm 0.51) \times 10^{-4}$
20	2.40×10^1	$(4.41 \pm 0.54) \times 10^{-4}$
22	1.60×10^1	$(6.62 \pm 0.76) \times 10^{-4}$
24	1.40×10^1	$(7.07 \pm 0.82) \times 10^{-4}$
26	1.26×10^1	$(1.29 \pm 0.23) \times 10^{-3}$
28	0.95×10^1	$(1.68 \pm 0.55) \times 10^{-3}$
30	0.84×10^1	$(1.94 \pm 0.22) \times 10^{-3}$
32	0.63×10^1	$(2.47 \pm 0.22) \times 10^{-3}$
34	0.29×10^1	$(5.49 \pm 0.32) \times 10^{-3}$
36	0.50×10^1	$(3.61 \pm 0.83) \times 10^{-3}$
38	0.67×10^1	$(2.97 \pm 0.53) \times 10^{-3}$
40	0.46×10^1	$(3.42 \pm 0.32) \times 10^{-3}$

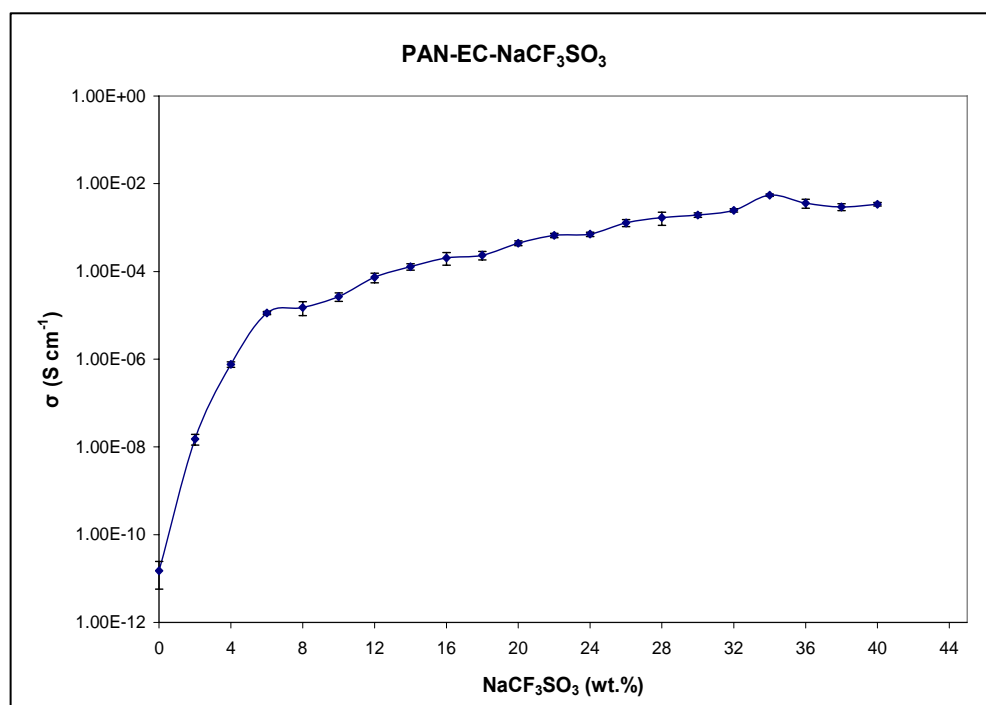


Figure 4.16: Conductivity versus amount of NaCF₃SO₃ in the PAN-EC-NaCF₃SO₃ system

Figure 4.17 and 4.18 show the variations of the dielectric constant, ϵ_r with frequency for different amounts of NaCF₃SO₃ in wt% for films in the PAN-EC-NaCF₃SO₃ system. The same behaviour as discussed in PAN-EC-LiCF₃SO₃ system can be observed in these figures. The dielectric constant, ϵ_r and dielectric loss, ϵ_i increase as frequency decreases. The film with 34 wt% of NaCF₃SO₃ has the highest conductivity value in the PAN-EC-NaCF₃SO₃ system, also has the highest dielectric constant, ϵ_r and dielectric loss, ϵ_i . This infers that the increase in conductivity is due to an increase in the number of free ions. Both dielectric constant, ϵ_r and dielectric loss, ϵ_i approach a constant value at high frequencies.

It also can be observed that this system has the highest dielectric constant, ϵ_r and dielectric loss, ϵ_i value compared to the PAN-EC-LiCF₃SO₃ system. This indicates that more Na⁺ ions are dissociated by EC in the PAN-EC-NaCF₃SO₃ system.

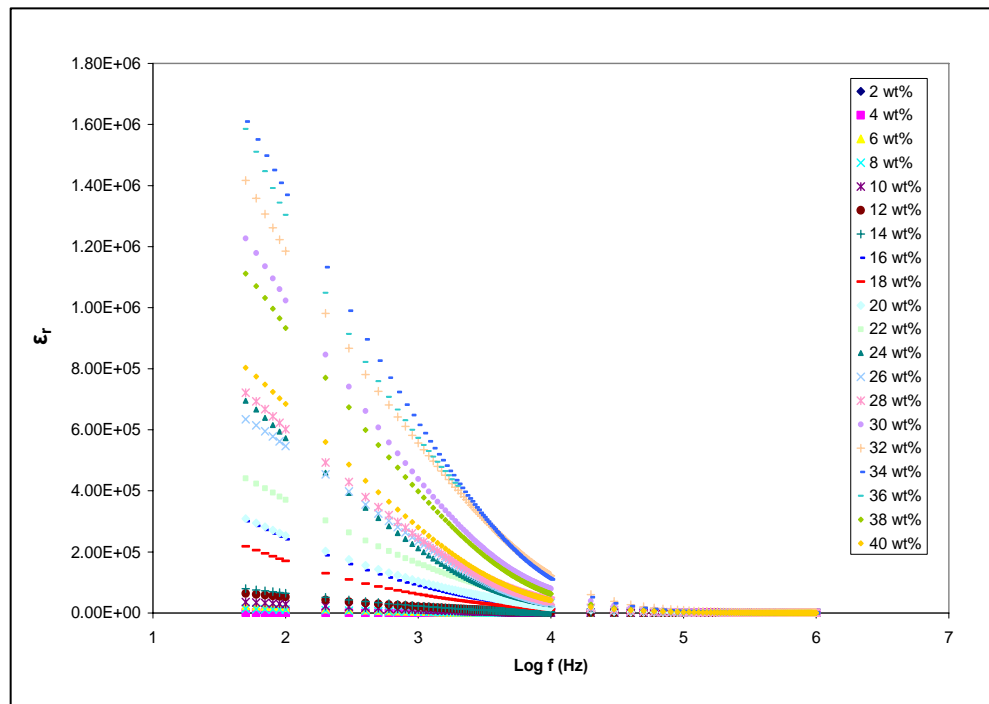


Figure 4.17: Dielectric constant versus frequency for films in the PAN-EC-NaCF₃SO₃ system.

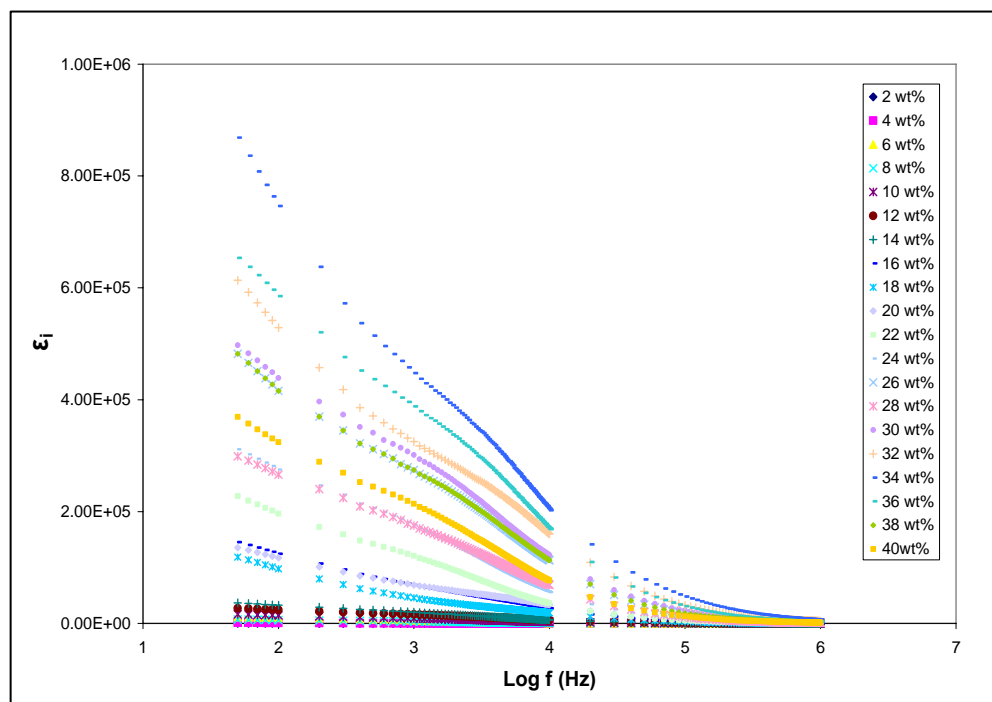


Figure 4.18: Dielectric loss versus frequency for films in the PAN-EC-NaCF₃SO₃ system

4.3 Conductivity-Temperature Dependence Studies

4.3.1 PAN - LiCF₃SO₃ System

In order to understand the mechanism of ionic conduction in polymer electrolytes system, conductivity-temperature dependence measurements are carried out from 303 K to 373 K. Figure 4.19 represents the variation of ionic conductivity with the reciprocal temperature for the highest conductivity film from PAN-LiCF₃SO₃ system containing 26 wt% of LiCF₃SO₃ and the plot shows the conductivity increases with temperature. The linear variation of $\log \sigma$ versus $1000/T$ plots revealed that in the temperature range of 303 K to 373 K, the ionic conductivity data follows Arrhenius equation, $\sigma(T) = \sigma_0 \exp(-E_a/RT)$, where σ_0 is the conductivity pre-exponential factor and E_a is the activation energy for conduction. As the conductivity temperature-dependence data obeys Arrhenius relationship, the nature of cation transport is quite similar to that occurring in ionic crystal, where ions jump into neighboring vacant sites and, hence, increase conductivity to higher value [74]. This is because as temperature increases, the polymer electrolyte can expand easily and produces free volume which ions can easily move [75]. In other words, as temperature increases, the free volume increases, the ions movement increase thus increasing the conductivity. The activation energy, E_a , which is a combination of the energy of defect formation and the energy of defect migration, can be evaluated from the slope of the plots [76]. The activation energy, E_a value obtained for this film is 0.28 eV.

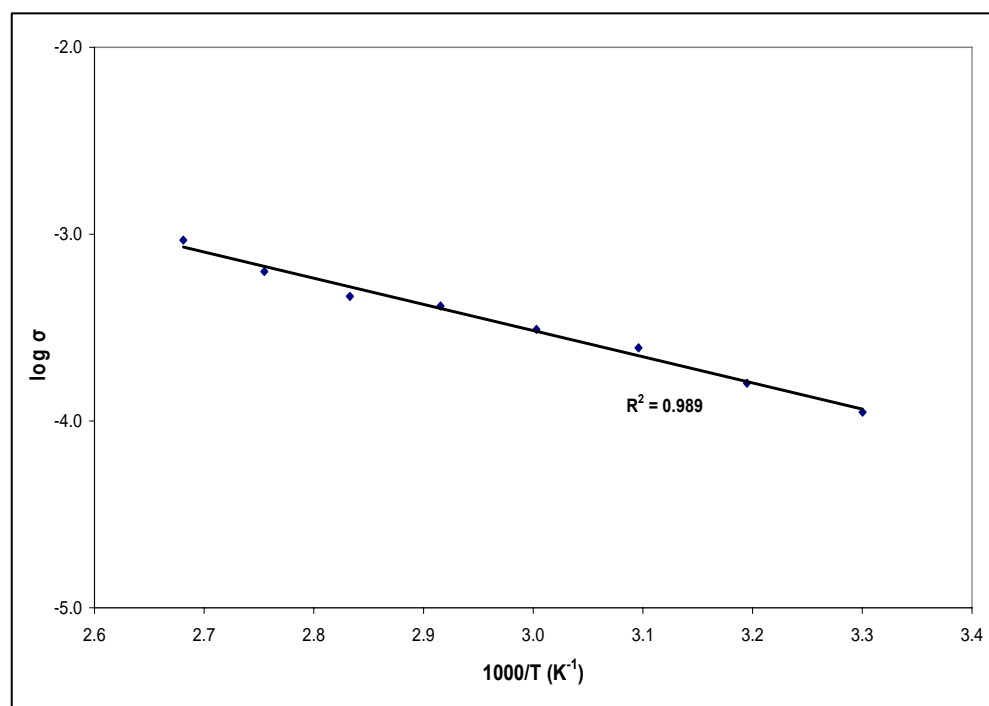


Figure 4.19: Arrhenius plot for the highest conducting film in the PAN-LiCF₃SO₃ system.

Figure 4.20 and 4.21 show the variation of the dielectric constant (ϵ_r) and dielectric loss (ϵ_i) as a function of frequency for LiCF₃SO₃ doped PAN polymer electrolytes at different temperatures. The dielectric constant (ϵ_r) plots indicated that at low frequencies the dielectric constant is high due to the accumulation of the charge carriers near the electrodes. At high frequencies, the periodic reversal of the electric field occurs so fast that there is no excess ion diffusion in the direction of the field. The polarization due to the charge accumulation decreases, leading to the decrease in the value of ϵ_r . The dielectric loss (ϵ_i) for this system becomes very large $\sim 10^3$ at lower frequencies and it increases with temperature due to free charge motion within the material. These values do not correspond to the bulk dielectric processes but are due to the free charges build up at the interface between the material and the electrodes. At very low frequencies there is particularly time or charges to build up at the interfaces

before the field changes the direction and this contributes to very large apparent values of ϵ_i . This phenomenon leads to the so called “conductivity relaxation” [77].

The relationship between the conductivity and the dielectric loss factor is given by $\epsilon_i = \sigma/\omega\epsilon_0$. Since σ is strongly dependent on temperature, the dielectric loss is strongly dependent on temperature and hence the ϵ_i value increase with temperature. From the Figure 4.20 and 4.21, the trends of dielectric constant (ϵ_r) and dielectric loss (ϵ_i), show an increasing value with increasing temperature for the PAN-LiCF₃SO₃ system. The dielectric constant, (ϵ_r) and dielectric loss, (ϵ_i) approach a constant value at high frequencies. This can be explained in terms of the rate of periodic reversal of the electric field, which is so high that there is no access diffusion of ions in the direction of the field. This leads to a decrease in the amount of charge accumulated which in turn results in a decrease in polarization effects causing a similar decrease in the value of the dielectric constant and dielectric loss [78-79].

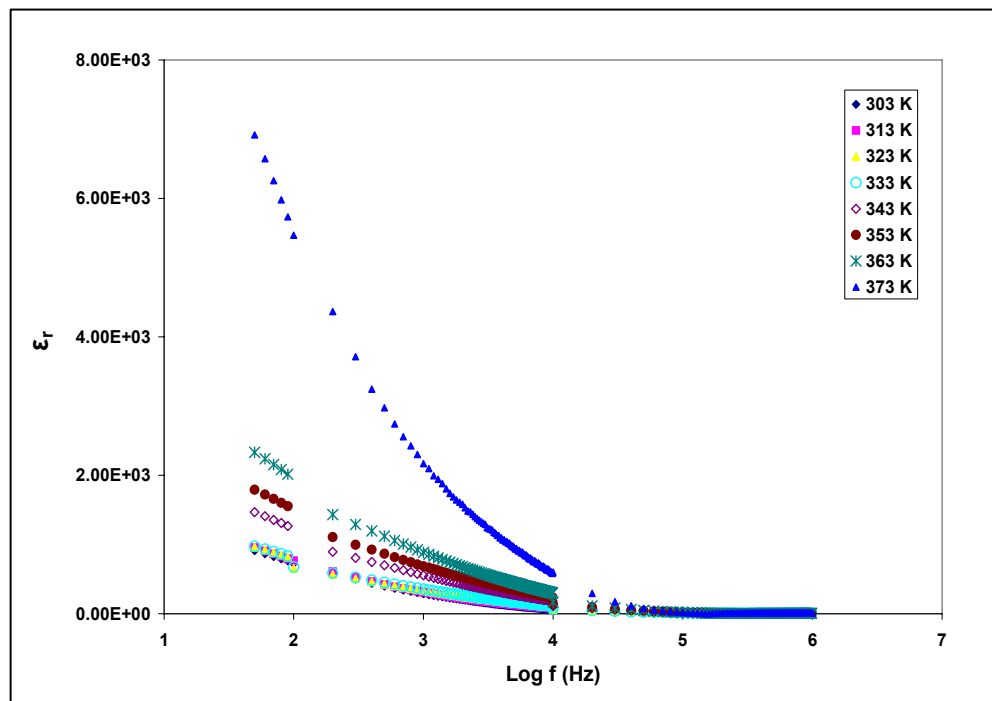


Figure 4.20: Dielectric constant versus frequency for the highest conducting film in the PAN-LiCF₃SO₃ system at different temperatures.

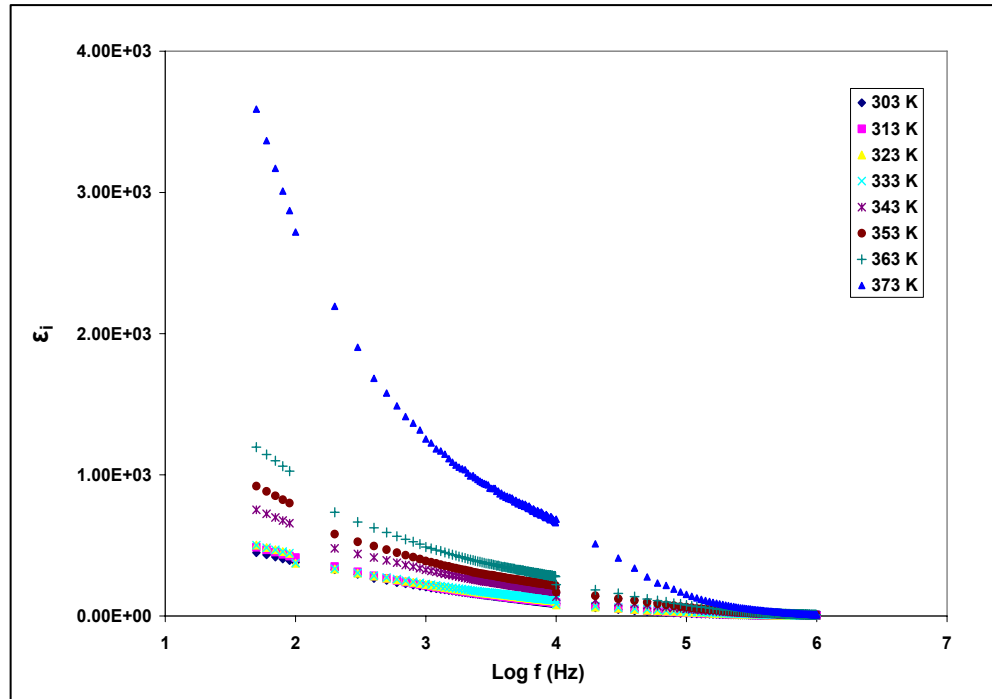


Figure 4.21: Dielectric loss versus frequency for the highest conducting film in the PAN-LiCF₃SO₃ system at different temperatures

4.3.2 PAN - NaCF₃SO₃ System

Figure 4.22 shows the variation of ionic conductivity with the reciprocal temperature for the highest conductivity film from PAN-NaCF₃SO₃ system. The points in the plot lie in an almost straight line and the plot obeys an Arrhenius relation. The activation energy, E_a has been evaluated from the Arrhenius plot using the equation (3.11). The E_a value obtained from this film is 0.23 eV.

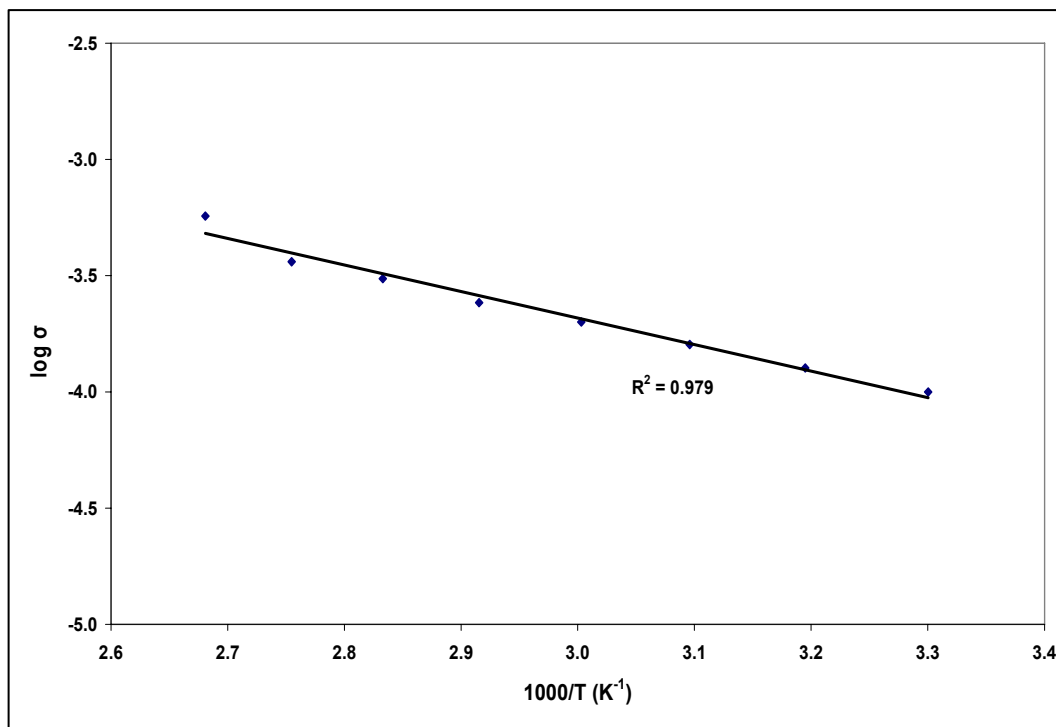


Figure 4.22: Arrhenius plot for the highest conducting film in the PAN- NaCF_3SO_3 system.

It can be observed that PAN- NaCF_3SO_3 system has a higher ionic conductivity and lower activation energy compared to PAN- LiCF_3SO_3 system. This result can be explained based on the Lewis acidity of the alkali ions (the Lewis acidity of Na^+ -ion is weaker than Li^+ -ion), i.e., the strength of the interaction of cations with the Lewis base of polymer electrolyte [80]. The size of Na^+ is larger than Li^+ , thus the interaction between Na^+ and nitrogen atom is weaker than Li^+ . Due to this weak interaction, the de-bonding process between Na^+ ions and nitrogen atom can easily take place, leading to an increase in the number of free ions. These free Na^+ ions then can move easily where ions can jump from one to another nitrogen atom along the backbone of polymer hence increase the conductivity.

The dependence of the dielectric constant, ϵ_r and dielectric loss, ϵ_i on frequency at various temperatures ranging from 303 K to 373 K for the highest conducting PAN- NaCF_3SO_3 film are given in Figure 4.23 and Figure 4.24,

respectively. It can be observed that the dielectric constant, ϵ_r and dielectric loss, ϵ_i appear to increase at higher temperature due to the higher charge carrier density. As temperature increases, the degree of salt dissociation and redissociation of ion aggregates increases resulting the increase in number of free ions due to the increase of free volume.

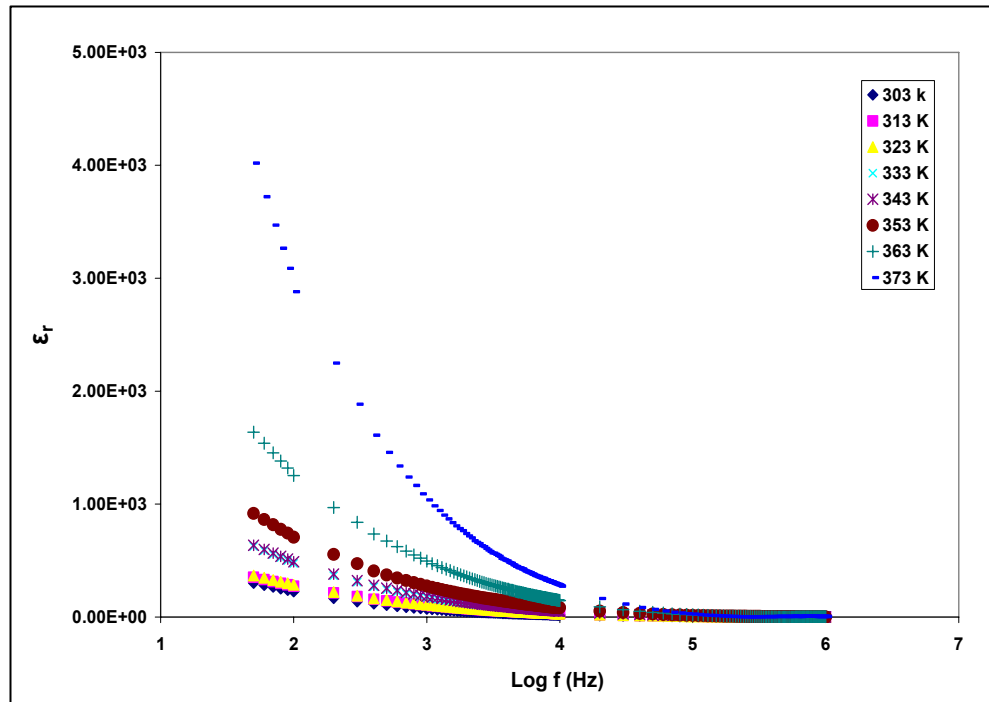


Figure 4.23: Dielectric constant versus frequency for the highest conducting film in the PAN-NaCF₃SO₃ system at different temperatures.

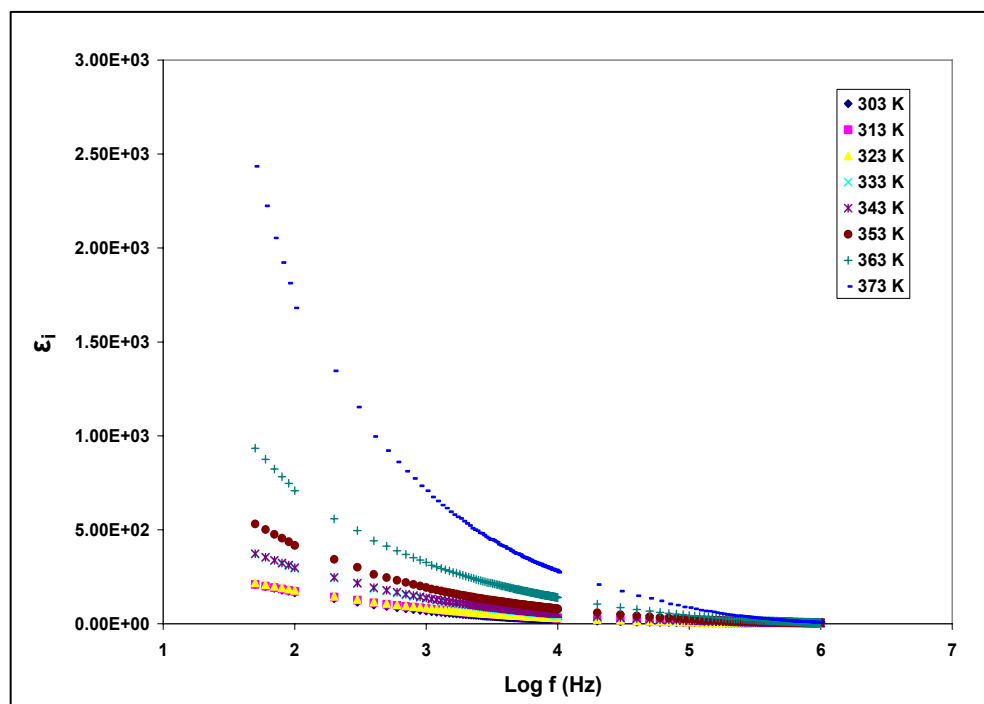


Figure 4.24: Dielectric loss versus frequency for the highest conducting film in the PAN-NaCF₃SO₃ system at different temperatures.

4.3.3 PAN - EC - LiCF₃SO₃ System

Figure 4.25 represents Arrhenius plot for the highest conductivity film from PAN-EC-LiCF₃SO₃ system containing 22 wt% of LiCF₃SO₃. The activation energy, E_a obtained from the film is 0.22 eV. This value is significantly low due to the completely amorphous nature of the polymer electrolytes that facilitates the fast Li-ion motion in the polymer network and it further provides a higher free volume in the ion conducting polymer upon increase in temperature [81].

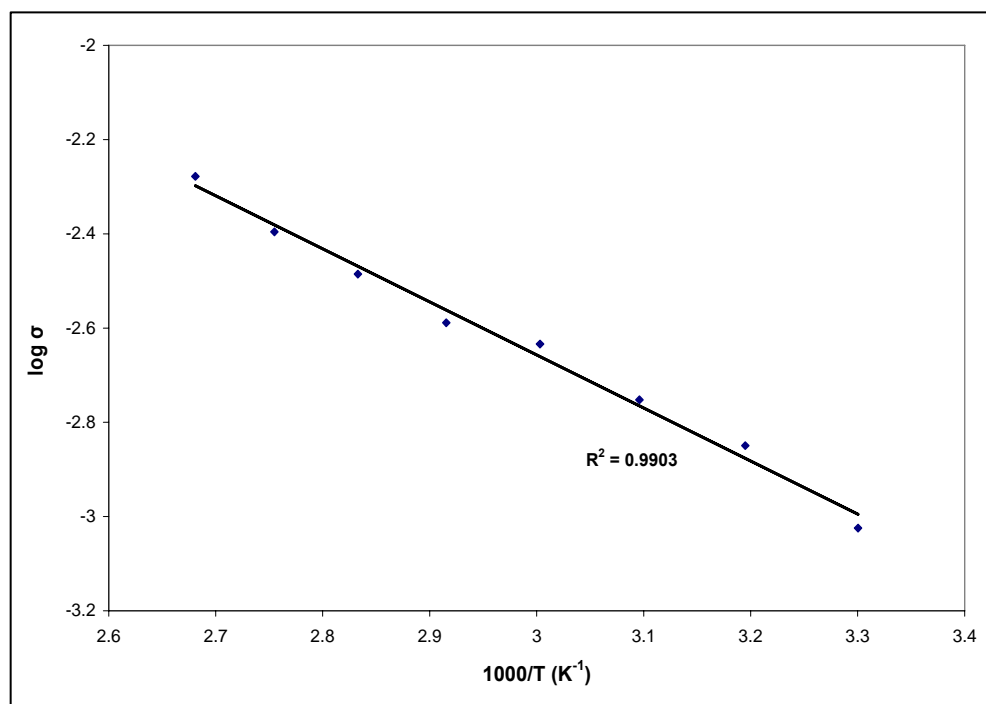


Figure 4.25: Arrhenius plot for the highest conducting film in the PAN-EC-LiCF₃SO₃ system.

Figure 4.26 and 4.27 show the variation of dielectric constant, ϵ_r and dielectric loss, ϵ_i respectively at various temperatures for the highest conducting film in PAN-EC-LiCF₃SO₃ system. The trends of the plots are similar to the plot of dielectric constant, ϵ_r and dielectric loss, ϵ_i at various temperatures discussed in the earlier system indicating that the same phenomenon applies. As the temperature increases, the value of dielectric constant, ϵ_r and dielectric loss, ϵ_i also increase due to the higher charge carrier density.

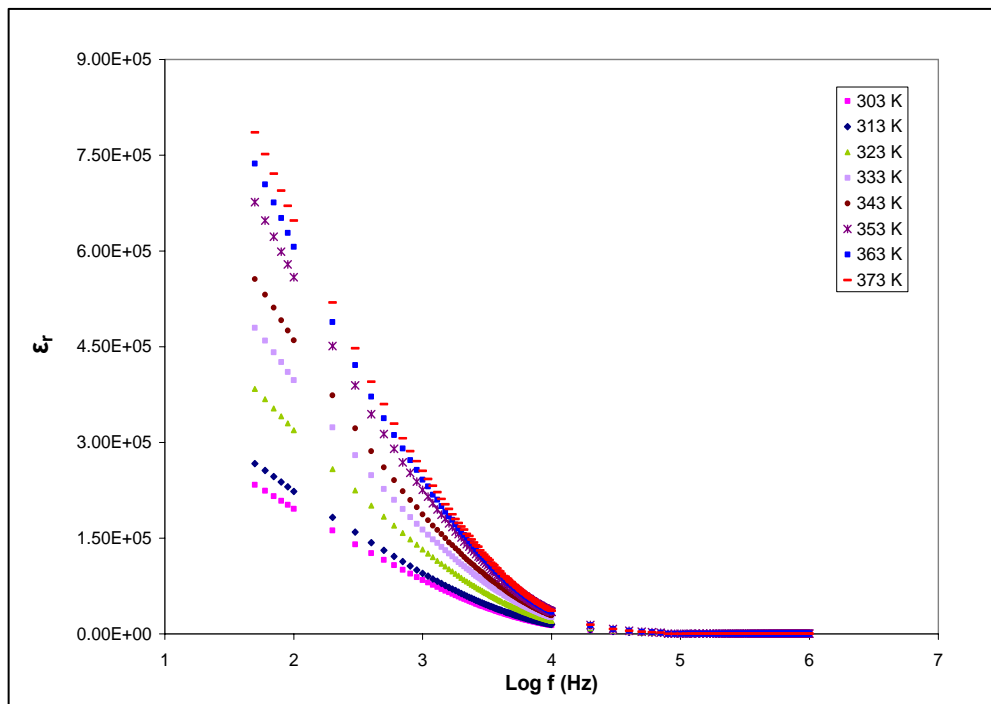


Figure 4.26: Dielectric constant versus frequency for the highest conducting film in the PAN-EC-LiCF₃SO₃ system at different temperatures.

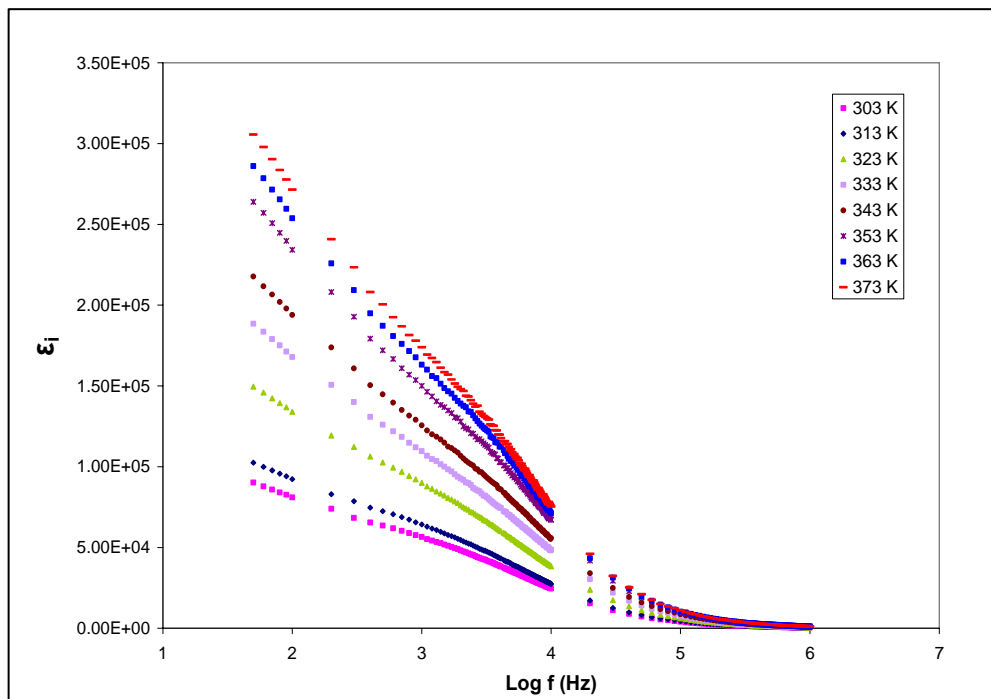


Figure 4.27: Dielectric loss versus frequency for the highest conducting film in the PAN-EC-LiCF₃SO₃ system at different temperatures.

4.3.4 PAN - EC - NaCF₃SO₃ System

Figure 4.28 represents Arrhenius plot for the highest conductivity film from PAN-EC-NaCF₃SO₃ system containing 34 wt.% of NaCF₃SO₃. The activation energy, E_a obtained from the film is 0.19 eV. The trends of dielectric constant, ϵ_r and dielectric loss, ϵ_i from Figure 4.29 and Figure 4.30, show an increasing value with increasing the temperature for the highest conducting film in the PAN-EC-NaCF₃SO₃ system. The higher dielectric constant, ϵ_r and dielectric loss, ϵ_i at higher temperature and hence higher conductivity with increasing temperature are due to the higher charge density. This also shows that the film has more ions movement which is assisted by heat when the temperature increases and this behaviour is the same as explained in the previous systems.

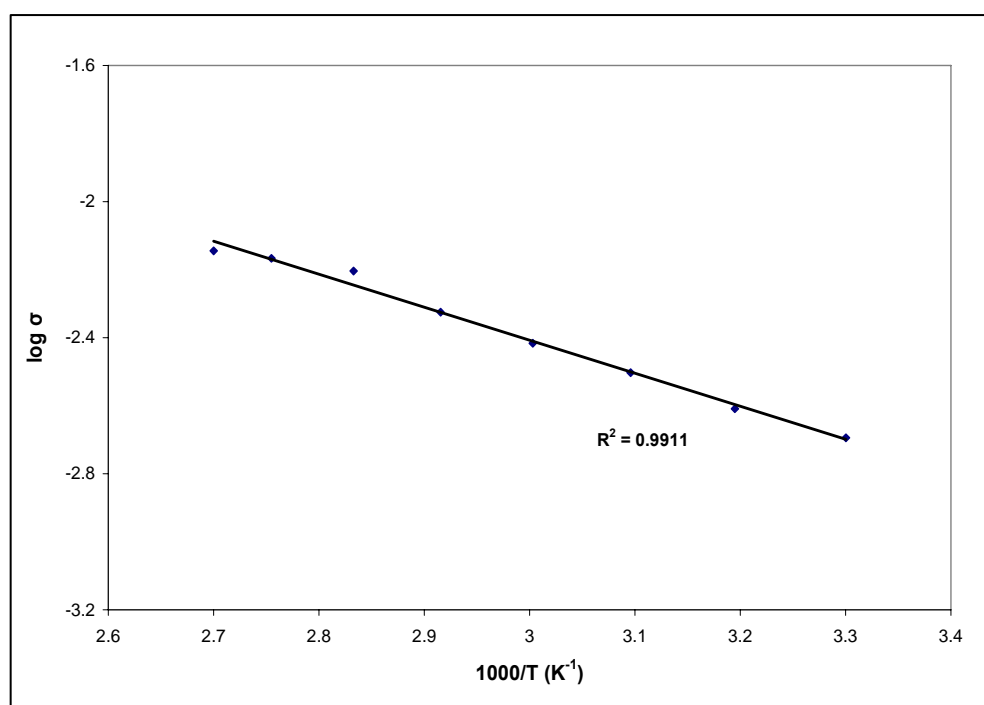


Figure 4.28: Arrhenius plot for the highest conducting film in the PAN-EC-NaCF₃SO₃ system.

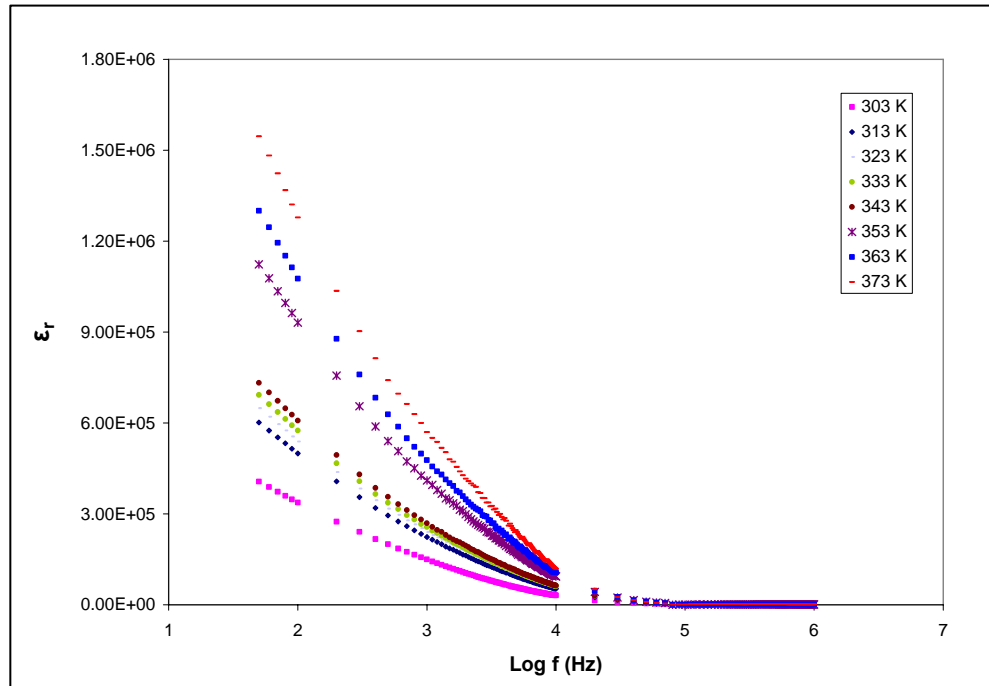


Figure 4.29: Dielectric constant versus frequency for the highest conducting film in the PAN-EC-NaCF₃SO₃ system at different temperatures.

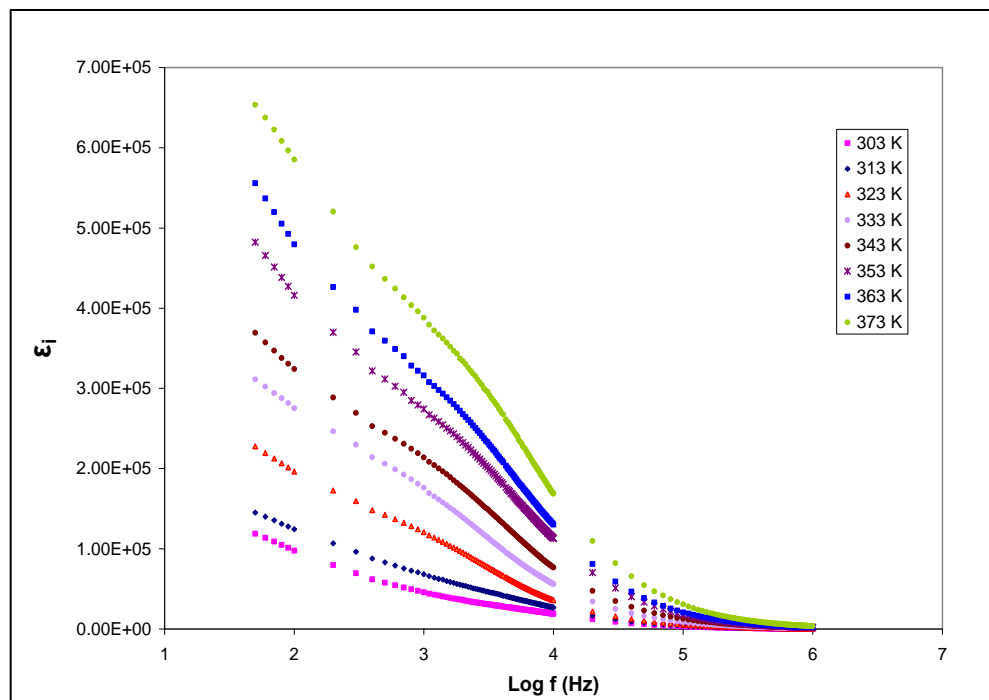


Figure 4.30: Dielectric loss versus frequency for the highest conducting film in the PAN-EC-NaCF₃SO₃ system at different temperatures.

4.4 Conductivity-Pressure Dependence Studies

The conductivity-pressure studies are carried out in the range of pressure between 0.01 MPa and 0.09 MPa for the highest room temperature conductivity from the PAN-LiCF₃SO₃, PAN-NaCF₃SO₃, PAN-EC-LiCF₃SO₃ and PAN-EC-NaCF₃SO₃ systems. Figure 4.31 (a), (b), (c) and (d) represented conductivity variations with pressure at room temperature for all system.

Conductivity is seen to decrease with increasing pressure for all systems. The conductivity decreases with the pressure, presumably because of a decrease in ionic mobility. This is because as pressure increases, defects are pushed closer together and become clustered, the free volume decreases thus decreases the conductivity [82]. In most previous works, the pressure variation of the electrical conductivity has been analyzed in terms of an activation volume [19, 83-85]. The observed linear dependence of logarithmic variation of electrical conductivity versus pressure allows a volume ΔV^* to be calculated by the equation (3.12).

Since the conductivities of all systems follow an Arrhenius type law at constant pressure, this volume is called an “activation volume”. The activation volume is the difference in volume between a mole of moving species in its activated transition state (at the top of the energy barrier) and its volume at normal equilibrium. The decrease of conductivity values with increasing pressure are related to the basis of the free volume model. Since free volume is the volume available for motion and the activation volume is the volume change required for motion, they behave oppositely i.e. large activation volumes are associated with small free volume and vice versa.

The activation volume, ΔV^* can be evaluated from the slope of the plots in Figure 4.31. The ΔV^* value obtained for all system are $3.04 \times 10^{-2} \text{ cm}^3/\text{mol}$, $2.86 \times 10^{-2} \text{ cm}^3/\text{mol}$, $1.37 \times 10^{-2} \text{ cm}^3/\text{mol}$ and $1.11 \times 10^{-2} \text{ cm}^3/\text{mol}$ for the highest conductivity films from the PAN-LiCF₃SO₃ system, the PAN-NaCF₃SO₃ system, the PAN-EC-LiCF₃SO₃

system and the PAN-EC- NaCF_3SO_3 system, respectively. For comparison, the activation volume values and the conductivity values for each system are summarized in Table 4.6. It can be observed that the system (PAN-EC- NaCF_3SO_3) with the highest conducting sample has the smallest activation volume. So, it can be concluded that only a small ΔV^* required for ion motion in this sample compared to other systems.

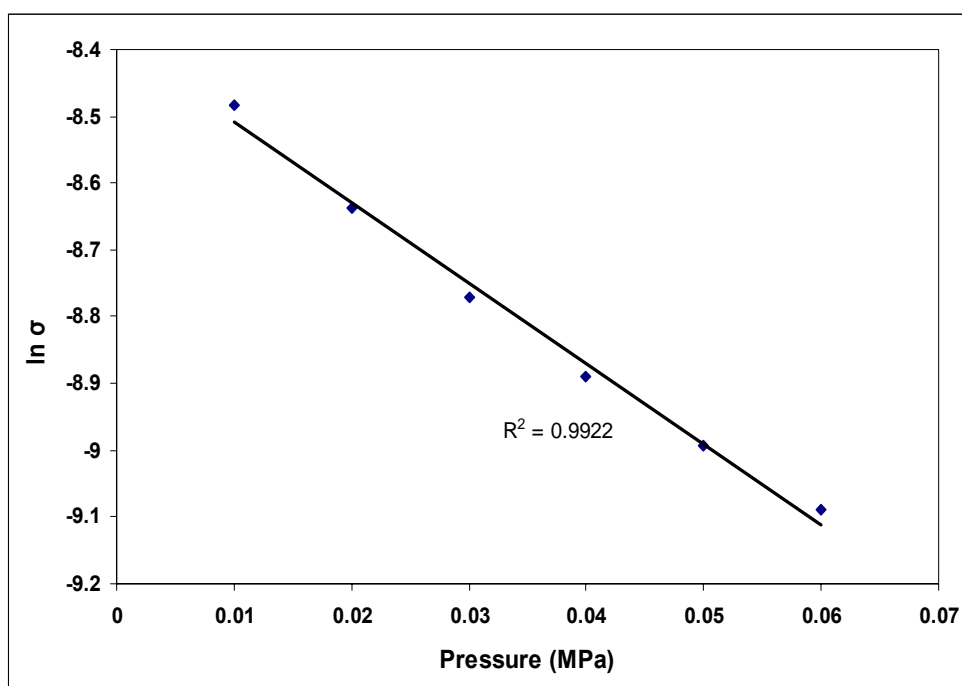


Figure 4.31 (a): The conductivity versus pressure for the highest conducting film in the PAN- LiCF_3SO_3 system.

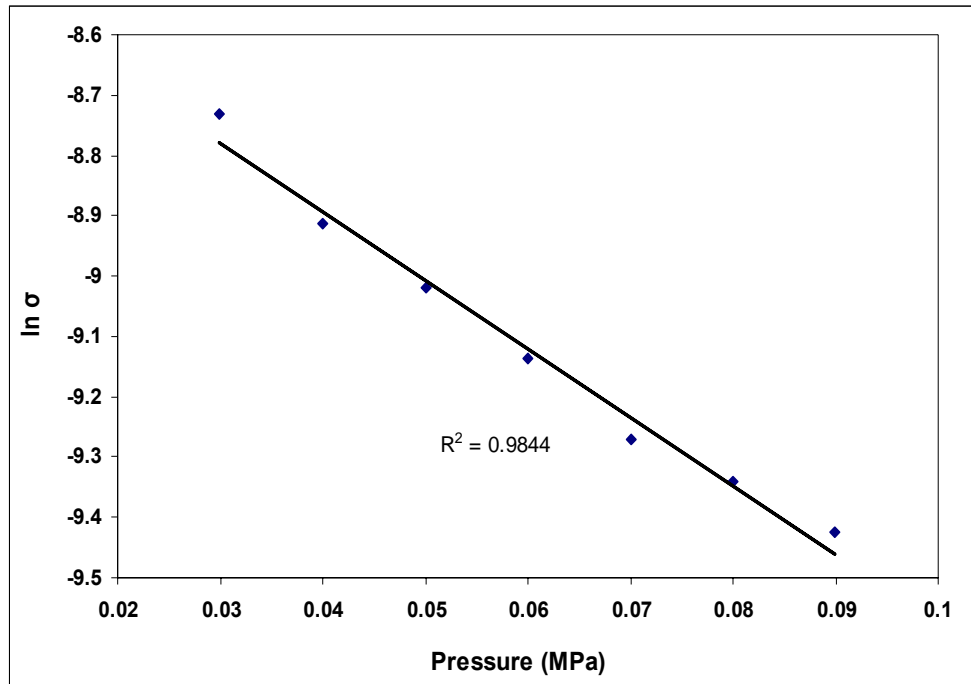


Figure 4.31 (b): The conductivity versus pressure for the highest conducting film in the PAN-NaCF₃SO₃ system.

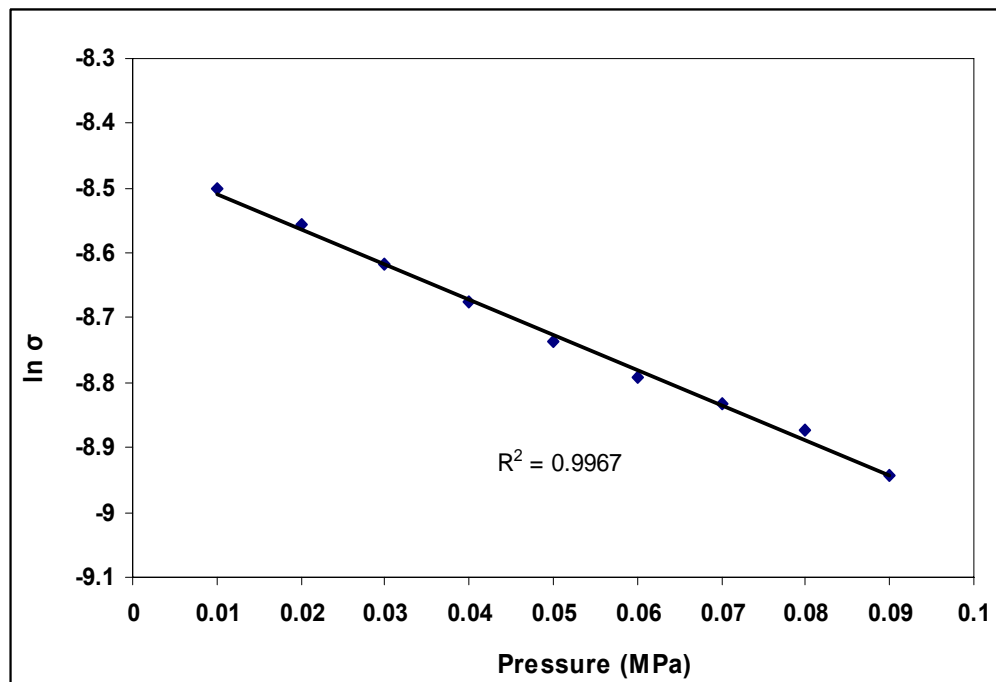


Figure 4.321 (c): The conductivity versus pressure for the highest conducting film in the PAN-EC-LiCF₃SO₃ system.

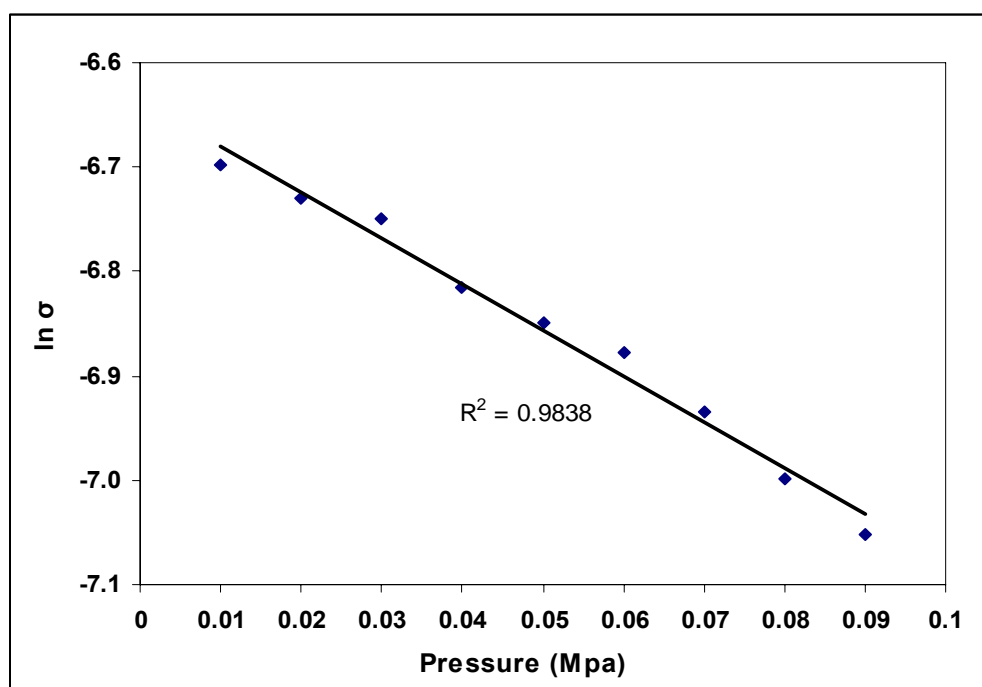


Figure 4.31 (d): The conductivity versus pressure for the highest conducting film in the PAN-EC-NaCF₃SO₃ system.

Table 4.6: The conductivity, σ and activation volume, ΔV^* for the highest conducting film from PAN-LiCF₃SO₃, PAN-NaCF₃SO₃, PAN-EC-LiCF₃SO₃ and PAN-EC-NaCF₃SO₃ systems.

System	Conductivity, σ	Activation Volume (ΔV^*)
PAN+26 wt.% LiCF ₃ SO ₃	$3.04 \times 10^{-4} \text{ S cm}^{-1}$	$3.04 \times 10^{-2} \text{ cm}^3/\text{mol}$
PAN+24 wt.% NaCF ₃ SO ₃	$7.13 \times 10^{-4} \text{ S cm}^{-1}$	$2.86 \times 10^{-2} \text{ cm}^3/\text{mol}$
PAN+EC+22 wt.% LiCF ₃ SO ₃	$1.32 \times 10^{-3} \text{ S cm}^{-1}$	$1.37 \times 10^{-2} \text{ cm}^3/\text{mol}$
PAN+EC+34 wt.% NaCF ₃ SO ₃	$5.49 \times 10^{-3} \text{ S cm}^{-1}$	$1.11 \times 10^{-2} \text{ cm}^3/\text{mol}$

CHAPTER 5:

Results and Discussion

-FTIR Studies-

5.1 FTIR Analysis

The Fourier Transform Infrared (FTIR) spectra were recorded in the range 4000–400 cm^{-1} using MAGNA-IR550 spectrophotometer to identify the complexation of the prepared polymer electrolytes films. The purpose of this analysis is also to study the effect of the plasticizer (EC) and salts (LiCF_3SO_3 and NaCF_3SO_3) on the pure PAN film.

5.2 Pure PAN Film

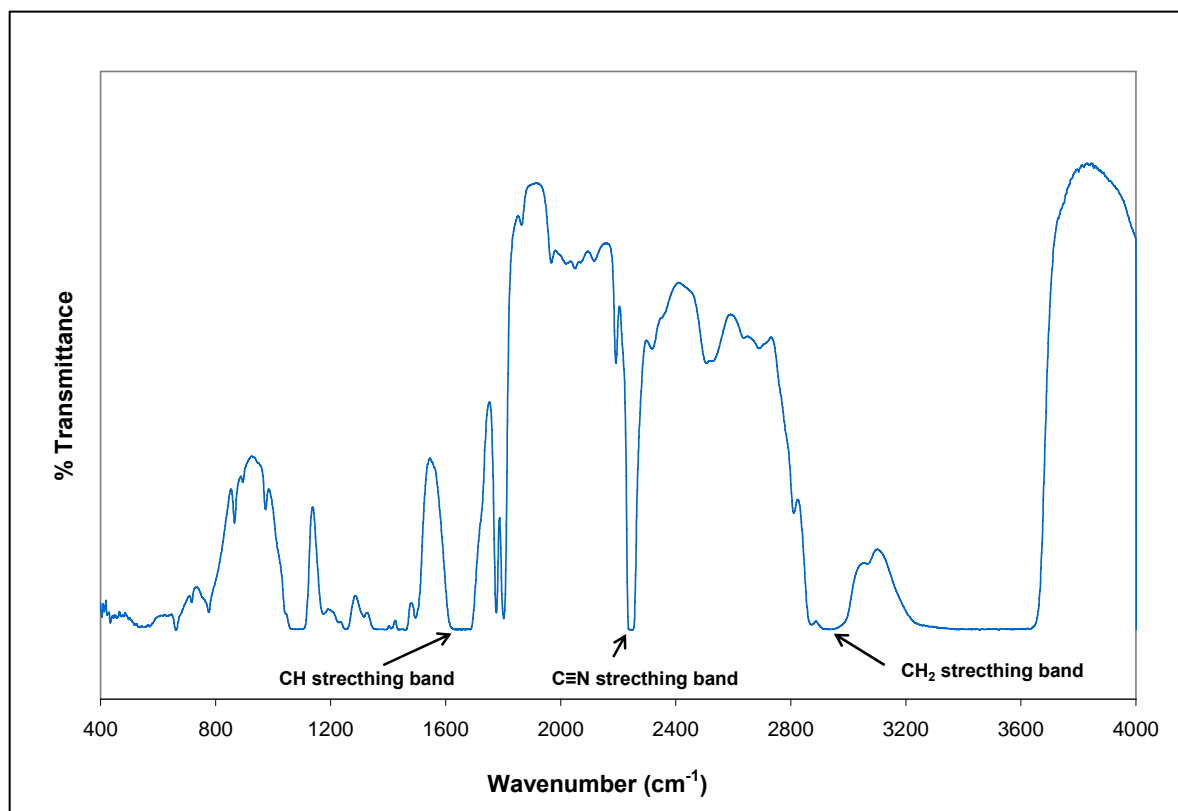


Figure 5.1: FTIR spectrum for pure PAN film in the region 400 cm^{-1} and 4000 cm^{-1}

Table 5.1: The vibrational mode and wavenumbers of pure PAN film.

Vibrational modes	Wavenumbers (cm ⁻¹)	References	Wavenumbers obtained from the work (cm ⁻¹)
C ≡ N (Symmetrical stretching)	1) 2248 2) 2239 3) 2241 4) 2240	[86] [87] [88] [25]	2247
CH ₂ (Symmetrical stretching)	2940	[86] [25] [43]	2933
CH (Asymmetrical stretching)	1623	[25] [43]	1655

Figure 5.1 shows FTIR spectrum of pure PAN in the region of 400 cm⁻¹ and 4000 cm⁻¹. The vibrational band in the pure PAN spectra obtained from this work and literature review is listed in Table 5.1. Band at 2247 cm⁻¹, 2933 cm⁻¹ and 1655 cm⁻¹ are assigned to C ≡ N stretching, CH₂ stretching and CH stretching, respectively. Since the structure of PAN involves only a high density of C ≡ N groups, this vibrational bands is expected to be changed in the plasticized PAN films, salted PAN films and also plasticized salted PAN films.

5.3 Pure EC

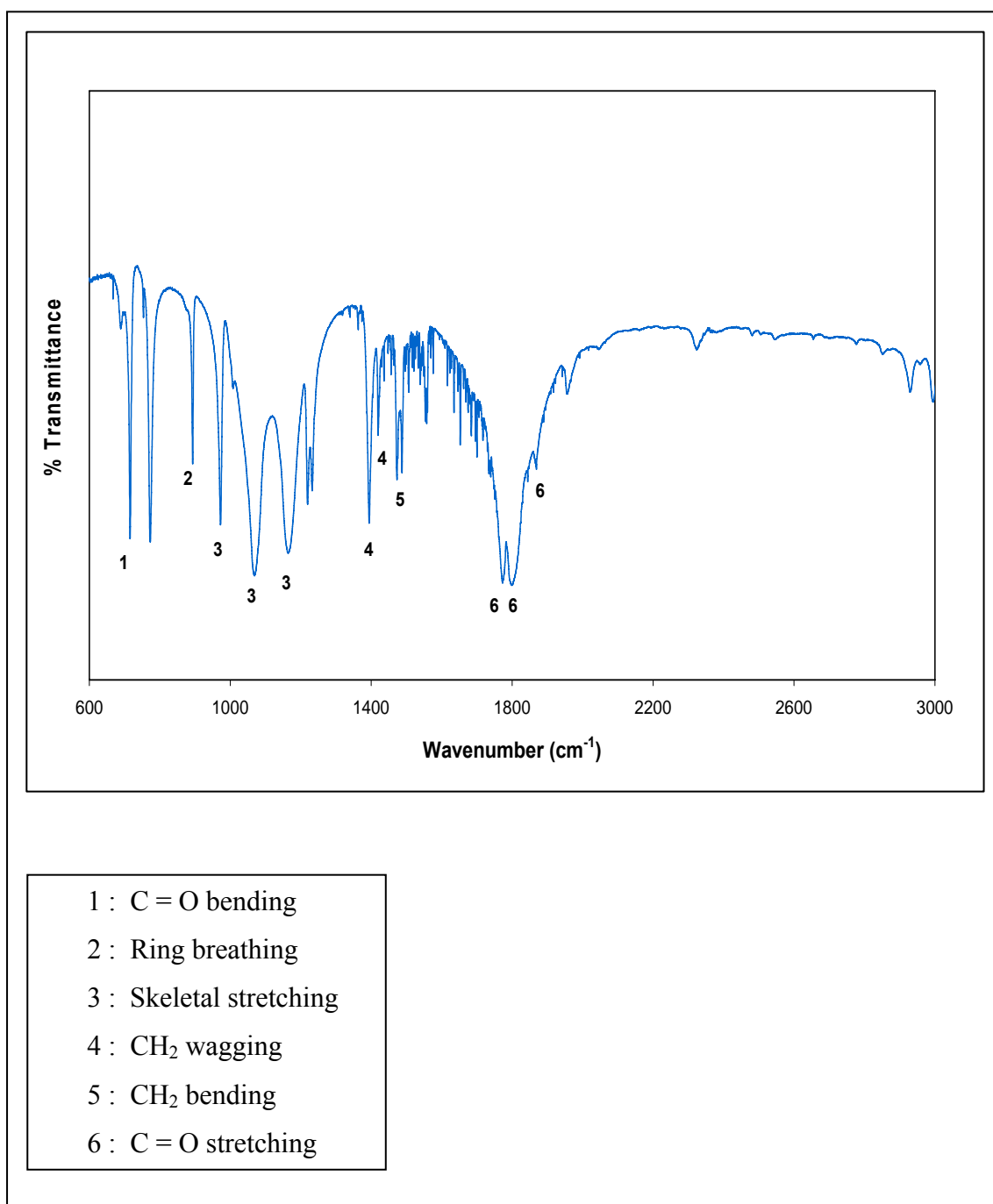


Figure 5.2: FTIR spectrum for pure EC in the region 600 cm⁻¹ and 3000 cm⁻¹

Table 5.2: The vibrational modes and wavenumbers of pure EC.

Vibrational modes	Wavenumbers (cm ⁻¹)	References	Wavenumbers obtained from the work (cm ⁻¹)
C = O bending	717	[89]	717
Ring breathing	1067, 890	[90]	893
Skeletal stretching	970,1076,1180	[91]	973, 1070, 1170
CH ₂ wagging	1394, 1420	[92]	1400, 1420
CH ₂ bending	1480	[91]	1470
C = O stretching	1810-1871, 1774 & 1803, 1773 & 1798, 1795	[91-93] [90]	1780, 1810, 1870

Figure 5.2 shows the FTIR spectrum of pure EC film in the region between 600 cm⁻¹ and 2000 cm⁻¹. The peaks appearing at 717 cm⁻¹ and 893 cm⁻¹ are due to C = O bending and ring breathing, respectively. The skeletal stretching frequencies are found at 973 cm⁻¹, 1070 cm⁻¹ and 1170 cm⁻¹. The group of frequencies at 1400 cm⁻¹ and 1420 cm⁻¹ are assigned to CH₂ wagging. The peak at 1470 cm⁻¹ may be assigned to CH₂ bending. Wang and co-workers reported that EC has a pair of intense doublets at 1770 cm⁻¹ and 1798 cm⁻¹ [90]. These doublets are due to C = O stretching mode. In this work, the doublets are found at 1780 cm⁻¹ and 1810 cm⁻¹. The C = O stretching band is also observed at 1870 cm⁻¹. Table 5.2 lists the vibrational band in the pure EC spectra obtained from this work and literature review.

Figure 5.3 shows the FTIR spectra of pure PAN, pure EC and films in the PAN-EC system in the region between 600 cm⁻¹ and 1000 cm⁻¹. The intensity of absorption peak observed at 717 cm⁻¹ in pure EC spectrum is found to be decreased in plasticized PAN films. It also can be observed from the figure some of the absorption peaks in pure

EC is shifted and broaden in PAN complexes. The FTIR spectra of pure PAN, pure EC and films in the PAN-EC system in the region between 1000 cm^{-1} and 1500 cm^{-1} is shown in Figure 5.4. The skeletal stretching peaks at 1070 cm^{-1} and 1170 cm^{-1} in pure EC film are broadening in the PAN complexes. Broad peaks that occurred at 1400 cm^{-1} and 1420 cm^{-1} in polymer complexes are assigned to CH_2 wagging in pure EC. The absorption peaks at 1470 cm^{-1} of pure EC which is due to CH_2 bending is shifted to 1481 cm^{-1} in the complexes. Figure 5.5 shows the FTIR spectra of pure PAN, pure EC and films in the PAN-EC system in the region between 1500 cm^{-1} and 2000 cm^{-1} . The common spectral features also can be observed in this figure. The $\text{C}=\text{O}$ stretching bands at 1780 cm^{-1} and 1810 cm^{-1} are shifted and broaden with further addition of plasticizer in PAN complexes. It also found that the intensity of absorption peak at 1870 cm^{-1} is increase in plasticized PAN system. The changes in the position of vibrational modes of pure EC in the polymer complexes indicate that the complexation between PAN and EC has occurred.

Figure 5.6 shows the FTIR spectra of pure PAN, pure EC and films in the PAN-EC system in the region between 2000 cm^{-1} and 3000 cm^{-1} . It can be observed from the figure, the intensity peak of $\text{C}\equiv\text{N}$ stretching band at 2247 cm^{-1} for pure PAN is increase in PAN complexes. It can be suggested that the interaction has occurred between carbon atom in the $\text{C}=\text{O}$ group of EC and the nitrogen atom of $\text{C}\equiv\text{N}$ group in PAN.

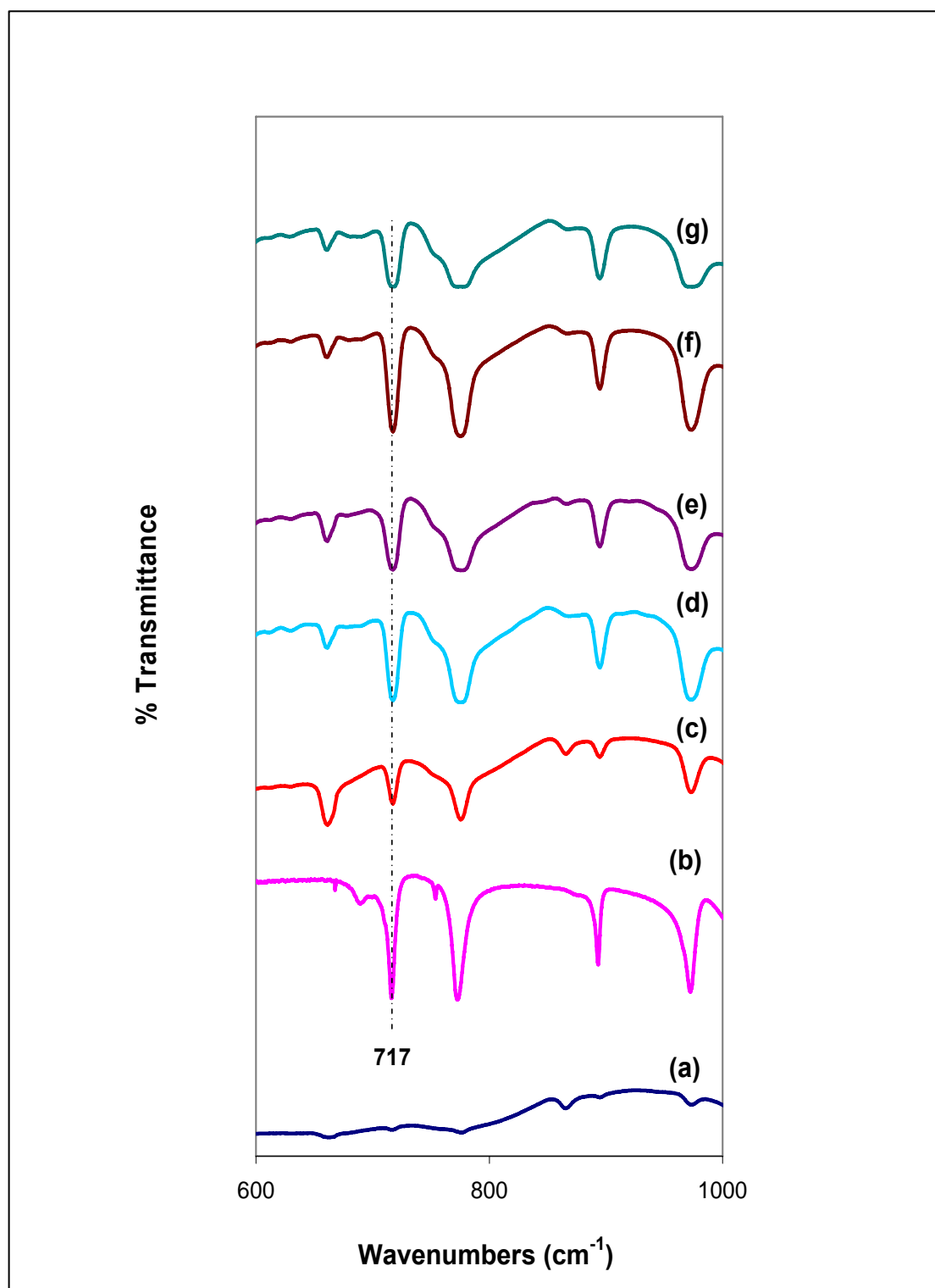


Figure 5.3: FTIR spectra of (a) pure PAN film (b) EC (c) PAN + 8 wt.% EC film (d) PAN + 16 wt.% EC film (e) PAN + 24 wt.% EC film (f) PAN + 26 wt.% EC film and (g) PAN + 30 wt.% EC film.

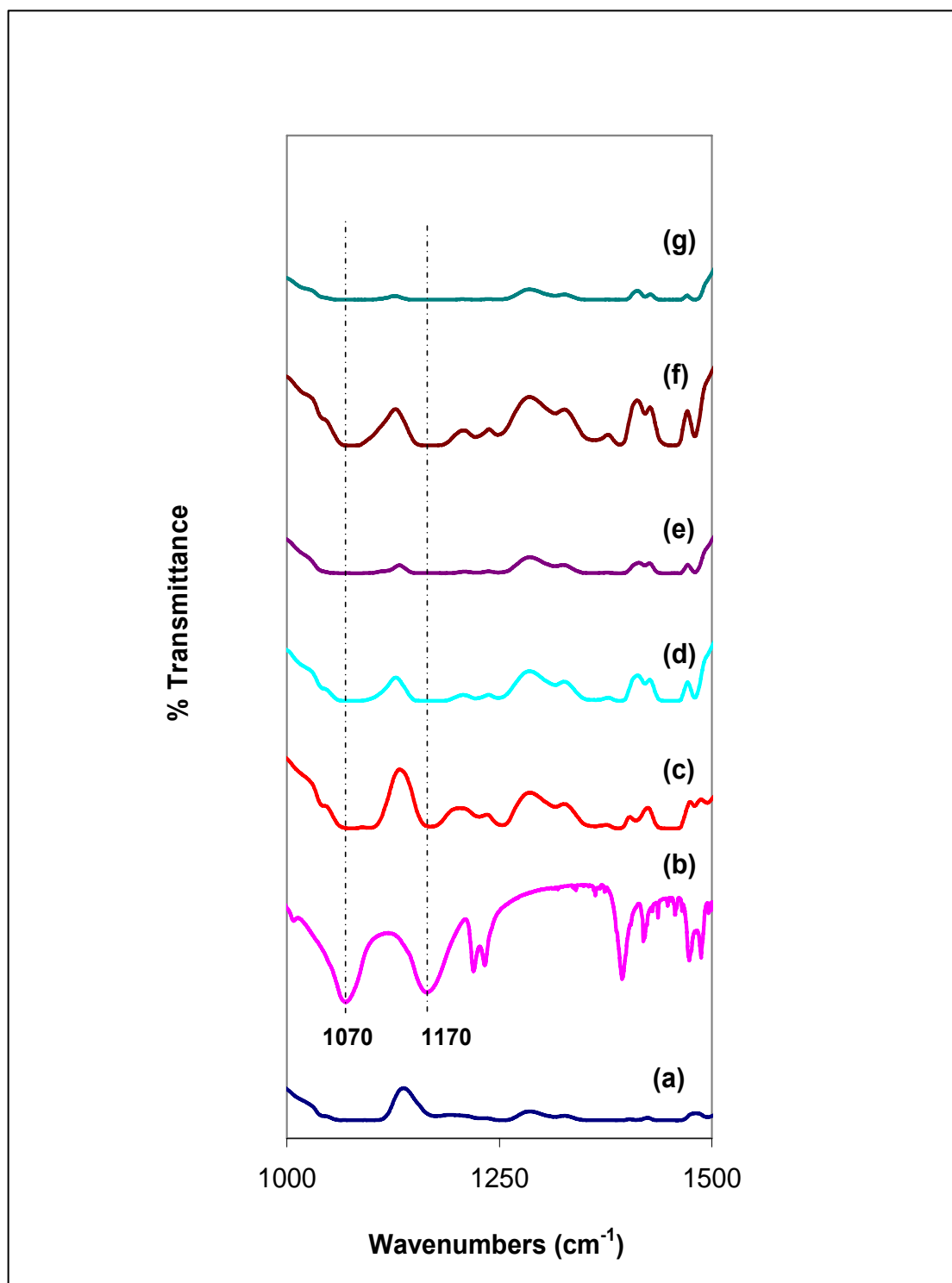


Figure 5.4: FTIR spectra of (a) pure PAN film (b) EC (c) PAN + 8 wt.% EC film (d) PAN + 16 wt.% EC film (e) PAN + 24 wt.% EC film (f) PAN + 26 wt.% EC film and (g) PAN + 30 wt.% EC film

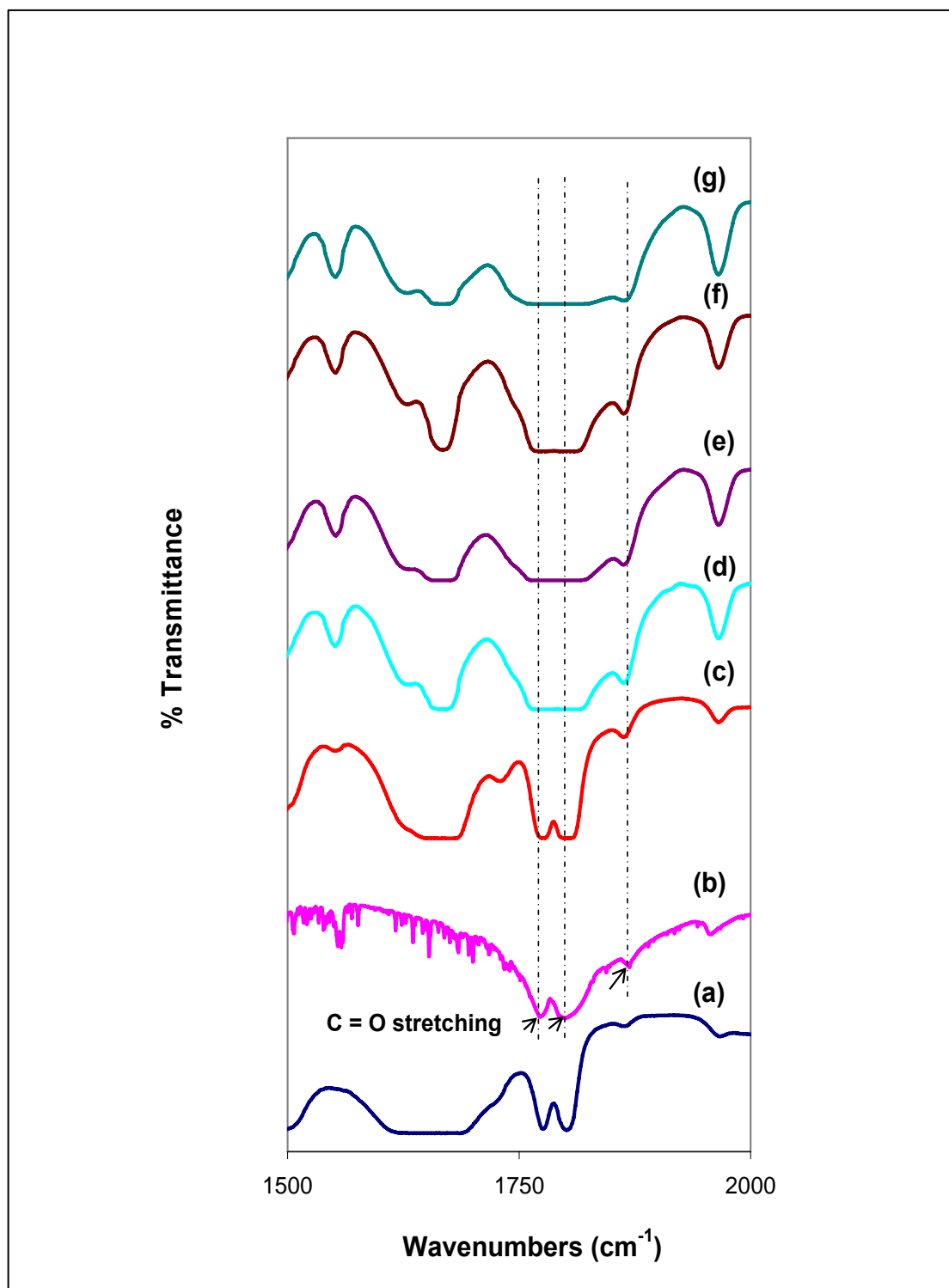


Figure 5.5: FTIR spectra of (a) pure PAN film (b) EC (c) PAN + 8 wt.% EC film (d) PAN + 16 wt.% EC film (e) PAN + 24 wt.% EC film (f) PAN + 26 wt.% EC film and (g) PAN + 30 wt.% EC film

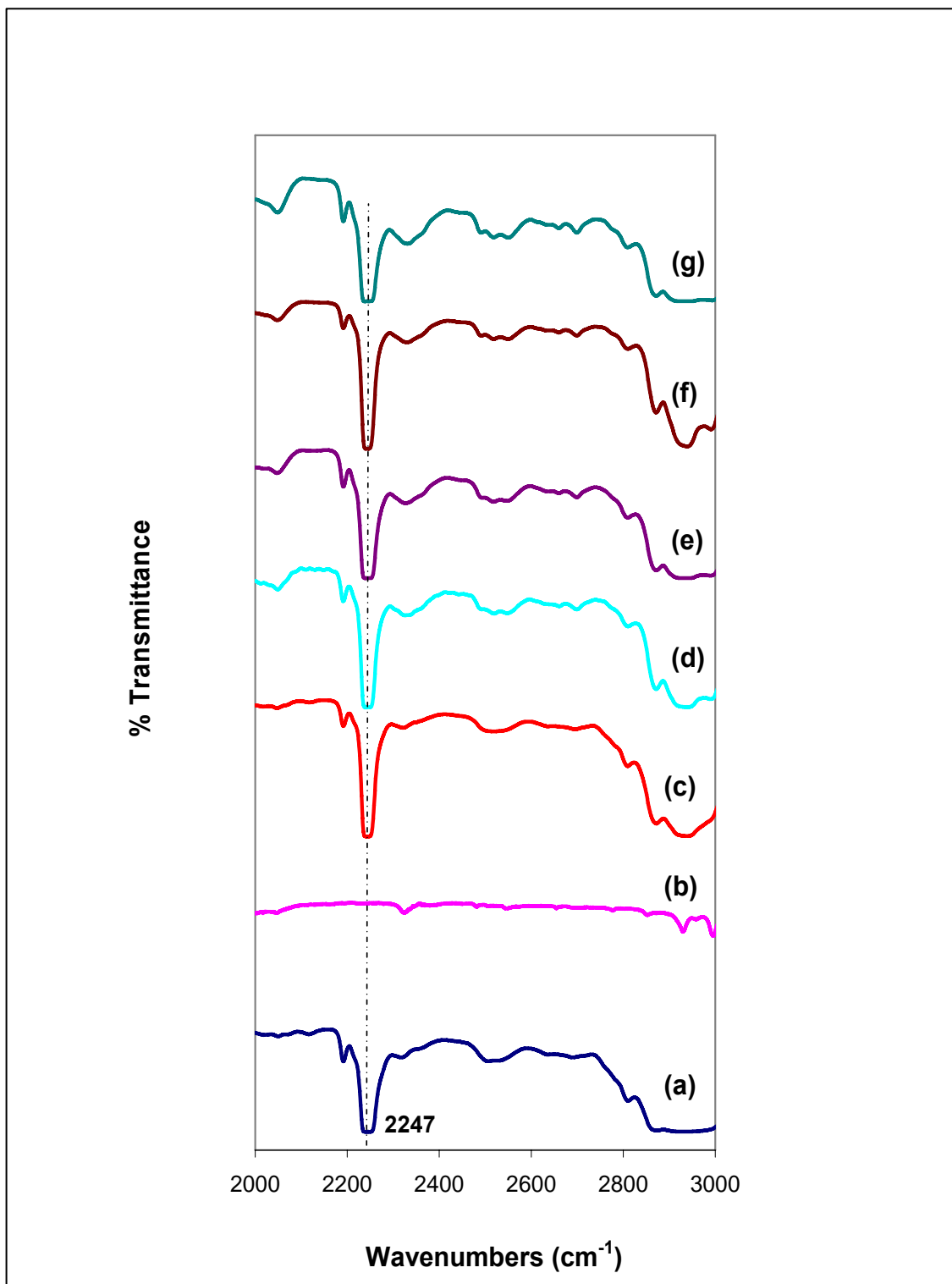


Figure 5.6: FTIR spectra of (a) pure PAN film (b) EC (c) PAN + 8 wt.% EC film (d) PAN + 16 wt.% EC film (e) PAN + 24 wt.% EC film (f) PAN + 26 wt.% EC film and (g) PAN + 30 wt.% EC film.

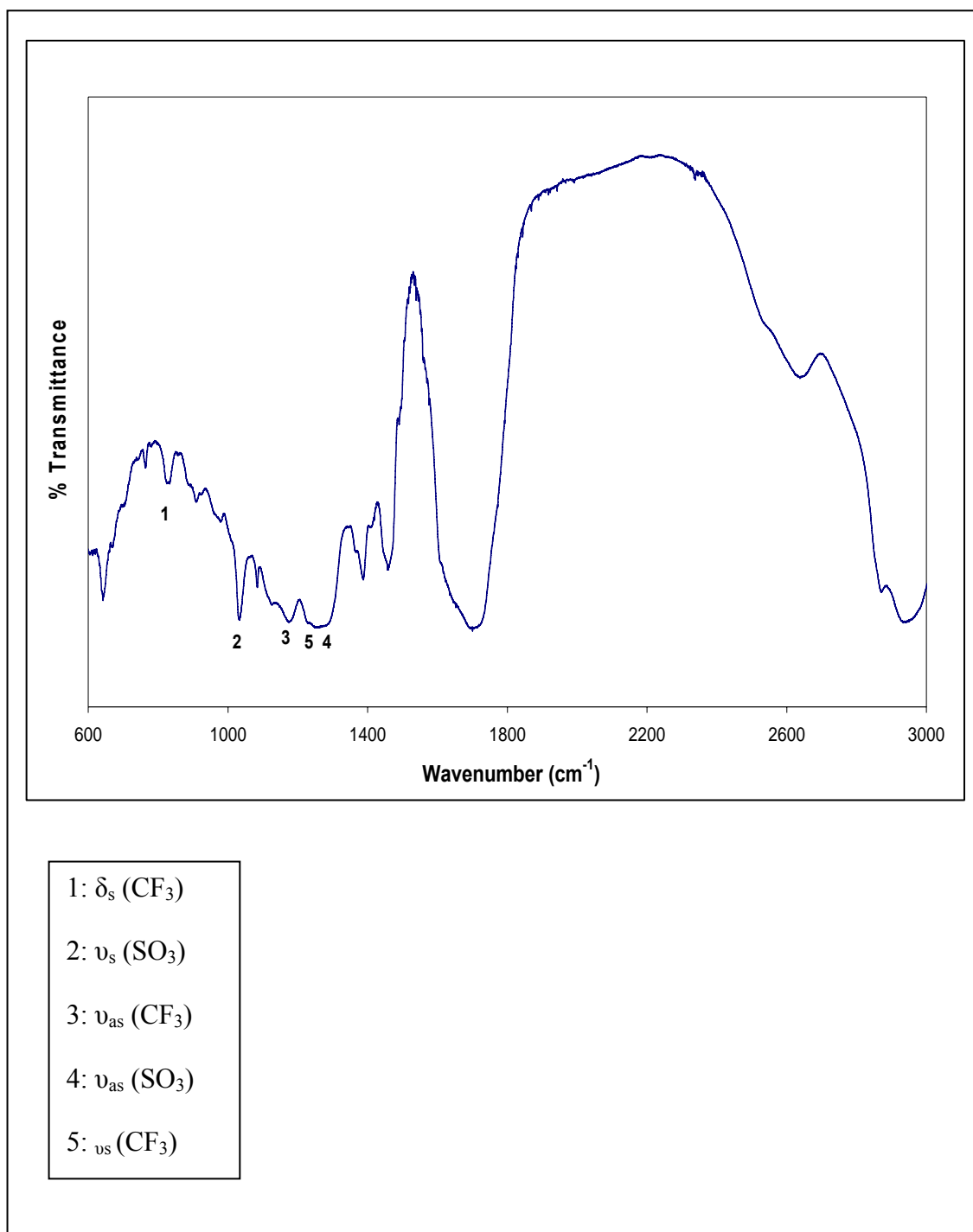
5.4 PAN - LiCF₃SO₃ System**Figure 5.7:** FTIR spectrum of LiCF₃SO₃ salt.

Table 5.3: The vibrational modes and wavenumbers of LiCF₃SO₃ salt.

Vibrational modes	Wavenumbers (cm ⁻¹)	References	Wavenumbers obtained from the work (cm ⁻¹)
δ_s (CF ₃)	766,757	[94,95]	766
ν_s (SO ₃)	1033, 1043,1053,1062	[90]	1036
ν_{as} (CF ₃)	1182	[91]	1186
ν_{as} (SO ₃)	1272, 1257, 1302, 1260.	[95]	1271
ν_s (CF ₃)	1230	[91]	1236

On addition of salt into polymer electrolytes, the cation of the salt is expected to coordinate with the polar groups in the host polymer matrix resulting in the complexation. This interaction will influence the local structure of the polymer backbone and certain modes of vibration will also be affected.

The vibrational modes and wavenumbers of LiCF₃SO₃ salt are listed in Table 5.3. Figure 5.7 shows the FTIR spectra for LiCF₃SO₃ salt in the region between 600cm⁻¹ and 3000 cm⁻¹. In spectroscopic studies of triflate containing polymer electrolytes, attention has been focused almost exclusively on the CF₃ symmetric deformation δ_s (CF₃) and SO₃ symmetric stretching ν_s (SO₃) modes. The δ_s (CF₃) have been well established to reflect the ionic association of the triflate anion at the SO₃ end through electronic distribution. The ν_s (SO₃) is particularly sensitive to ionic association since the oxygens of the triflate interact with the cations of the salt [96].

Figure 5.8 presents the FTIR spectra of pure PAN, LiCF₃SO₃ and films in the PAN-LiCF₃SO₃ system in the region between 650 cm⁻¹ and 850 cm⁻¹. The band at 766 cm⁻¹ in pure LiCF₃SO₃ shows a symmetric deformation δ_s (CF₃) peak. The CF₃ symmetric deformation δ_s (CF₃) spectral region contains distinct band due to several

ionically associated species i.e “free” ions, contact ion pairs (LiCF_3SO_3) and the aggregate species (associated triflate ion) $[\text{Li}_2\text{CF}_3\text{SO}_3]^+$ [10]. This peak was shifted into distinct doublet at 760 cm^{-1} and 766 cm^{-1} for the films containing below than 26 wt.%. It should also be noted that the peak is absent in the higher salt concentrations. The disappearance of this band indicates that there is possible interaction between the polymer and Li ions in the system.

Figure 5.9 depicts the FTIR spectra of pure PAN, LiCF_3SO_3 and films in the PAN- LiCF_3SO_3 system in the region between 900 cm^{-1} and 1800 cm^{-1} . The band at 1036 cm^{-1} is assigned to symmetric stretching modes (SO_3) of triflate. According to many studies [96-97], it could be assigned that the component is ascribed to ion pairs, free ions, ion triple and ion cluster. Intensity of this peak was drastically decreased when less than 22 wt% of salt was added. When more than 22 wt % of salt was added, it is observed that the peaks are absent. It indicates that a strong interaction between polymer and the salt has occurred in the PAN-salt complexes.

The FTIR spectra of pure PAN, LiCF_3SO_3 and films in the PAN- LiCF_3SO_3 system in the region between 2000 cm^{-1} and 3000 cm^{-1} is shown in Figure 5.10. In Figure 5.10 (c) to (g), it has been observed the stretching frequency at 2247 cm^{-1} , which corresponds to $\text{C}\equiv\text{N}$ of pure PAN, is shifted to 2244 cm^{-1} in the complexes. It also can be observed that this band broaden with the addition of salt. Its represents the Li^+ ions coordinate with the $\text{C}\equiv\text{N}$ group of PAN [98]. This also agrees with the analysis of the chemical structure of PAN i.e. there is a pair of unbounded electrons in the nitrogen atom from the $\text{C}\equiv\text{N}$ group and the Li^+ ion has an empty orbital. Therefore, it is possible for Li^+ to bond with the nitrogen atom of $\text{C}\equiv\text{N}$ group and the complexes are formed.

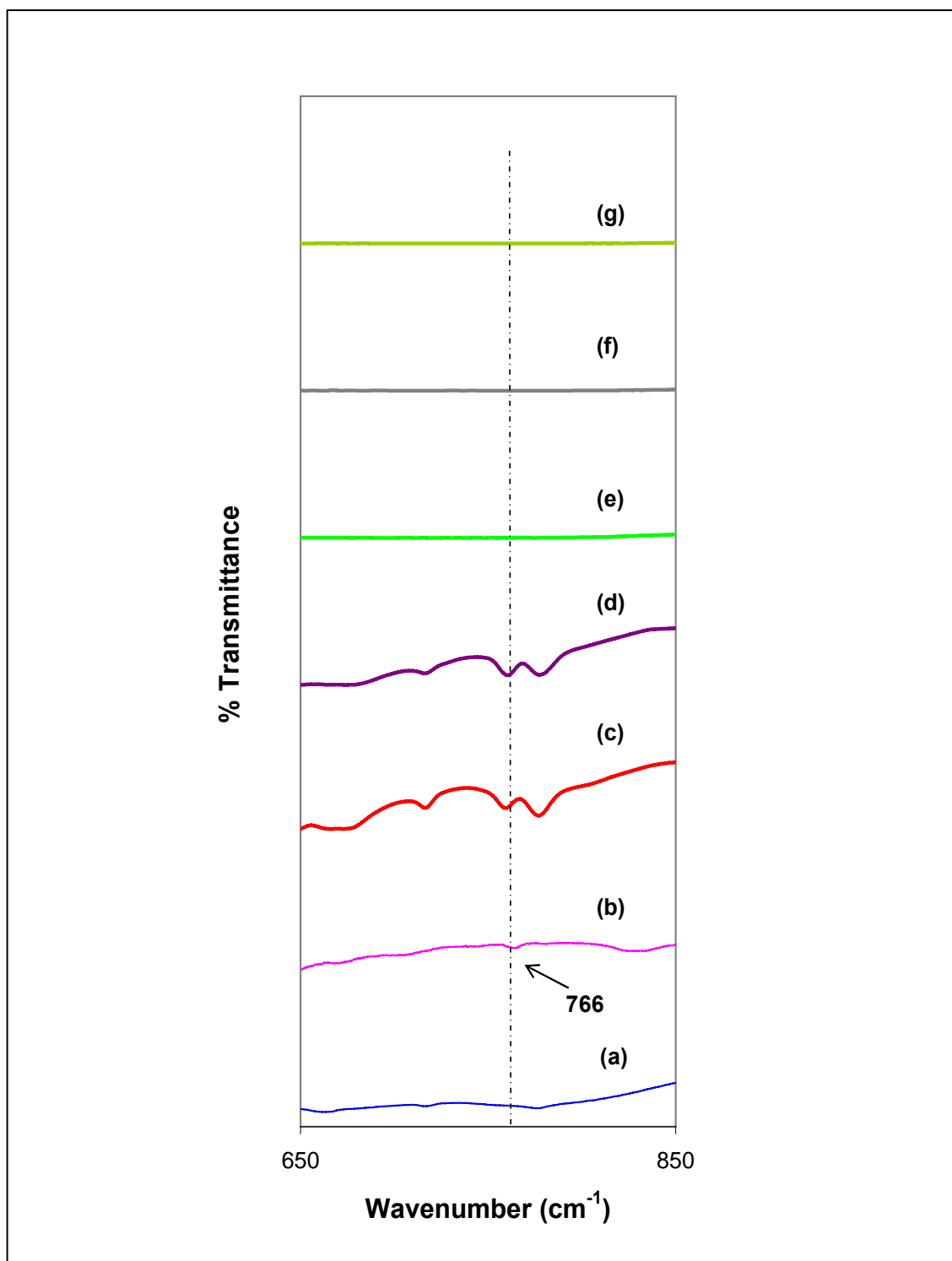


Figure 5.8: FTIR spectra of (a) pure PAN film (b) LiCF₃SO₃ (c) PAN + 8 wt.% LiCF₃SO₃ film (d) PAN + 18 wt.% LiCF₃SO₃ film (e) PAN + 22 wt.% LiCF₃SO₃ film (f) PAN + 26 wt.% LiCF₃SO₃ film and (g) PAN + 30 wt.% LiCF₃SO₃ film.

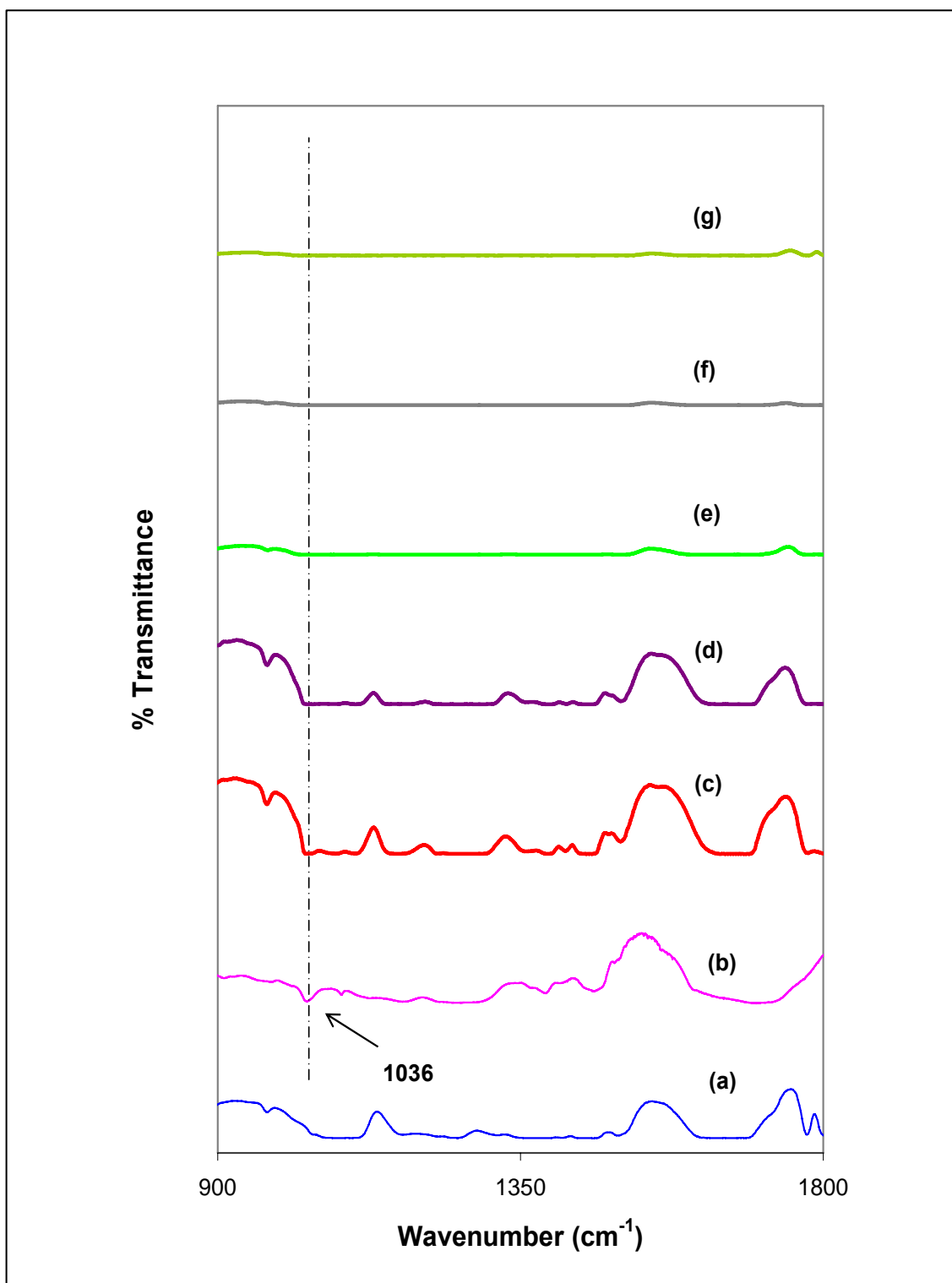


Figure 5.9: FTIR spectra of (a) pure PAN film (b) LiCF₃SO₃ (c) PAN + 8 wt.% LiCF₃SO₃ film (d) PAN + 18 wt.% LiCF₃SO₃ film (e) PAN + 22 wt.% LiCF₃SO₃ film (f) PAN + 26 wt.% LiCF₃SO₃ film and (g) PAN + 30 wt.% LiCF₃SO₃ film.

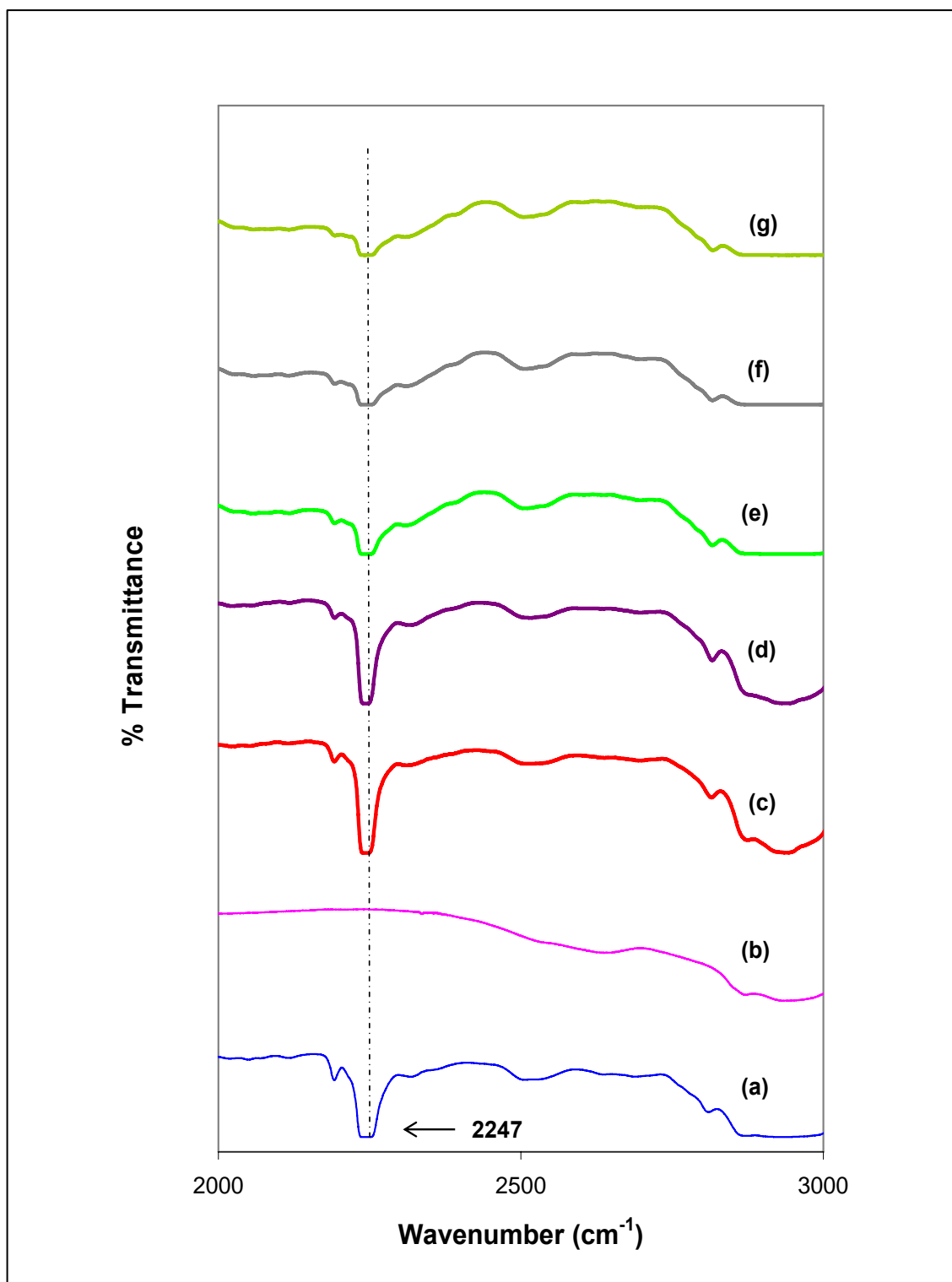


Figure 5.10: FTIR spectra of (a) pure PAN film (b) LiCF₃SO₃ (c) PAN + 8 wt.% LiCF₃SO₃ film (d) PAN + 18 wt.% LiCF₃SO₃ film (e) PAN + 22 wt.% LiCF₃SO₃ film (f) PAN + 26 wt.% LiCF₃SO₃ film and (g) PAN + 30 wt.% LiCF₃SO₃ film.

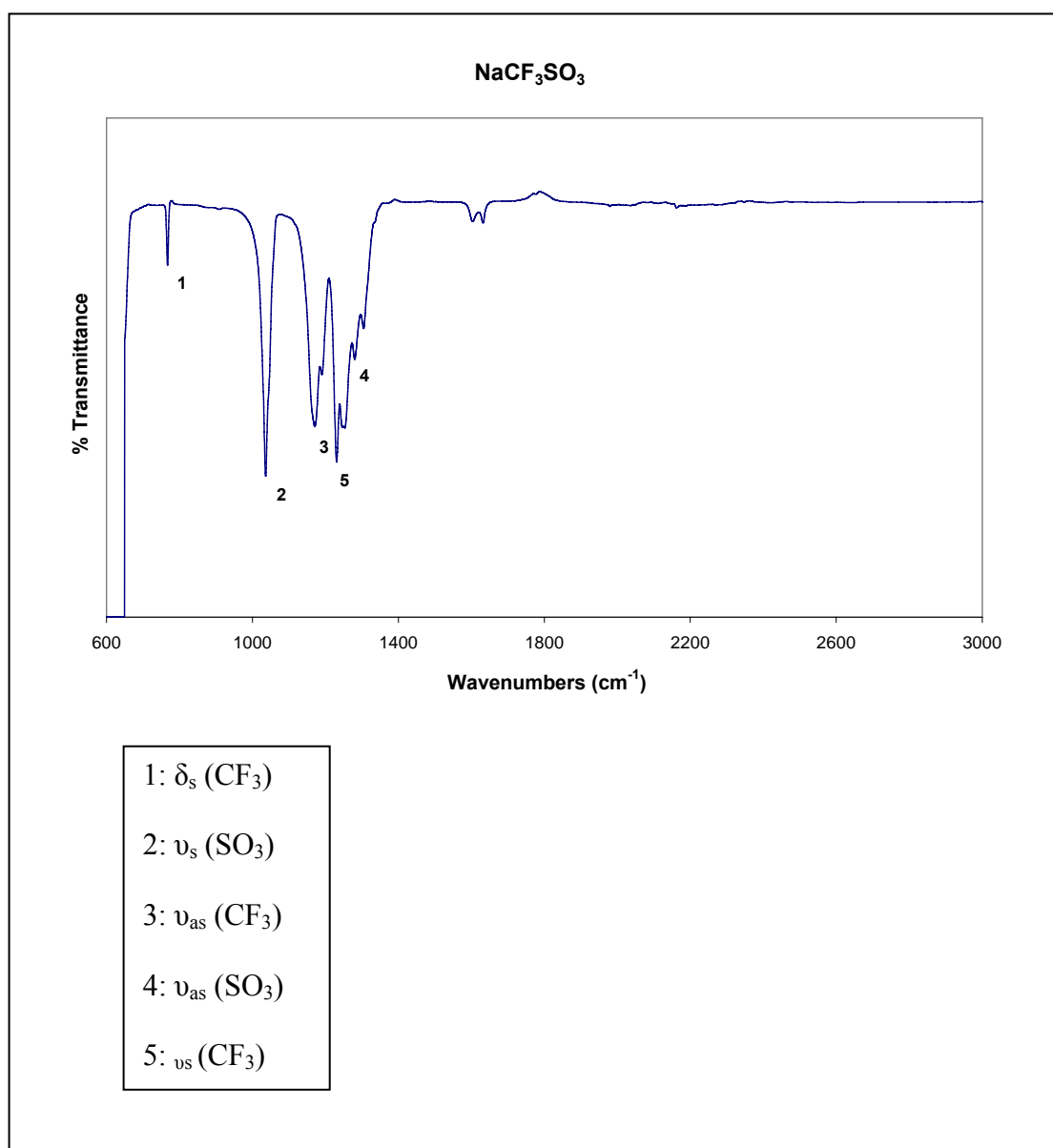
5.5 PAN - NaCF₃SO₃ System**Figure 5.11:** FTIR spectrum of NaCF₃SO₃ salt.

Table 5.4: The vibrational modes and wavenumbers of NaCF₃SO₃ salt.

Vibrational modes	Wavenumbers (cm ⁻¹)	References	Wavenumbers obtained from the work (cm ⁻¹)
δ_s (CF ₃)	766, 757	[94, 95]	769
ν_s (SO ₃)	1033, 1043, 1053, 1062	[91]	1037
ν_{as} (CF ₃)	1182, 1157	[90, 95]	1174
ν_{as} (SO ₃)	1272, 1257, 1302, 1271	[95]	1282
ν_s (CF ₃)	1230	[91]	1232

Figure 5.11 depicts the FTIR spectrum of NaCF₃SO₃ salt in the region between 600 cm⁻¹ and 3000 cm⁻¹. The vibrational modes and wavenumbers of NaCF₃SO₃ salt are listed in Table 5.4. Since the anion of this salt is triflate [CF₃SO₃], it was expected to have a similar appearance (frequency bands) with the spectrum of LiCF₃SO₃ in Figure 5.7.

Figure 5.12 shows the FTIR spectra of pure PAN film, NaCF₃SO₃ salt and the films from the PAN-NaCF₃SO₃ system in the region between 650 cm⁻¹ and 950 cm⁻¹. The band at 769 cm⁻¹ is assigned to δ_s (CF₃) mode of triflate. The addition of NaCF₃SO₃ results in two very distinct bands of medium intensity at 760 cm⁻¹ and 777 cm⁻¹. However, these bands completely disappear at the higher salt concentrations i.e. above 18 wt% of NaCF₃SO₃. Again, it implies the complexation has occurred in the PAN-NaCF₃SO₃ films.

In Figure 5.13, FTIR spectra of pure PAN, NaCF₃SO₃ and the films from the PAN-NaCF₃SO₃ system in the region between 900 cm⁻¹ and 1800 cm⁻¹ are presented. The band that appears at 1037 cm⁻¹ is due to the triflate symmetric (SO₃) stretching modes. According to many studies [96-97], it could be assigned that the component is ascribed to ion pairs, free ions, ion triple and ion cluster. It can be observed from the

figure the intensity of this band decreases with increasing salt concentration until the band intensity completely disappears at the higher salt concentrations i.e. above 18 wt% of NaCF₃SO₃. It indicates that there is stronger interaction between Na⁺ ions and the polymer than interaction of anions-cations of the salt. At higher salt concentrations, most of the band in this region slightly broadened. The change in intensity, shape and position of the peaks in this region confirms the complexation of PAN and NaCF₃SO₃.

The FTIR spectra of pure PAN, NaCF₃SO₃ salt and the films from the PAN-NaCF₃SO₃ system in the region between 2000 cm⁻¹ and 3000 cm⁻¹ is shown in Figure 5.14. The peak at 2247 cm⁻¹ is identified as C ≡ N stretching of pure PAN film. The intensity of this peak is decreases with increasing salt concentration. It shows that the interaction inside the system mainly occurred between the Na⁺ ions and the polymer chain molecule.

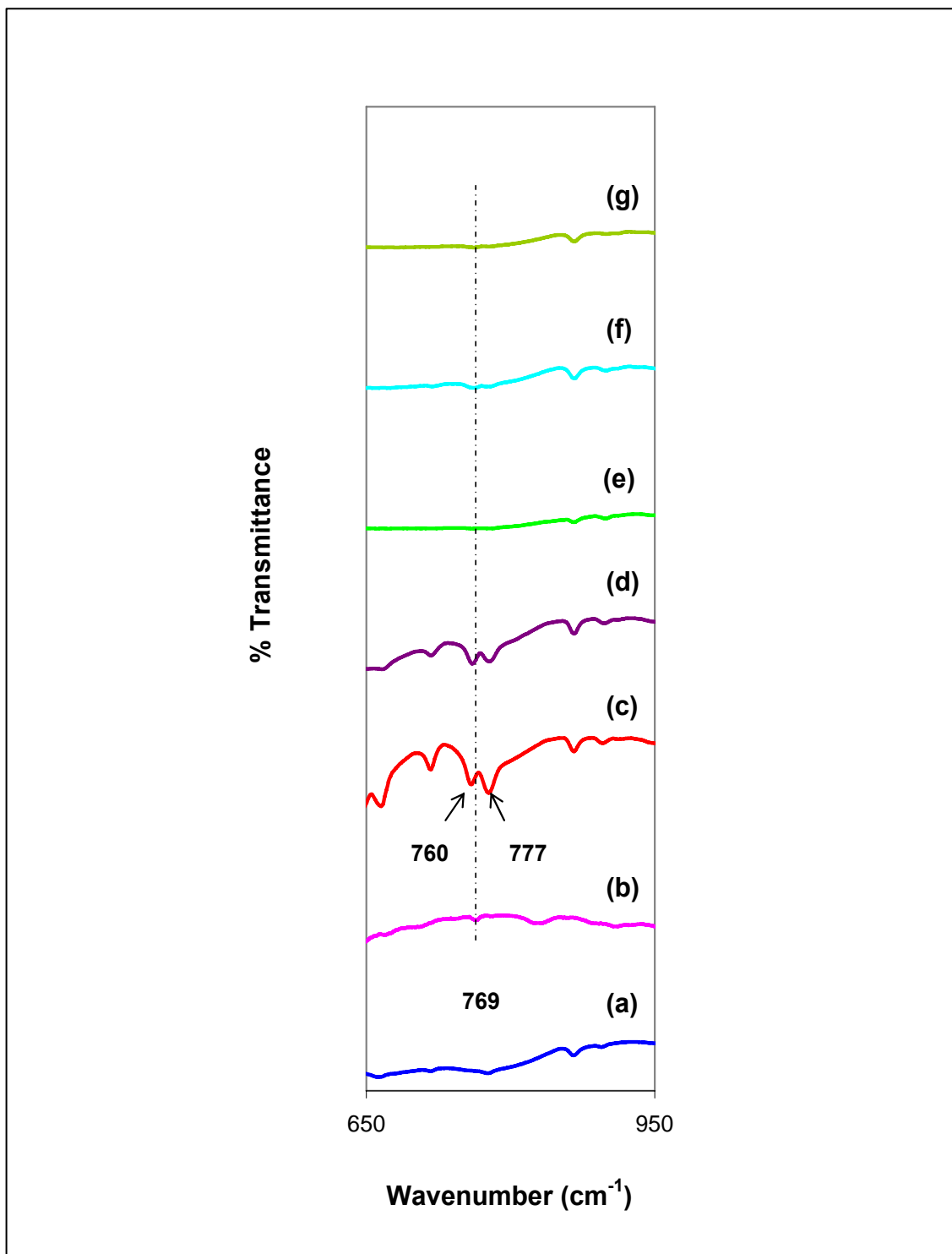


Figure 5.12: FTIR spectra of (a) pure PAN film (b) NaCF₃SO₃ (c) PAN + 8 wt.% NaCF₃SO₃ film (d) PAN + 18 wt.% NaCF₃SO₃ film (e) PAN + 24 wt.% NaCF₃SO₃ film (f) PAN + 26 wt.% NaCF₃SO₃ film and (g) PAN + 30 wt.% NaCF₃SO₃ film.

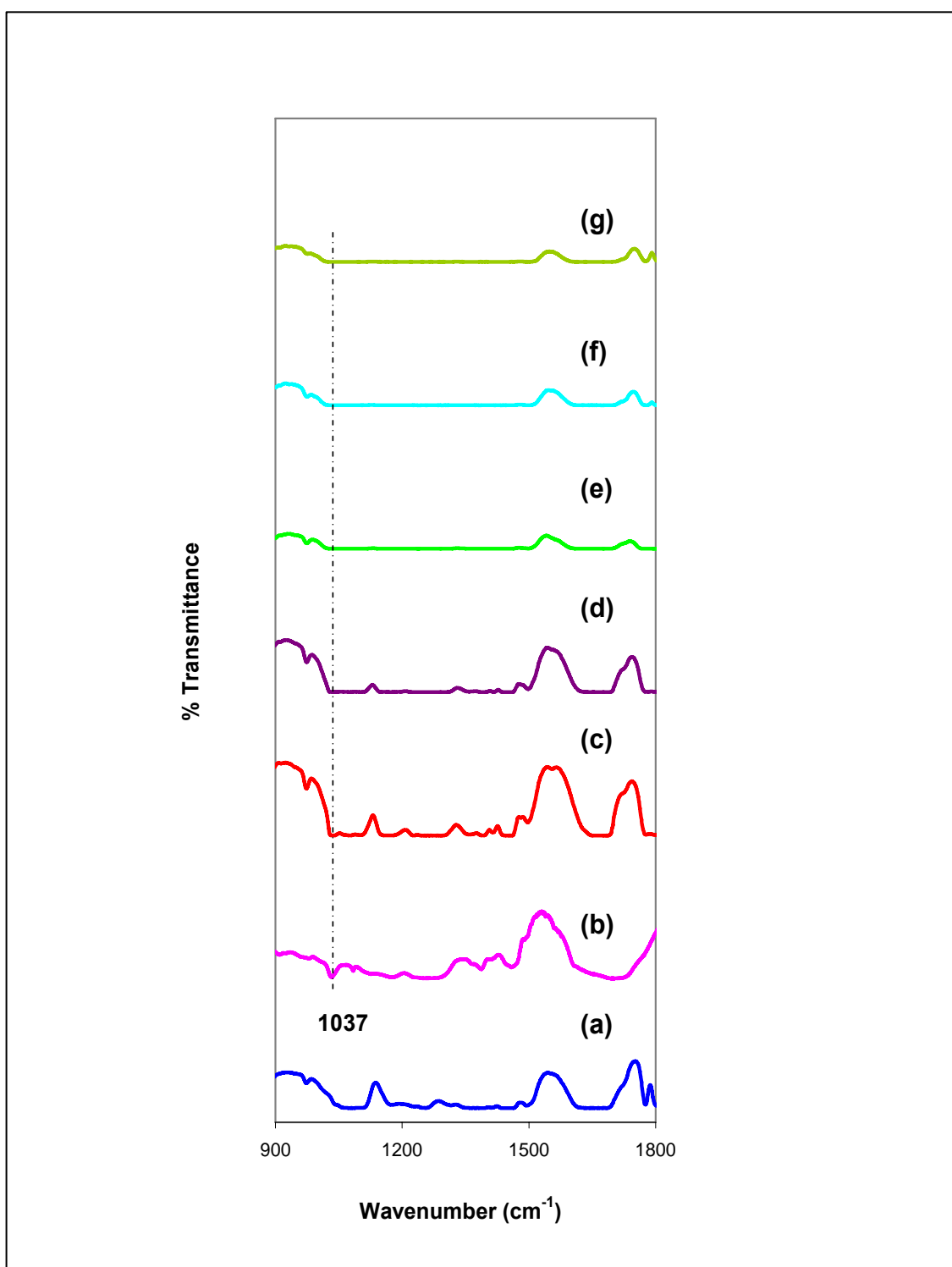


Figure 5.13: FTIR spectra of (a) pure PAN film (b) NaCF₃SO₃ (c) PAN + 8 wt.% NaCF₃SO₃ film (d) PAN + 18 wt.% NaCF₃SO₃ film (e) PAN + 24 wt.% NaCF₃SO₃ film (f) PAN + 26 wt.% NaCF₃SO₃ film and (g) PAN + 30 wt.% NaCF₃SO₃ film.

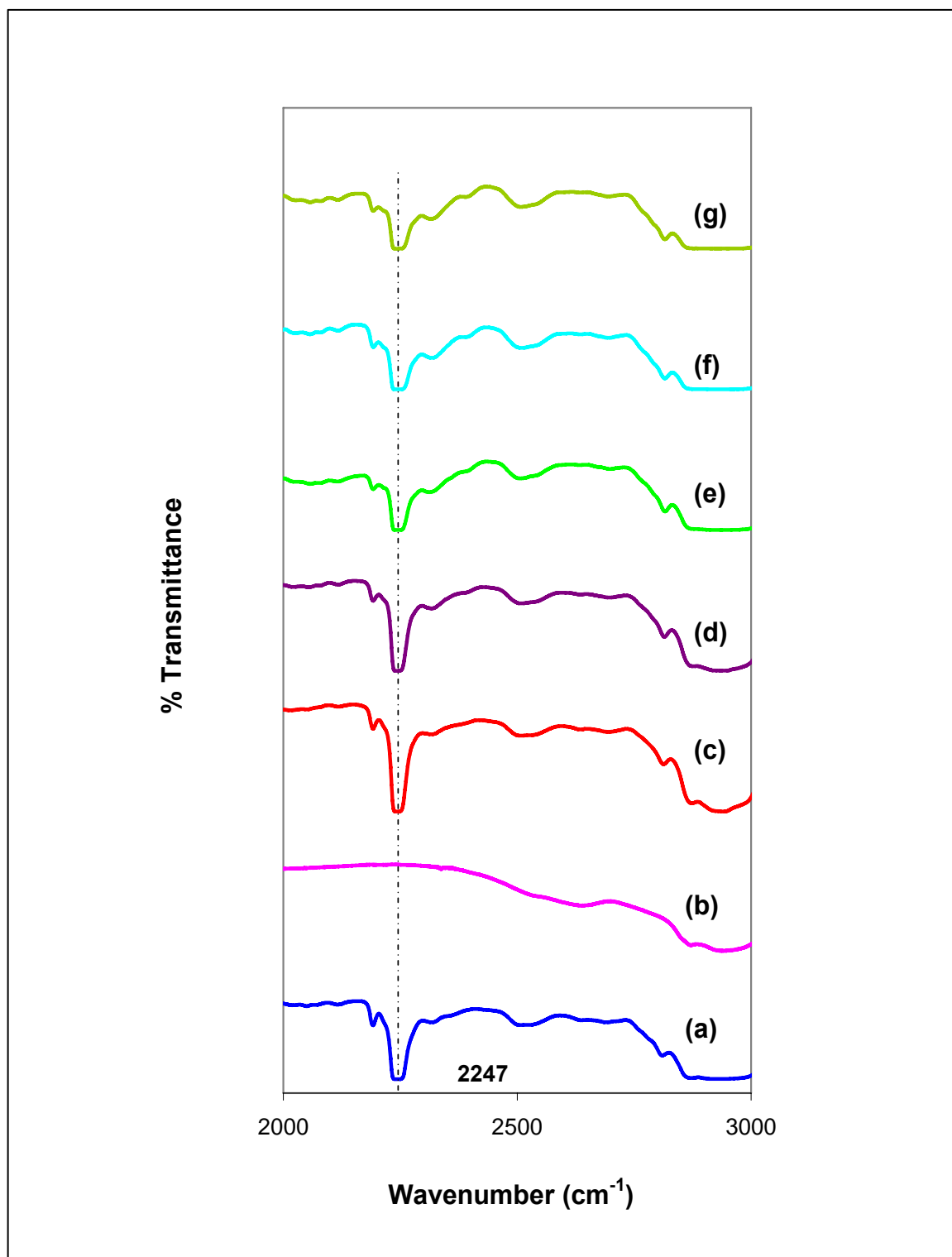


Figure 5.14: FTIR spectra of (a) pure PAN film (b) NaCF₃SO₃ (c) PAN + 8 wt.% NaCF₃SO₃ film (d) PAN + 18 wt.% NaCF₃SO₃ film (e) PAN + 24 wt.% NaCF₃SO₃ film (f) PAN + 26 wt.% NaCF₃SO₃ film and (g) PAN + 30 wt.% NaCF₃SO₃ film.

5.6 PAN - EC - LiCF₃SO₃ System

The roles of the plasticizer in the polymer electrolytes system are to decrease the glass transition temperature, dissolve salt, make the polymer becomes more amorphous and therefore allow the ionic or charge carriers to move freely resulting in the increase of the conductivity. In the PAN-salt system, the cations associate only with nitrogen in PAN. However, on the addition of plasticizer, EC the new route for the ions to move in the polymer electrolytes is formed through the interaction between oxygen atoms in EC with the cations.

Figure 5.15 shows the FTIR spectra of pure PAN film, EC, LiCF₃SO₃ salt and the films from the PAN-EC-LiCF₃SO₃ system in the region between 600 cm⁻¹ and 1000 cm⁻¹. The peaks appearing at 717 cm⁻¹ and 766 cm⁻¹ are due to C = O bending of pure EC and δ_s (CF₃) of pure LiCF₃SO₃ salt, respectively. It is found that these peaks are absent in the complexes. This again implies the interaction between Li⁺ ions in lithium salt with the oxygen group in EC has occurred and it is also confirmed that the complex formation between the salt, PAN and EC has taken place.

Figure 5.16 shows the FTIR spectra of pure PAN film, EC, LiCF₃SO₃ salt and the films from the PAN-EC-LiCF₃SO₃ system in the region between 1000 cm⁻¹ and 1500 cm⁻¹. The peak appearing at 1036 cm⁻¹ is assigned to ν_s (SO₃) modes of triflate. The peaks at 1070 cm⁻¹ and 1170 cm⁻¹ has been assigned to skeletal stretching in pure EC. They seem to disappear in the complexes which confirmed that the interaction between EC and the salt has been occurred.

The FTIR spectra of pure PAN, EC, LiCF₃SO₃ and films in the PAN-EC-LiCF₃SO₃ system in the region between 1500 cm⁻¹ and 2000 cm⁻¹ are presented in Figure 5.17. The C = O stretching peak at 1780 cm⁻¹ and 1810 cm⁻¹ of pure EC disappear in the salted plasticized PAN complexes which may due to the addition of

salt. The peak at 1870 cm^{-1} is shifted to 1860 cm^{-1} . This infers that EC interact with the salt in the complexes.

Figure 5.18 depicts the FTIR spectra of pure PAN film, EC, LiCF_3SO_3 salt and the films from the PAN-EC- LiCF_3SO_3 system in the region between 2000 cm^{-1} and 3000 cm^{-1} . From the figure, the intensity of the peak at 2247 cm^{-1} which is due to $\text{C}\equiv\text{N}$ group of PAN is decreased when the salt is added. It also observed that this peak became narrower when the salt content is further increased. As explained before, this may be due to the interaction through the Li^+ ion and the nitrogen atom of $\text{C}\equiv\text{N}$ group.

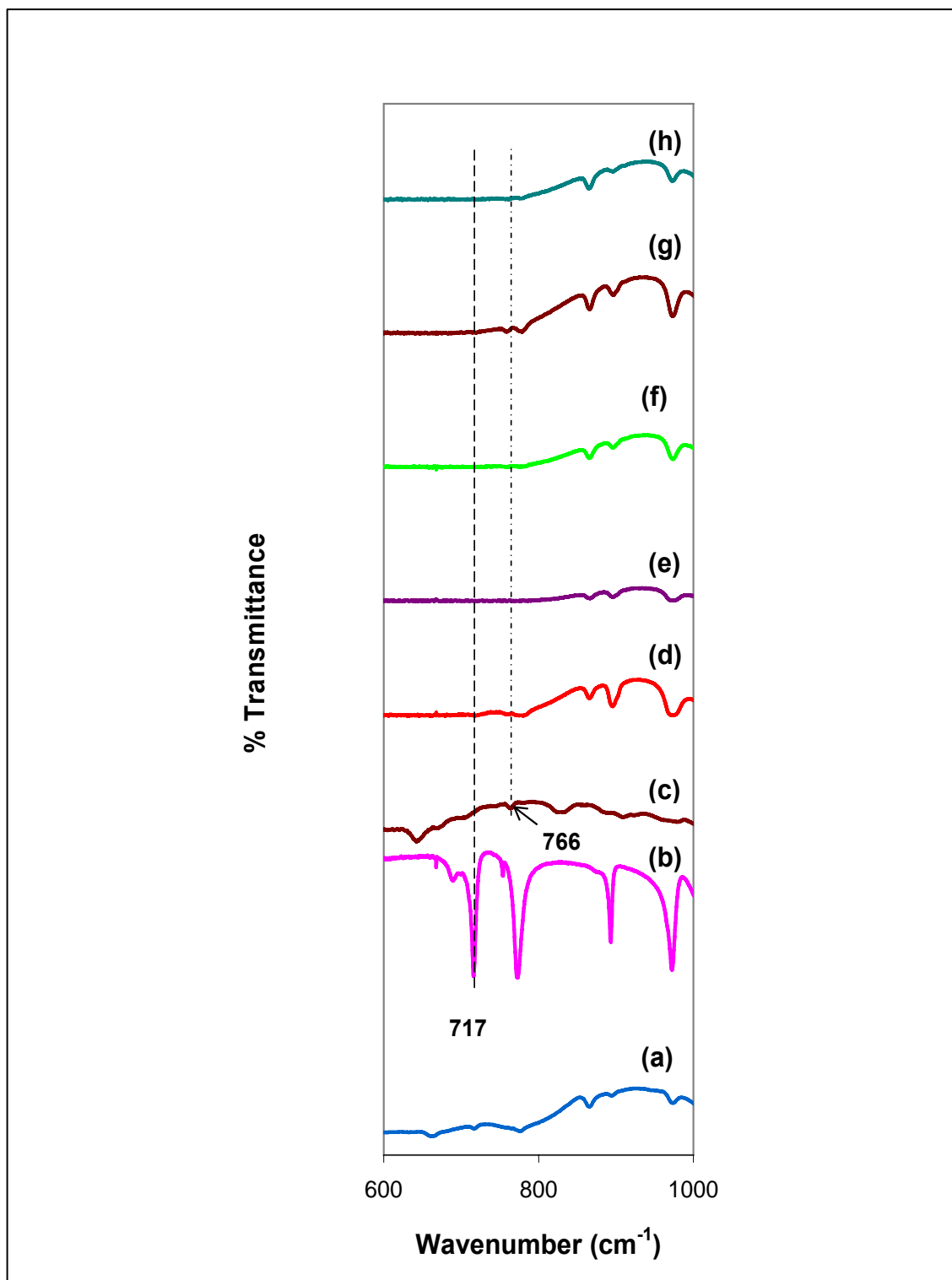


Figure 5.15: FTIR spectra of (a) pure PAN film (b) EC (c) LiCF₃SO₃ (d) PAN + EC + 8 wt.% LiCF₃SO₃ film (e) PAN + EC + 16 wt.% LiCF₃SO₃ film (f) PAN + EC + 22 wt.% LiCF₃SO₃ film (g) PAN + EC + 28 wt.% LiCF₃SO₃ film and (h) PAN + EC + 36 wt.% LiCF₃SO₃ film.

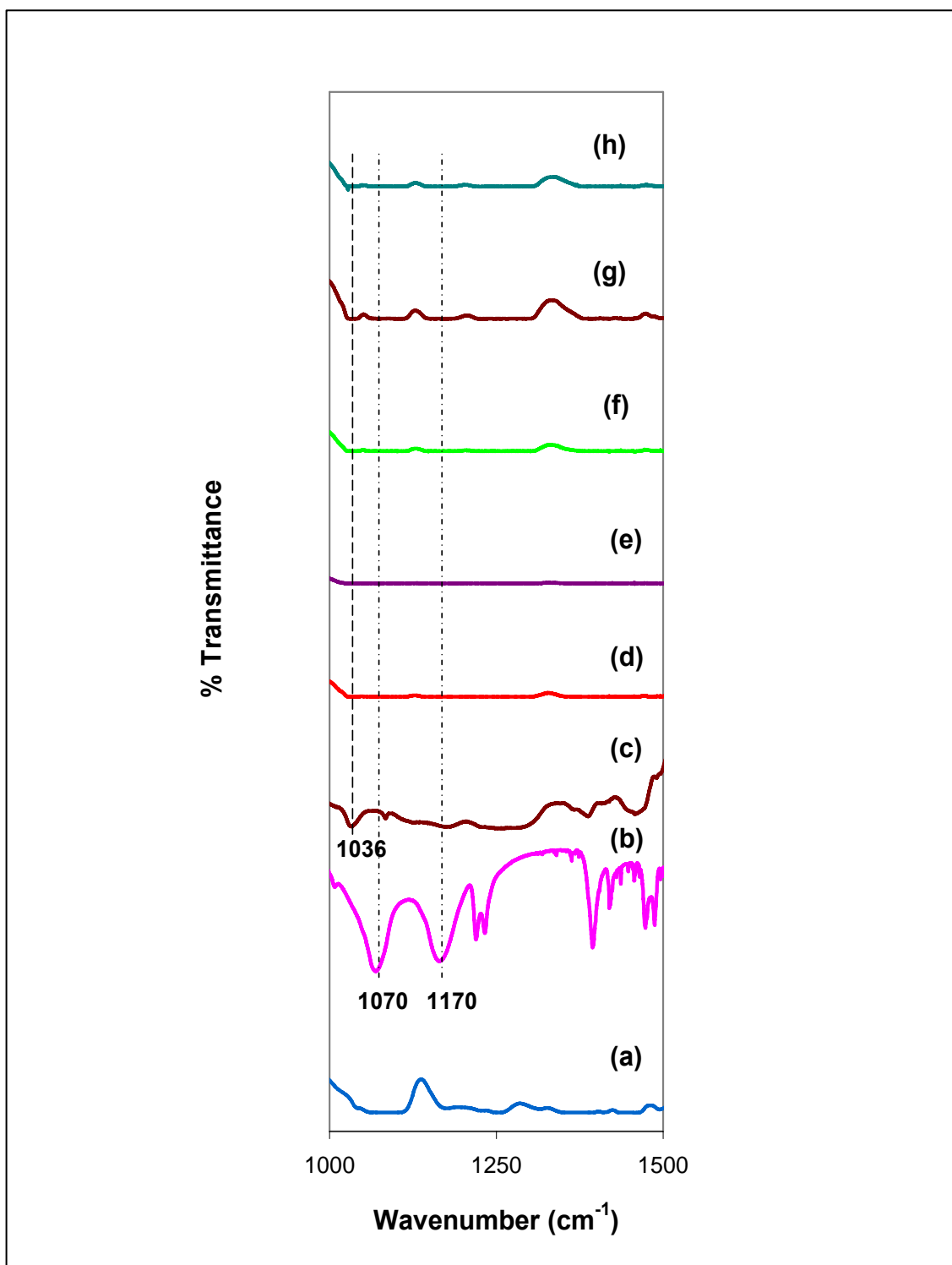


Figure 5.16: FTIR spectra of (a) pure PAN film (b) EC (c) LiCF₃SO₃ (d) PAN + EC + 8 wt.% LiCF₃SO₃ film (e) PAN + EC + 16 wt.% LiCF₃SO₃ film (f) PAN + EC + 22 wt.% LiCF₃SO₃ film (g) PAN + EC + 28 wt.% LiCF₃SO₃ film and (h) PAN + EC + 36 wt.% LiCF₃SO₃ film.

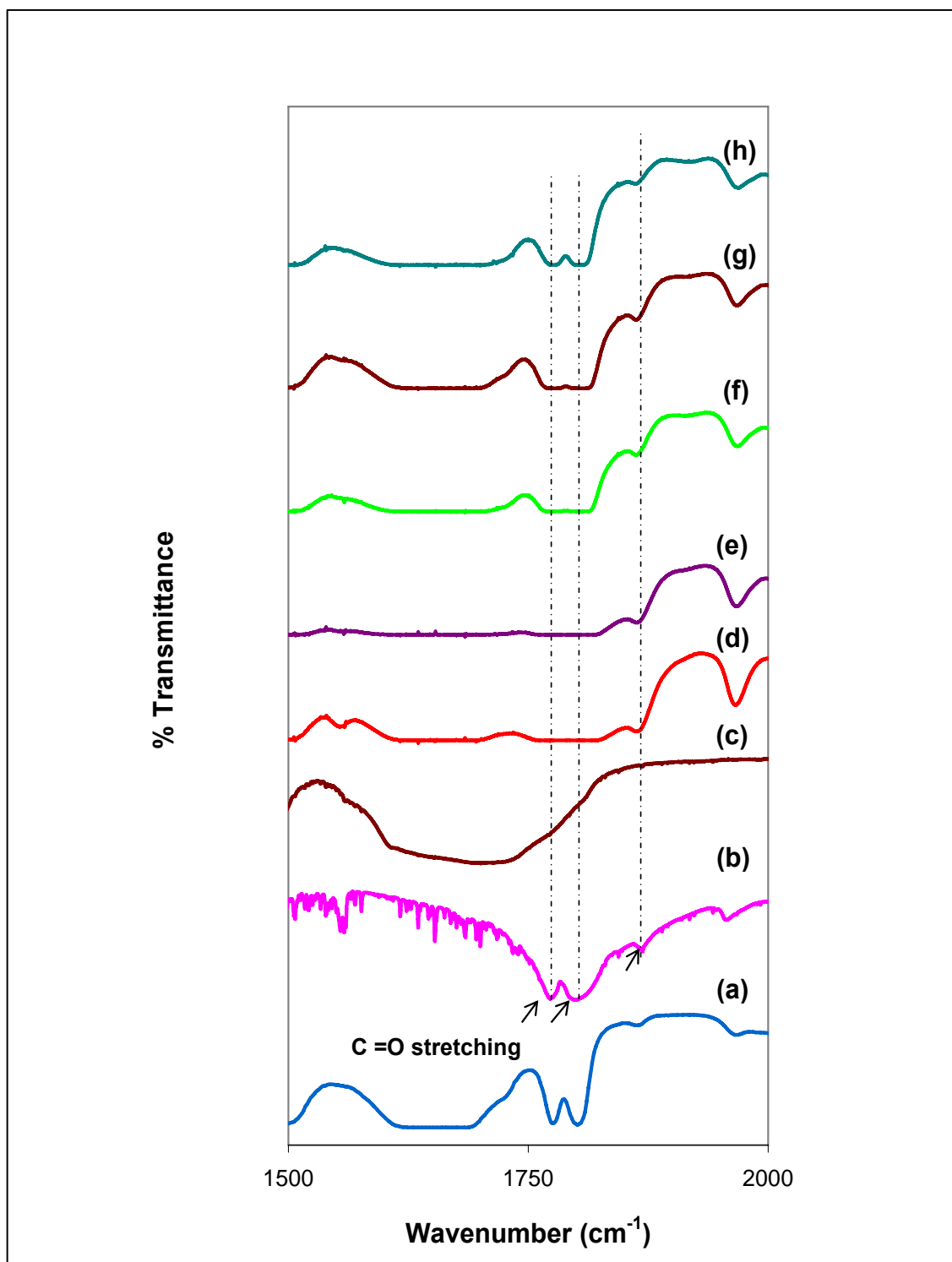


Figure 5.17: FTIR spectra of (a) pure PAN film (b) EC (c) LiCF₃SO₃ (d) PAN + EC + 8 wt.% LiCF₃SO₃ film (e) PAN + EC + 16 wt.% LiCF₃SO₃ film (f) PAN + EC + 22 wt.% LiCF₃SO₃ film (g) PAN + EC + 28 wt.% LiCF₃SO₃ film and (h) PAN + EC + 36 wt.% LiCF₃SO₃ film.

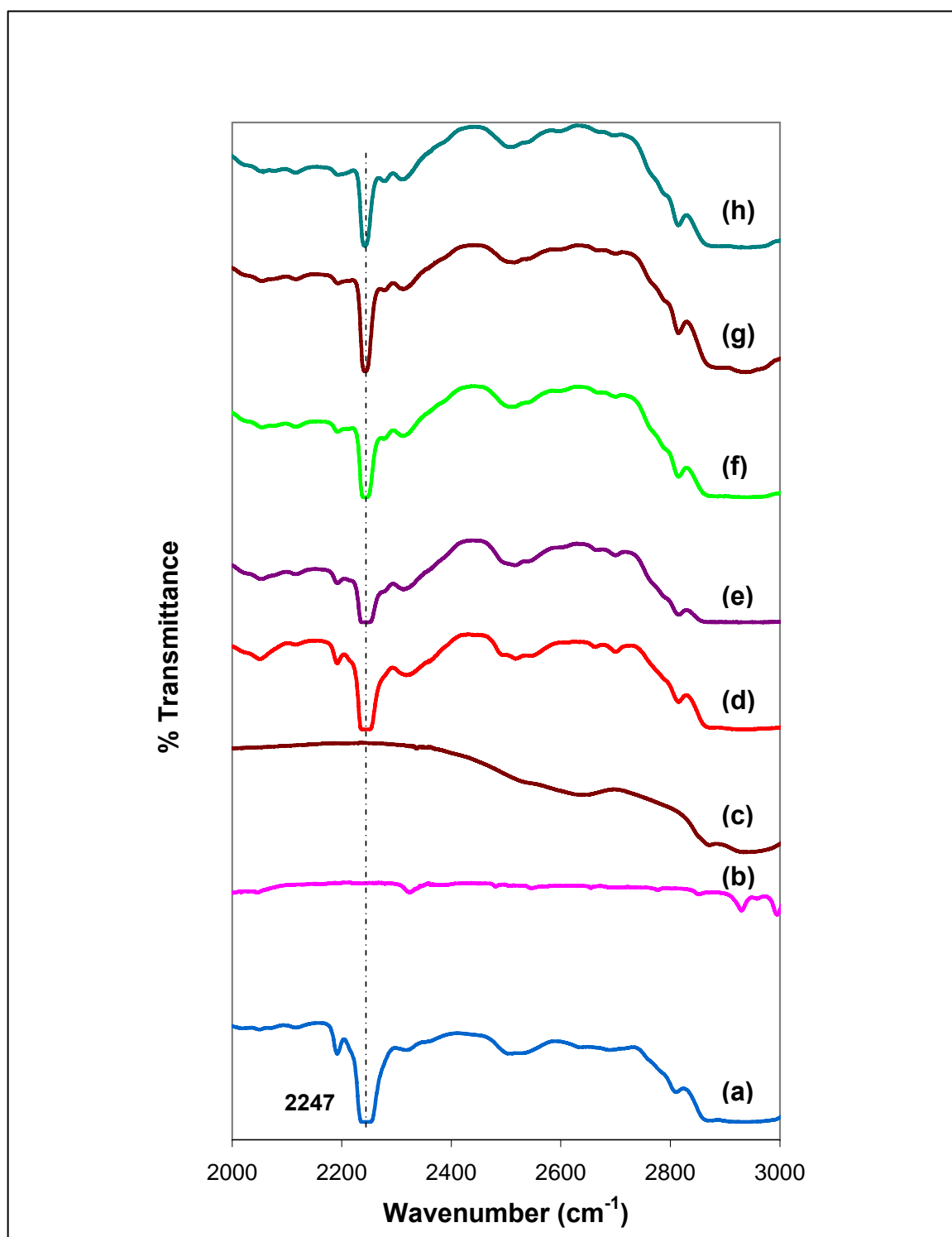


Figure 5.18: FTIR spectra of (a) pure PAN film (b) EC (c) LiCF₃SO₃ (d) PAN + EC + 8 wt.% LiCF₃SO₃ film (e) PAN + EC + 16 wt.% LiCF₃SO₃ film (f) PAN + EC + 22 wt.% LiCF₃SO₃ film (g) PAN + EC + 28 wt.% LiCF₃SO₃ film and (h) PAN + EC + 36 wt.% LiCF₃SO₃ film.

5.7 PAN - EC - NaCF₃SO₃ System

The FTIR spectra of pure PAN, EC, NaCF₃SO₃ salt and the films from the PAN-EC-NaCF₃SO₃ system in the region between 650 cm⁻¹ and 950 cm⁻¹ are presented in Figure 5.19. The peak at 769 cm⁻¹ is assigned to δ_s (CF₃) of triflate. Similar trend is seen in this region which is the peaks also found to be absent in the plasticized PAN containing LiCF₃SO₃ salt.

Figure 5.20 shows the FTIR spectra of pure PAN, EC, NaCF₃SO₃ and films in the PAN-EC-NaCF₃SO₃ system in the region between 1000 cm⁻¹ and 1500 cm⁻¹. The strong peaks at 1037 cm⁻¹, 1174 cm⁻¹ and 1232 cm⁻¹ are assigned to ν_s (SO₃), ν_{as} (CF₃) and ν_s (CF₃) of triflate. These peak are observed to be absent in the PAN complexes due to the interaction between the polymer, the plasticizer and the salt. The FTIR spectra of pure PAN film, EC, NaCF₃SO₃ salt and the films from the PAN-EC-NaCF₃SO₃ system in the region between 1500 cm⁻¹ and 2000 cm⁻¹ are presented in Figure 5.21. The C = O stretching band of EC is observed to decrease with the addition of salt concentration. It indicates that there are interaction between EC, PAN and Na⁺ ions.

Figure 5.22 depicts the FTIR spectra of pure PAN film, EC, NaCF₃SO₃ salt and the films from the PAN-EC-NaCF₃SO₃ system in the region between 2000 cm⁻¹ and 3000 cm⁻¹. The same trend is observed in this system as in the PAN-EC-LiCF₃SO₃ system which is the intensity peak at 2247 cm⁻¹ is decreases with the addition of sodium triflate. This change is caused by the sodium ions interacting with the nitrogen atoms in the polymer as the lithium ions coordinated by the polymer. In the spectra of PAN-EC-NaCF₃SO₃ films in the region between 650 cm⁻¹ and 3000 cm⁻¹ as shown in Figure 5.19 to 5.22, most of the peaks became shallow compared to unsalted plasticized PAN (Section 5.3) and unplasticized salted PAN (Section 5.4 and 5.5) spectra. This indicates that the complexation has occurred due to the interaction between the salt and PAN and also the plasticizer.

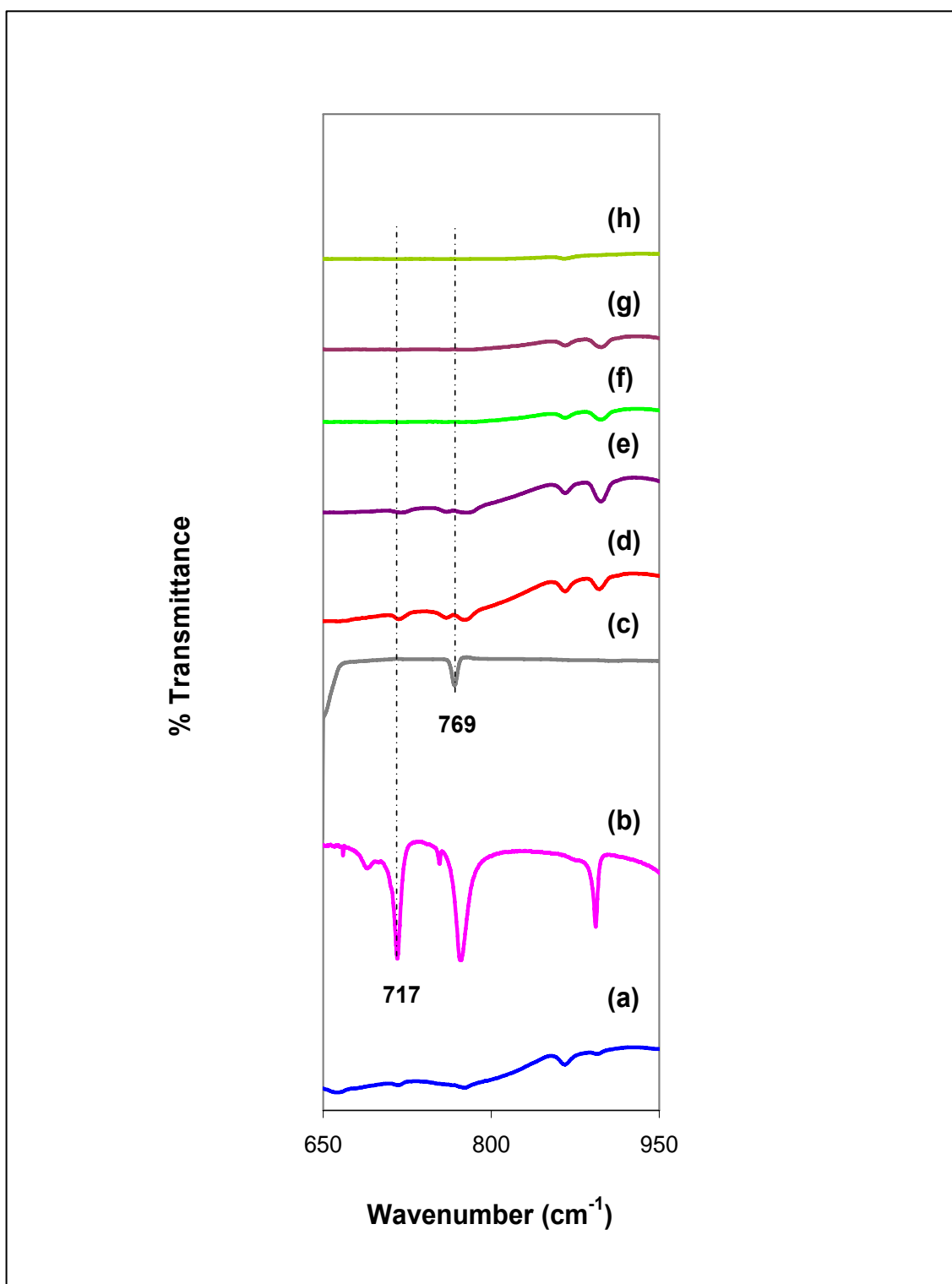


Figure 5.19: FTIR spectra of (a) pure PAN film (b) EC (c) NaCF₃SO₃ (d) PAN + EC + 8 wt.% NaCF₃SO₃ film (e) PAN + EC + 16 wt.% NaCF₃SO₃ film (f) PAN + EC + 22 wt.% NaCF₃SO₃ film (g) PAN + EC + 34 wt.% NaCF₃SO₃ film and (h) PAN + EC + 38 wt.% NaCF₃SO₃ film.

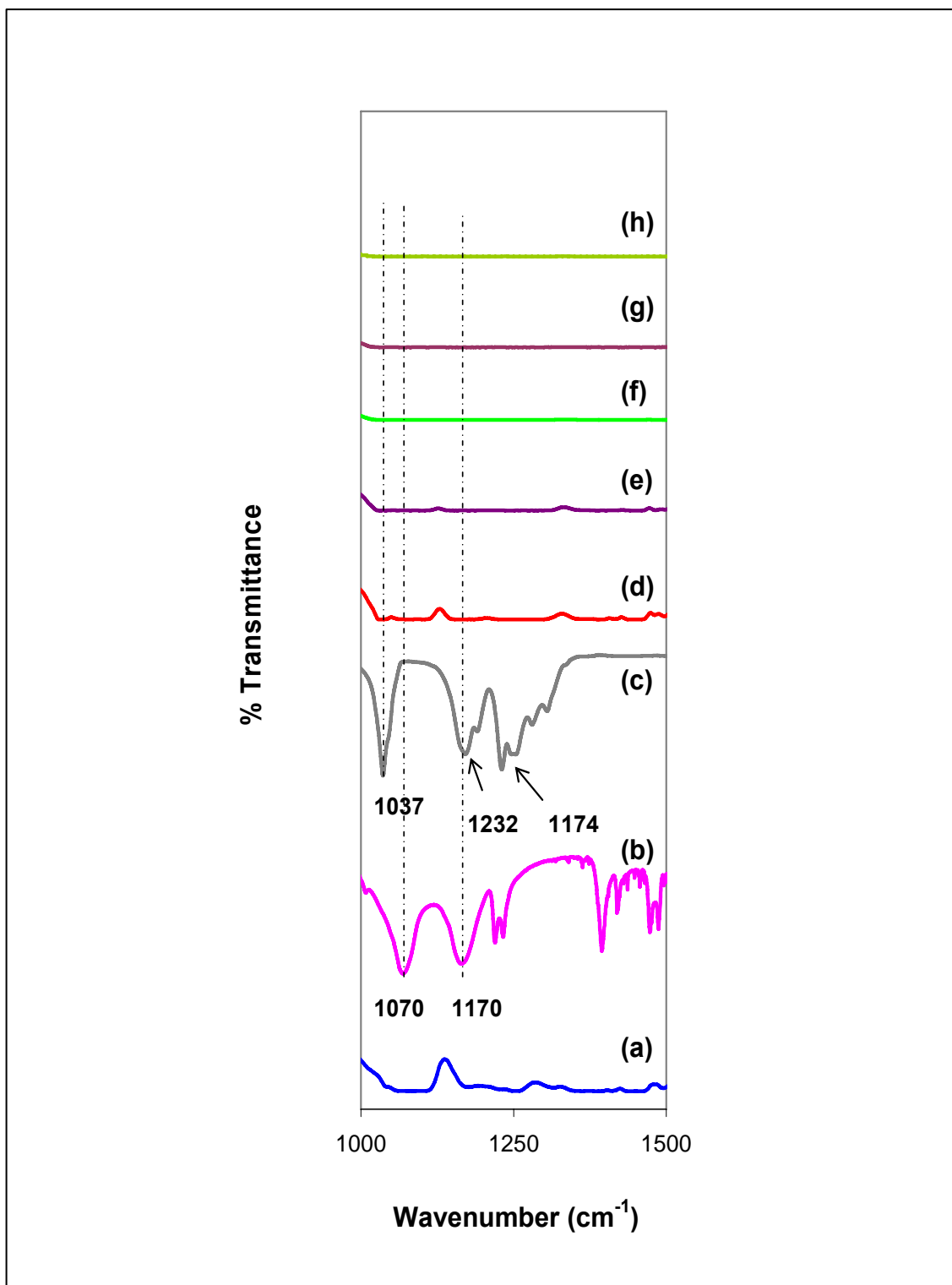


Figure 5.20: FTIR spectra of (a) pure PAN film (b) EC (c) NaCF₃SO₃ (d) PAN + EC + 8 wt.% NaCF₃SO₃ film (e) PAN + EC + 16 wt.% NaCF₃SO₃ film (f) PAN + EC + 22 wt.% NaCF₃SO₃ film (g) PAN + EC + 34 wt.% NaCF₃SO₃ film and (h) PAN + EC + 38 wt.% NaCF₃SO₃ film.

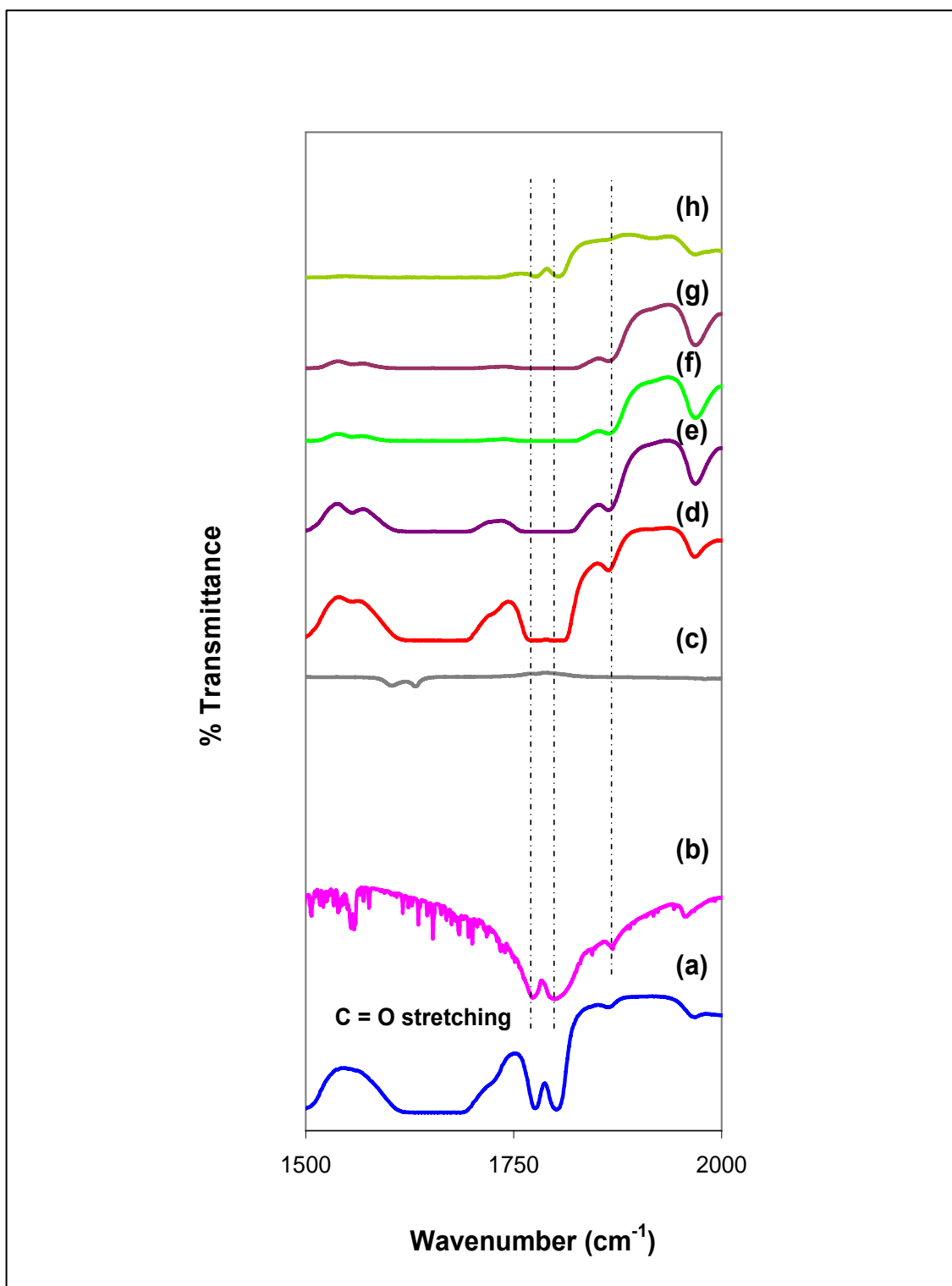


Figure 5.21: FTIR spectra of (a) pure PAN film (b) EC (c) NaCF₃SO₃ (d) PAN + EC + 8 wt.% NaCF₃SO₃ film (e) PAN + EC + 16 wt.% NaCF₃SO₃ film (f) PAN + EC + 22 wt.% NaCF₃SO₃ film (g) PAN + EC + 34 wt.% NaCF₃SO₃ film and (h) PAN + EC + 38 wt.% NaCF₃SO₃ film.

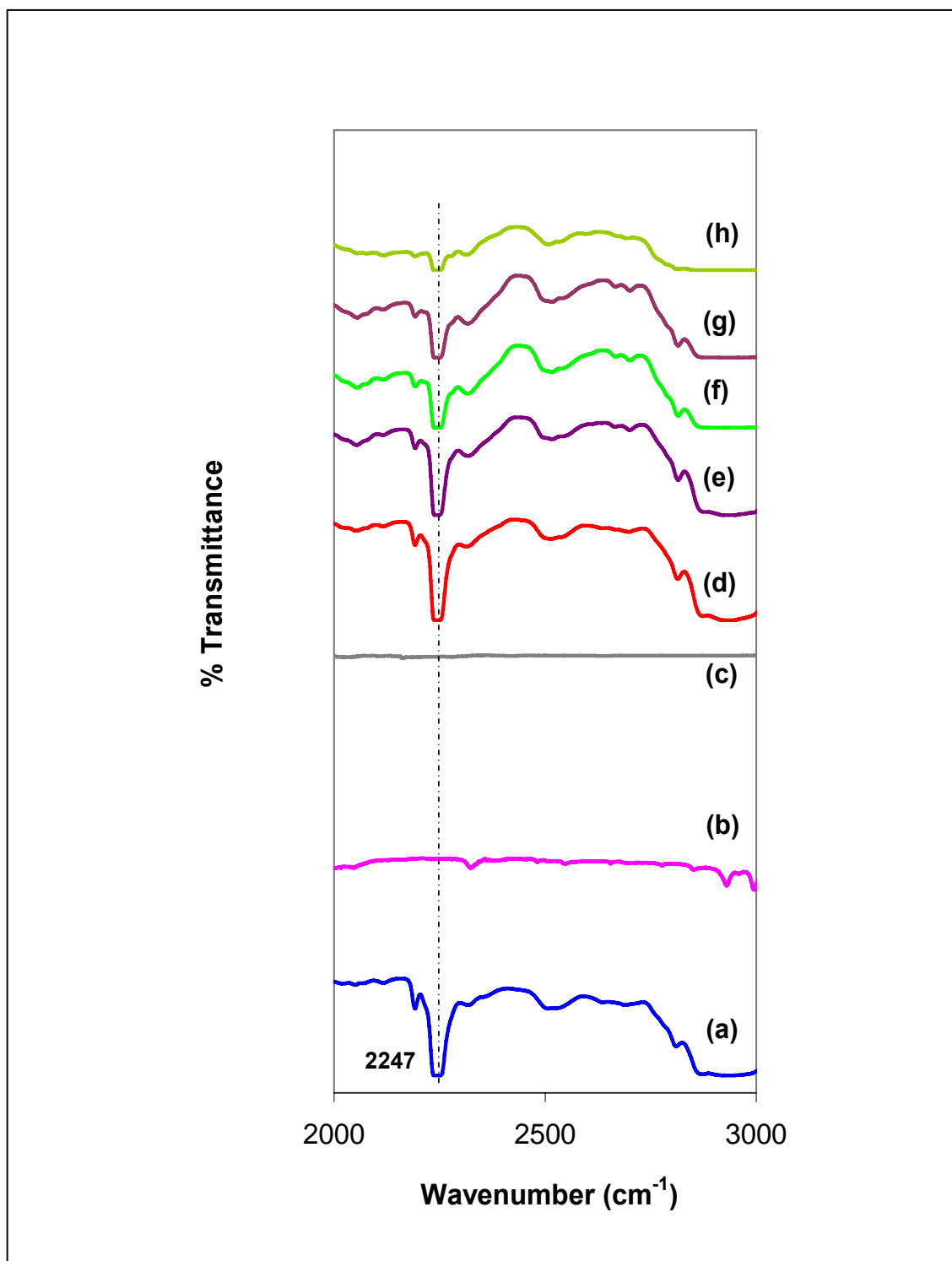


Figure 5.22: FTIR spectra of (a) pure PAN film (b) EC (c) NaCF₃SO₃ (d) PAN + EC + 8 wt.% NaCF₃SO₃ film (e) PAN + EC + 16 wt.% NaCF₃SO₃ film (f) PAN + EC + 22 wt.% NaCF₃SO₃ film (g) PAN + EC + 34 wt.% NaCF₃SO₃ film and (h) PAN + EC + 38 wt.% NaCF₃SO₃ film.

CHAPTER 6:

Results and Discussion

-XRD Studies-

6.1 X-ray Diffraction Analysis

X-ray Diffraction (XRD) can determine whether a material is amorphous, crystalline or both. It also show that the introduction of an additive such plasticizer or salt to a polymer can make it more or less crystalline. In this work, the XRD analysis was performed on the films of pure PAN, EC, LiCF_3SO_3 and NaCF_3SO_3 salts and also the PAN based complexes from each system.

6.2 Pure PAN film

Figure 6.1 shows the x-ray diffractogram of pure PAN film. The XRD pattern exhibits the pure PAN film is semicrystalline with a diffraction peak is observed at $2\theta = 17.4^\circ$.

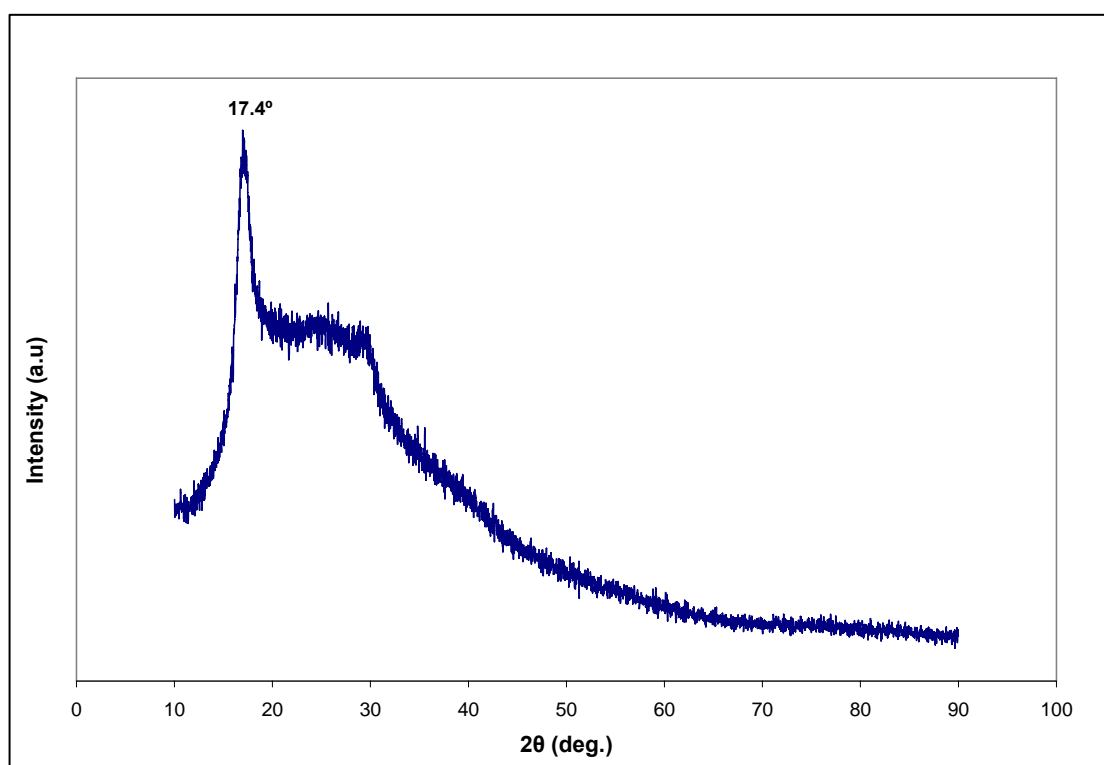


Figure 6.1: X-ray diffractogram of pure PAN film

6.3 Pure EC

Figure 6.2 shows the x-ray diffractogram of pure EC film. Several sharp peaks present signify the crystalline state of EC and the peaks can be found at $2\theta = 17.4^\circ$, 20.1° , 25.9° , 30.1° , 38.1° . This reveals that EC is crystalline in nature.

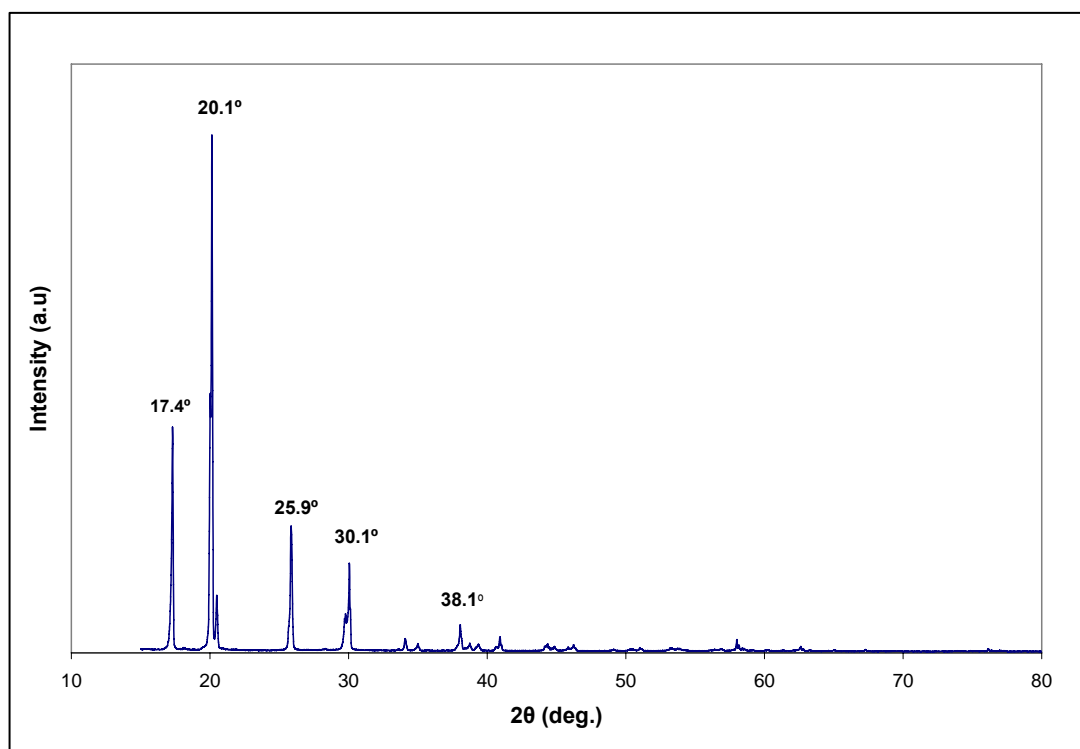


Figure 6.2: X-ray diffractogram of pure EC.

6.4 LiCF_3SO_3 and NaCF_3SO_3 Salts

Figure 6.3 and 6.4 present the x-ray diffractogram of LiCF_3SO_3 and NaCF_3SO_3 salts. The XRD pattern of LiCF_3SO_3 shows peaks at $2\theta = 16.7^\circ$, 19.8° , 20.3° , 22.5° , 24.6° , 25.5° , 33.0° , 33.6° and 41.7° . The strong peaks also can be found in NaCF_3SO_3 diffractogram which is observed at $2\theta = 23.7^\circ$, 32.9° , 34.8° , 42.7° , 48.7° , 53.5° and 56.20° . These reveal that both salts are crystalline in nature.

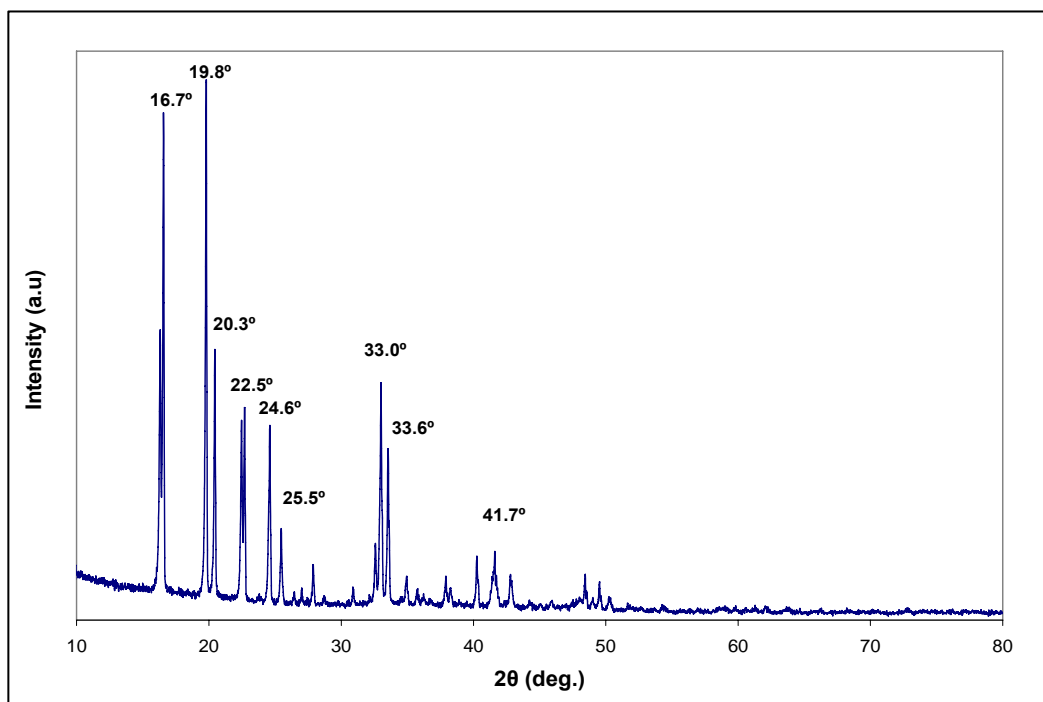


Figure 6.3: X-ray diffractogram of LiCF₃SO₃ salt.

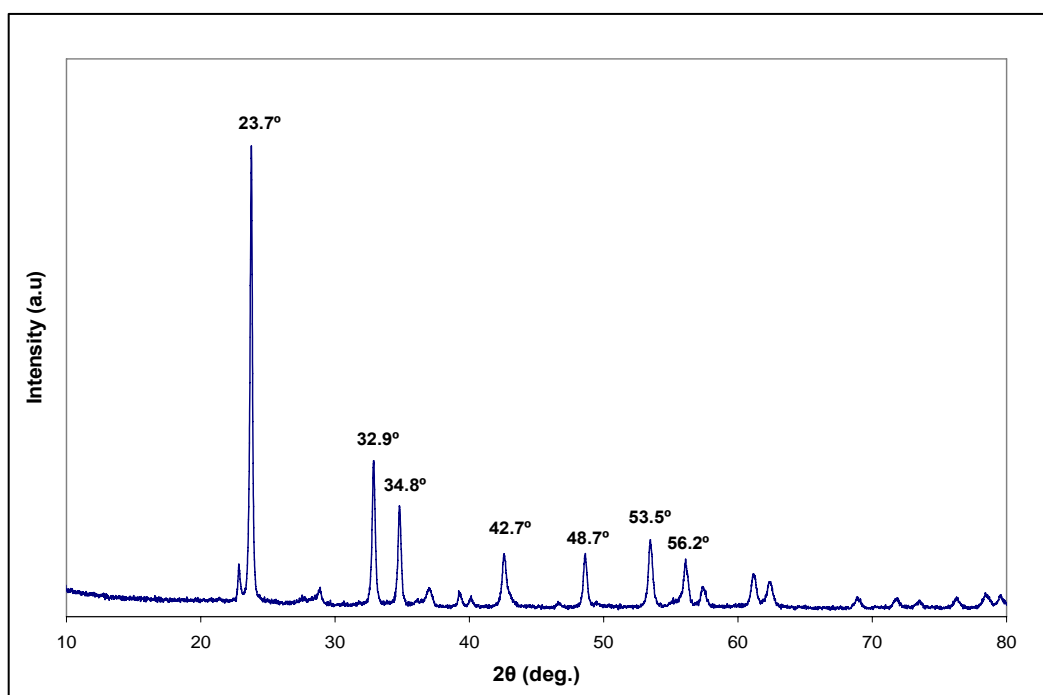


Figure 6.4: X-ray diffractogram of NaCF₃SO₃ salt.

6.5 PAN - EC System

The XRD patterns for pure PAN and PAN-EC films containing different amounts of EC are shown in Figure 6.5. On addition of different concentration of plasticizer, EC, the diffraction peak of pure PAN at $2\theta = 17.4^\circ$ shifted to 17.0° and the intensity of the peak is reduced about 25.0 %. This peak is also broaden when the plasticizer was added and the Full Width at Half Maximum (FWHM) value is increased. This suggests that the decrease in the degree of crystallinity of plasticized PAN films. A new broad peaks at $2\theta = 26.8^\circ$, 27.1° , 28.7° also appear in the films containing 20 wt.%, 24 wt.% and 30 wt.% of EC, respectively. This is due to the incorporation of plasticizer, EC and polymer matrices, PAN. It also can be observed that the crystalline nature of EC is completely disappears in the complexes which indicated the complexation has occurred between PAN and EC.

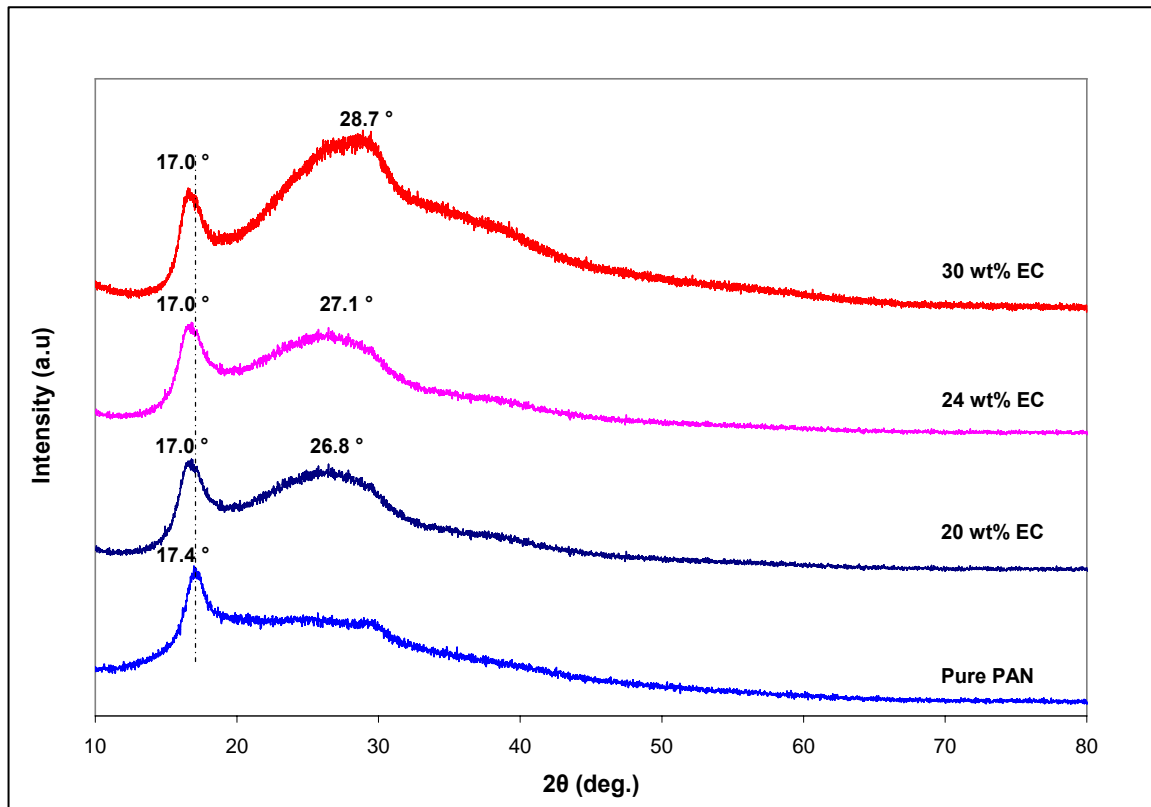


Figure 6.5: X-ray diffractogram of the films in the PAN-EC system.

6.6 PAN-LiCF₃SO₃ System

Figure 6.6 shows the XRD patterns for pure PAN film and PAN-LiCF₃SO₃ films containing different amounts of LiCF₃SO₃. It can be observed that most of the peaks pertaining to pure LiCF₃SO₃ are absent in the polymer electrolyte films and indicates the complete dissolution of the salt in the polymer matrix PAN. Thus, the XRD studies confirm that complexation has occurred in the polymer matrices and the complex formed are amorphous. Berthier et al. [26] established that ionic conductivity in polymer electrolytes is associated with the amorphous phase of the studied samples. It can also be observed that the film with 26 wt.% of LiCF₃SO₃ is the most amorphous film thus leading to a highest conductivity in this system. This observation is in good agreement with the work done by Berhier and co-workers [99]. They reported that ionic conductivity in polymer electrolytes is associated with the amorphous phase of the studied samples.

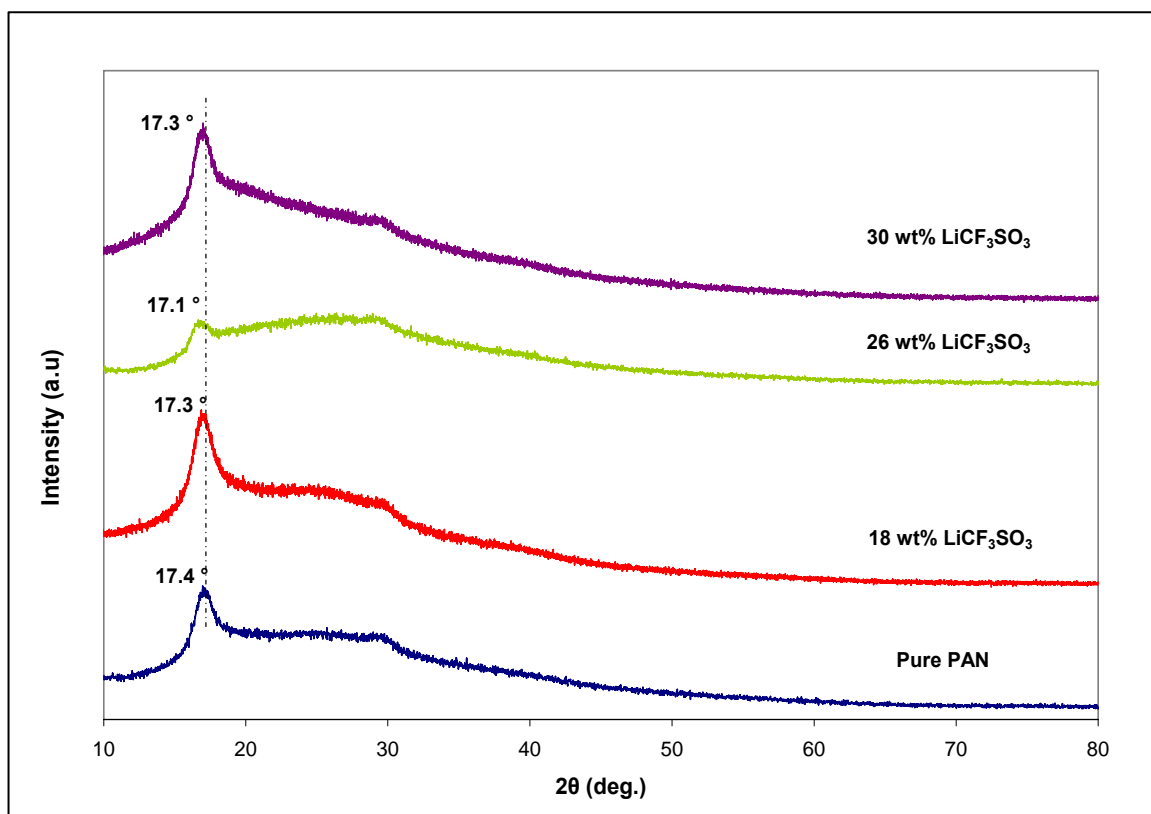


Figure 6.6: X-ray diffractogram of the films in the PAN-LiCF₃SO₃ system.

6.7 PAN- NaCF_3SO_3 System

Figure 6.7 depicts the XRD patterns for pure PAN film and PAN- NaCF_3SO_3 films containing different amounts of NaCF_3SO_3 salt. All sharp crystalline peaks noticed in NaCF_3SO_3 are absent in all complexes indicating the complexation has occurred between PAN and NaCF_3SO_3 salt. The highest conductivity for this system is obtained from film containing 24 wt.% of NaCF_3SO_3 . It can be observed that the intensity of the peak at $2\theta = 17.3^\circ$ for this film is lower than the other films which revealed that the film is the most amorphous film.

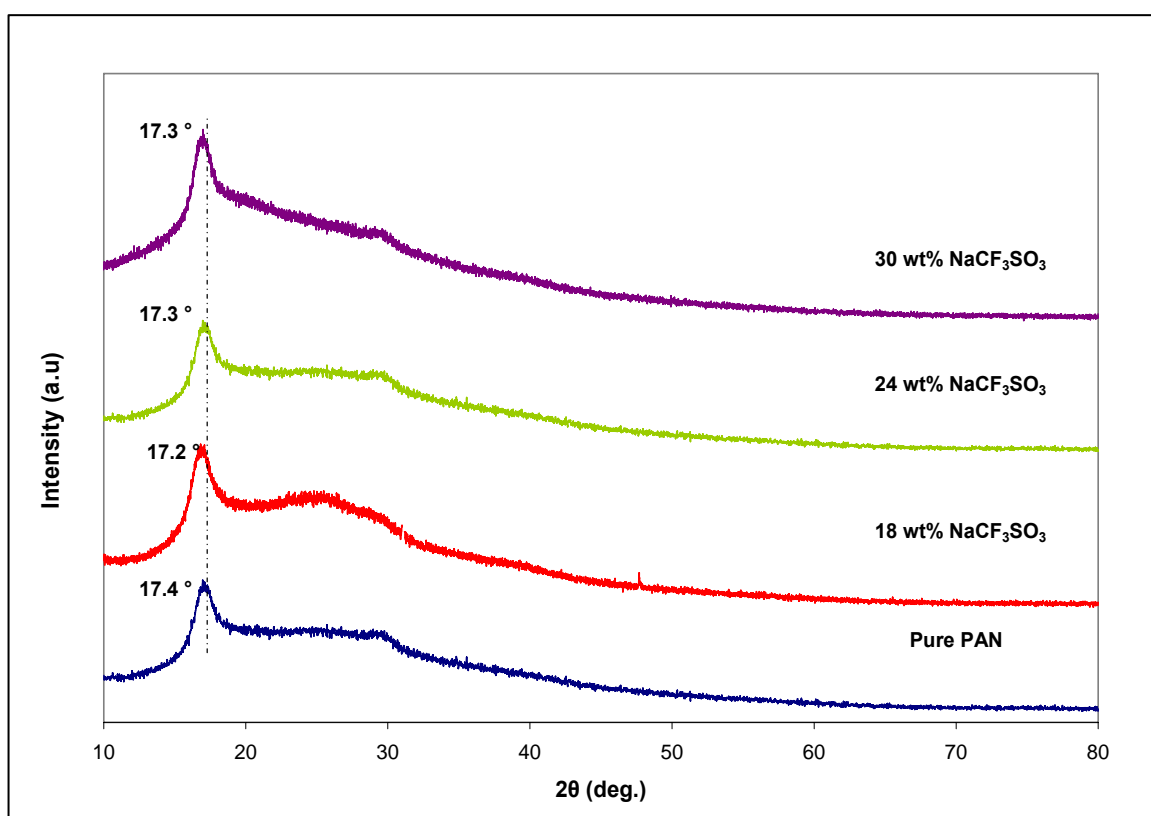


Figure 6.7: X-ray diffractogram of films in the PAN- NaCF_3SO_3 system

6.8 PAN-EC-LiCF₃SO₃ System

The XRD pattern of PAN-EC-LiCF₃SO₃ system is shown in Figure 6.8. The diffraction peaks of LiCF₃SO₃ salt is found to be absent in the complexes indicate that the complete dissolution of the salt in the plasticized polymer matrix. The intensity of the diffraction peak of pure PAN at $2\theta = 17.4^\circ$ is reduced in the complexed films. This peak is also shifted to $2\theta = 17.2^\circ$, 17.1° and 17.3° in the 18 wt.% LiCF₃SO₃, 22 wt.% LiCF₃SO₃ and 30 wt.% LiCF₃SO₃, respectively. This reveals the decrease in the degree of crystallinity of PAN with increasing concentration of the salt. The film containing 22 wt.% of LiCF₃SO₃ has the highest conductivity at the room temperature, hence it has lower degree of crystallinity as compared to the other films and causes a reduction in the energy barrier to the segmental motion of the polymer electrolytes.

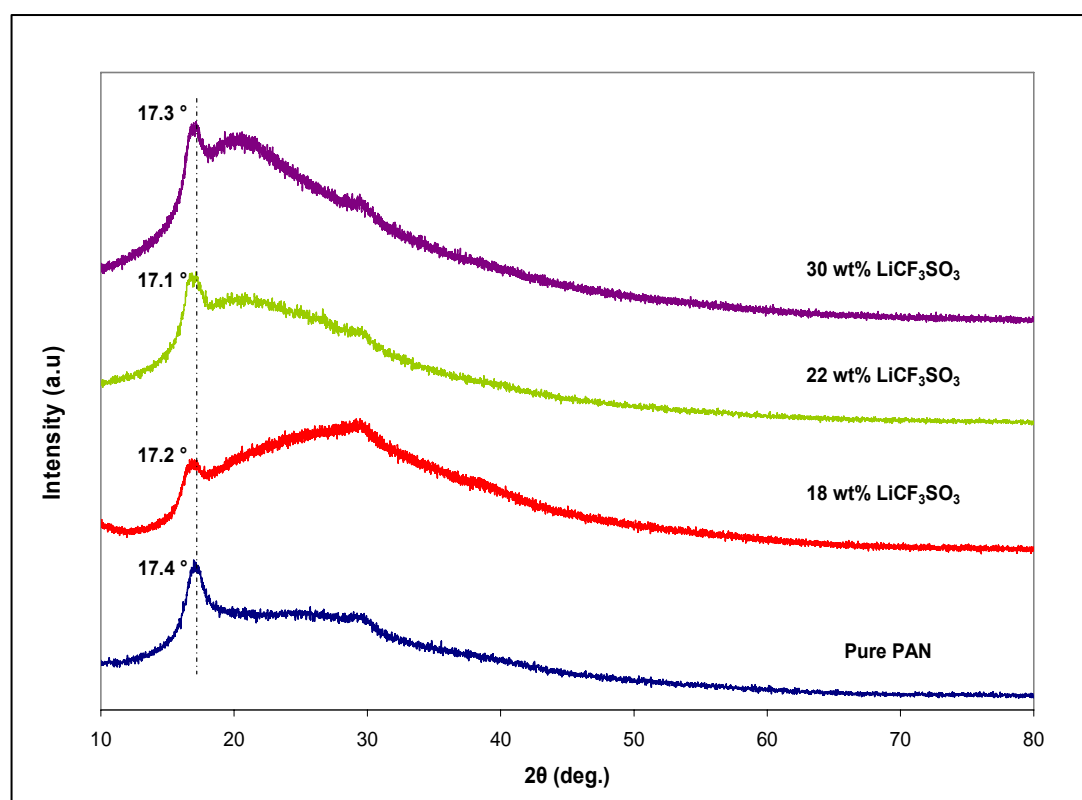


Figure 6.8: X-ray diffractogram of the films in the PAN-EC-LiCF₃SO₃ system.

6.9 PAN-EC- NaCF_3SO_3 System

Figure 6.9 depicts the XRD patterns of the films in the PAN-EC- NaCF_3SO_3 system. The intensity of peak at $2\theta = 17.4^\circ$ is decreased with increasing of salt concentration and shifted to $2\theta = 17.1^\circ$, 17.0° and 17.1° in the 28 wt.% NaCF_3SO_3 , 34 wt.% NaCF_3SO_3 and 40 wt.% LiCF_3SO_3 , respectively. This indicates the films are amorphous and complexation has occurred in the complexes films. The highest conductivity at room temperature is obtained from the film containing 34 wt.% of NaCF_3SO_3 as discussed in Chapter 4. It also can be observed that the XRD pattern of this film has the lowest intensity peak indicating the film is the most amorphous film.

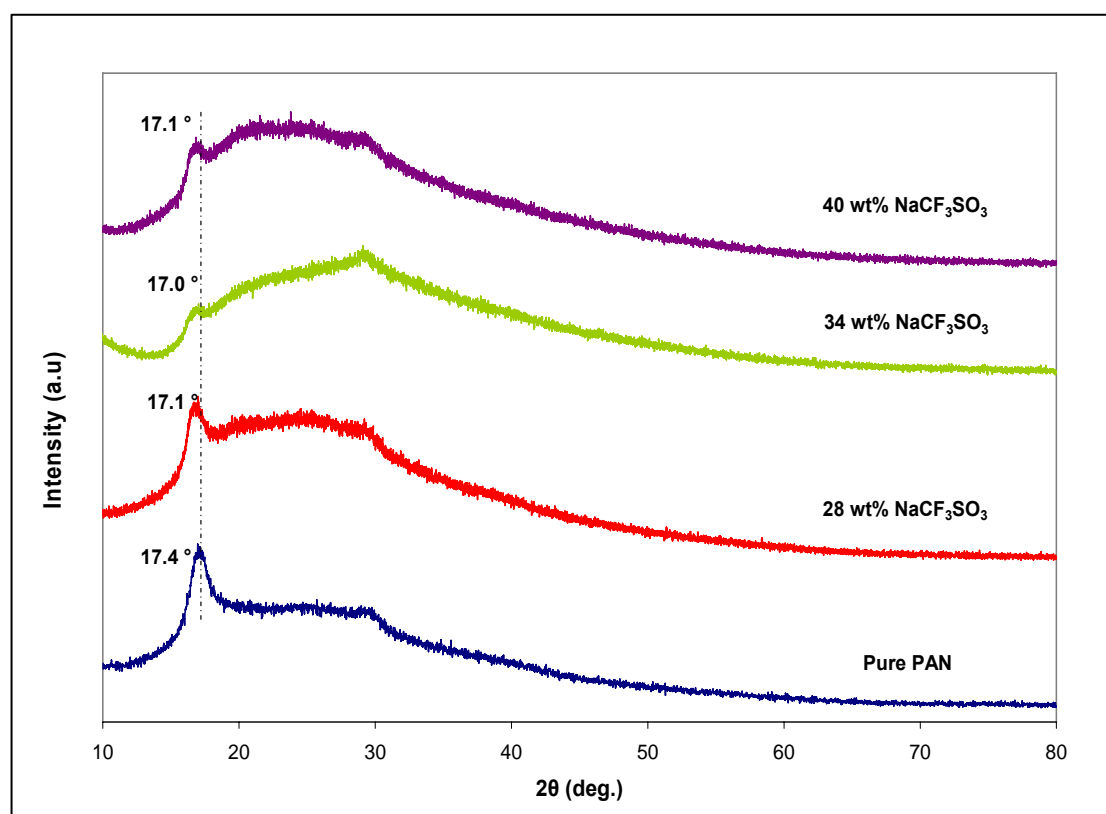


Figure 6.9: X-ray diffractogram of the films in the PAN-EC- NaCF_3SO_3 system.

CHAPTER 7:

Results and Discussion

-SEM Studies-

7.1 Scanning Electron Microscopy (SEM)

Scanning electron microscopy was used to study the surface morphology of the polymer electrolytes films with the highest conductivity at room temperature from each system. SEM micrographs of the films were obtained at a magnification of 3000X. The films were vacuumed after coated with gold at 25 mA for 2 minutes and 40 s.

7.2 Pure PAN Film

Figure 7.1 depicts the SEM micrographs of pure PAN film. A smooth and homogenous surface was discovered in the micrograph of pure PAN film.

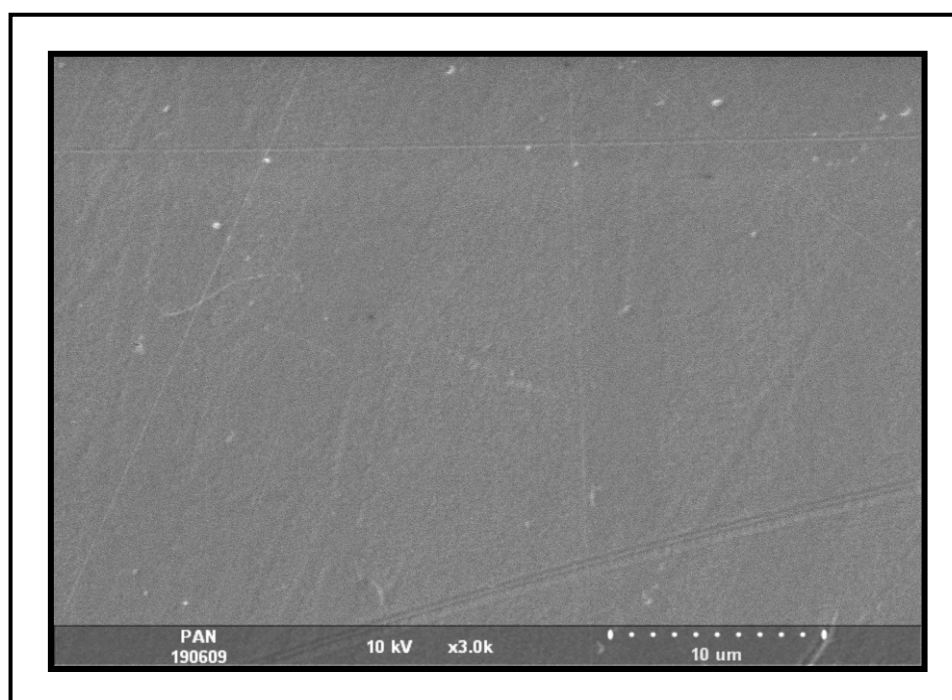


Figure 7.1: SEM micrograph for pure PAN film

7.3 PAN-EC System

Figure 7.2 shows SEM micrograph for the highest conducting film of the PAN-EC system. With addition of plasticizer, it is observed that the amorphous phase is seen to be prominent in this image. The surface appears smooth and homogenous. It can therefore be inferred that the complexation between the polymer, PAN and plasticizer, EC has occurred. This result is consistent with the FTIR and XRD results that discussed in Chapter 5 and Chapter 6.

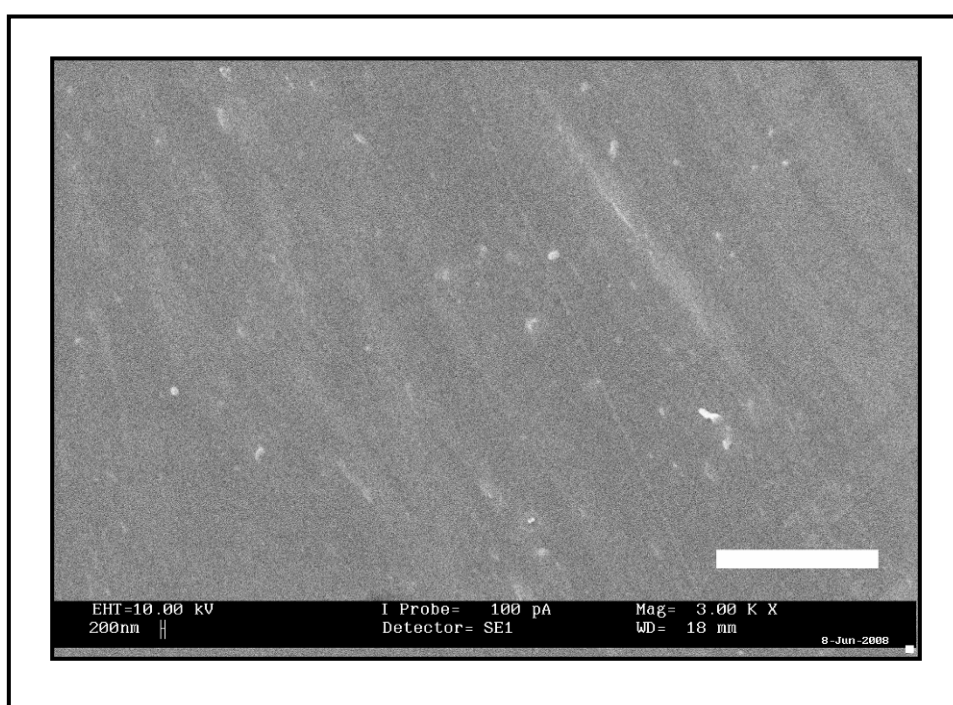


Figure 7.2: SEM micrograph for the highest conducting film in the PAN-EC system.

7.4 PAN-LiCF₃SO₃ and PAN-NaCF₃SO₃ Systems

Figure 7.3 (a) and (b) show SEM micrographs for the highest conducting film in the PAN-LiCF₃SO₃ system and the PAN-NaCF₃SO₃ system, respectively. The smooth and homogenous surface that observed in Figure 7.1 are absent in this film. The surface morphology of the films becomes rough and uneven due to the interaction between PAN and the salt. It can also be observed that the pores appear in the films. This reveals that LiCF₃SO₃ and NaCF₃SO₃ salts are strongly interact with polymer host as observed in the FTIR spectra.

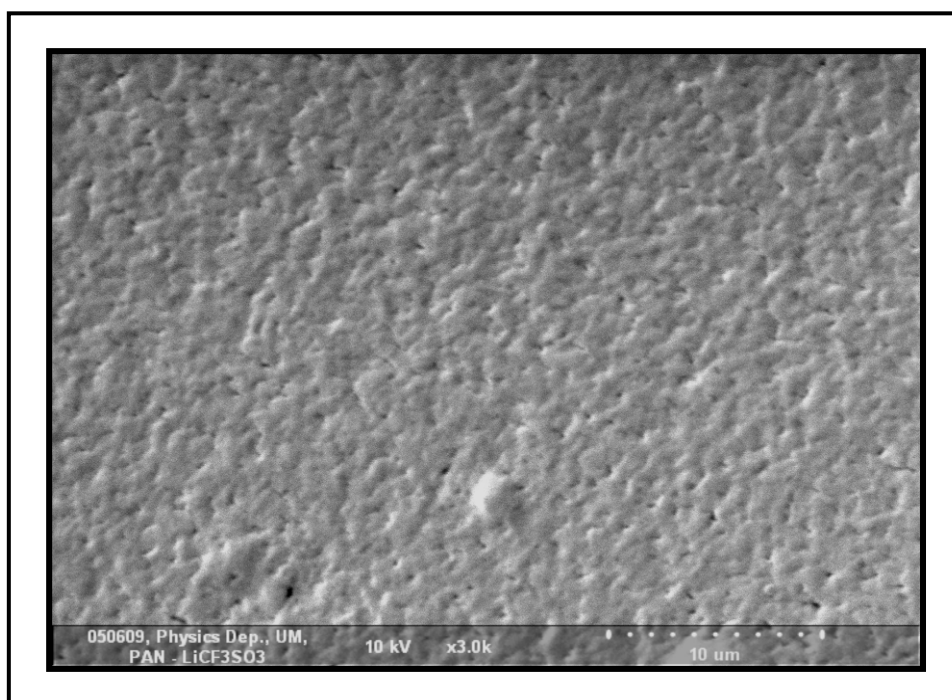


Figure 7.3 (a): SEM micrograph for the highest conducting film in the PAN-LiCF₃SO₃ system

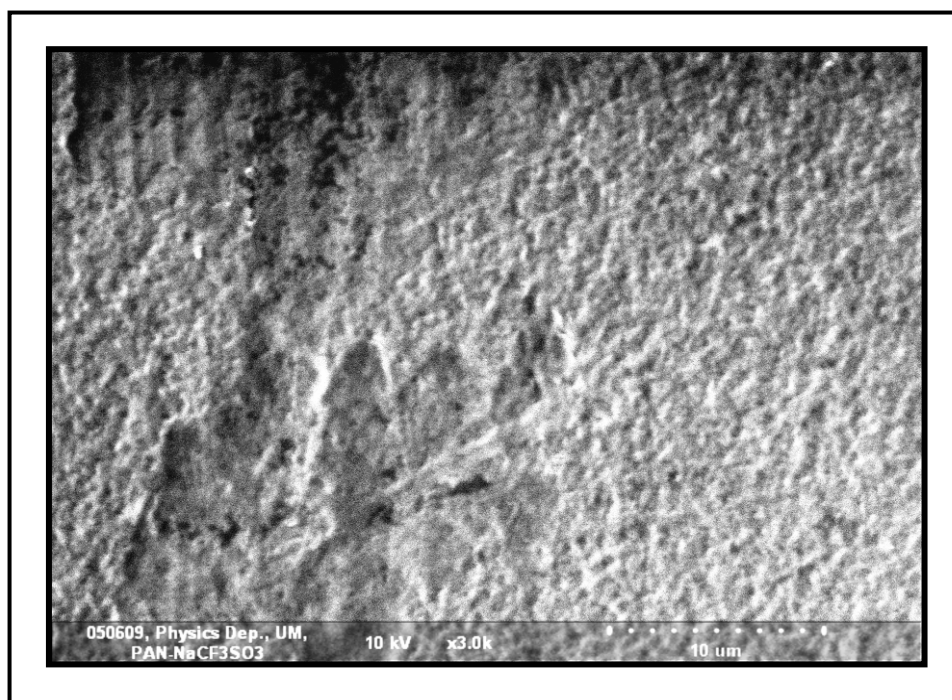


Figure 7.3 (b): SEM micrograph for the highest conducting film in the PAN-NaCF₃SO₃ system

7.5 PAN-EC-LiCF₃SO₃ and PAN-EC-NaCF₃SO₃ Systems

The SEM micrographs for the highest conducting films in the PAN-EC-LiCF₃SO₃ and PAN-EC-NaCF₃SO₃ systems are presented in Figure 7.4 (a) and (b), respectively. It can be seen that the granular and porous surface is appear in these films. This is the effect from the interaction between PAN, EC and the salts. It also can be observed clearly that the pores size in plasticized containing NaCF₃SO₃ film is larger than in the film containing LiCF₃SO₃. The difference in the pores size between both films could be due to the size of Na⁺ ion is bigger than Li⁺ ion. Since the conductivity values for both plasticized films is higher than the unplasticized films, it can be concluded that the presence of plasticizer in PAN-salt film will helps to obtain a regular pore structure, which lead to ion mobility hence higher conductivity.

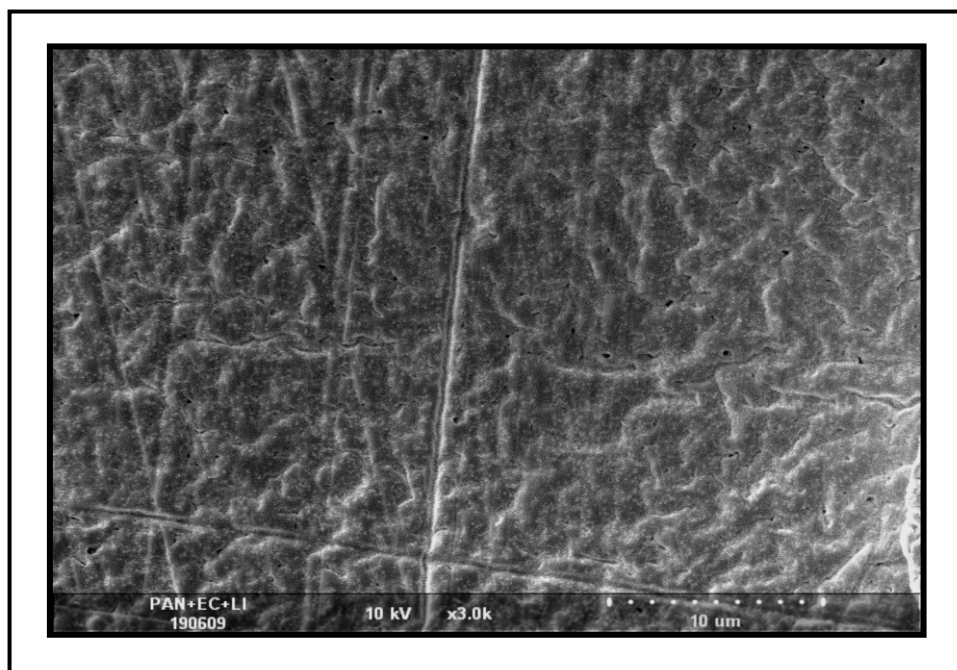


Figure 7.4 (a): SEM micrograph for the highest conducting film in PAN-EC-LiCF₃SO₃ system

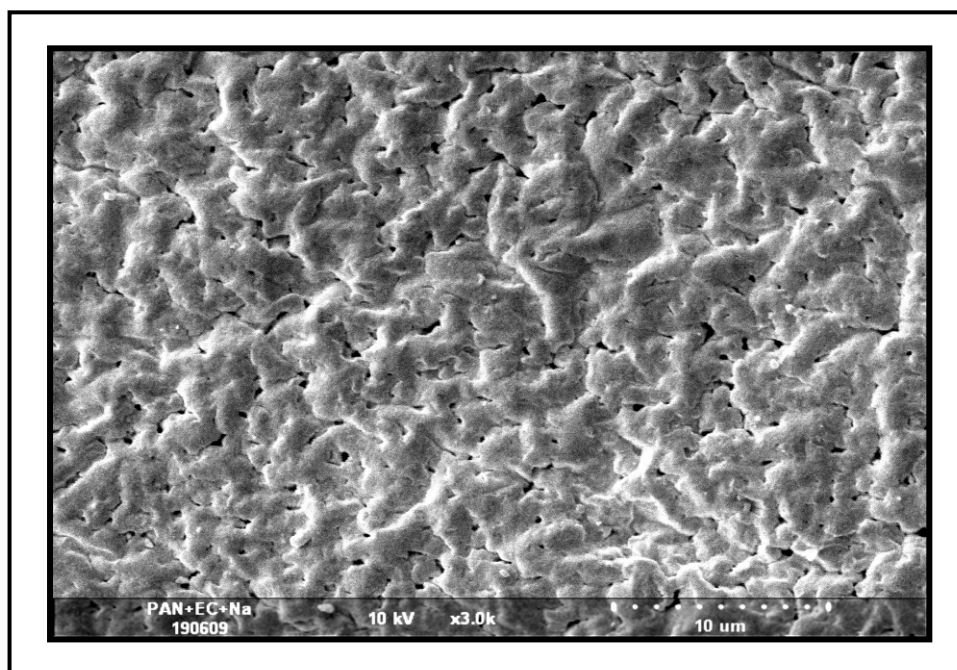


Figure 7.4 (b): SEM micrograph for the highest conducting film in PAN-EC-NaCF₃SO₃ system

CHAPTER 8:

Results and Discussion

-DSC Studies-

8.1 Differential Scanning Calorimetry (DSC)

Thermal analysis using Differential Scanning Calorimeter has been performed in order to observe the change in transition temperature that is caused by the blending of polymer, salt and plasticizer. The DSC thermograms in this chapter show the glass transition temperature, T_g values for all the samples with the highest conductivity at room temperature from each polymer electrolyte system. The T_g values were obtained by using Pyris 6 series thermal software package in the computer that connected to the DSC equipment. The samples were measured in the temperature range between $-50\text{ }^\circ\text{C}$ to $300\text{ }^\circ\text{C}$.

8.2 Pure PAN Film

DSC thermogram of pure PAN sample heated at control rate of $10\text{ }^\circ\text{C}/\text{min}$ has been depicted in Figure 8.1. As shown by the DSC curve, the recorded T_g for pure PAN is $85.4\text{ }^\circ\text{C}$. In general, polymer electrolyte films have a complete amorphous phase structure and it is believed that the ionic conduction occurs more readily in the amorphous phase [95]. Therefore, DSC analysis can be used to determine the T_g values for all polymer electrolyte systems where the T_g value is decreased with the increased of amorphous phase.

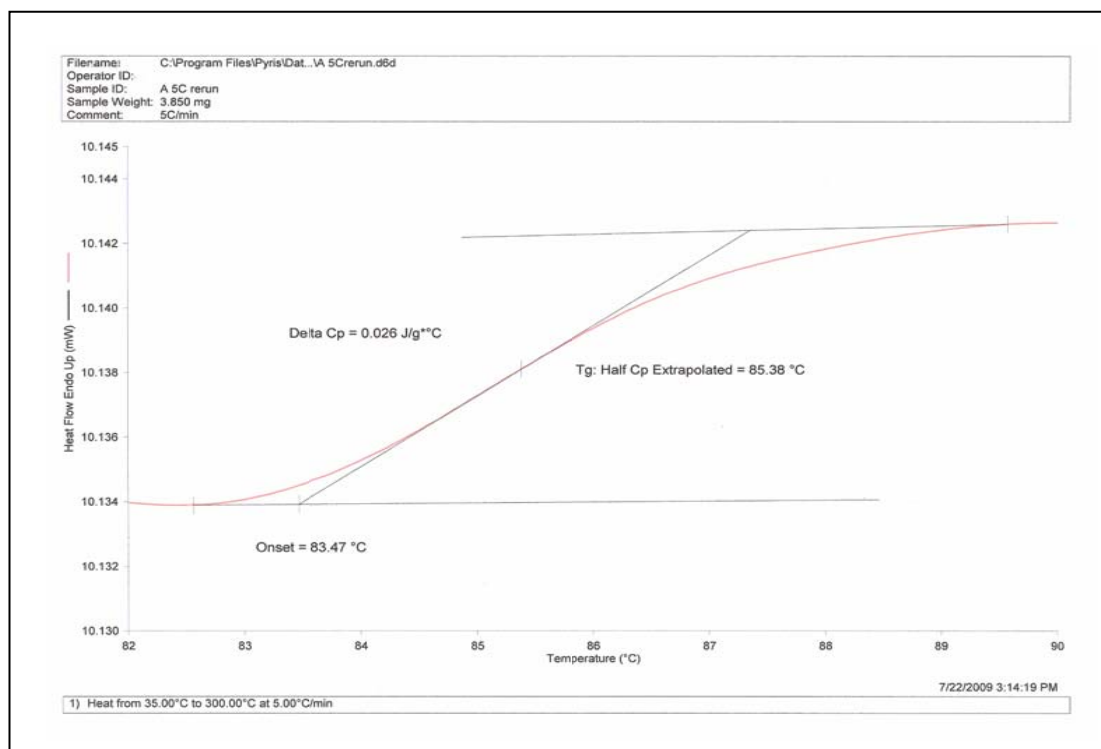


Figure 8.1: DSC thermogram of pure PAN

8.3 PAN - EC System

Figure 8.2 shows the DSC thermogram of the highest conducting film in the PAN-EC system. It was observed that the T_g value of PAN-EC system is decreased to 79.2 °C. The decrease in T_g of pure PAN when the plasticizer is added can be explained by morphological changes in PAN system due to the plasticizing effect of the PAN as observed in SEM image, Figure 7.2. It also indicates that the film becomes more amorphous through the addition of plasticizer. This is in agreement with the conductivity, FTIR and XRD results as discussed in chapter 5, 6 and 7.

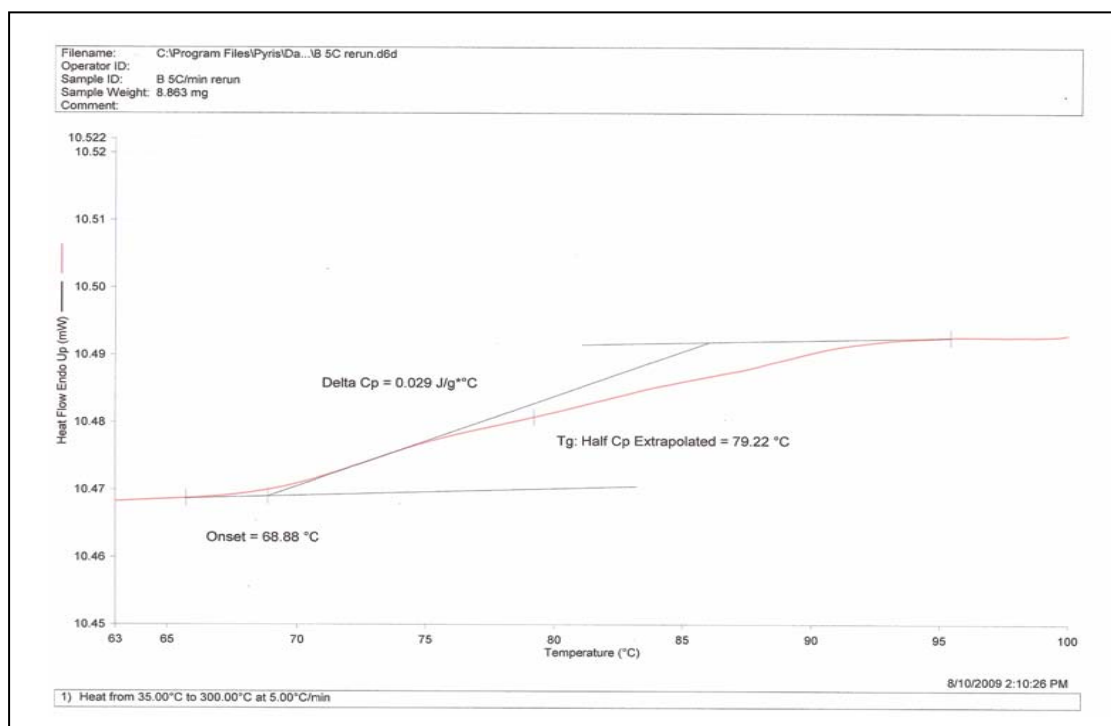


Figure 8.2: DSC thermogram of highest conducting film in the PAN-EC system

8.4 PAN - LiCF₃SO₃ and PAN - NaCF₃SO₃ Systems

DSC thermograms of the highest conducting film in the PAN-LiCF₃SO₃ and PAN-NaCF₃SO₃ systems have been depicted in Figure 8.3 and 8.4 respectively. It can be seen that T_g of the PAN containing salt films has decreased compared to that of pure PAN film. The T_g values for PAN+26 wt.% LiCF₃SO₃ and PAN+24wt.% NaCF₃SO₃ films are 76.9°C and 76.2 °C, respectively. The change in T_g is due to the interaction of Li⁺ and Na⁺ cations with the C \equiv N in the PAN as discusses in FTIR analysis. In fact, the lowering of T_g values result in increasing of amorphous phase in this system with the addition of LiCF₃SO₃ and NaCF₃SO₃ as confirmed by XRD patterns. These results also confirmed the effect of salts on PAN. It also noticed that the T_g value of PAN+24 wt.% NaCF₃SO₃ film is lower than PAN+26 wt.% LiCF₃SO₃ film. This result consistent

with the impedance studies of PAN containing salt system where the conductivity value of PAN+24 wt.% NaCF_3SO_3 sample is higher than PAN+26 wt.% LiCF_3SO_3 samples.

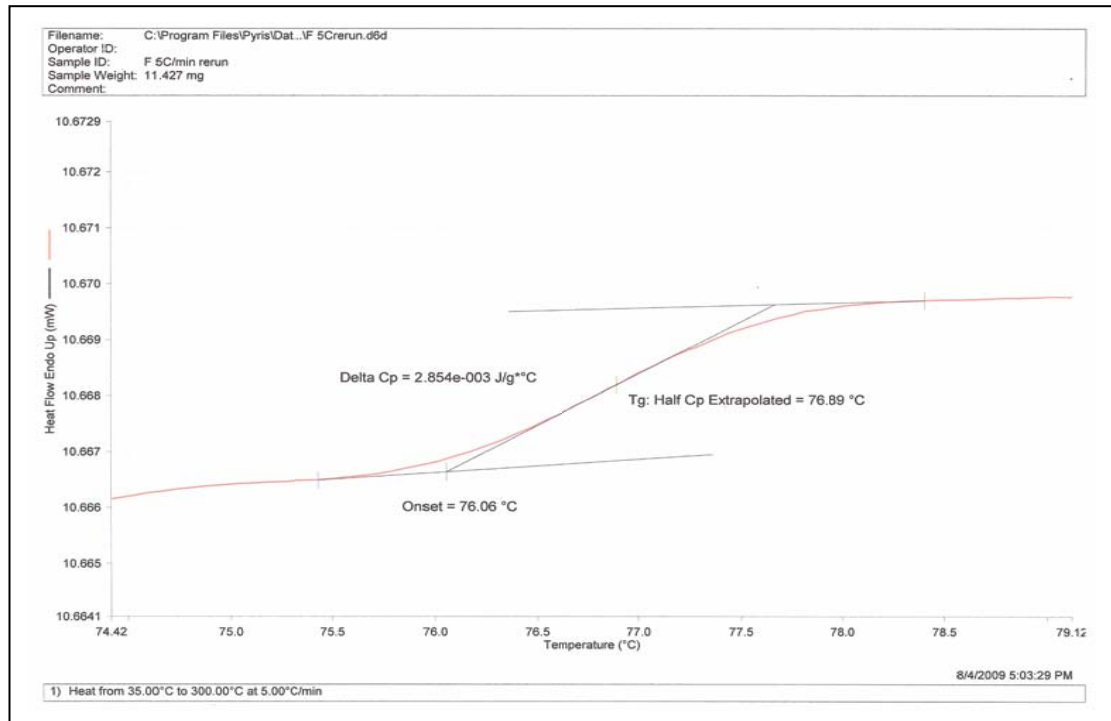


Figure 8.3: DSC thermogram of the highest conducting film in the PAN- LiCF_3SO_3 system

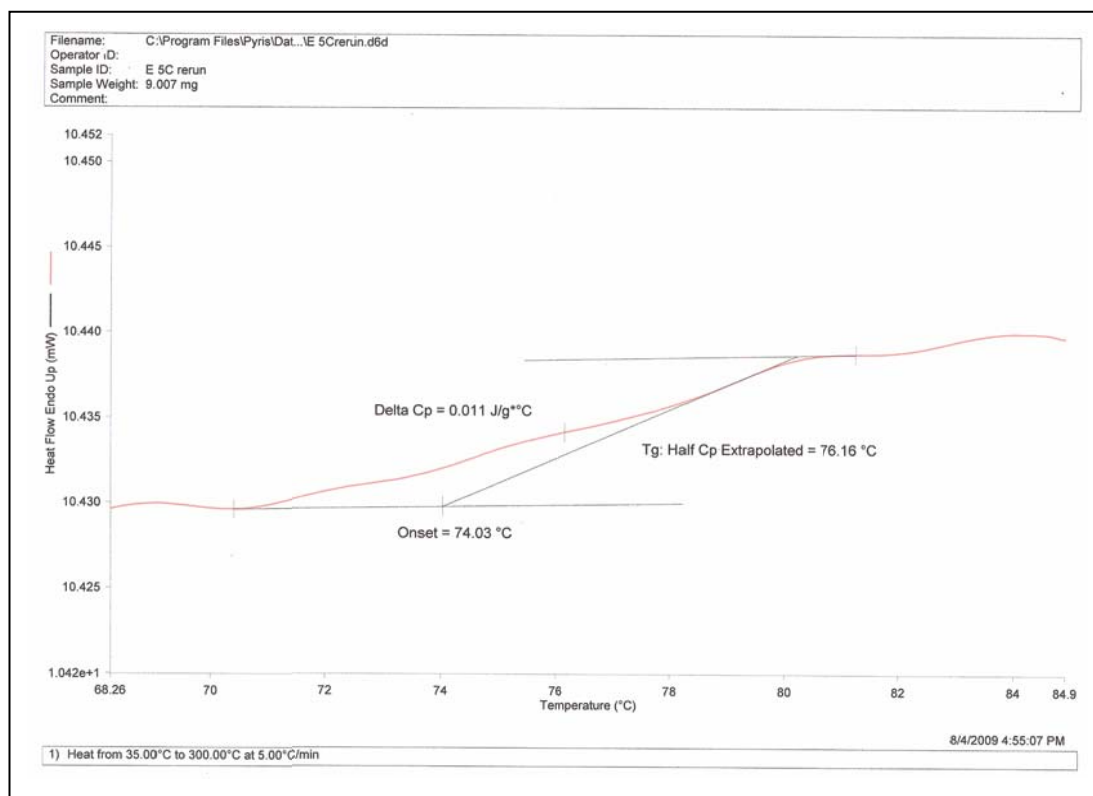


Figure 8.4: DSC thermogram of the highest conducting film in the PAN- NaCF_3SO_3 system

8.5 PAN - EC - LiCF_3SO_3 and PAN - EC - NaCF_3SO_3 systems

DSC thermograms of PAN-EC- LiCF_3SO_3 and PAN-EC- NaCF_3SO_3 samples are shown in Figure 8.5 and 8.6, respectively. The T_g value for PAN-EC- LiCF_3SO_3 sample is 72.9 °C and 63.1 °C for PAN-EC- NaCF_3SO_3 samples. The addition of plasticizer, EC into both PAN-salt systems present lower value of T_g than other system. The decrease of the T_g value is attributed to the increase of amorphous phase and the reduce in crystallinity of the system. The systems also have higher conductivity than the unplasticized PAN systems. This shows that the conductivity is associated with the amorphous phase of the system. Table 8.1 summarizes the T_g values for the highest conducting film from all systems.

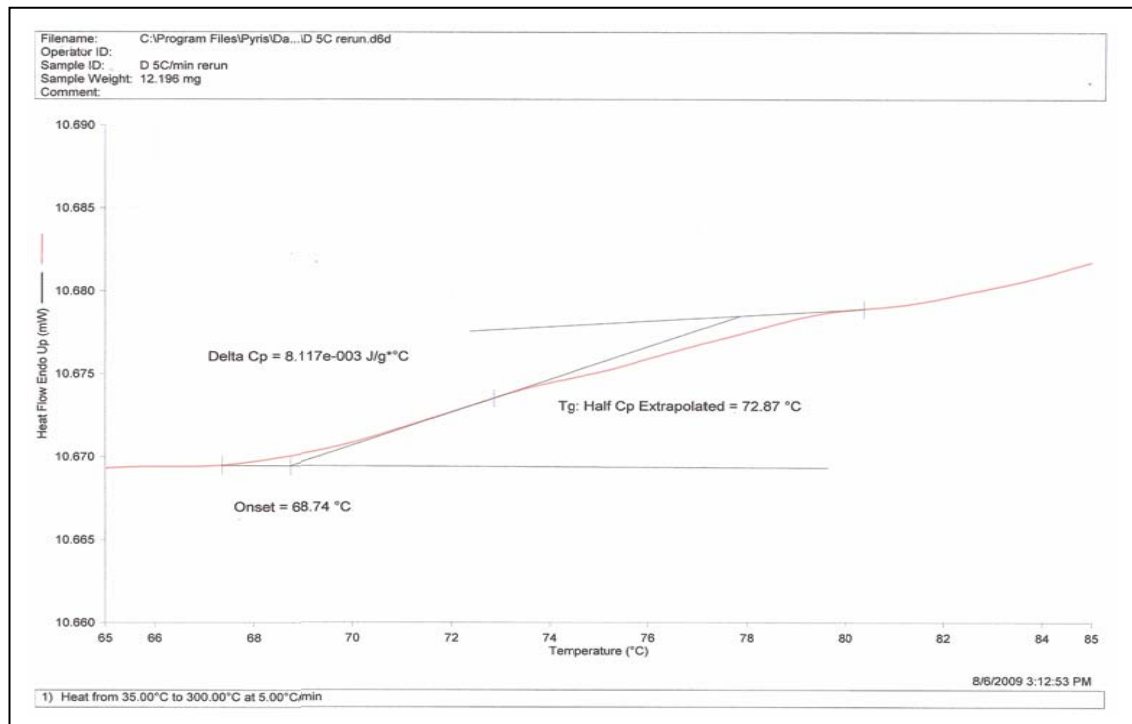


Figure 8.5: DSC thermogram of PAN-EC-LiCF₃SO₃ system

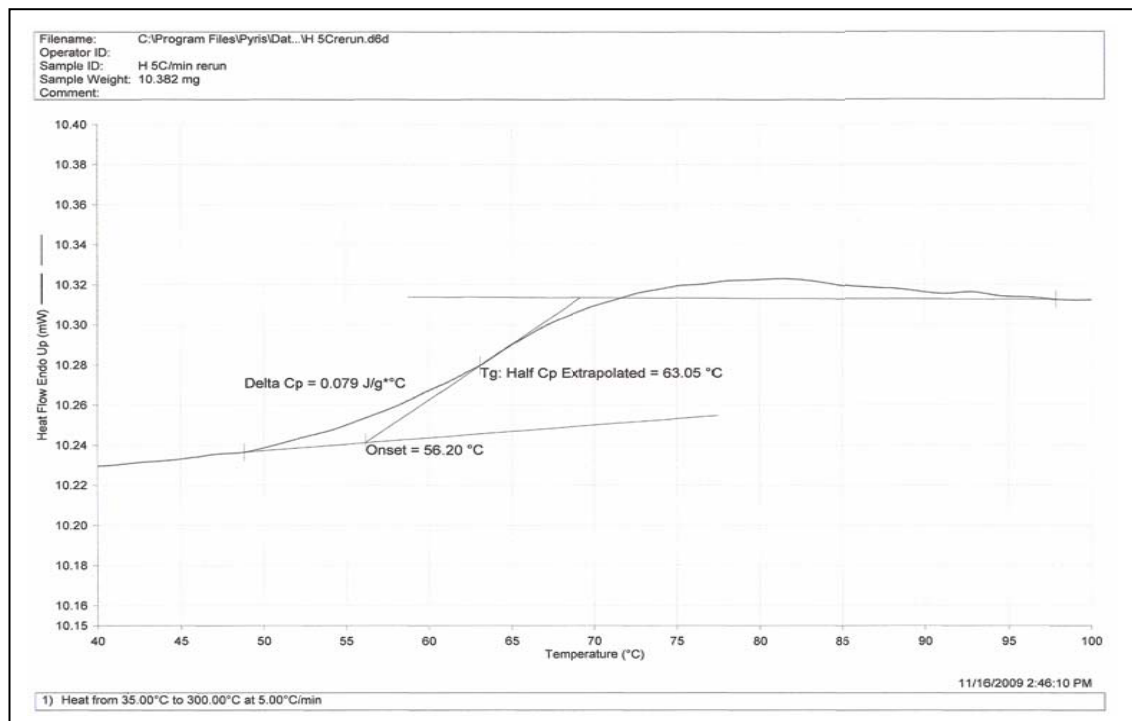


Figure 8.6: DSC thermogram of PAN-EC-NaCF₃SO₃ system

Table 8.1: T_g values from the highest conducting film of PAN-EC, PAN-LiCF₃SO₃, PAN-NaCF₃SO₃, PAN-EC-LiCF₃SO₃ and PAN-EC-NaCF₃SO₃ systems.

System	Glass transition temperature, T_g (°C)
PAN+24 wt.% EC	79.2
PAN+26 wt.% LiCF ₃ SO ₃	76.9
PAN+ 24 wt.% NaCF ₃ SO ₃	76.2
PAN+EC+22 wt.% LiCF ₃ SO ₃	72.9
PAN+EC+34 wt.% NaCF ₃ SO ₃	63.1

CHAPTER 9:

**DISCUSSION, CONCLUSIONS
AND SUGGESTIONS FOR
FURTHER WORK**

DISCUSSION, CONCLUSIONS AND SUGGESTIONS FOR FURTHER WORK

In this work, five systems of PAN based polymer electrolytes have been prepared with various compositions of salts and plasticizer by using solution casting technique. Several experimental methods have been done on these systems to study the effect of plasticizer and salts on ionic conductivity, structural, morphology and thermal properties of the prepared samples.

Charge carrier concentration and ionic mobility are two important factors which influence the conductivity of the polymer electrolyte. The conductivity generally depends on the concentration of salt and the degree of salt dissociation. Higher dissociation of salt resulting in higher number of mobile ions that is available for conduction. Adding plasticizers to polymer electrolytes is useful technique to enhance the conductivity of polymer system. These plasticizers increase the amorphous content of the polymer matrix and tend to dissociate ion-pairs into free cations and anions thereby leading to an overall enhancement in conductivity.

The room temperature conductivity for pure PAN film was achieved at $1.51 \times 10^{-11} \text{ Scm}^{-1}$. On addition of salts and plasticizer, the ionic conductivity of this film increases with increasing salt and plasticizer contents. Table 9.1 summarizes the composition of the films that achieved the highest conductivity for the five systems of polymer electrolytes.

Table 9.1: The highest conductivity at room temperature for each system.

No	System	Conductivity obtained from this work (S cm ⁻¹)	Conductivity (from Literature) (S cm ⁻¹)
1.	PAN+26 wt.% LiCF ₃ SO ₃	3.04 x 10 ⁻⁴	1.32 x 10 ⁻³
2.	PAN+24wt.% NaCF ₃ SO ₃	7.13 x 10 ⁻⁴	*
3.	PAN+EC+22 wt.% LiCF ₃ SO ₃	1.32 x 10 ⁻³	3.53 x 10 ⁻³ (containing EC and PC)
4.	PAN+EC+34 wt.%NaCF ₃ SO ₃	5.49 x 10 ⁻³	*

* *To our knowledge, there is no conductivity value reported for these films.*

At room temperature, the value of the dielectric constant, ϵ_r and dielectric loss, ϵ_i increase as frequency decreases. The film that has the highest conductivity also has the highest value of dielectric constant, ϵ_r and dielectric loss, ϵ_i . This infers that the increase in conductivity is due to an increasing the diffusion of ions through their free volume.

The conductivity-temperature studies are carried out from 303 K to 373 K to understand the effect of temperature on the conductivity. These studies indicate that the conductivity is increased when the temperature is increased. The Arrhenius plots for the highest conducting films in the PAN-LiCF₃SO₃, PAN-NaCF₃SO₃, PAN-EC-LiCF₃SO₃ and PAN-EC-NaCF₃SO₃ systems show that the points lie in an almost straight line and obey Arrhenius relation. Since the conductivity-temperature data obeys Arrhenius relationship, the nature of cation transport is quite similar to that occurring in ionic crystal, where ions jump into neighbouring vacant sites and hence increase the ionic conductivity. The activation energy, E_a values obtained from these systems is 0.28 eV, 0.23 eV, 0.22 eV and 0.19 eV, respectively. The film containing NaCF₃SO₃ salt has

higher ionic conductivity and lower activation energy as compared to film containing LiCF_3SO_3 salt. This result can be explained based on the Lewis acidity of the alkali ions i.e., the strength of the interaction of cations with the nitrogen atoms of PAN. The interaction between Li^+ ion and the nitrogen atom of PAN is stronger than that of Na^+ ion. Thus, Li^+ ion transfer requires higher activation energy than Na^+ ion in polymer electrolytes. These results agree well with the works reported by Sagane et al. and Abe et al. [80, 100-101].

The value of dielectric constant, ϵ_r and dielectric loss, ϵ_i for each system increase with the increasing of temperature and vice versa. This is due to the higher charge carrier density. As temperature increases, the degree of salt dissociation and redissociation of ion aggregates increases resulting the increase in number of free ions due to the increase of free volume.

The conductivity-pressure dependence studies are carried out in the range of pressure between 0.01 MPa to 0.09 MPa for the highest conducting films from the PAN- LiCF_3SO_3 and PAN- NaCF_3SO_3 , PAN-EC- LiCF_3SO_3 and PAN-EC- NaCF_3SO_3 systems. Conductivity is observed to decrease with increasing pressure for all systems. The linear dependence of logarithmic variation of electrical conductivity versus pressure allows a volume ΔV^* can be calculated by using equation;

$$\delta \ln \sigma / \delta P = - (\Delta V^*/RT) \quad (3.12)$$

Since the conductivities of all systems follow an Arrhenius type law at constant pressure, this volume is called an “activation volume”. The activation volume is the difference in volume between a mole of moving species in its activated transition state and its volume at normal equilibrium. The decrease of conductivity values with increasing pressure are related to the basis of the free volume model. The activation

volume, ΔV^* values obtained from these systems are $3.04 \times 10^{-2} \text{ cm}^3 \text{ mol}^{-1}$, $2.86 \times 10^{-2} \text{ cm}^3 \text{ mol}^{-1}$, $1.37 \times 10^{-2} \text{ cm}^3 \text{ mol}^{-1}$ and $1.11 \times 10^{-2} \text{ cm}^3 \text{ mol}^{-1}$, respectively. It can be observed that the highest conducting sample from the PAN-EC- NaCF_3SO_3 system has the smallest activation volume. So, it can be concluded that only a small ΔV^* required for ion motion in this film compared to other films.

FTIR spectra studies have proven that the EC, LiCF_3SO_3 salt and NaCF_3SO_3 salt have form complexes with the polymer host, PAN. The complexation can be determined by the appearance of new peaks, the absence of peaks, the decrease or increase in intensity of the existing peaks in the FTIR spectra. The nitrile band, $\text{C}\equiv\text{N}$ assigned to stretching band in the FTIR spectrum is appeared at 2247 cm^{-1} for pure PAN. The nitrile band is displaced towards the lower frequency around 2244 cm^{-1} due to inductive effect created by the interaction between the nitrogen atom in $\text{C}\equiv\text{N}$ with Li^+ and Na^+ ions from the salts. It also can be observed that the intensity of this band is reduced with increases of salts and plasticizer concentration. This indicates that the complexation has occurred between the polymer, PAN, the salts and the plasticizer.

The XRD diffractograms that have been presented in Chapter 6 reveal that the film with the highest conductivity at room temperature is the amorphous film. Generally, the conductivity increases as the degree of crystallinity decreases with increase of the flexibility of the polymer backbone.

The SEM micrographs presented in Chapter 7 show that the films with the highest conductivity at room temperature from each polymer electrolytes system have the amorphous phase. The presence of plasticizer in PAN-salt system helps to obtain regular pore structure, which lead to ion mobility, hence higher conductivity. These results are fully supported by the XRD and conductivity results.

DSC studies show that the pure PAN has glass transition temperature, T_g at 85.4°C . The T_g of the film decrease upon addition of plasticizer and salts. This

consistent with the room temperature conductivity studies where conductivity is increased with the decrease of due to increased in the segmental motion of the PAN backbone.

In this work, the highest conductivity obtained is $5.49 \times 10^{-3} \text{ S cm}^{-1}$. Therefore, work should be continued to improve the conductivity of the polymer electrolytes to as $\sim 10^{-2} \text{ S cm}^{-1}$. There are some suggestions that could be done to improve the conductivity of polymer electrolytes containing PAN as a polymer matrix. The first suggestion to enhance the conductivity is to blend the PAN with other polymer such as PEO and PVC. Blending polymer is a useful method to develop new materials with improved mechanical stability. As a second suggestion, the use of the different salts such lithium perchlorate (LiClO_4), lithium hexafluorophosphate (LiPF_6), sodium perchlorate (NaClO_4), sodium hexafluorophosphate (NaPF_6) and sodium tetrafluoroborate (NaBF_4) should be considered in an attempt to look for good lithium and sodium ion conducting polymer electrolytes. Final suggestion is the incorporation of double plasticizers such as ethylene carbonate (EC): propylene carbonate (PC) in the polymer electrolytes.

REFERENCES

REFERENCES

- [1] Wolfgang Sigmund, University of Florida, Gainesville, USA; Hassan El-Shall; Dinesh O. Shah, University of Florida, Gainesville, USA; Brij. M. Moudgil, University of Florida, Gainesville, USA editors of Particulate Systems in Nano- and Biotechnologies
- [2] S. Schantz, J. Sandahl, L. Bořjesson, L.M. Torell, *Solid State Ionics* 28–30 (1988) 1047
- [3] *Fundamentals of Polymer Engineering* Author: Arie Ram, Plenum Press, New York (1997)
- [4] Servos, John W., *Physical Chemistry from Ostwald to Pauling*, Princeton University Press, Princeton, New Jersey, 1990
- [5] M. Armand, *Solid State Ionics* 69 (1994) 309
- [6] S. York, R. Frech, A. Snow, D. Glatzhofer, *Electrochim. Acta* 46 (2001) 1533-1537.
- [7] C. P. Rhodes and R. Frech, *Solid State Ionics* 136-137 (2000) 1131-1137
- [8] R. A. Sanders, A. G. Snow, R. Frech and D. Glatzhofer, *Electrochimica Acta* 48 (2003) 2247-2253
- [9] B.L. Papke, M.A. Ratner, D.F. Shriver, *J. Electrochem. Soc.* 129 (1982) 1434-1438.
- [10] M. B. Armand, J. M. Chabagno, M. J. Duclot, *Fast Ion Transport in Solids*, Elsevier, North Holland, New York, (1979) 131
- [11] M. H. Cohen, D. J. Turnbull, *J. Chem. Phys.* 31 (1959) 1164
- [12] H. Cheradame, In *IUPAC Macromolecules*, Benoit, P. Rempp. Eds.; Pergamon Press; New York, (1982) 2.
- [13] A. Killis, J. F. LeNest, A. Gandini, H. Cheradame, J. P. Cohen-Addad, *Solid State Ionics* 14 (1984) 231
- [14] M. A. Ratner, In *Polymer Electrolyte Reviews*; J. R. MacCallum, C. A. Vincent, Eds.; Elsevier: London, (1987) 173.
- [15] A. Killis, J. F. LeNest, H. Cheradame, A. Gandini, *Makro mol. Chem.* 183 (1982) 2835
- [16] A. Killis, J. F. LeNest, A. Gandini, H. Cheradame, *Makro mol. Chem.* 183 (1982) 1037

-
- [17] C. A. Angell, *Solid State Ionics* 9/10 (1983) 3
- [18] C. A. Angell, *Solid State Ionics* 18/19 (1986) 72
- [19] L. M. Torrell, C. A. Angell, L. Borjesson, S. W. Martin, *Solid State Ionics* 18/19 (1986) 431
- [20] J. J. Fontanella, M. C. Wintersgill, M. K. Smith, J. Samancik, C. G. Andeen, *J. Appl. Phys.* 60 (1986) 2665
- [21] J. J. Fontanella, M. C. Wintersgill, J. P. Calame, J. P. Pursel, D. R. Figueroa, C. G. Andeen, *Solid State Ionics* 9/10 (1983) 1139
- [22] A. V. Chadwick, J. H. Strange, M. R. Worboys, *Solid State Ionics* 9/10 (1983) 1155
- [23] M. B. Armand, J. M. Chabagno, M. Duclot, In *Fast Ion Transport in Solids*; M. J. Duclot, P. Vashishta, N. Mundy, G. K. Shenoy, Eds.; North-Holland, New York (1979) 131
- [24] D. E. Fenton, J. M. Parker, P. V. Wright, *Polymer* 14 (1973) 589-1589.
- [25] S. Rajendran, R. S. Babu and P. Sivakumar, *Journal of Membrane Science* 315 (2008) 67-73
- [26] F. Yuan, H. Z. Chen, H.Y. Yang, H. Y. Li, M. Wang, *Materials Chemistry and Physics* 89 (2005) 390-394
- [27] R. Koksang I.I Olsen and D. Shackle, *Solid State Ionic* 69 (1994) 320-335
- [28] Hae-Kwon Yoona, Won-Sub Chungb, Nam-Ju Jo, *Electrochimica Acta* 50 (2004) 289–293.
- [29] Songklanarin *J. Sci. Technol.*, Vol 24 (Suppl.) 2002: Membrane Sci. & Tech.
- [30] O. Bohnke, C. Rousselot, P. A. Gillet, C. Truche, *J. Electrochem. Soc.* 1 (1992) 1862
- [31] E. Tsuchida, H. Ohno, K. Tsunami, N. Kobayashi, *Solid State Ionics* 11 (198) 227.
- [32] S. Reich and I. Michaeli, *J. Polym. Sci. Polym. Phys. Ed.* 13 (1) (1975) 9-18
- [33] J. M. G. Lowie in *Polymer Electrolyte Reviews 1* ; Edited by J. R. MacCallum and C. A. Vincent, Elsevier New York (1987) p. 94
- [34] M. Watanabe, M. Togo, K. Sanui, N. Ogata, T. Kobayashi, Z. Ohtaki, *Macromolecules* 17 (1984) 2902
- [35] S. S. Selchon, N. Arora, H. P. Singh, *Solid State Ionics* 160 (2003) 301
- [36] B. Huang, Z. Wang, L. Chen, R. Xue, F. Wang, *Solid State Ionics* 91 (1996) 279

-
- [37] A. M. Stephan, *European Polymer Journal* 42 (2006) 21
- [38] J. Saunier, N. Chaix, F. Allion, J. P. Belieres, J. Y. Sanchez, *Electrochimica Acta* 47 (2002) 1321
- [39] H. Akashi, K. Sekai, K. Tanaka, *Electrochim. Acta* 43 (1998) 1193
- [40] Watanabe M, Togo M, Sanui K, Ogata N, Kobayashi T, Ohtaki Z, *Macromolecules* 17 (1984) 2908
- [41] Abraham KM, Choe HS, Rasquariello DM, *Electrochim Acta* 43 (1998) 2399
- [42] P. P. Chu, Z.P. He, *Polymer* 42 (2001) 4743-4749.
- [43] S. Rajendran, R. Kannan, O. Mahendran, *Materials Letters* 48 (2001) 331-335
- [44] M.B. Armand, J.M. Chabagno, M. J. Duclot, *Fast Ion Transport in Solids*, Elsevier, North Holland, New York, (1979) 131
- [45] R. Larsson and O. Anderson, *Electrochimica Acta* 48 (2003) 3481-3489
- [46] Chemical structure of Ethylene carbonate , Author, date of creation: selfmade by Shaddack, 5 December 2006 , from the Wikipedia web: http://en.wikipedia.org/wiki/File:Ethylene_carbonate.png
- [47] Z. Wang, B. Huang, R. Xue, X. Huang, L. Chen, *Solid State Ionics* 121 (1999) 141–156
- [48] G. Long and M.E. Meek, Environmental Health Directorate, Health Canada, and M. Lewis, Commercial Chemicals Evaluation Branch, Environment Canada, (2001), Concise International Chemical Assessment Document 31, from the web: <http://www.inchem.org/documents/cicads/cicads/cicad31.htm>
- [49] AroKor Holdings Inc. Seoul, Korea, *N,N-DIMETHYLFORMAMIDE*, from the web: <http://www.chemicaland21.com/industrialchem/solalc/DMF.htm>
- [50] *N,N-Dimethylformamide Draft*, California Environmental Protection Agency, August 2008
- [51] Marshall Brain and Charles W. Bryant, *How Batteries Work*, from the web: <http://electronics.howstuffworks.com/battery6.htm>
- [52] *Lithium-ion Polymer Batteries: A Look to the Future*, Edited by Chris Warner, ECN, August 2001
- [53] O. Tillement, *Solid State Ionics* 68 (1994) 9-33
- [54] C. G. Granqvist, *Solid State Ionics* 53-56 (1992) 479-489
- [55] R. B. Goldner, F.O. Arntz, G. Berera, T. Haas, W. Wie, K.K. Wong, P.C. Yu, *Solid State Ionics* 53- 56 (1992) 617-627

-
- [56] M. Armand, D. Deroo, D. Pedone, Proc. Int. Seminar Solid State Ionic Devices, Singapore (1988) 515-520
- [57] H. Ohno, H. Yamazaki, Solid State Ionics 59 (1993) 217-222
- [58] Types of Fuel Cells, 1999-2001 FuelCellWorks.com from the Web: <http://fuelcellworks.com/Typesoffuelcells.html>
- [59] Chapter 2: Electrochemical Sensors, from the Web: <http://www.intlsensor.com/pdf/electrochemical.pdf>
- [60] Application Note, Gamry Instrument, from the web: www.gamry.com/App_Notes/EIS_Primer/EIS_Primer.htm
- [61] N. M. Morni, N. S. Mohamed, A. K. Arof, Materials Science and Engineering 845 (1997) 140.
- [62] A.S.A. Khair, R. Puteh, A. K. Arof, Physica B 373 (2006) 2
- [63] W. Van Gool, Paul Hagenmuller (Eds.), Solid Electrolytes General Principles, Characterization, Materials, Applications, Material Science and Technology, Academic Press, USA, 1978
- [64] C. Julien, Gholam-Abbas Nazri, Solid State Batteries: Materials Design and Optimization, Kluwer Academic Publishers, London, 1994.
- [65] M. Duclot, F. Alloin, O. Brylev, J. Sanchez, Jean L. Souquet, Solid State Ionic 136-137 (2000) 1153-1160
- [66] J. Ross MacDonald, Impedance Spectroscopy, John Wiley & Sons, USA, (1987)
- [67] Introduction to Fourier Infrared Spectroscopy, Thermo Nicolet (2001), from the web: <http://www.thermonicolet.com>
- [68] Powell, D. Handout on X-Ray Diffraction generated for 626 instrumentations course, UW--Madison Chemistry Department, Spring, 1992, figure from the Web: <http://www.chem.wisc.edu/~newtrad/CurrRef/BDGTopic/BDGtext/BDGGraph.html>
- [69] Optics basics: Young's double slit experiment by skullsinthestars, references: T. Young, "On the Theory of Light and Colours," Proc. Roy. Soc. Lond. A 92 (1802), 12-48, figure from the web: <http://skullsinthestars.com/2009/03/28/optics-basics-youngs-double-slit-experiment/>
- [70] Diagram courtesy of Iowa State University SEM Homepage
- [71] Differential Scanning Calorimetry by Gürther Höhne, W. Hemminger, H Flammersheim ISBN 3-540-00467-x Springer-Verlag Berlin Heidelberg 2003
- [72] C. S. Ramya, S. Selvasekarapandian, T. Savitha, G. Hirankumar, Physica B 393 (2007) 2672

-
- [73] R. Mishra and K. J. Rao *Solid State Ionics* 106 (1998) 113- 127.
- [74] J. L. Souquet, M. Levy, M. Duclot, *Solid State Ion* 70/71 (1994) 337–345
- [75] M. L. Williams, R. F. Landell, J. D. Ferry, *J. Am. Chem. Soc* 77 (1955) 3701
- [76] S. Ramesh, A. K. Arof *Mat Sci Eng B85* (2001) 11
- [77] J.C. Dyre, *J. Non-Cryst. Solids* 135 (1991) 219
- [78] S. Ramesh and A.K Arof, *Mat Sci. Eng B85* (2001) 11
- [79] S. Ramesh, A. H. Yahya, A.K. Arof, *Solid State Ionics*, 152-153 (2002) 291
- [80] F. Sagane, T. Abe, Y. Iriyama, Z. Ogumi, *Journal of Power Sources* 146 (2005) 749–752
- [81] M. S. Michael, M. M. E. Jacob, S. R. S. Prabakaran, S. Radhakrishna, *Solid State Ionics* 98 (1997) 167
- [82] J. T. Bendler, J. J. Fontanella, M. F. Shlesinger, M. C. Wintersgill, *Electrochimica Acta* 48 (2003) 2267
- [83] J. J. Fontanella, *J. Chem. Phys.* 111 (1999) 7103
- [84] M. C. Wintersgill, J. J. Fontanella, P. E. Stallworth, S. A. Newman, S. H. Chung, S. G. Greenbaum, *Solid State Ionics* 135 (2000) 155
- [85] J. J. Fontanella, M. C. Wintersgill, J. P. Calame, M. K. Smith, C. G. Andeen, *Solid State Ionics* 18–19 (1986) 253.
- [86] F. A Amaral et.al *Journal of Power Sources* 164 (2007) 379-385
- [87] P. Basak and S. V. Manorama, *Solid State Ionics* 167 (2004)113-121
- [88] H. K. Yoon, W. S Chung and N. J. Jo, *Electrochimica Acta* (2004) 289-293
- [89] S. Chintapalli, R. Frech, *Electrochimica Acta* 42 (1997) 471.
- [90] Z. Wang, B. Huang, H. Huang, L. Chen, R. Xue, F. Wang, *Solid State Ionics* 85 (1996) 143-148
- [91] C. L. Angell, *Trans, Faraday Soc.* 52 (1956) 1178
- [92] B. Huang, Z. Huang, G. Li, H. Huang, R. Xue, L. Chen, F. Wang, *Solid State Ionics* 85 (1996) 79
- [93] C. H. Kim, J. K. Park, S. I. Moon, M. S. Yoon, *Electrochimica Acta* 43, Nos 10-11 (1998) 1421-1427
- [94] Z. Osman, A.K. Arof, *Electrochimica Acta* 48 (2003) 993
- [95] R.A. Sanders, G. S. Albert, R. Frech, D. Glatzhofer, *Electrochimica Acta* 48 (2003) 2247-2253

-
- [96] W. Huang, R. Frech, R.A. Wheeler, *J. Phys. Chem.* 98 (1994) 100
- [97] A. Ferry, G. Orlandi, P. Jacobsson, *Electrochimica Acta* 43 (1998) 1471
- [98] H.W. Chen, F.C. Chan, *Journal Polymer Sciences, Part: Polymer Physics*, 39 (2001) 2407
- [99] C. Berthier, W. Gorecki, M. Minier, M. B. Armand, J. M Chabagno, P. Rigaud *Solid State Ionics* 11 (1983) 91-95.
- [100] T. Abe, H. Fukuda, Y. Iriyama, Z. Ogumi, *J. Electrochem. Soc.* 151, 8 (2004) A1120-A1123.
- [101] T. Abe, H. Fukuda, Y. Iriyama, Z. Ogumi, *J. Electrochem. Soc.* 151, 11 (2004) A1950-A1153.
- [102] M. Jaipal Reddy, J. Siva Kumar, U. V. Subba Rao, P. Chu, *Solid State Ionics* 177 (2006) 253–256